Mohamed Abdelrahman

A contribution to the development of a special-purpose vehicle for handicapped persons

A contribution to the development of a special-purpose vehicle for handicapped persons

Dynamic simulations of mechanical concepts and the biomechanical interaction between wheelchair and user

Mohamed Abdelrahman

Impressum

Titelfoto: Veit Henkel | Fakultät für Maschinenbau, TU Ilmenau

__Abstract__

This thesis discusses the mathematical modeling of wheeled locomotion systems. More precisely, the kinematics and the dynamics of a Mecanum wheeled vehicle are studied. The dynamic and kinematic models are introduced for the practical and industrial applications. Also, the motion behavior of the handicapped is captured and analyzed during the propulsion of the wheelchair for different operation conditions.

The motivations of this study are introduced in the beginning of the thesis. The state of the art, in the field of Mecanum wheels based vehicles, is presented. A general overview for nowadays aspects in the field of locomotion systems for handicapped and their advantages has been discussed.

Chapter 2 discusses the mathematical basics, which are deployed in this thesis. Different theories and principles of the kinematics and dynamics are summarized and presented. The transformation matrices, types of the kinematic constraints, the dynamics of rigid multibody systems with a special focus on the LAGRANGE's equation of the second kind are presented.

The locomotion systems are analyzed analytically from the kinematic and dynamic point of views. It focuses mainly on two important designs, which are commonly used in our everyday life. The first is a model for the two wheels locomotion system such as wheelchairs and similar systems. The second type is a model for the four wheeled Mecanum vehicle. A detailed derivation for the kinematic and dynamic models for both locomotion systems is introduced. Two different ways have been used to model the four wheels Mecanum vehicle. The first method is called the suggested method and the second is the approximation method. In the suggested method, the LAGRANGE's equation of the second kind is used to introduce a precise dynamic model, which can model all kinds of motion trajectories for the discussed system. The approximation method is estimated using the pseudo inverse matrix and can be used for simulating the standard motion trajectories.

The simulation results for different motion trajectories are presented in chapter 4. The second order differential equations of the dynamic models, for both the suggested and approximation models, are numerically integrated and the resulted motion trajectories for predefined driving

moments are presented. A 3D Virtual model for the four wheeled Mecanum vehicle is programmed using MATLAB®, SIMULINK® and the VIRTUAL REALITY TOOLBOX®, that to show the combination between the translational and rotational motion in 3D environment. Two different experimental platforms were constructed for realizing the special-purpose vehicle for the handicapped. The platforms move typical to the simulation results.

Finally, the characteristics of the wheelchair propulsion for two test volunteers have been discussed. The motion of the human body has been captured using special experimental setup and has implemented and analyzed using ALASKA® and ERGO TOOL® software.

Kurzfassung

Die Arbeit diskutiert die mathematische Modellbildung von ausgewählten Fortbewegungssystemen mit Rädern. Die Kinematik und Dynamik eines radgetriebenen Fahrzeuges mit Mecanum-Rädern wird beschrieben. Die dynamischen und kinematischen Modelle sind die Voraussetzung für Simulationsrechnungen und gleichzeitig für die praktische Anwendung beim Betrieb der Systeme. Außerdem wird das Bewegungsverhalten von Behinderten während der Fahrt im Rollstuhl für verschiedene Umgebungsbedingungen analysiert.

Nach der Darlegung der Motivation der Arbeit wird eine Analyse des Standes der Technik auf dem Gebiet der Fahrzeuge mit Mecanum-Rädern vorgestellt. Eine Übersicht über aktuelle Aspekte der Fortbewegungssysteme für Behinderte und ihre Vor- und Nachteile ist ein weiterer Gegenstand der Arbeit. Im Kapitel 2 sind die mathematischen Grundlagen, die in dieser Arbeit verwendet werden, zusammengefasst. Es handelt sich um die Kinematik der starren Körper und ausgewählte Prinzipien und Gleichungen der analytischen Mechanik. Die Transformationsmatrizen für ebene Drehungen, die Arten der kinematischen Zwangsbedingungen, die Dynamik der starren Körper mit einem speziellen Fokus auf die LAGRANGE Gleichung 2. Art mit Multiplikatoren werden vorgestellt. Die Fortbewegungssysteme sind vor allem mit analytischen Methoden in der Kinematik und Dynamik beschrieben worden. Der Fokus liegt auf 2 Grundmodellen, die auch aktuell technisch genutzt werden. Das erste Modell gilt für zweirädrige Bewegungssysteme, wie zum Beispiel für einen Rollstuhl. Das zweite Modell wurde für ein vierrädriges Fahrzeug mit Mecanum-Rädern entwickelt. Detaillierte Herleitungen für die kinematischen und dynamischen Modelle sind für beide Fortbewegungssysteme dargestellt. Für die Dynamik des Fahrzeuges mit Mecanum-Rädern wird eine exakte Methode, basierend auf den Grundlagen der nichtholonomen Mechanik mit einer zweiten, häufig in der Literatur angeführten, Näherungsmethode verglichen. Aus der nichtholonomen Mechanik werden die LAGRANGE Gleichungen mit Multiplikatoren als effizientes Verfahren eingesetzt, um ein exaktes Modell zu generieren. Diese Modellgleichungen können alle möglichen Bewegungsbahnen des Fahrzeuges mit vier Mecanum-Rädern erfassen. Das Approximationsverfahren aus der Literatur nutzt eine Pseudoinverse Matrix und kann nur ausgewählte Standardtrajektorien abbilden. Simulationsergebnisse, basierend auf der numerischen Integration der Dynamikgleichungen aus beiden Verfahren werden in Kapitel 4 vorgestellt.

Die resultierenden Bewegungsbahnen sind für vorgegebene Antriebsmomente dargestellt. Ein virtuelles 3D-Modell des vierrädriges Mecanum-Fahrzeuges ist mit Hilfe von MATLAB®, SIMULINK® und VIRTUAL REALITY TOOLBOX® erstellt worden. Ein Vorteil der 3D-Umgebung ist die anschauliche Darstellung komplexer Bewegungsbahnen bei kombinierten Translations- und Rotationsbewegungen des Systems.

Zwei Experimentalfahrzeuge, eines mit klassischer Vierradstruktur inklusive Vorderachslenkung und ein weiteres mit vier omnidirektionalen Rädern vom Typ Mecanum, wurden aufgebaut. Sie dienen als Demonstratoren eines möglichen Plattformkonzeptes für Behindertenfahrzeuge. In der Arbeit werden die aus Simulationsrechnungen gewonnenen Trajektorien mit den tatsächlichen Bahnen des Prototyps verglichen. In einem abschließenden Kapitel wird für ausgewählte Szenarien mittels Motion Capturing Verfahren die Mensch-Maschine-Interaktion am Beispiel von Rollstuhlfahrern untersucht. Die Bewegung des menschlichen Körpers und des Rollstuhls wurde in ihren kinematischen Daten erfasst und mit den Werkzeugen ALASKA-DYNAMICUS® und ERGO TOOL® analysiert.

<u>Acknowledgment</u>

```
291
292      % Line Segment modified to create MarkerExtrusion instead of MarkerLine
293      % JD, 10.12.2013
294      % create a line segment if enabled in block mask
```

Table of Contents

Nomenclatures and Symbols

$\vec{r}(\cdot)$	Position vector of a point in the motion space
q^a	Generalized coordinate
$\dot{q}^a$	Generalized velocity
$\ddot{q}^a$	Generalized acceleration
$\vec{\omega}_i$	Angular velocity of the body i
μ	Coefficient of dry friction
x_i, y_i, z_i	Cartesian coordinates relative to x , y and z axis for i-th body in Cartesian coordinates
x_C, y_C, z_C	Coordinates of the center of mass
$\dot{x}_C, \dot{y}_C, \dot{z}_C$	Velocity components of the mass center
$\vec{e}_x, \vec{e}_y, \vec{e}_z$	Unity vectors of the global coordinate system
$\vec{E}_x, \vec{E}_y, \vec{E}_z$	Unity vectors of the body-fixed coordinate system
$\mathbb{E}$	Rotation matrix
$\bar{E}$	Column vector of the body-fixed unity vectors
$\bar{e}$	Column vector of the unity vectors of the global coordinate system
$\vec{\omega}$	Angular velocity
V	Volume of the rigid body
$\vec{D}_0$	Angular momentum vector relative to the origin of the global coordinate system
$\vec{D}_C$	Angular momentum vector relative to the center of mass C
$\dot{\vec{D}}_A$	Angular momentum vector relative to point A
$\vec{M}_0$	Moment vector relative to the origin of the global coordinate system
$\vec{M}_C$	Moment vector relative to the center of mass C
$\vec{F}$	Resultant force
L	LAGRANGE function
T	Kinetic energy
U	Potential energy
λ_b	LAGRANGE multiplier
$\alpha_{a_1}^{a_2}$	Coefficient scheme
dm	Mass element in the rigid body
S	Acceleration energy, APPELL function
Π	Generalized force

v_{C_i}	Velocity for the wheel center of rotation
v_{r_i}	Velocity of the roller contact point
J_C	Mass moment of inertia for the complete vehicle relative to the center of mass of the vehicle
$\mathbb{J}^+$	Pseudo-inverse matrix
$\vec{M}^C$	Moment vector at point C
$\vec{M}_{ix}^C, \vec{M}_{iy}^C, \vec{M}_{iz}^C$	Moment components in the direction of the reference coordinates (x, y, z) for body number i
$\vec{F}^C$	Force vector at point C
$\vec{F}_{ix}^C, \vec{F}_{iy}^C, \vec{F}_{iz}^C$	Force components in the direction of reference coordinates (x, y, z) for body number i at point C
$\vec{F}^A$	Force vector at point A
$\vec{F}_{ix}^A, \vec{F}_{iy}^A, \vec{F}_{iz}^A$	Force components in the direction of reference coordinates (x, y, z) for body number i at point A
J_{xx}, J_{yy}, J_{zz} $\scriptstyle i \quad i \quad i$	Mass moment of inertia for body number i relative to the main body reference axes x, y, z
$\dot{\varphi}_i$	Angular velocity of wheel i
fc_i	Friction coefficient between wheel i and the contact surface
$F_R(\cdot)$	Friction force
$\text{sgn}(\cdot)$	Signum function
m_0	Mass of the vehicle chassis
m_1	Mass of the Mecanum wheel
m	Total mass of the four-wheeled Mecanum vehicle
J_0	Mass moment of inertia of the vehicle chassis relative to body-fixed perpendicular axis $\vec{E}_3$
J_1	Mass moment of inertia for a Mecanum wheel relative to rotating axis $\vec{\underline{E}}_{2}$ of the wheel
J_2	Mass moment of inertia for a Mecanum wheel relative to perpendicular wheel local axis $\vec{\underline{E}}_{3}$
ρ_1	Distance from the center of mass to the rear axle
ρ_2	Distance from the center of mass to the front axle
l	One-half the width of the vehicle
R	Wheel radius
$M_i(\cdot)$	Driving moment of wheel i
f_a^b, F^b, g^b	Functions, constraints
J_{ik}	Mass moment of inertia relative to axes i and k
$J_{i'k'}$	Mass moment of inertia relative to the translated and

	rotated axes i' and k'
ω_i	Angular velocity relative to axis i
$\vec{E}_k$	Unity vector in the direction of axis k
$\vec{a}$	Linear displacement vector
a_i	Linear displacement in the direction of axis i
a_j	Linear displacement in the direction of axis j
a_k	Linear displacement in the direction of axis k
δ_{ik}	KRONECKER symbol
δq^{a_1} or $\delta\vec{r}$	Virtual displacement
$\vec{p}$	Linear momentum vector
$\dot{\vec{p}}$	Resultant force on a rigid body
$E_{i'i}$	Rotation matrix about axis i
$E_{k'k}$	Rotation matrix about axis k
Q_a	Generalized forces where $(a = 1,2,\ldots,n)$
R_a	Reaction force
P	Electrical driving power
η	Mechanical efficiency
m_t	Total mass
θ_P	Propulsion angle or effective pushing cycle
θ_R	Release angle
θ_C	Contact angle
C	Center of gravity for the rigid body
DOF	Degrees of freedom
4WMV	Four-wheeled Mecanum vehicle
MS	Motion span
MBS	Multibody system
Mr. J.	Test volunteer 1
Mr. K.	Test volunteer 2
RD	Direction of rotation
Sugg.	The suggested model for 4WMV
Aprox	The approximated model for 4WMV

In setting the notations and symbols of this thesis, the symbols for vectors contain the arrow and the standard matrix form is used as appropriate.

The wheelchair is one of the most commonly used assistive devices for enhancing personal mobility, which is a precondition for enjoying human rights and living in dignity and assists people with disabilities to become more productive members of their communities.

(WHO, 2008)

1 Introduction

1.1 Social and technical aspects of physical disabilities

Developing a locomotion system which fulfills the motion requirement in different environments and can overcome all the surrounding obstacles is still a dream for all scientists working in the field of locomotion and transportation systems. The needs of physically disabled persons are especially important with respect to new facilities for both ordinary wheelchairs and specially designed, high-tech wheelchair, the choice of which mostly depends on the level of luxury desired by the patient. It is difficult to find concrete official statistics about the number of wheelchair users in developed and developing countries. The lack of information about the number of wheelchair users is one parameter limiting the services and facilities available to them. For this reason, MCKEE from MONASH University, England [81] published his statistics about the number of wheelchair users in different countries to contribute to better understanding of the breadth of this market. It states that

■ Number of wheelchair users
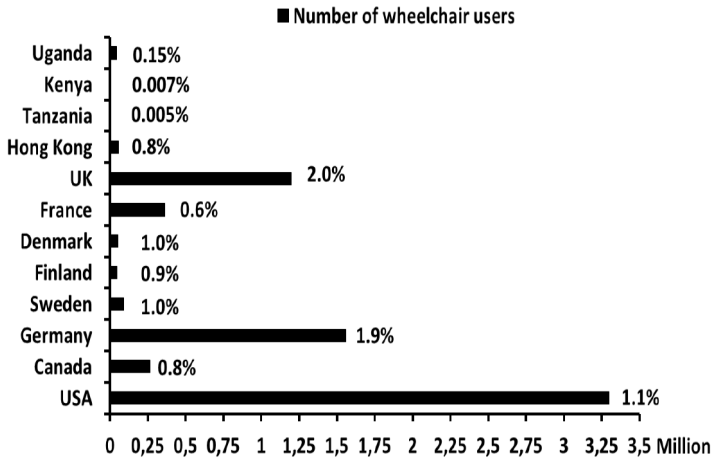
Figure 1.1 The number of wheelchair users in different countries and percentage relative to the respective population – based on the statistics in [81]

From the previous statistics, it is clear that there are no exact reliable numbers for wheelchair users, especially in developing countries, where wars and internal conflicts are the cause most cases of physical disabilities. The number cannot reflect reality in a developing country at all. On the other hand, in developed countries, available numbers for wheelchair users have mostly come from organizations for the disabled, which sometimes may not be accurate for reasons such as missing government support for providing these statistics and the limited capability of such organizations and unions for covering the different regions in the country. Missing an accurate number as well as details about the number of wheelchair users and the type of their disability are still a huge problem facing developers of these products. Additional statistics about the physically disabled in the US is presented in [7].

The following flow diagram presents an overview from different sides of the mobility problems facing disable persons in the modern world.
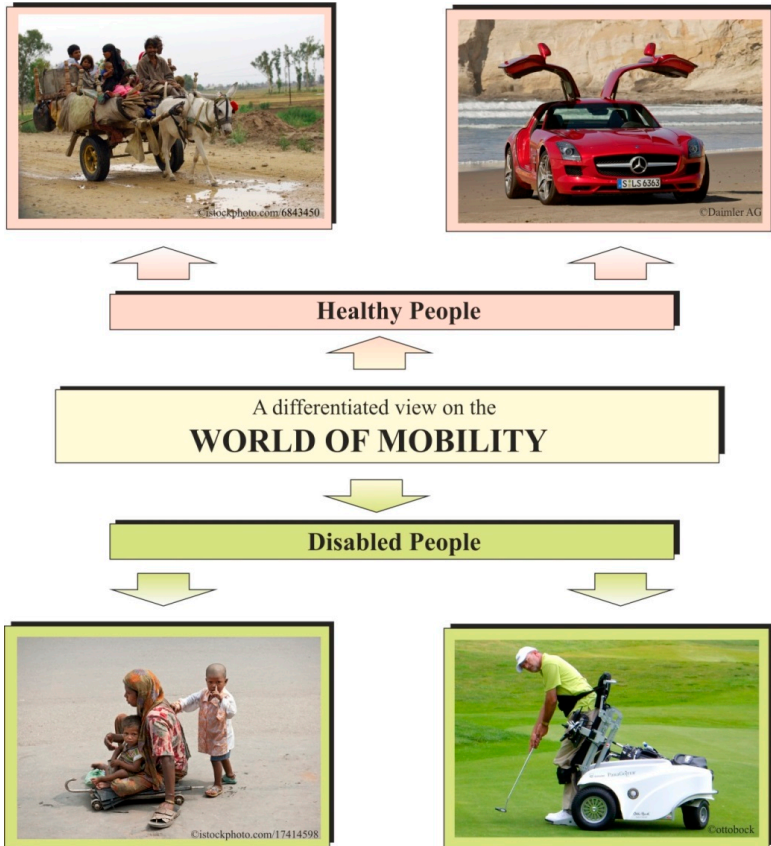
Figure 1.2 A differentiated view of the world of mobility

The cycle of life turns a child into an adolescent, into a young adult and then a strong adult, who will eventually become a weaker elderly person. In some places of the world, the percentage of the elderly within the population is increasing rapidly due to high standards of health care and a significant shortage of an equivalent percentage of newborns. Therefore, the need arises to compensate for the weakness of the older generations in order to help them to continue to be able to contribute economically through production or other work. Many scientific research institutes and many scientists have worked and are still working on that objective.

On the other hand, some places in this world experience significant conflict and war, which are a direct reason for an increasing percentage of disabilities among the people in those places. The Middle East, central Africa and south Asian countries have suffered and are still experiencing bloody conflicts, which have only produced hatred, death and wounded disabled victims. This brings about the need to compensate for the disabilities of those victims especially those suffering from a motion disability in an arm or leg in order to put them back on the road of positive economic integration. The countries themselves as well as other friendly countries helping to effect peace in those countries are funding research projects to help these victims to retrain their societal capabilities and the capability to work in order to remain productive members of those societies.

Traffic accidents have left a lot of disabled victims who need help to retrain their movement capability. The victims lose their extremities and sometimes their hope in life. The duty of their own societies is to bring them hope, to draw a smile on sad faces. In some countries such as Egypt for example, the number of traffic accident victims in one year is more than number of victims lost in all political conflicts in the Arabic region. Some statistics discussed the percentages of dead victims and wounded victims in all countries of the world. They determined that the actual percentage of victims becoming disabled after accidents is a terrible number and the statistics showed the direct relationship between the disabilities and the amount of developmental progress in countries experiencing a high percentage of traffic accidents. The only solution to overcome the disabilities suffered by traffic accidents victims is to find a treatment for their disability through the invention of new clever solutions to compensate for the loss of one or more of their extremities, namely by providing those handicapped with wheelchairs or advanced locomotion units. These units can adapt themselves to different driving and environmental conditions. They are designed and configured based on the needs of each user. These units offer the solution for every kind of disability, whatever it is and wherever it occurred. They can realize the dream of movement and put a great smile on the faces of their users.

When practicing hobbies for example, there is a specific degree of danger for the occurrence of accidents. Accidents due to hobbies are considered a low percentage of all reasons behind disabilities and are usually due to such events as practicing for car races, paragliding, kite surfing and balloon flights. All these sports or hobbies involve a degree of danger stemming from faults in safety systems or human errors, both

directly leading to an accident. Most research aspects concentrate on eliminating the errors leading to accidents during participation in hobbies or sports, but it is impossible to attain 100% safe participation, especially if the human element plays a role in controlling any part of the system. Then if an accident occurs, the possibility for paralyzing one or more of the body extremities is significant. Past research projects have taken into consideration the consequences of practicing such hobbies and the type of disabilities which can result from and offer more intelligent solutions to compensate the disabled extremities by applying prosthetics or by facilitating transportation using suitable locomotion systems.

Based on the reasons mentioned above for sources of disabilities in certain parts of the body, it is clear that requirement common among them is the straightforward development of new intelligent motion aids to retrain motion capability in the disabled body part or to assist when there is difficulty in treating the disability as in its involving multiple body parts. New locomotion systems can be suggested as a solution to compensate part or all of a disability. Within the last few decades a lot of money and efforts have been invested to find a solution for the disability of the human body parts. The social aspects governing the life of disabled persons and relating to the wheelchair industry have been discussed previously in [34, 120].

1.2   <u>State of the art</u>

1.2.1   General overview

A short overview of developed designs is given here to more fully understand the different activities and contributions in the field of designing, modeling and controlling locomotion systems, especially with respect to the physically disabled. The selected examples are presented in the context of this thesis. The researchers have concentrated on two main directions. The first aspect involves assisting the body using an external, or exoskeleton, system; the second direction concerns the development of a locomotion system, such as a wheelchair, which can offer a wide variety of different assistance methods in addition to comfortable transportation for the disabled person. Also the wheelchair industry provides the disabled with new facilities and equipment which can be attached to the wheelchair in order to assist in many aspects of life in general or even to be able to participate in sports.

The first idea came to the engineers researching solutions for disabled extremities involved maintaining and assisting the motion capability of the disabled person. The research institutes, both civilian and military, have been working on a project to develop a mechanical suit for the human body to assist motion – widely known as an exoskeleton suit. The mechanical suit consists of an external structure surrounding mechanical muscles, which operate using a pneumatic or electrical driving system. The mechanical suit is still under development and enhancement. So far, it has shown limited success in achieving its development purposes. The source of energy for driving the mechanical muscles needs more development in order to reduce weight and increase efficiency. The structural elements of the suit have thus far been manufactured from material with special mechanical properties. This material is strong enough to withstand the body load and light enough to prevent exhaustion in the disabled body parts by carrying external weights. Generally, the exoskeleton concept has not been used widely among the disabled because of its high costs. Successful prototypes of the exoskeleton concept can be seen in the robotics field and in the military research field. One of the most difficult challenges in developing the exoskeleton suit is the combination and integration of the mechanical parts together in addition to the high sensitivity required during motion of the paralyzed parts, without needing a high level of driving power or expensive electronics. The Japanese company CYBERDYNE® INC has developed a suit for different ages and levels of paralysis.

Figure 1.3 Exoskeleton suit from CYBERDYNE INC® – Japan (Ref.: www.cyberdyne-studio.com/hf_english.html)

The second aspect in the suggested solutions for disabled persons is the development of a transportation unit or locomotion system that can be modified to match the basic requirements of the user. An example for such locomotion systems is the wheelchair. The wheelchair has grown in recent times into a large category, encompassing many different special-purpose vehicles. The real challenge in designing an optimum wheelchair is to determine how the locomotion system can be suitable for all motion conditions with a reasonable level of comfort and stability in different surroundings. Besides that, the developers of disabled assistance systems offer a wide range such systems, from parts useful to facilitate driving the wheelchair, which can now be considered a special-purpose vehicle. Capabilities added to wheelchairs have included adding a joystick for driving the wheelchair, controlling motion using voice commands or even using direct signals from the brain as well as adding a special camera to detect the body of the user and translate the body's motion into commands. All of these components have been added to the wheelchair to make it easier to use and suitable for a wide range of users with different disabilities.

The second challenge facing the industry for special-purpose vehicles for the disabled is power consumption. More power is needed due to the increase in capabilities built into the unit. The duration of the working time of the moving units reflected directly on the size of the used battery. The second example for driving the wheelchair is based on manual propulsion, which means the wheelchair is equipped with large-radius wheels, which help to make the propulsion process easy for the user. However, not all disabled users have enough manual power to drive the wheels for long time. In this case, assistance systems must be added to aid in manually driving the wheelchairs. Long rotational arms, chained sprockets or similar systems can used to assist in manual rotation. If the disable person suffers from a higher-degree disability, it is recommended to switch to an electrically driven vehicle.

Table 1.1 Different driving concepts for wheelchairs and similar systems

Additional motorized wheel Z50	Otto Bock (Ref.:www.ottobock.de/cps/rde/xbcr/ob_de_de/ifu_647g315_z50.pdf)
	Description: Motorized wheels with additional battery pack. It has the features of both an ordinary wheelchair and a motorized wheelchair. The user can rotate the wheels manually or electrically using a joystick. Each wheel is equipped with an electric motor at its hub.
Additional driving units Z10 & Z10-ce	Otto Bock (Ref.: www.ottobock.de/cps/rde/xbcr/ob_de_de/64 6D379-D-02-1006w.pdf)
	Description: The driving unit can be attached to the wheelchair to convert it from a manually driven unit into a motorized wheelchair. It is suitable for long-distance travel. It can be controlled by patients themselves or an assistant.
Pivot wheelchair with propulsion arms	RIO Mobility (Ref.: www.riomobility.com/en/leverdrive/userma nual.pdf)
Description: The wheelchair is equipped with two levers along with a special mechanism to rotate the wheels.	

Heliumls – manually propelled, manual stand-up	Permobil (Ref.: www.permobilus.com/pdf/Heliumls.pdf)

Description:
The position of the wheelchair user can be changed manually from a sitting position to a standing position.

K450 – powered wheelchair with wheelchair position adaptability	Permobil (Ref.: www.permobilus.com/manuals/47.pdf)

Description:
The position of the seat can be changed using an additional pneumatic lifting system.

Scalamobil – Stair climbing unit	Alber (Ref.: www.alber.de/fileadmin/content/schulung/Prospekt_scalamobil_S35_deutsch_37.0001.6.01.04.pdf)

Description:
It can be attached directly to the wheelchair using special connecting elements; step-by-step stair climbing unit; there is another design from the same company with an additional seat.

Electric single wheel drives for a wheelchair	EUROPÄISCHE PATENTSCHRIFT - EP 2 360 045 B1 Inventor(s): Oliver BORNGRÄBER, Michael Hungerbühler 05.09.2012 Patentblatt 2012/36 Owner of the patent Micro-Motor AG - http://www.micromotor.ch/ Patent site address (Ref.: worldwide.espacenet.com/publicationDetails/biblio? CC=EP& NR= 2360045B1&KC=B1&FT=D)
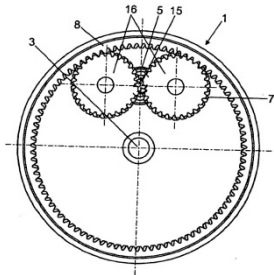
FIG. 1	**Description:** The ordinary wheel is equipped with a couple of gears for wheel propulsion; an electric motor drives the gears
COYOTE Dual-Drive Handcycle	Team Hybrid (Ref.: www.teamhybrid.co.uk/handcycles2/dualdrive.php)
Description: A third wheel can be connected to the wheelchair; it is driven by a chain, a sprocket and a hand pedal.	
ScoutCrawler	Otto Bock (Ref.: www.ottobock.de/cps/rde/xbcr/ob_de_de /646D587-DE-04-1203w.pdf)
	Description: A chained motorized vehicle which can transport different types of wheelchairs on rough terrain; easy to use and compatible with different environments.
Super Four	Otto Bock (Ref.: www.ottobock.de/cps/rde/xbcr/ob_de_de /646D363_3DD_OBH _SuperFour_web.pdf)

	Description: An electric vehicle for the disabled which can move on different roads and different terrains. It provides the user with various capabilities to make transportation easier.

The short overview of the existing systems in Table 1.1 and the contents of Figure 1.2 show the complexity of the development process for an assistant system for the disabled. The history of wheelchair development and the new intelligent wheelchairs were discussed in [59, 119]. The basic requirements to be considered in wheelchair designs according to the standards of developed countries such as England can be found in [51].

This thesis will discuss the state of the art for the mechanical aspects from an engineering point of view. The wheel is the basic element in wheelchair construction and varies widely, depending on user capability and the nature of the surroundings through which the motion is to take place. Different kinds of wheels have been developed to match the user requirements. It was found that the optimal design for any wheelchair begins by selecting a suitable type of wheel.

1.2.2   Wheels – design and mechanical aspects

This section discusses the state of the art of research in the field of locomotion and transportation systems, including an analysis and summary of the advantages and disadvantages. The ideas of locomotion systems vary widely depending on the purpose and the available design budgets. Because of that, finding a solution for a locomotion system which fulfills the requirements of all aspects and is also suitable for all financial budgets is simply a dream. However, in some developed countries, inventors have faced this challenge and have built cheap designs from available materials and technologies in their societies, thus decreasing the design costs and increasing unit durability and overall lifetime. By avoiding the use of expensive spare parts or complicated technologies, they developed simple designs which were compatible with societal and environmental conditions. There are several basic, important requirements that have to be fulfilled by any locomotion system:

1. Ease of driving.
2. Relative acceptable range of payload capacity.
3. Ease of maintenance.

A successful completion of these requirements is possible only using model-based design. Thus, rigorous computer-aided design of locomotion systems is actually the state of the art. A general step forward in the direction of introducing new concepts of wheels used in the engineering field is the development of omnidirectional wheels. They are special designs for wheels with rollers distributed along the circumference of the wheel, see Figure 1.4. When the angle between the wheel contact motion plane and the roller axis is $\pi/4$, the wheel is called a Mecanum wheel. It has previously appeared in some literature sources under the name "Swedish wheel" because this type of wheel is based on a patent from BENGT ILON (Swedish inventor, 1973) [49]. BECKER et al. [13] presented a new type of wheel called Wheg, which combines the characteristics of rolling and stepping over an obstacle in one configuration.

(a)   (b)   (c)
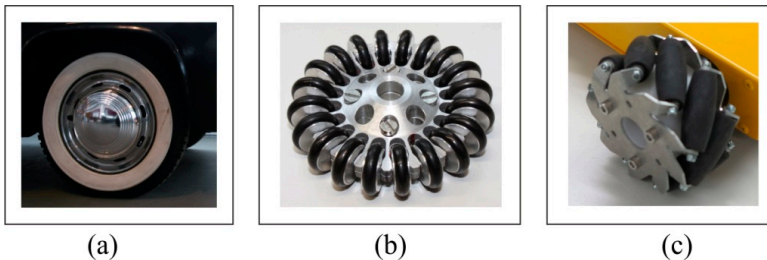
Figure 1.4 Different kinds of wheel designs used in mechanical applications, (a) classical wheel, (b) classical omnidirectional wheel, (c) Mecanum wheel

In a detailed survey ADASCALITE and DOROFTEI [4] discussed the most important applications of the Mecanum wheels in the field of mobility and industry. They presented the most common configurations of a Mecanum-wheeled vehicle as well as advantages and disadvantages and suggested solutions for overcoming negatives in performance. Also, they compared the Mecanum wheel with the standard wheel in order to show how the former is important for the next generation of locomotion systems, especially in fields such as military, health care, logistics and transportation. Different structures for the Mecanum wheel have been included from

different scientific resources. The designs discussed help in solving the problem of lost kinetic energy during wheel rotation and facilitating the motion of the locomotion system on different types of terrain.

DIEGEL, BADVE, BRIGHT, POTGIETER and TLALE suggested in [26] different designs for Mecanum wheel or for a nonholonomic mobile platform. Through the designs presented in the article, a series of problem associated with the Mecanum wheel has almost been solved, especially the problem of losing kinetic energy due to slippage of the rotating rollers on the surface. To concentrate the driving force on the contact area between the exterior roller and the contact area, they presented a new design for the Mecanum wheel under the title "Mecanum wheel with lockable rollers", the free rollers of the wheel are locked using an additional brake disc, which is rotated to the lock position using a small actuator; this actuator can be mechanically or electrically actuated as shown on the left side of Figure 1.5. This design prevents some of the bleeding of driving energy while the vehicle moves in the longitudinal direction but does not solve that problem during motion in the other directions.

A second mechanical design for the Mecanum wheel as previously mentioned is the "Mecanum wheel with rotatable rollers". This design is effective in retaining some of the driving energy normally lost but complicates design and control. The idea behind this design is that the rollers are fixed on a rotatable axis, which can rotate from -45 degree to 135 degree as illustrated on the right side of Figure 1.5-right. The position of the roller changes according to the direction of motion. During diagonal motion, the inclination angle of the rollers is the same in order to increase travelling speed in the desired direction. As an adaptation to the mobile platform suitable for all terrains, it was suggested in the article to combine the conventional wheel with the Mecanum wheel in one set. Both wheels are mounted in one unit. This entire assembly is rotatable on a pivot and driven by same electric motor. The vehicle will automatically detect the change in terrain and respond by changing which set of driving wheels is in contact with the surface. The Mecanum wheels are for indoors and high-maneuverability requirements and the conventional wheels are for outdoors and rough terrain, see Figure 1.6.
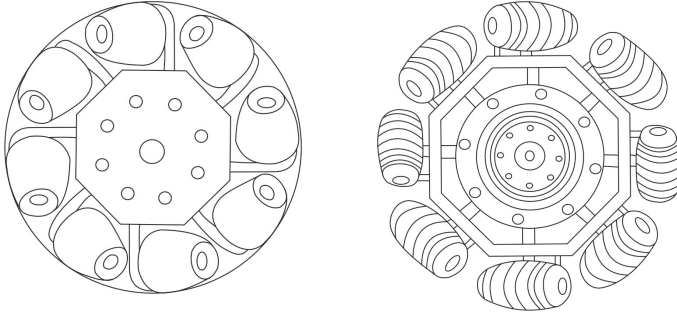
Figure 1.5 Mecanum wheel with lockable rollers (left) and rotatable rollers (right) [26]
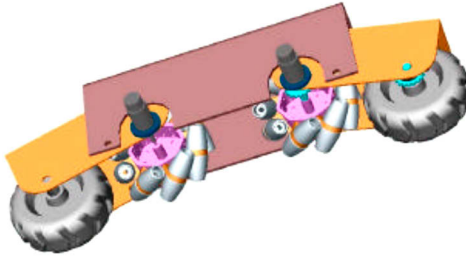
Figure 1.6 Combined vehicle with Mecanum and conventional wheels [26]

As a new contribution to solving the poor performance of the Mecanum wheel on rough terrain, RAMIREZ-SERRANO and KUZYK suggested a new design for the Mecanum wheel in their article [99]. From Ar² S-Lab, Calgary, Canada comes one of the most important improvements on the design of the Mecanum wheel in suggesting the Mecanum double-wheel design. This kind of wheel can overcome obstacles of up to 75% of its diameter through lateral motion. The assembled elliptical Mecanum double wheel is constructed from two elliptically shaped Mecanum wheels, which are connected together using a special mechanism. The elliptical wheel has two different types of rollers. The types and the number of the rollers are selected to construct the elliptical shape of the single wheel. Each wheel in the design rotates at its own speed. The distance between the two parts of the design expands and contracts as the wheels rotate. This leads to a changing attitude of the wheels; the wheel goes up and down during the motion to step over the obstacles, as shown in Figure 1.7. However, there

are still a lot of disadvantages for such a design, such as complexity, cost, reliability and size.

Ar² S-Lab's team discussed in [99] a different design for the Mecanum wheels, which they the "semicircular Mecanum double wheel". It is simply a wheel having a half-circular and half-elliptical profile. Two wheels with this profile are mounted together on one pivot but with a 180° offset side-to-side. This wheel can overstep obstacles up to 37.5% of the wheel radius. This type of Mecanum wheel consists of three different types of rollers to form the combined shape of the half-circle and half-ellipse as shown in Figure 1.8. The disadvantages of this wheel can be summarized in the cost and the additional number of parts required. Still the previously mentioned designs are still in the conceptual profile stage and still need practical experiments to prove their reliability and durability with respect to different types of terrain.

DE VILLIERS and BRIGHT presented in [24] a test platform to test the motion of a single Mecanum wheel at different rotation speeds and with different roller inclination angles. They proved experimentally that the theoretical results do not match practical measurements of their test platform. A detailed kinematic analysis for the Mecanum wheel and a vehicle with four Mecanum wheels is also presented.
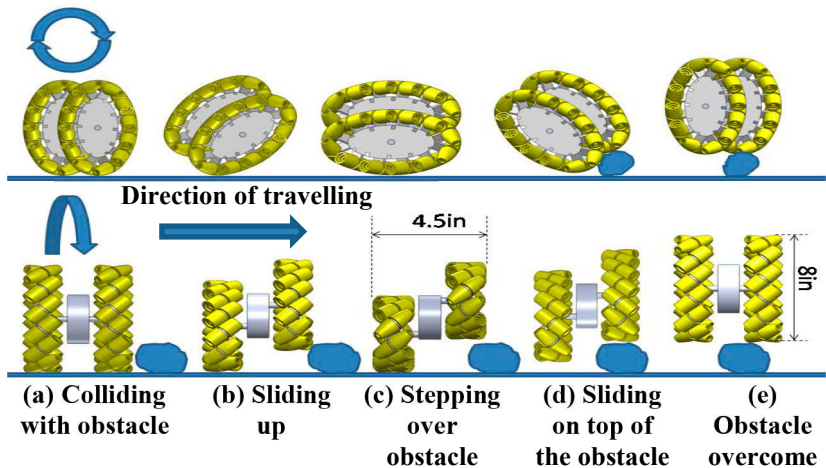
Figure 1.7 The elliptical Mecanum double wheel moving sideways [99]
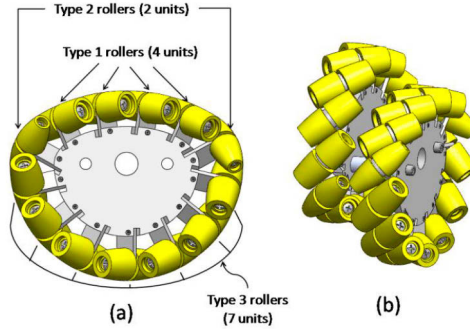
Figure 1.8 (a) Side view of the semicircular Mecanum double wheel, (b) final assembly of the semicircular Mecanum double wheel [99]

1.3   State of the art in the mechanics and control of nonholonomic systems

NOETHER and his son derived their theories about finding conserved quantities from symmetries, infinite-dimensional LIE algebras and differential equations and finitely generated algebra over a field. The principle of the least action, which is NOETHER's first theorem, states that the action of a physical system is the integration over time of a Lagrangian function, this physical system, state and phenomena may or may not be integrable over the space of the Lagranigain density function. NOETHER theories are the fundamentals of LAGRANGE's and HAMILTON's theories of mechanics, which were developed in 1788 and 1833, respectively. In 1949, HAMEL [36] discussed the famous example of a specific nonholonomic system: "the ice skate with two axles and two rigid wheels and they are affected by lateral friction"; nonholonomic mechanics are very important for those who are working in the field of dynamics of autonomous vehicles, especially if such autonomous vehicles are combined with robot's applications.

In 1967 NEIMARK and FUFAEV [94] presented their classical work "Dynamics of Non-holonomic Systems", which was translated into English in 1972 and until now this masterpiece of NIEMARK and FUFAEV is the fundamental base for new concepts and methods concerning analyzing the mechanics of nonholonomic systems and vehicle dynamics. At the same

time KANE [60] published his fundamental work "Dynamics of nonholonomic systems" for the first time in 1961.

Non-holonomic systems have been discussed in many articles and text books. In 1997, SCHIEHLEN [108] discussed most of the literature representing real scientific trials to solve the problem of nonholonomic systems from the mechanics point of view and as an application of control theories. BATES and SNIATYCKI [12] discussed the reduction of the mathematical model of the system's state space, which they called the reduced minimal state space of the nonholonomic system. Analysis of the dynamic behavior of the nonholonomic system from the geometrical point of view was discussed by ESSEN [31]. Based on Gauss's principle, KALABA and UDWADIA [58] presented the dynamics of a nonholonomic system in the form of mathematical equations and a mathematical model. Initially, they considered the dynamics of the nonholonomic system as a vibration problem and LIANG and LI-FU [70] estimated the dynamic behavior based on that assumption.

Subsequently in 1991 and 1993, LUO [72] and YU, ZHANG and XU [160] discussed the advantages of NEOTHER's theories and suggested a theoretical approach for solving the systems based on NEOTHER's theory. Studying variable-mass nonholonomic system behavior based on ROUTH's criteria was done by LUO and ZHAO [73]. MLADENOVA [85] discussed the kinematics and dynamics of a rigid body with nonholonomic constraints. The impulsive motion of multibody dynamic system with nonholonomic constraint was studied by RISMANTAB-SANY [102] and by SHABANA [103]; they suggested a numerical solution for the differential equations of that system. SCHIEHLEN [107] discussed a nonholonomic mobile robot, both from dynamics and control points of view.

Any multibody dynamic system, usually referred to as a plant, attempts to react to an external force or torque and usually needs to be controlled. The science of mechatronics deals with modeling and controlling all types of multibody systems. A lot of researchers have discussed the topic of vehicle dynamics and the modeling of the dynamics of multibody systems, such as POPP and SCHIEHLEN [98], SEGEL [112], STADLER [123] and VUKOBRATOVIC and STOKIC [139]. A general overview for the control of mechanical systems was presented by SCHWEITZER and MANSOUR [111]. Elastic multibody systems and control was discussed by PFEIFFER and GEBLER [96]. MODI and SULIMAN [86] suggested a new approach

for controlling the motion of flexible structures based on modeling their dynamics. Presenting a progress report regarding the modeling and control of actively controlled multibody systems was given by HAUG [42]. It is important to distinguish between a simple dynamic or kinematic model for aspects of control design and a complex dynamic and kinematic model for validating control laws according to SCHIEHLEN [108].

This kind of considerations for nonholonomic systems was presented by a large group of mathematicians in different fundamental literature sources, such as BULLO and LEWIS [15], MARSDEN and SCHEURLE [57, 56], MURRAY, LI, SASTRY [91] and others. JARZEBOWSKA discussed the relation between mechanics and control theories in [55] and [54]. There is a contribution from a polish mechanics school for modeling these mechanical systems and solution of the equation of motion from GUTOWSKI [35] und ARCZEWSKI [9]. WANG and XU [155] discussed the internal dynamics of nonholonomic wheeled mobile robots. More examples of the nonholonomic systems are presented in [77], [168] and [78] by MARTYNENKO, FORMALSKII and others.

Finally, HILLER in [45], [46] and [47] briefly discussed aspects of mechatronics and as well as primary aspects for controlling and simulating the behavior of a multibody dynamic system, such as modeling, control design and simulation. These fields have affected each other and no single one can be ignored when discussing or implementing a model for a multibody system.

1.4 Thesis motivation, formulation of the problems and structured plan

The survey about the state of the art showed that the development of a mobility system for the disabled, the injured and the elderly is a complex task. This author defined a target for this thesis, which is to write a contribution to discuss the enhancements of these systems from a mechanics point of view. Therefore, this thesis will focus on studying the basic mechanical element of any locomotion system: the wheel. Different layouts and topologies of the wheel in the locomotion systems will be considered. A new solution for mechanical analysis of this nonholonomic system will be introduced using Mecanum wheels.

Because the efficiency of the motion assistance system, whether the form is that of a wheelchair, walking suit or electric vehicle, mostly depends on the interaction and interface between the locomotion system and the user. Therefore, it also is important to study the biomechanical aspects of the user during motion. Based on the basic assumptions previously mentioned, the thesis will discuss the following points:

1. Exact description of the kinematics and dynamics of Mecanum wheels and Mecanum-wheel-based locomotion systems and a comparison to already existing, dominant driving and control solutions

2. Comparison and evaluation of wheelchair driving strategies for both trained and untrained users, of biomechanical parameters such as body joint angles and and body part position using motion-capture methods and the dynamic simulation of these multibody systems

3. Development of new practical concepts for driving the mobility system and comparison with the theoretical results

The tasks given for the thesis are presented in 5 chapters. Figure 1.9 gives an overview of the contents and the tasks dealt with.
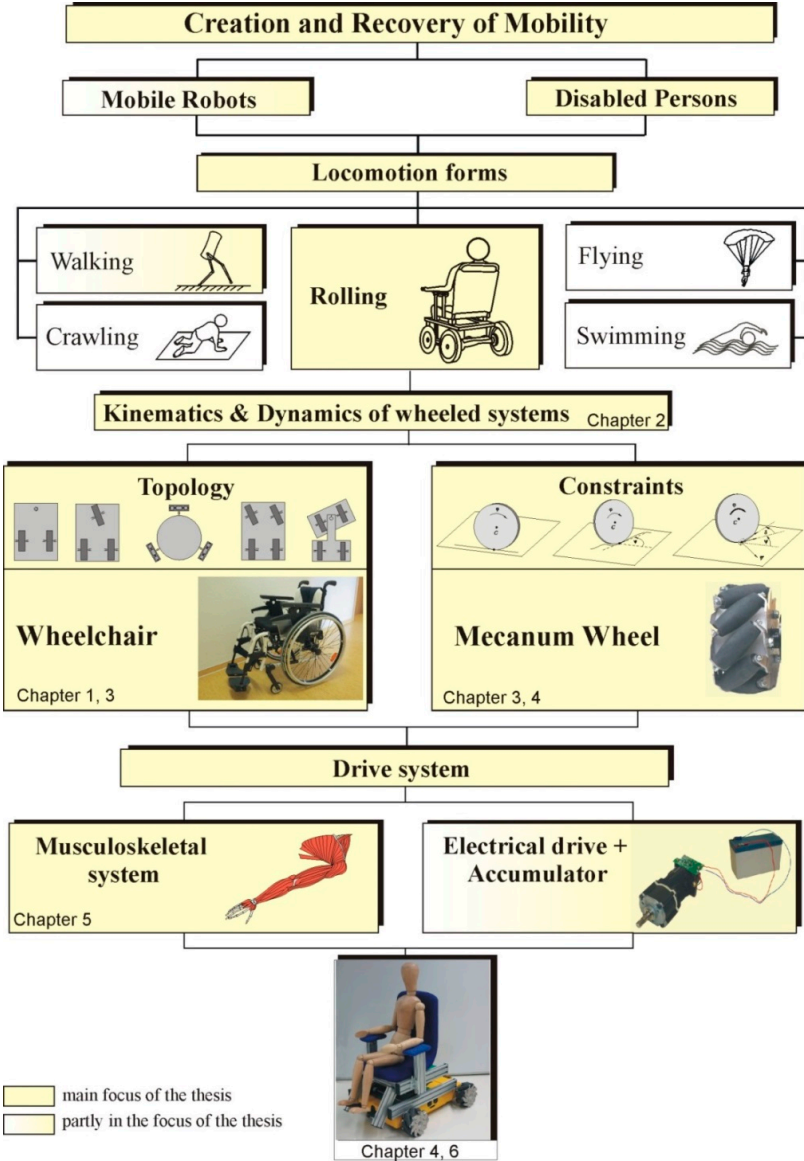
Figure 1.9 Content and structure of the thesis

The methods that I explain in it require neither constructions nor geometrical or mechanical arguments, but only the algebraic operations inherent to a regular and uniform process. Those who love Analysis will, with joy, see mechanics become a new branch of it and will be grateful to me for thus having extended its field.

(J.L. LAGRANGE)

2 <u>Theoretical background – mathematical and mechanical basics</u>

2.1 <u>Definition of the system and the model</u>

According to HILLER [45], the mechanical system is defined as "a group of elements (bodies and joints), which act on each other (interaction), on this interaction affects external influences (inputs) and produce as result to these external influences an action (output)".
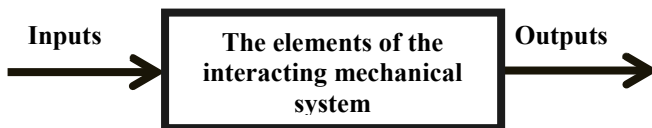
Figure 2.1 Symbolic representation of a system definition according to Hiller [45]

The objectives behind studying the system dynamics include:

- Building a mathematical model for the mechanical system
- Studying system stability

- Selection of the inputs to be controlled
- Simulation of system performance.
- Building a mathematical model for the mechanical system

The mathematical model is a set of mathematical relationships to describe the behavior of the system. These mathematical relationships are mostly a set of differential equations for either translational or rotational motion in case of rigid body.

The mathematical model cannot fully represent the actual mechanical system because it only presents the ideal, abstracted performance of the system – i.e. the differential equations describing the motion of the vehicle – and do not take slip into consideration. Hence anytime slip occurs, these equations will no longer describe the performance of the vehicle accurately.

Also, the equations of motion must be made more complicated in order to increase the applicability of the mathematical model to the actual system. For example, the vehicle could be modeled as five rigid bodies connected to each other (body and four wheels) or it could be modeled as multibody dynamic system with a higher number of elements or bodies, such as the frame, doors, wheels, motor and driveline parts in addition to the joints connecting the rigid bodies of the vehicle.

- Studying system stability

In this section, this researcher is interested in understanding the characteristics of the mechanical system and finding a solution for the estimated or calculated equations of motion for the system under investigation. More simply, this will be achieved by uncovering the behavior of the system under different operating conditions. Several methods of approximation are available and stability examination methods are used to study the behavior of the system by finding a solution to the mathematical differential equations of the system. All the available numerical methods for investigating the solutions for the differential equations mostly depend on linearizing the second-order differential equations. Some numerical software can linearize the second-order differential equations without input from the user.

- Selection of the controlled input

The inputs for the mechanical system (multibody dynamic system) have to be controlled and regulated to attain the required system behavior. As part of this requirement, it will be suitable to add an objective to the researcher's list of duties: studying the possibility of implementing a controller within the investigated system in order to enhance the behavior of the system. For example the mechanical parts of the investigated system have to be actuated by an exact method, which can help achieve the main objective of the mechanical system. Here, finding a suitable actuation method and direction are important demands on the research.

- Simulation of system performance

Nowadays, there are a lot of simulation packages for simulating the kinematics and dynamics of the multibody dynamic systems such as ADAMS®, DADS®, SIMPACK®, ALASKA® and similar software. The kinematic and dynamic behavior resulting from these software packages mostly depends on the exactness of the system model. Either by modeling the system as a set of differential equations or building the system completely from discrete mechanical components such as massless bodies or those with mass, connection joints (different types such as prismatic, rotational etc.) and defining the moving surfaces with different friction characteristics. A secondary requirement is the evaluation stage. Here, the task is to decide the strengths and weaknesses of the model and the real system, depending on the simulation results. It is also necessary to evaluate how the suggested inputs for the system will assist in attaining the optimal behavior for the system. Examination the system model has to be carried out for a wide range of different inputs and under different actuation conditions.

The most important model for the configurations used in kinematic theories is the multibody system. A multibody system (MBS) is a finite set of rigid bodies that are physically and/or geometrically interconnected with each other and with a ground base not belonging to the MBS. Physical coupling is specified by the applied forces and torques (e.g. spring and damper forces). The constraints describe the geometric interconnections (e.g. prismatic and rotational joints).
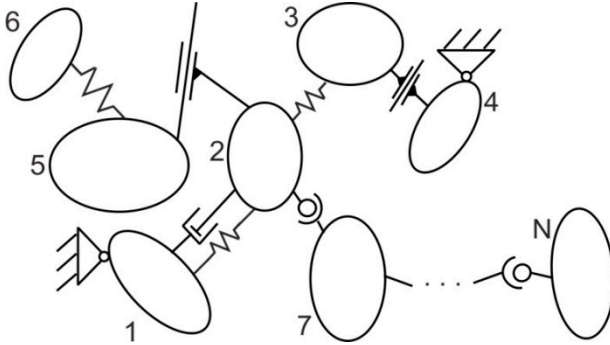
Figure 2.2 Example of a multibody system

     Classification of MBSs based on topology (i.e. based on the alignment of the bodies) in connection with the context here indicates that the constraints of the mechanical system (as in the case of closed kinematic chains) play an important role. This is because of the permanent contact with the ground. Additionally, one of the problems in modeling the mechanical systems is how to describe the contact between the bodies and the ground in a realistic way, Figure 2.3.
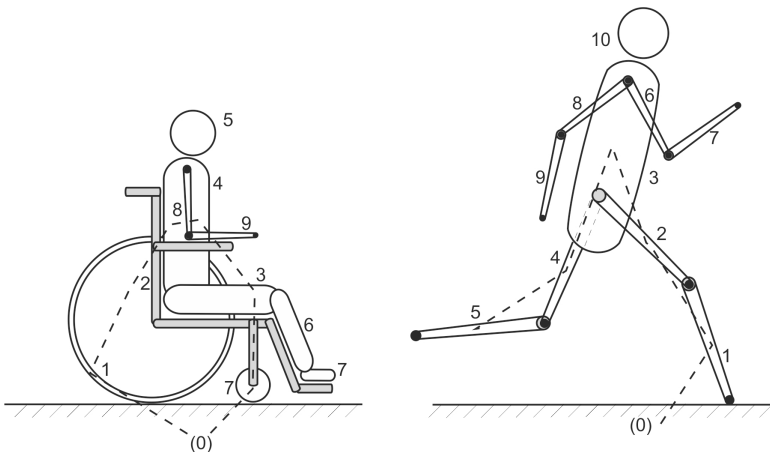
Figure 2.3 Topologies for MBSs: open kinematic chain (right) and closed kinematic chain (left)

2.2   Kinematics and dynamics of an MBS

2.2.1   Basic kinematics of an MBS

Studying the kinematics of MBSs is a very important requirement for understanding and representing the dynamics of the MBS. The formulation of the position, velocity and acceleration vectors of any MBS, relative to the global coordinate system, is required for applying momentum and angular momentum theories. Here, it is important to mention that momentum and angular momentum theories are combined with the cutting principle in studying the dynamics of the MBS. Thus, the compact form of the position, velocity and acceleration vectors will be presented and discussed.

The following chapter presents a formulation of the MBS's differential equations of motion using methods of analytical mechanics such as the LAGRANGE equation, the APPELL equation and others using the previous theories. The results of the kinematics described in this chapter are output points for the scalar values from the process of simulating the dynamic model, such as the kinetic energy T or the APPELL function S. Using this method the formulation of dynamics of the MBS does not depend on the coordinate system used because the model is based on scalar functions. Both the global (inertial) coordinate system S and the local (body-fixed) coordinate system S' can be used in the formulation of the kinetic energy or APPELL function. The formulation of the aforementioned quantities as a function in the local (body-fixed) coordinate system is widely found in the application of vehicle mechanics. For that, this formulation will be discussed in section 2.2.2.

Figure 2.4 shows a rigid body with a fixed-body coordinate system S' and a fixed point Ω. Point C is the center of gravity.
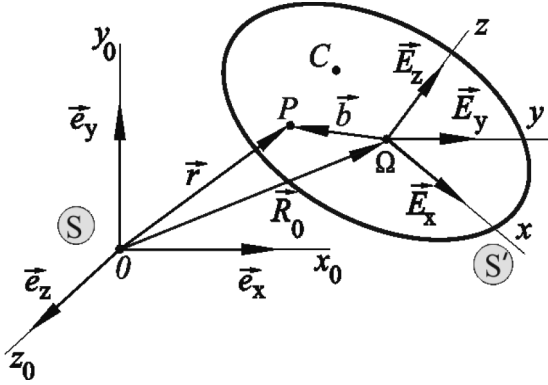
Figure 2.4 Kinematics of a rigid body

The position of the rigid body relative to the global (inertial) coordinate system can be described using the position vectors $\vec{r}(P)$ from the origin 0 of the system S to point P on the rigid body.

$$\overrightarrow{OP} = \overrightarrow{O\Omega} + \overrightarrow{\Omega P} \,,$$
$$\vec{r}(P) = \vec{R}_0 + \vec{b} \,. \tag{2.1}$$

Equation (2.1) is valid for any selected fixed point Ω on the rigid body and it does not matter whether that point is the center of gravity C of the rigid body or not. Using the unit vectors $\vec{e}_x$, $\vec{e}_y$, $\vec{e}_z$ of the global coordinate system S and the unit vectors $\vec{E}_x$, $\vec{E}_y$, $\vec{E}_z$ of the body-fixed coordinate system S', equation (2.1) can be written as

$$\vec{r}(P) = x_0\vec{e}_x + y_0\vec{e}_y + z_0\vec{e}_z + x\vec{E}_x + y\vec{E}_y + z\vec{E}_z \,, \tag{2.2}$$

where the vector components x, y and z are constant from the characteristics of the rigid body. In the case that $\Omega = C$, then the dyxycoordinates x_0, y_0, z_0 are the coordinates x_C, y_C, z_C of the rigid body's center of gravity relative to the global coordinate system S.

$$x_C = \frac{\displaystyle\int_{(V)} x \, dm}{\displaystyle\int_{(V)} dm} \quad , \quad y_C = \frac{\displaystyle\int_{(V)} y \, dm}{\displaystyle\int_{(V)} dm} \quad , \quad z_C = \frac{\displaystyle\int_{(V)} z \, dm}{\displaystyle\int_{(V)} dm} \qquad (2.3)$$

The motion of the rigid body can be described by the equations:

$$\vec{R}_0 = \vec{R}_0(t) , \qquad \vec{E}_x = \vec{E}_x(t) , \qquad \vec{E}_y = \vec{E}_y(t) , \qquad \vec{E}_z = \vec{E}_z(t) . \qquad (2.4)$$

Function $\vec{R}_0(t)$ describes the translational motion of the rigid body and the unit vectors $\vec{E}_x(t)$, $\vec{E}_y(t)$, $\vec{E}_z(t)$ represent the rotational motion of the rigid body. Inserting equation (2.4) into equation (2.2) and differentiating the resultant equation with respect to time gives the velocity vector of point P on the rigid body as follows

$$\dot{\vec{r}}(P) = \dot{\vec{R}}_0 + \dot{\vec{b}} = \dot{\vec{R}}_0 + x\dot{\vec{E}}_x + y\dot{\vec{E}}_y + z\dot{\vec{E}}_z . \qquad (2.5)$$

The unit vectors $\vec{E}_x$, $\vec{E}_y$ and $\vec{E}_z$ and their time derivatives can be determined using the rotation matrix $\mathbb{E}$ and the angular velocity $\vec{\omega}$ of the rigid body. For transforming the body-fixed (local) S' coordinate components into the global coordinate system S, the following mathematical expression is used

$$\begin{pmatrix} \vec{E}_x \\ \vec{E}_y \\ \vec{E}_z \end{pmatrix} = \mathbb{E} \cdot \begin{pmatrix} \vec{e}_x \\ \vec{e}_y \\ \vec{e}_z \end{pmatrix} , \qquad \bar{E} = \mathbb{E} \cdot \bar{e} \qquad (2.6)$$

where

$$\mathbb{E} = \begin{pmatrix} E_{xx} & E_{xy} & E_{xz} \\ E_{yx} & E_{yy} & E_{yz} \\ E_{zx} & E_{zy} & E_{zz} \end{pmatrix} . \qquad (2.7)$$

Matrix $\mathbb{E}$ is an orthonormal matrix, meaning $\mathbb{E}^{-1} = \mathbb{E}^T$, and it describes the rotation of the body-fixed S' coordinate system relative to the global coordinate system S. The elements of the rotation matrix $\mathbb{E}$ are functions of three time-variant parameters such as EULER angles, BRYANT angles etc. From equations (2.5), (2.6) and (2.7), the time derivatives of the body-fixed unit vectors $\dot{\vec{E}}_x$, $\dot{\vec{E}}_y$, $\dot{\vec{E}}_z$ can be written in the following form

$$\dot{\vec{E}}_x = \dot{E}_{xx}\vec{e}_x + \dot{E}_{xy}\vec{e}_y + \dot{E}_{xz}\vec{e}_z$$
$$\dot{\vec{E}}_y = \dot{E}_{yx}\vec{e}_x + \dot{E}_{yy}\vec{e}_y + \dot{E}_{yz}\vec{e}_z \ , \qquad\qquad \dot{\vec{E}} = \dot{\mathbb{E}} \cdot \bar{e} \ . \quad (2.8)$$
$$\dot{\vec{E}}_z = \dot{E}_{zx}\vec{e}_x + \dot{E}_{zy}\vec{e}_y + \dot{E}_{zz}\vec{e}_z$$

Similarly, by using the matrix $\mathbb{E}^{-1}$ from the inverse transformation $\bar{e} = \mathbb{E}^{-1}\bar{E}$ it follows

$$\dot{\vec{E}} = \dot{\mathbb{E}} \cdot \bar{e} = \dot{\mathbb{E}} \cdot \mathbb{E}^{-1}\bar{E} = \dot{\mathbb{E}} \cdot \mathbb{E}^T\bar{E} \ . \tag{2.9}$$

From the skew-symmetric matrix $\bar{\bar{\omega}} = \dot{\mathbb{E}} \cdot \mathbb{E}^T$, the elements of the angular velocity vector are

$$\vec{\omega} = \omega_x\vec{E}_x + \omega_y\vec{E}_y + \omega_z\vec{E}_z \tag{2.10}$$

with

$$\omega_x = \dot{E}_{yx}E_{zx} + \dot{E}_{yy}E_{zy} + \dot{E}_{yz}E_{zz}$$
$$\omega_y = \dot{E}_{zx}E_{xx} + \dot{E}_{zy}E_{xy} + \dot{E}_{zz}E_{xz} \tag{2.11}$$
$$\omega_z = \dot{E}_{xx}E_{yx} + \dot{E}_{xy}E_{yy} + \dot{E}_{xz}E_{yz} \ .$$

Then equation (2.8) can be rewritten as a function of the angular velocity vector $\vec{\omega}$ as follows

$$\dot{\vec{E}}_x = \vec{\omega} \times \vec{E}_x \ , \qquad\qquad \dot{\vec{E}}_y = \vec{\omega} \times \vec{E}_y \ , \qquad\qquad \dot{\vec{E}}_z = \vec{\omega} \times \vec{E}_z \ . \tag{2.12}$$

Accordingly, the velocity of the rigid body will be EULER's equation

$$\dot{\vec{r}} = \dot{\vec{R}}_0 + \vec{\omega} \times \vec{b}.$$ (2.13)

The vector $\dot{\vec{R}}_0$ represents the translation velocity for any point on the rigid body and the term $\vec{\omega} \times \vec{b}$ stands for the specific rotational velocity of each point of the rigid body. The instantaneous rotation axis of the rigid body is defined by point Ω and angular velocity vector $\vec{\omega}$. Through time differentiation of the EULER form in equation (2.13), the acceleration vector of any point on the rigid body $\ddot{\vec{r}}(P)$ can be calculated from the following relation

$$\ddot{\vec{r}} = \ddot{\vec{R}}_0 + \vec{\omega} \times (\vec{\omega} \times \vec{b}) + \dot{\vec{\omega}} \times \vec{b}.$$ (2.14)

Example (1)

In context of discussions of the rotating wheel concepts at the motion level, it is important to estimate the velocity and acceleration vectors for the wheel's center point, i.e. mass center point or center of gravity and also for a peripheral point P, see Figure 2.5.
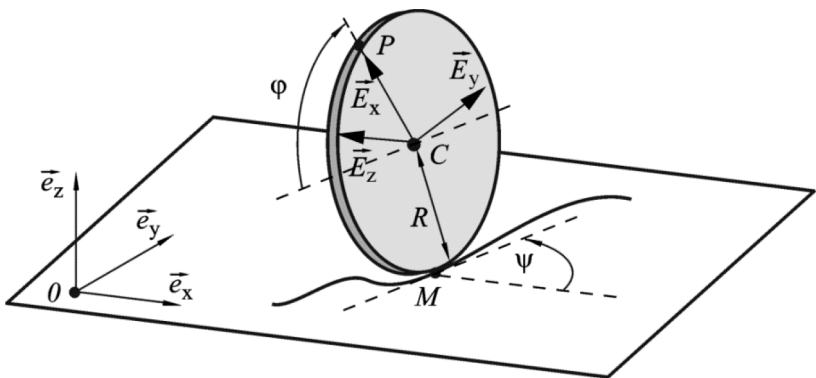
Figure 2.5 Rolling wheel

Considering that the contact point is the instantaneous center of rotation M, the wheel's motion is pure rotation without slippage. The velocity vector for the center of mass of the rotating wheel is

$$\dot{\vec{r}}_C = \dot{\vec{r}}_M + \vec{\omega} \times \overrightarrow{MC} \;. \tag{2.15}$$

Since M is the instantaneous center of rotation (i.e., $\dot{\vec{r}}_M = \vec{0}$) equation (2.15) can be rewritten as follows

$$\dot{\vec{r}}_C = \vec{\omega} \times \overrightarrow{MC} = \left(\dot{\psi}\, \vec{e}_z + \dot{\varphi}\, \vec{E}_z \right) \times (R\, \vec{e}_z) = \dot{\varphi}\, R \left(\vec{E}_z \times \vec{e}_z \right)$$
$$\vec{E}_z = -\sin\psi\; \vec{e}_x + \cos\psi\; \vec{e}_y$$
$$\dot{\vec{r}}_C = \dot{\varphi}\, R \left(-\sin\psi\; \vec{e}_x + \cos\psi\; \vec{e}_y \right) \times \vec{e}_z$$
$$= \dot{\varphi}\, R \left(-\sin\psi\, (-\vec{e}_y) + \cos\psi\; \vec{e}_x \right)$$
$$\dot{\vec{r}}_C = \dot{\varphi}\, R\; \cos\psi\; \vec{e}_x + \dot{\varphi}\, R\; \sin\psi\, \vec{e}_y \;.$$

From

$$\dot{\vec{r}}_C = \dot{x}_C\, \vec{e}_x + \dot{y}_C\, \vec{e}_y + \dot{z}_C\, \vec{e}_z$$

it follows that

$$\begin{aligned}
\dot{x}_C &= \dot{\varphi}\, R\; \cos\psi \\
\dot{y}_C &= \dot{\varphi}\, R\; \sin\psi \\
\dot{z}_C &= 0 \;.
\end{aligned} \tag{2.16}$$

By applying a similar sequence to find the vector $\dot{\vec{r}}_P$, the next sequence of equations can be determined as

$$\dot{\vec{r}}_P = \dot{\vec{r}}_M + \vec{\omega} \times \overrightarrow{MP} = \vec{\omega} \times \overrightarrow{MP} \;.$$

Using the previously known velocity of point C, it is also possible to find that

$$\dot{\vec{r}}_P = \dot{\vec{r}}_C + \vec{\omega} \times \overrightarrow{CP} \;.$$

Then

$$\dot{\vec{r}}_P = \dot{\varphi}\, R\; \cos\psi\, \vec{e}_x + \dot{\varphi}\, R\; \sin\psi\, \vec{e}_y + \left(\dot{\psi}\, \vec{e}_z + \dot{\varphi}\, \vec{E}_z \right) \times (R\, \vec{E}_x)$$

and with

$$\vec{E}_x = -\cos\varphi \cos\psi\, \vec{e}_x - \cos\varphi \sin\psi\, \vec{e}_y + \sin\varphi\, \vec{e}_z$$

it follows

$$\dot{\vec{r}}_P = \dot{\varphi}\, R\, \cos\psi\, \vec{e}_x + \dot{\varphi}\, R\, \sin\psi\, \vec{e}_y + \big(\dot{\psi}\, \vec{e}_z + \dot{\varphi}(-\sin\psi\, \vec{e}_x + \cos\psi\, \vec{e}_y)\big) \\ \times \Big(R\big(-\cos\varphi\cos\psi\, \vec{e}_x - \cos\varphi\sin\psi\, \vec{e}_y + \sin\varphi\, \vec{e}_z\big)\Big)$$

then

$$\dot{x}_P = R\big(\dot{\varphi}\cos\psi + \dot{\psi}\cos\varphi\sin\psi + \dot{\varphi}\sin\varphi\cos\psi\big)$$
$$\dot{y}_P = R\big(\dot{\varphi}\sin\psi + \dot{\varphi}\sin\psi\sin\varphi - \dot{\psi}\cos\psi\cos\varphi\big) \qquad (2.17)$$
$$\dot{z}_P = \dot{\varphi}R\cos\varphi\,.$$

Vectors $\ddot{\vec{r}}_C$ and $\ddot{\vec{r}}_P$ can be estimated from equation (2.14) and (2.17). But in practical applications, they are usually calculated from the time derivatives of equations (2.14) and (2.17). This yields the following equations

$$\ddot{x}_C = \ddot{\varphi}\, R\, \cos\psi - \dot{\varphi}\, R\, \dot{\psi}\, \sin\psi = R\big(\ddot{\varphi}\, \cos\psi - \dot{\varphi}\dot{\psi}\sin\psi\,\big)$$
$$\ddot{y}_C = \ddot{\varphi}\, R\, \sin\psi + \dot{\varphi}\, R\, \dot{\psi}\cos\psi = R\big(\ddot{\varphi}\sin\psi + \dot{\varphi}\,\dot{\psi}\cos\psi\big) \qquad (2.18)$$
$$\ddot{z}_C = 0$$

and

$$\ddot{x}_P = R\big[\,\ddot{\varphi}\,(\cos\psi + \sin\varphi\cos\psi) + \ddot{\psi}\cos\varphi\sin\psi$$
$$\qquad - \dot{\varphi}\dot{\psi}(\sin\psi + 2\sin\varphi\sin\psi) + \cos\varphi\cos\psi\,(\dot{\psi}^2 + \dot{\varphi}^2)\big]\,,$$
$$\ddot{y}_P = R\big[\,\ddot{\varphi}\,(\sin\psi + \sin\varphi\sin\psi) - \ddot{\psi}\cos\varphi\cos\psi \qquad (2.19)$$
$$\qquad + \dot{\varphi}\dot{\psi}(\cos\psi + 2\sin\varphi\cos\psi) + \cos\varphi\sin\psi\,(\dot{\psi}^2 + \dot{\varphi}^2)\big]\,,$$
$$\ddot{z}_P = R\big[\ddot{\varphi}\cos\varphi - \dot{\varphi}^2\sin\varphi\big]\,.$$

To describe the kinematics of a multibody system, recursive enhancements have been applied to the previously mentioned forms of the rigid bodies. Using the EULER form, it is possible to describe also the kinematics of a MBS.
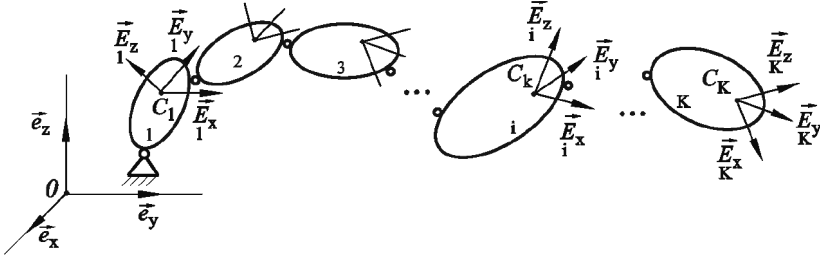
Figure 2.6 Multibody system with body-fixed coordinate systems and the generalized coordinate system

The new aspect in MBSs is that there now exists **absolute** rotation matrices $\underset{i,0}{\mathbb{E}}$, which are used to transform the unit vectors of the ith body-fixed (local) coordinate system into the absolute (global) coordinate system

$$\bar{E}_i = \underset{i,0}{\mathbb{E}} \cdot \bar{e} \qquad (2.20)$$

and **relative** rotation matrices $\underset{i,i-1}{\mathbb{E}}$, which describe the relationship between two in-sequence body-fixed coordinate system, i.e. successive coordinates for successive bodies in the same system, as follows

$$\bar{E}_i = \underset{i,i-1}{\mathbb{E}} \cdot \bar{E}_{i-1} . \qquad (2.21)$$

Then, the following relation is valid

$$\overrightarrow{OP_i} = \vec{r}_i = \vec{R}_i + \vec{b}_i = \vec{R}_i + x\vec{E}_{ix} + y\vec{E}_{iy} + z\vec{E}_{iz} \qquad (2.22)$$

where

$$
\begin{aligned}
\vec{E}_{ix} &= \underset{i,0}{E}_{xx}\,\vec{e}_x + \underset{i,0}{E}_{xy}\,\vec{e}_y + \underset{i,0}{E}_{xz}\,\vec{e}_z \\
\vec{E}_{iy} &= \underset{i,0}{E}_{yx}\,\vec{e}_x + \underset{i,0}{E}_{yy}\,\vec{e}_y + \underset{i,0}{E}_{yz}\,\vec{e}_z \\
\vec{E}_{iz} &= \underset{i,0}{E}_{zx}\,\vec{e}_x + \underset{i,0}{E}_{zy}\,\vec{e}_y + \underset{i,0}{E}_{zz}\,\vec{e}_z .
\end{aligned}
\qquad (2.23)
$$

According to equation (2.20), the velocity vector of point $\vec{P}_i$ on the rigid body with order i can be described according to

$$\dot{\vec{r}}_i = \dot{\vec{R}}_i + \underset{i,0}{\vec{\omega}} \times \vec{b}_i \ . \tag{2.24}$$

Due to the sophistication in this method for finding the angular velocity component $\underset{i,0}{\vec{\omega}}$, it will be calculated using the skew-symmetric matrix $\underset{i,0}{\bar{\bar{\omega}}}$ from the absolute rotation matrix $\underset{i,0}{\mathbb{E}}$ and its time derivative $\underset{i,0}{\dot{\mathbb{E}}}$ according to equation (2.11). A simplification of the last method can be made by applying the following form

$$\underset{i,0}{\vec{\omega}} = \underset{i,i-1}{\vec{\omega}} + \underset{i-1,0}{\vec{\omega}} \ . \tag{2.25}$$

This will especially be used in cases where a moving coordinate system can be obtained by a sequence of planar rotations.

Example (2)

The angular velocity $\underset{2,0}{\vec{\omega}}$ of the wheels in a vehicle equipped with two wheels is to be determined while it is moving on the plane as shown in Figure 2.7.
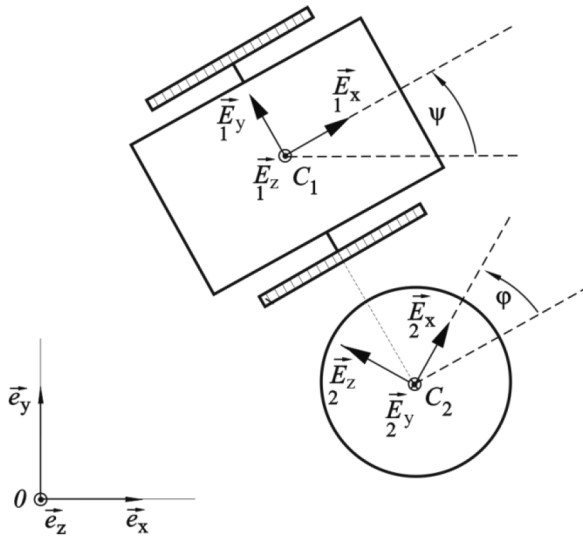
Figure 2.7 Two body-fixed coordinate systems in a two-wheeled vehicle

The solution

The first method

By using the rotation matrices and their time derivatives according to equation (2.11), the angular velocity $\vec{\omega}_{2,0}$ in this case can be obtained as follows:
The rotation matrix $\underset{2,0}{\mathbb{E}}$, and then its time derivative $\underset{2,0}{\dot{\mathbb{E}}}$ can be computed by the relation

$$\underset{2,0}{\mathbb{E}} = \underset{2,1}{\mathbb{E}} \cdot \underset{1,0}{\mathbb{E}}$$

where

$$\underset{2,1}{\mathbb{E}} = \begin{pmatrix} \cos\varphi & 0 & \sin\varphi \\ 0 & 1 & 0 \\ -\sin\varphi & 0 & \cos\varphi \end{pmatrix}, \qquad \underset{1,0}{\mathbb{E}} = \begin{pmatrix} \cos\psi & \sin\psi & 0 \\ -\sin\psi & \cos\psi & 0 \\ 0 & 0 & 1 \end{pmatrix}$$

Then, it follows from the multiplication of the matrices that

$$\underset{2,0}{\mathbb{E}} = \begin{pmatrix} \cos\varphi\cos\psi & \cos\varphi\sin\psi & \sin\varphi \\ -\sin\psi & \cos\psi & 0 \\ -\sin\varphi\cos\psi & -\sin\varphi\sin\psi & \cos\varphi \end{pmatrix}$$

And

$$\underset{2,0}{\dot{\mathbb{E}}} = \begin{pmatrix} -\dot\varphi\sin\varphi\cos\psi - \dot\psi\cos\varphi\sin\psi & -\dot\varphi\sin\varphi\sin\psi + \dot\psi\cos\varphi\cos\psi & \dot\varphi\cos\varphi \\ -\dot\psi\cos\psi & -\dot\psi\sin\psi & 0 \\ -\dot\varphi\cos\varphi\cos\psi + \dot\psi\sin\varphi\sin\psi & -\dot\varphi\cos\varphi\sin\psi - \dot\psi\sin\varphi\cos\psi & -\dot\varphi\sin\varphi \end{pmatrix}.$$

Finally, using equation (2.11)

$$\begin{aligned} \omega_x &= \dot{E}_{yx}E_{zx} + \dot{E}_{yy}E_{zy} + \dot{E}_{yz}E_{zz} = \dot\psi\,\sin\varphi \\ \omega_y &= \dot{E}_{zx}E_{xx} + \dot{E}_{zy}E_{xy} + \dot{E}_{zz}E_{xz} = \dot\varphi \\ \omega_z &= \dot{E}_{xx}E_{yx} + \dot{E}_{xy}E_{yy} + \dot{E}_{xz}E_{yz} = \dot\psi\,\cos\varphi \end{aligned} \qquad (2.26)$$

and

$$\vec{\omega}_{2,0} = \dot\psi\sin\varphi\,\vec{\underset{2}{E}}_x + \dot\varphi\,\vec{\underset{2}{E}}_y + \dot\psi\,\cos\varphi\,\vec{\underset{2}{E}}_z.$$

The second method uses equation (2.25).

Since

$$\vec{\omega}_{2,0} = \vec{\omega}_{2,1} + \vec{\omega}_{1,0} ,$$

where body (1) is the chassis of the vehicle. The body rotates in the motion plane (x-y) around the z-axis by angle ψ. Then, the angular velocity of body (1) can be found from $\vec{\omega}_{1,0} = \dot{\psi} \, \vec{E}_{1z}$. Wheel (2) rotates in motion plane (x-z) by angle φ around the y-axis relative to body (1); this means that $\vec{\omega}_{2,1} = \dot{\varphi} \, \vec{E}_{2y}$. Then, it follows that

$$\vec{\omega}_{2,0} = \dot{\varphi} \, \vec{E}_{2y} + \dot{\psi} \, \vec{E}_{1z} .$$

The equality of unity vectors $\vec{E}_{2y}$ and $\vec{E}_{1y}$ means that the representation of angular velocity $\vec{\omega}_{2,0}$ in the first system is

$$\vec{\omega}_{2,0} = \dot{\varphi} \, \vec{E}_{1y} + \dot{\psi} \, \vec{E}_{1z} .$$

Generally, the representation of the angular velocity of ith body is also written in the ith body-fixed coordinate system, i.e. using the following transformation

$$\vec{E}_{1,0} = \mathbb{E}_{1,2} \cdot \vec{E}_{2,0} ,$$

with

$$\mathbb{E}_{1,2} = \mathbb{E}_{2,1}^{-1} = \mathbb{E}_{2,1}^{T} = \begin{pmatrix} \cos\varphi & 0 & \sin\varphi \\ 0 & 1 & 0 \\ -\sin\varphi & 0 & \cos\varphi \end{pmatrix}^{T} = \begin{pmatrix} \cos\varphi & 0 & -\sin\varphi \\ 0 & 1 & 0 \\ \sin\varphi & 0 & \cos\varphi \end{pmatrix}$$

Then, the required angular velocity is

$$\begin{aligned} \vec{\omega}_{2,0} &= \dot{\varphi} \, \vec{E}_{2y} + \dot{\psi} \left(-\sin\varphi \, \vec{E}_{2x} + \cos\varphi \, \vec{E}_{2z} \right) \\ &= \dot{\psi} \, \sin\varphi \, \vec{E}_{2x} + \dot{\varphi} \, \vec{E}_{2y} + \dot{\psi} \, \cos\varphi \, \vec{E}_{2z} . \end{aligned}$$

As the elements of rotation matrix $\underset{i,0}{\mathbb{E}}$ also the position vector $\vec{R}_i$ of the free-moving rigid body in general depends on three parameters (i.e. cylinder coordinates, spherical coordinates). For each free i^{th} rigid body, the following form is valid

$$\dot{\vec{R}}_i = \dot{\vec{R}}_i \left(\underset{i}{y_1}, \underset{i}{y_2}, \underset{i}{y_3} \right) \quad , \quad \underset{i,0}{\mathbb{E}} = \underset{i,0}{\mathbb{E}} \left(\underset{i}{y_4}, \underset{i}{y_5}, \underset{i}{y_6} \right).$$

For any multibody system, the components $(\underset{i}{y_1}, \underset{i}{y_2}, \dots, \underset{i}{y_6})$ for (i=1,2,…,K) cannot be freely selected. These kinematic constraints will be discussed later in brief. In the following section, the specific vehicle kinematics will be considered in detail.

2.2.2 A specific form for describing MBS kinematics in vehicle mechanics

In vehicle dynamics, the differential equations of vehicle motion are often written with the help of the body-fixed coordinate system (local coordinates). That is an advantage because some terms of the model equations will no longer depend on the system's states. Then, the mechanics of the modeling will be "easier". The disadvantage of this modeling method is the loss of accuracy in the physical interpretation of the terms in the model's equations. However, this method has a clear efficiency advantage for numerical applications such as real-time processing and numerical integration. Therefore, this modeling method is widely used for vehicle dynamics modeling.

What consequences follow from this point of view for the kinematic description of vehicle motion?

The equations presented in section (2.2.1) dealing with the kinematics of rigid bodies and multibody systems are also valid for the kinematics of land vehicles. Those forms are simpler in the case of land vehicles than in the previous section due to their limited capability (planar motion). This simplification in the model equations occurs in the velocity vector projections v_x and v_y of the absolute velocity of the vehicle center of mass into the body-fixed coordinate system of the vehicle. A vehicle with three omnidirectional wheels is considered as an example in Figure 2.8. Here, only the relationship is given between the velocities in the absolute and body-fixed coordinate systems.
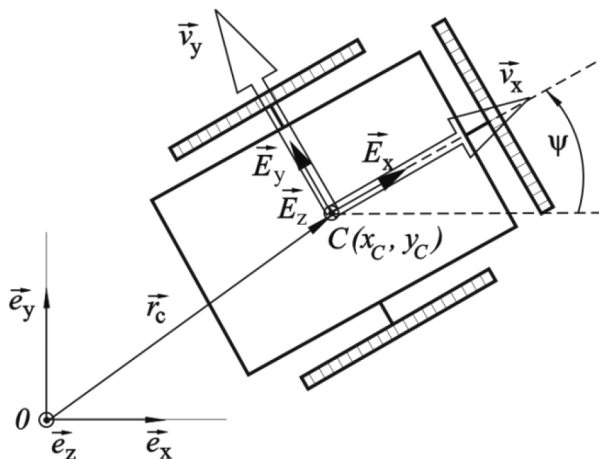
Figure 2.8 Inertial and body-fixed coordinate systems in a vehicle

$$\dot{\vec{r}}_C = (\dot{x}_C, \dot{y}_C)^T_{abs} = \dot{x}_C \vec{e}_x + \dot{y}_C \vec{e}_y$$

$$\vec{v}_C = \left(v_x, v_y\right)^T_{local} = v_x \vec{E}_x + v_y \vec{E}_y$$

$$\dot{x}_C \vec{e}_x + \dot{y}_C \vec{e}_y = v_x \vec{E}_x + v_y \vec{E}_y$$

$$\begin{pmatrix} \vec{e}_x \\ \vec{e}_y \end{pmatrix} = \begin{pmatrix} \cos\psi & -\sin\psi \\ \sin\psi & \cos\psi \end{pmatrix} \begin{pmatrix} \vec{E}_x \\ \vec{E}_y \end{pmatrix}$$

$$\dot{x}_C\left(\cos\psi \ \vec{E}_x - \sin\psi \ \vec{E}_y\right) + \dot{y}_C\left(\sin\psi \ \vec{E}_x + \cos\psi \ \vec{E}_y\right) = v_x \vec{E}_x + v_y \vec{E}_y$$

By comparing the coefficients of unity vectors $\vec{E}_x$ and $\vec{E}_y$ of both sides of the equation, it follows that

$$v_x = \dot{x}_C \ \cos\psi + \dot{y}_C \ \sin\psi$$
$$v_y = -\dot{x}_C \ \sin\psi + \dot{y}_C \ \cos\psi$$

$$\begin{pmatrix} v_x \\ v_y \end{pmatrix} = \mathbb{E} \cdot \begin{pmatrix} \dot{x}_C \\ \dot{y}_C \end{pmatrix}, \mathbb{E} = \begin{pmatrix} \cos\psi & \sin\psi \\ -\sin\psi & \cos\psi \end{pmatrix}. \tag{2.27}$$

Thus, equation (2.27) gives the dependency between the velocity vector components in the global and the body-fixed coordinate systems for a vehicle with three omnidirectional wheels.

Using these kinematic equations, it is possible to describe the velocity vectors of the wheel's center of gravity and the angular velocity vectors for any defined vehicle's maneuver in a relatively simple and illustrative form. In the following selected examples, the previously mentioned topic will be explained briefly, especially in light of its relevance in determining the vehicle's instantaneous center of rotation. Also, in the same sequence, the following examples will discuss the consequences of using the EULER form and the projection of the velocity vectors onto the vehicle-fixed coordinate system.

Example (3)

The illustration in Figure 2.9 shows a vehicle equipped with two classical (ordinary) wheels and a differential drive. Given v_1, v_2, l the required parameters are $v_C, \dot{\psi}, r_M$, with $r_M = \left| \overrightarrow{MC} \right|$.
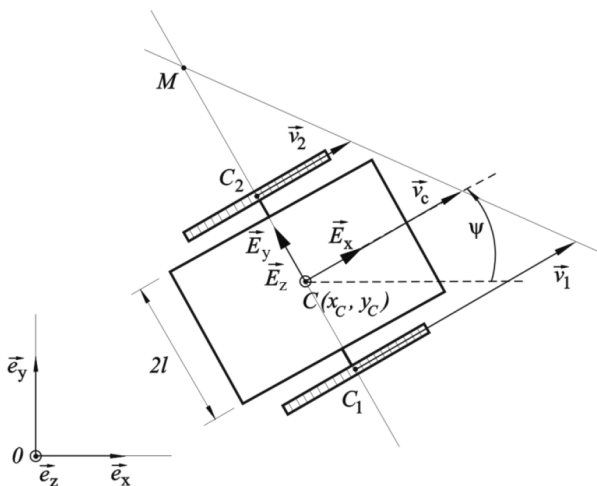
Figure 2.9 Determination of the vehicle center of rotation

First, the velocities are determined as follows

$$\vec{v}_C = \vec{\omega} \times \overrightarrow{MC} = \dot{\psi}\,\vec{E}_z \times \left(-r_M\vec{E}_y\right) = r_M\dot{\psi}\,\vec{E}_x$$
$$v_C = r_M\dot{\psi}$$
$$\vec{v}_1 = \vec{\omega} \times \overrightarrow{MC_1} = \dot{\psi}\,\vec{E}_z \times \left(-(r_M + l)\,\vec{E}_y\right) = (r_M + l)\,\dot{\psi}\,\vec{E}_x$$
$$v_1 = (r_M + l)\,\dot{\psi}$$
$$\vec{v}_2 = \vec{\omega} \times \overrightarrow{MC_2} = \dot{\psi}\,\vec{E}_z \times \left(-(r_M - l)\,\vec{E}_y\right) = (r_M - l)\,\dot{\psi}\,\vec{E}_x$$
$$v_2 = (r_M - l)\,\dot{\psi}\,,$$

By using the theorem of intersecting lines

$$v_C = \frac{v_1 + v_2}{2}$$

it follows that

$$\dot{\psi} = \frac{v_1 + v_2}{2\,r_M}.$$

By substituting the last relationship of $\dot{\psi}$ into the equations for v_1 and v_2, it is evident that

$$v_1 = (r_M + l)\,\frac{v_1 + v_2}{2\,r_M}$$
$$2\,r_M v_1 = (r_M + l)(v_1 + v_2)$$
$$2\,r_M v_1 - r_M v_1 - r_M v_2 = l\,(v_1 + v_2)\,.$$

From

$$r_M = \frac{v_1 + v_2}{v_1 - v_2}\,l$$

and

$$\dot{\psi} = \frac{v_1 - v_2}{2\,l}\,,$$

it follows that

$$\begin{pmatrix} v_C \\ \dot\psi \end{pmatrix} = \frac{1}{2} \begin{pmatrix} 1 & 1 \\ \frac{1}{l} & -\frac{1}{l} \end{pmatrix} \begin{pmatrix} v_1 \\ v_2 \end{pmatrix}. \tag{2.28}$$

Example (4)

A vehicle is equipped with three omnidirectional wheels and it has an inclination angle of 90° between the wheels axles and the wheel plane. Given the center of mass for the wheels v_1 , v_2 , v_3 the required parameters are v_x , v_y , $\dot\psi$.
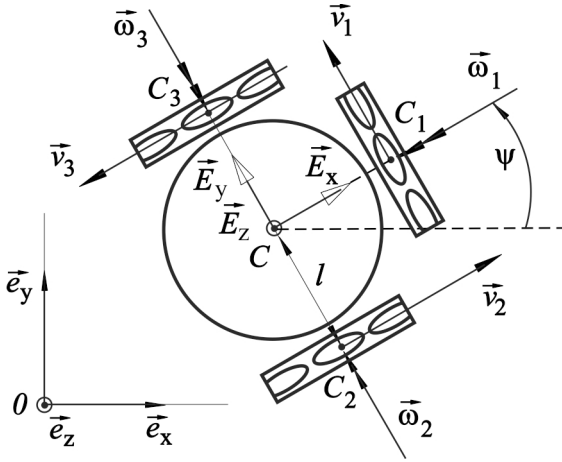
Figure 2.10 Three-wheel vehicle

The solution

$$\dot{\vec{r}}_{C1} = \dot{\vec{r}}_C + \vec\omega \times \overrightarrow{CC_1} = \dot{\vec{r}}_C + (\dot\psi \vec{E}_z) \times l \vec{E}_x = \dot{\vec{r}}_C + \dot\psi l \vec{E}_y$$
$$v_1 = \dot{\vec{r}}_{C1} \cdot \vec{E}_y = \dot{\vec{r}}_C \cdot \vec{E}_y + \dot\psi l = (\dot{x}_C \vec{e}_x + \dot{y}_C \vec{e}_y) \cdot \vec{E}_y + \dot\psi l$$
$$v_1 = [\dot{x}_C(\cos\psi\ \vec{E}_x - \sin\psi\ \vec{E}_y) + \dot{y}_C(\sin\psi \vec{E}_x + \cos\psi\ \vec{E}_y)] \cdot \vec{E}_y + \dot\psi l$$
$$v_1 = -\dot{x}_C \sin\psi + \dot{y}_C \cos\psi + \dot\psi l$$

By substituting equation (2.27) it can be determined that

$$v_1 = v_y + \dot\psi l \tag{2.29}$$

$$\dot{\vec{r}}_{C2} = \dot{\vec{r}}_C + \vec{\omega} \times \overrightarrow{CC_2} = \dot{\vec{r}}_C + (\dot{\psi}\,\vec{E}_z) \times (-l\,\vec{E}_y) = \dot{\vec{r}}_C + \dot{\psi}\,l\,\vec{E}_x$$

$$v_2 = \dot{\vec{r}}_{C2} \cdot \vec{E}_x = \dot{\vec{r}}_C \cdot \vec{E}_x + \dot{\psi}\,l = (\dot{x}_C\,\vec{e}_x + \dot{y}_C\,\vec{e}_y) \cdot \vec{E}_x + \dot{\psi}\,l$$

$$v_2 = [\dot{x}_C(\cos\psi\,\vec{E}_x - \sin\psi\,\vec{E}_y) + \dot{y}_C(\sin\psi\,\vec{E}_x + \cos\psi\,\vec{E}_y)] \cdot \vec{E}_x + \dot{\psi}\,l$$

$$v_2 = \dot{x}_C \cos\psi + \dot{y}_C \sin\psi + \dot{\psi}\,l\,.$$

By substituting equation (2.27), then

$$v_2 = v_x + \dot{\psi}\,l \tag{2.30}$$

$$\dot{\vec{r}}_{C3} = \dot{\vec{r}}_C + \vec{\omega} \times \overrightarrow{CC_3} = \dot{\vec{r}}_C + (\dot{\psi}\,\vec{E}_z) \times l\,\vec{E}_y = \dot{\vec{r}}_C - \dot{\psi}\,l\,\vec{E}_x$$

$$v_3 = \dot{\vec{r}}_{C3} \cdot (-\vec{E}_x) = \dot{\vec{r}}_C \cdot (-\vec{E}_x) + \dot{\psi}\,l = (\dot{x}_C\,\vec{e}_x + \dot{y}_C\,\vec{e}_y) \cdot (-\vec{E}_x) + \dot{\psi}\,l$$

$$v_3 = [\dot{x}_C(\cos\psi\,\vec{E}_x - \sin\psi\,\vec{E}_y) + \dot{y}_C(\sin\psi\,\vec{E}_x + \cos\psi\,\vec{E}_y)] \cdot (-\vec{E}_x)$$
$$+ \dot{\psi}\,l$$

$$v_3 = -(\dot{x}_C \cos\psi + \dot{y}_C \sin\psi) + \dot{\psi}\,l$$

and by substituting equation (2.27), it follows that

$$v_3 = -v_x + \dot{\psi}\,l\,. \tag{2.31}$$

Summing equations (2.30) and (2.31) yields

$$v_x = \frac{1}{2}\,(v_2 - v_3)\,. \tag{2.32}$$

Substituting equation (2.32) into equation (2.31) leads to

$$\dot{\psi} = \frac{v_x + v_3}{l} = \frac{\frac{1}{2}v_2 - \frac{1}{2}v_3 + v_3}{l} = \frac{1}{2l}(v_2 + v_3) \tag{2.33}$$

and substituting equation (2.33) into equation (2.29) yields

$$v_y = v_1 - \dot{\psi}\,l = v_1 - \frac{1}{2l}(v_2 + v_3)\,l = v_1 - \frac{1}{2}(v_2 + v_3)\,. \tag{2.34}$$

From the previous equations, it is possible to represent the body-fixed velocity coordinates of the vehicle's center of gravity v_x and v_y and also its

angular velocity $\dot{\psi}$ as a function of the velocity components of the wheel's center of gravity v_1, v_2 and v_3 in the following simple form:

$$\begin{pmatrix} v_x \\ v_y \\ \dot{\psi} \end{pmatrix} = \begin{pmatrix} 0 & 1/2 & -1/2 \\ 1 & -1/2 & -1/2 \\ 0 & 1/2l & 1/2l \end{pmatrix} \begin{pmatrix} v_1 \\ v_2 \\ v_3 \end{pmatrix} \tag{2.35}$$

For comparison, the representation of the previous form in the global coordinate system by applying the inverse rotation matrix of equation (2.27) can be given as:

$$\mathbb{E}^{-1} = \mathbb{E}^T = \begin{pmatrix} \cos\psi & -\sin\psi \\ \sin\psi & \cos\psi \end{pmatrix}$$

$$\begin{pmatrix} \dot{x}_C \\ \dot{y}_C \\ \dot{\psi} \end{pmatrix} = \begin{pmatrix} \left(\dfrac{v_2 + v_3}{2} - v_1\right)\sin\psi + \left(\dfrac{v_2 - v_3}{2}\right)\cos\psi \\ \left(\dfrac{v_2 - v_3}{2}\right)\sin\psi + \left(\dfrac{-(v_2 + v_3)}{2} + v_1\right)\cos\psi \\ \dfrac{1}{2l}(v_2 + v_3) \end{pmatrix} \tag{2.36}$$

As mentioned before, the representational form of the velocity components shown in equation (2.36) is more complicated than in the form of equation (2.35). Another example for an application using this type of kinematic constraints for four-wheeled Mecanum vehicles can be found in section 3.3.

Example (5)

Figure 2.11 illustrates a vehicle equipped with four Mecanum wheels distributed on two parallel axles. The required parameters are the angular velocities of the four wheels v_1, v_2, v_3 and v_4 as a function of the velocity components of the vehicle's center v_x, v_y and $\dot{\psi}$. The constraint equations will be considered in detail later in chapter 3 (see equations (3.81), (3.84), (3.87) and (3.91)). The final equations are given here in the context demonstrating the advantages of applying the body-fixed coordinate system

$$v_1 = v_x - v_y - (\rho + l)\dot{\psi}$$
$$v_2 = v_x + v_y + (\rho + l)\dot{\psi}$$
$$v_3 = v_x + v_y - (\rho + l)\dot{\psi}$$
$$v_4 = v_x - v_y + (\rho + l)\dot{\psi}\,.$$
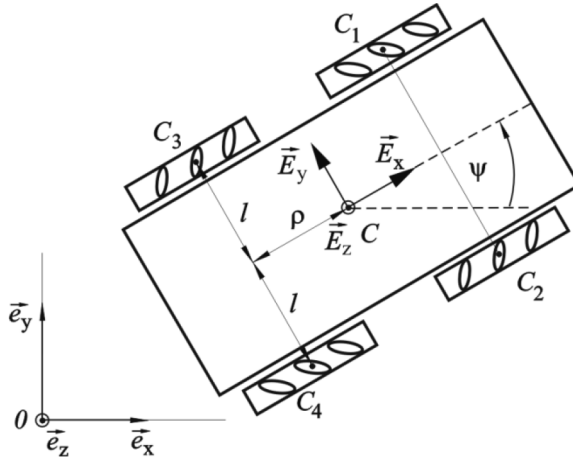
Figure 2.11 A vehicle equipped with four Mecanum wheels

It is not possible to find the inverse of the previous velocity components because the size of matrix in this case is (4×3). But it has been found by several authors, e.g. [137, 129], that it is possible to determine the inverse using the pseudo-inverse matrix method. This solution method brings about a limitation in the results and in the possible motion of the system.

$$\begin{pmatrix} v_x \\ v_y \\ \dot{\psi} \end{pmatrix} = \begin{pmatrix} 1 & 1 & 1 & 1 \\ -1 & 1 & 1 & -1 \\ -\dfrac{1}{(\rho + l)} & \dfrac{1}{(\rho + l)} & -\dfrac{1}{(\rho + l)} & \dfrac{1}{(\rho + l)} \end{pmatrix} \begin{pmatrix} v_1 \\ v_2 \\ v_3 \\ v_4 \end{pmatrix}. \qquad (2.37)$$

In order to solve the over-defined set of equations in the previous expression (i.e. to find an approximated value for the vehicle velocity vector $\vec{V}_C = (v_x, v_y, \dot{\psi})^T$ from the angular velocities $\vec{v} = (v_1, v_2, v_3, v_4)^T$ of the wheels, one possible method uses a so-called pseudo-inverse matrix as described in GANTMACHER [33]. The pseudo-inverse matrix method is formed as follows

$$\vec{V}_C = \mathbb{J}^+ \cdot \vec{v} + (\mathbb{I} - \mathbb{J}^+ \cdot \mathbb{J}) \cdot \tilde{H} \,, \tag{2.38}$$

where $\mathbb{J}^+ = (\mathbb{J}^T \cdot \mathbb{J})^{-1} \cdot \mathbb{J}^T$, the diagonal matrix $\mathbb{I} = \mathbb{J}^+ \cdot \mathbb{J}$ and the parameter $\tilde{H} \in \mathbb{R}$. In the case of $\tilde{H} = 0$, there is a solution to minimize the Euclidean norm $\|\mathbb{J} \cdot \vec{V}_C - \vec{v}\|$. In this case, the solution has been found to be

$$\vec{V}_C = \mathbb{J}^+ \cdot \vec{v} \,. \tag{2.39}$$

2.3   <u>Constraints</u>

The term "constraint" is used to describe a fundamental mechanical characteristic for an MBS. Using the constraints of the MBS, it is possible to define its generalized coordinates and its degree of freedom. Any mechanical system whose center of mass moves without restrictions during motion can be called free. The most relevant technical systems are subjected to certain restrictions on its position and/or its velocity. The mathematical representations of these restrictions are known as constraint equations or "constraints" for short. Depending on the form of these restrictions on motion, it is possible to distinguish between different types of constraints.

Remark: Beginning here with the basics of analytical mechanics, it is convenient to use a special mathematical notation. EINSTEIN's summation convention states that "repeated indices are implicitly summed over".

2.3.1   Bilateral holonomic constraints

The position of the mechanical system can be described using m coordinates in the form $q^1, q^2,..., q^m$. These coordinates can be Cartesian coordinates for example. If there are restrictions for these coordinates with respect to changes, then these restrictions are called holonomic constraints (geometric). The mathematical equations for these restrictions are called bilateral holonomic constraints.

Definition (1)

The mathematical form of bilateral holonomic constraints are as follows

$$f^b(q^1, q^2, ..., q^m, t) = f^b(\vec{q}, t) = 0, \quad (b = 1,2, ..., r < m), \tag{2.40}$$

where $\vec{q} = (q^1, q^2, ..., q^m)$, $\text{rank}\left(\frac{\partial f^b}{\partial q^a}\right) = r$, $(a = 1,2, ..., m)$ and t is time. The independent coordinates $n = m - r$ are called generalized coordinates and n is the number of degrees of freedom of the mechanical system. The generalized coordinates are linearly independent parameters used to determine the position of the mechanical system at any moment.

Example (6)

A wheel (thin disk) with radius R rotates without slipping along the x-axis and the wheel's plane is perpendicular to the contact surface, as shown in Figure 2.12.
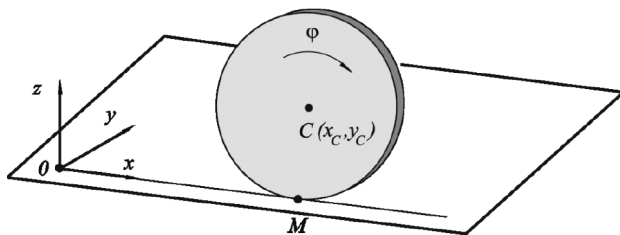
Figure 2.12 A wheel in a plane (I)

The position of the showed wheel is defined by the vector $\vec{q} = (q^1, q^2, q^3, q^4) = (x_C, y_C, z_C, \varphi)$. The coordinates (x_C, y_C, z_C) determine the position of the wheel's center of mass C and the angle φ is the rotation angle. In this case, the motion constraints are

$$x_C - R\varphi = 0, \ \ y_C = 0, \ \ z_C - R = 0.$$

For $m = 4$ parameters there exist $r = 3$ constraints, i.e. the system has $n = m - r = 4 - 3 = 1$ degree of freedom.

2.3.2   Kinematic constraints

If the restrictions in the rigid body's motion result in a restriction of velocities $\dot{q}^1, \dot{q}^2, ..., \dot{q}^m$, then these restrictions are known as kinematic constraints.

Definition (2)

The mathematical representation of bilateral kinematical constraints is as follows

$$f_a^b(q^1, q^2, \ldots, q^m, t)\, \dot{q}^a \; + \; g^b(q^1, q^2, \ldots, q^m, t)$$
$$= f_a^b(\vec{q}, t)\, \dot{q}^a \; + \; g^b(\vec{q}, t) = 0 \,, \qquad (b = 1,2, \ldots, r < m) \,, \tag{2.41}$$

where $\vec{q} = (q^1, q^2, \ldots, q^m)$ and $\operatorname{rank}\left(\frac{\partial f^b}{\partial q^a}\right) = r$, $(a = 1,2, \ldots, m)$ and t is time. If a differentiable function $F^b(\vec{q}, t)$ does not exist such that

$$\frac{d}{dt} F^b(\vec{q}, t) = f_a^b(\vec{q}, t)\, \dot{q}^a + g^b(\vec{q}, t) \,,$$

then the kinematic constraint is a nonholonomic constraint, i.e. not integrable.

Analogous to geometrical constraints, an idea has been presented to also create a more general form in the context in which there are non-linear relationships between the velocities. However, only linear relationships between the velocities are known in practical applications. A correct example (correct with respect to the mechanics and physics points of view) with non-linear kinematical constraints is not known. The number $n = m - r$ also defines the number of degrees of freedom for the mechanical system when considering kinematic constraints.

From the historical standpoint, it is known that the terms "holonomic" and "nonholonomic" as kinematic constraints were first introduced by H. HERTZ (1857-1894). It also seems that he was the first to mention that it is not valid to describe nonholonomic systems using the LAGRANGE equations of the second type. He answered these questions in his fundamental work "Prinzipien der Mechanik in neuem Zusammenhange dargestellt" (Leipzig, 1899) [44]. Previous authors have considered all constraints not having the form $f^b(\vec{q}, t) = 0$ as nonholonomic constraints. In this case a problem arises since it follows from this definition that unilateral constraints are also automatically nonholonomic constraints.

Example (7)

A wheel with radius R rotates without slippage in the x-y-plane and the wheel's plane is perpendicular to the contact surface as shown in Figure 2.13.
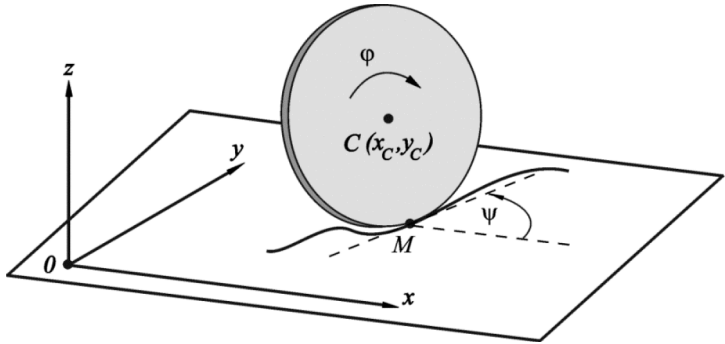
Figure 2.13 A wheel in a plane (II)

The position of the wheel is now defined using the vector $\vec{q} = (q^1, q^2, q^3, q^4, q^5) = (x_C, y_C, z_C, \varphi, \psi)$. The coordinates (x_C, y_C, z_C) define the position of the wheel's center of mass C, φ defines the rotation angle about a center line (i.e. a body-fixed axis) perpendicular to the wheel plane and ψ is the angle between the wheel plane and the x-axis. In this case, the constraints will be

$$\dot{x}_C - R\dot{\varphi}\cos\psi = 0, \ \ \dot{y}_C - R\dot{\varphi}\sin\psi = 0, \ \ z_C - R = 0.$$

Without taking into account the differential equations of motion, these constraints are not integrable.

In the general case, the integration conditions for the constraints are determined from FROBENIUS's law in [3] and have been used to estimate optimal maneuvering for nonholonomic mobile robots in [11]. The question arises as to the qualitative difference in the motion of mechanical systems having holonomic versus nonholonomic constraints.

A mechanical system with nonholonomic constraints can reach any point within the configuration space (set of all generalized coordinates of the system), with the motion starting at any point in the configuration space

by applying the required force. But, a mechanical system with holonomic constraints can only move from point $\vec{q}_A$ to point $\vec{q}_B$ in the case

$$f^b(\vec{q}_A, t) = f^b(\vec{q}_B, t), \quad (b = 1,2, \ldots, r) \ .$$

The previous definitions were used to classify the mechanical systems into holonomic and nonholonomic systems without applying FROBENIUS's law [3].

Example (8)

According to the kinematic constraints in example (6), it is not possible for point P to be on the wheel's circumference, which is momently in contact with the surface (instantaneous center of rotation M) and can only take a position on a straight line through rotation without slipping. Point P can only reach the points on a straight line having a distance from the instantaneous center of rotation M equal to $n \cdot 2\pi R$, where $n = 1,2, \ldots$. The behavior of a steerable wheel during motion oriented as shown in example (7) is different than the previously mentioned wheel in example (6). By assuming that this wheel moves from point $\vec{q}_A = (x_A, y_A, z_A, \varphi_A, \psi_A)$ to point $\vec{q}_B = (x_B, y_B, z_B, \varphi_B, \psi_B)$ with $(0 \leq \varphi_A, \varphi_B \leq 2\pi)$. Points $A(x_A, y_A, 0)$ and $B(x_B, y_B, 0)$ are connected together by a curve whose length is $l = R(\varphi_B - \varphi_A) + n \cdot 2\pi R$ as shown in the following Figure 2.14.
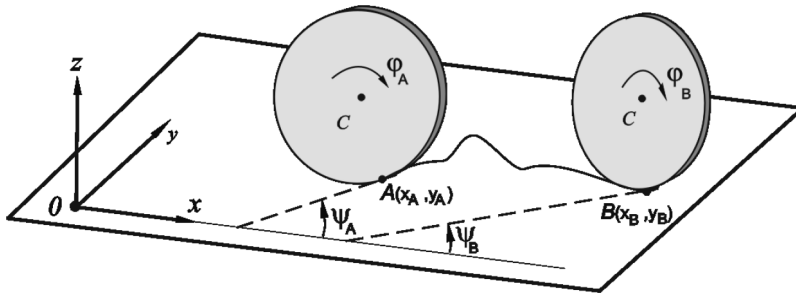
Figure 2.14 Illustration of the difference between holonomic and nonholonomic constraints

The rotating wheel experiencing the motion shown above moves without slippage on the given curve from point A to point B. Finally, the rotation angle ψ about the z-axis should be made equal to ψ_B. All these motions correspond to the formulated kinematic constraints. Thus, the

wheel in example (7) can reach any point in the configuration space. From the kinematic constraints $\dot{x}_C = R\dot{\varphi}\cos\psi$ and $\dot{y}_C = R\dot{\varphi}\sin\psi$ it is not possible to obtain a constraint equation of the form $f(x, y, z, \varphi, \psi) = 0$. The constraints in this case are nonholonomic.

2.3.3   Unilateral constraints

If the restrictions of both the coordinates and the velocities are formulated in the form of inequalities, the constraints are called unilateral. Usually, these kinds of constraints are not classified as holonomic or nonholonomic constraints. In this case, the one-sided constraints take the mathematical form $f^b(\dot{\vec{q}}, \vec{q}, t) \geq 0$, $(b = 1, 2, \ldots, r)$ and these constraints indicate a linear relationship among the velocities.

However, it is also possible to classify one-sided constraints into holonomic and nonholonomic constraints.

Definition (3)

One-sided holonomic constraints can be represented by the following form

$$f^b(q^1, q^2, \ldots, q^m, t) = f^b(\vec{q}, t) \geq 0 , \qquad (2.42)$$

where $\vec{q} = (q^1, q^2, \ldots, q^m)$ and t is time.

Example (9)

The motion characteristics of the wheel in example (6) will be used for this example as well. Two additional constraints will be assumed here. First, a rigid wall stands at $x = 0$. Second, there is a thread between the wall and the wheel's center of mass C. The thread's length is $L \geq R$ and it will limit the motion of the wheel to a certain area. The schematic drawing in Figure 2.15 shows the wheel, the thread and the wall.
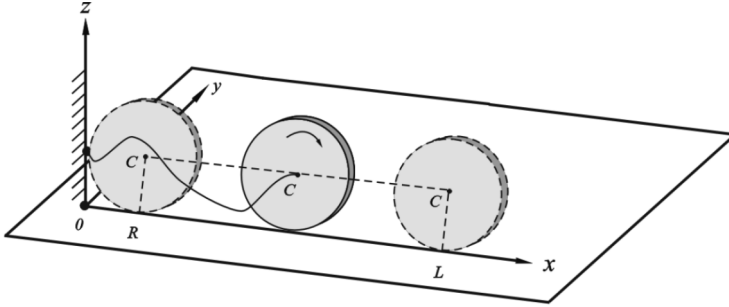
Figure 2.15 An example of unilateral holonomic constraints

The constraints of this mechanical system take the following form

$$R \leq x_C \leq L, \qquad x_C = R\varphi + R, \qquad y_C = 0, \qquad z_C = R.$$

Obviously, it is possible for the inequality $R \leq x \leq L$ to be formulated into $x - R \geq 0$ and $L - x \geq 0$. The one-sided nonholonomic constraints can be defined analogous to definition (2).

Definition (4)

The one-sided nonholonomic constraint is called a restriction and has the following form

$$f_a^b(q^1, q^2, \dots, q^m, t)\dot{q}^a + g^b(q^1, q^2, \dots, q^m, t) \qquad (2.43)$$
$$= f_a^b(\vec{q}, t)\dot{q}^a + g^b(\vec{q}, t) \geq 0, \qquad (b = 1, 2, \dots, r),$$

where $\vec{q} = (q^1, q^2, \dots, q^m)$, and $(a = 1, 2, \dots, m)$ and t is time.

Example (10)

The constraints of the wheel's motion in example (6) will be extended in this example. A ratchet mechanism only allows motion of the wheel towards the right side (in the positive x-direction), see Figure 2.16.
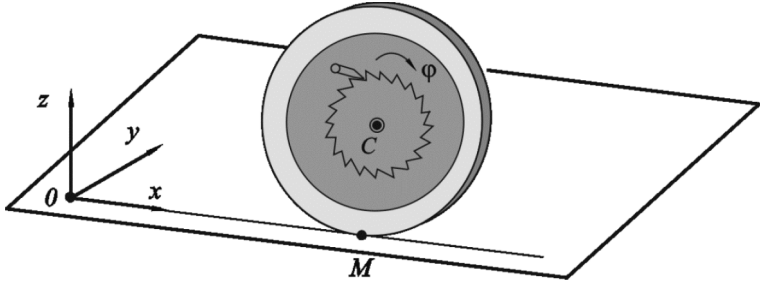
Figure 2.16 A wheel with a ratchet mechanism

The constraints in this case will be as follows

$$\dot{x}_C \geq 0 \,, \qquad x_C = R\varphi \,, \qquad y_C = 0 \,, \qquad z_C = R \,.$$

It follows that the function $x_C(t)$ does not decrease with time, i.e. $x_C(t) \geq x_0$, even with unknown values of x_0. Therefore, the additional constraints of one coordinate, in contrast to nonholonomic bilateral constraints, cannot be rewritten in the form $f(x, t) \geq 0$.

2.3.4   Scleronomic constraints

If all the previously discussed constraints are not explicitly time-dependent, then it follows that:

$f^b(\vec{q}) = 0$ for holonomic bilateral constraints,

$f_a^b(\vec{q})\dot{q}^a + g^b(\vec{q}) = 0$ for nonholonomic bilateral constraints,

$f^b(\vec{q}) \geq 0$ for holonomic unilateral constraints and

$f_a^b(\vec{q})\dot{q}^a + g^b(\vec{q}) \geq 0$ for nonholonomic unilateral constraints.

These types of constraints are called scleronomic.

2.3.5   Virtual displacement

The dependencies between the system's coordinates of motion and the corresponding velocities also leads to dependencies between the virtual

displacement of the system δq^a $(a = 1,2, \ldots, m)$. In the case of holonomic constraints, the virtual displacements are necessarily connected through this system of equations

$$\frac{\partial f^b}{\partial q^a} \delta q^a = 0 \,, \qquad (a = 1,2, \ldots, m) \,, \qquad (b = 1,2, \ldots r).$$

For nonholonomic bilateral constraints, the virtual displacements yield the following system

$$f_a^b(\vec{q}) \, \delta q^a = 0, \qquad (a = 1,2, \ldots, m) \,, \qquad (b = 1,2, \ldots, r).$$

The analogous mathematical representation of unilateral constraints is

$\frac{\partial f^b}{\partial q^a} \delta q^a \geq 0 \; \rightarrow$ holonomic constraints

and

$f_a^b(\vec{q}) \delta q^a \geq 0 \;\; \rightarrow \;$ nonholonomic constraints.

2.3.6   Ideal constraints

A two-sided constraint can be considered ideal if the virtual work of the reaction forces vanishes for any virtual displacement δq^a. The reaction forces resulting from the constraints (or better: the forces as the physical realization of these constraints) should be denoted in a LAGRANGE equation of the second kind using the term "additional generalized forces R_a" in addition to the generalized forces Q_a, which result from the applied forces. These reaction forces act on the mechanical system such that the motion of the system fulfills the constraints. Then, the equations of motion for the mechanical system, according to LAGRANGE, are

$$\frac{d}{dt}\left(\frac{\partial T}{\partial \dot{q}^a}\right) - \frac{\partial T}{\partial q^a} = Q_a + R_a \,, \qquad (a = 1,2, \ldots, m).$$

The mathematical formulation of ideal bilateral constraints is given by

$$R_a \, \delta q^a = 0 \,, \qquad (a = 1,2, \ldots, m).$$

For unilateral constraints, the following conditions should be considered separately:

(1) the equality to zero such as $f_a^b(\vec{q})\dot{q}^a + g^b(\vec{q}) = 0$ and $f^b(\vec{q}) = 0$, respectively, and one occurrence of the inequality case and

(2) the reverse case, i.e. the change from inequality to equality to zero in the constraints.

In the first case, the virtual work of the reaction forces is equal to zero for any virtual displacement. In the second case, the motion of the mechanical system is combined with an impact and the constraint will be ideal if at the moment of impact the kinetic energy is still a continuous function. This means that the kinetic energy T_- before impact is equal to the kinetic energy T_+ after the impact, i.e. $T_- = T_+$.

2.4   Dynamics of rigid multibody systems

The differential equation of motion for any rigid multibody system can be estimated using different physical principles. But most of the commonly used methods can be classified under two main groups:

- Synthetic methods
- Analytical method.

The synthetic methods category lists the principle of linear momentum (NEWTON's second law) and the principle of angular momentum which per se use the method of sections. Generally the synthetic method group covers NEWTON-EULER mechanics. On the other hand, analytical methods deal with the multibody system as one huge entity and the differential equation for this large complex system can be derived from studying the kinetic energy as in LAGRANGE's equation of the second kind or LAGRANGE's equation with multipliers. In this part of the thesis, the analytical methods will be highlighted and the focus is mainly on LAGRANGE's equation with multipliers to model the dynamics of nonholonomic multibody systems.

2.4.1   Synthetic methods

2.4.1.1   *Principle of linear momentum*

Let the force $d\vec{F}$ acts on a mass element dm in a rigid body. The position vector $\vec{r}_C$ of the center of mass of the rigid body can be found from the relation

$$\vec{r}_C = \dfrac{\displaystyle\int_{(V)} \vec{r}\, dm}{\displaystyle\int_{(V)} dm} \quad , \tag{2.44}$$

The summation of the force vector $d\vec{F}$ exerting on the mass elements dm is determined by the equation $\vec{F} = \int_{(V)} d\vec{F}$, see Figure 2.17. $\vec{F}$ is the resultant force acting on the rigid body.
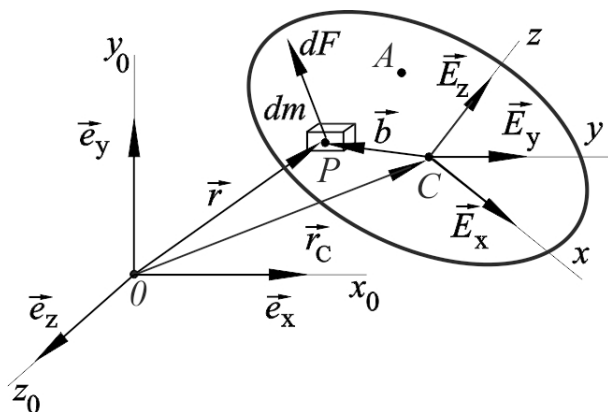
Figure 2.17 Rigid body with mass element dm and distributed forces $d\vec{F}$

The total linear momentum of a rigid body is the vector $\vec{p}$, which is defined as

$$\vec{p} = \int\limits_{(V)} \dot{\vec{r}}\, dm = m\, \dot{\vec{r}}_C\,. \tag{2.45}$$

Principle of linear momentum (NEWTON's second law):

The center of mass of a rigid body moves as a particle (mass point) with mass $m = \int_{(V)} dm$ and with a force acting on it equal to the resultant external force applied to the body:

$$\dot{\vec{p}} = m\, \ddot{\vec{r}}_C = \vec{F}\,. \tag{2.46}$$

2.4.1.2   Principle of angular momentum

The principle of angular momentum describes the rotation of a rigid body similar to the principle of linear momentum used for transitional motion of those rigid bodies. According to the EULER theorem, the angular momentum and the moment of the applied forces on the mass element dm with respect to the origin of the inertial coordinate system 0 can be calculated from the following relationship

$$\vec{D}_0 = \int\limits_{(V)} \vec{r} \times \dot{\vec{r}}\, dm\,, \qquad \vec{M}_0 = \int\limits_{(V)} \vec{r} \times d\vec{F}\,, \tag{2.47}$$

where V is the volume of the rigid body, see Figure 2.17. With respect to the center of mass of the rigid body C, the equation of the angular momentum can be rewritten as follows

$$\vec{D}_C = \int\limits_{(V)} \vec{b} \times \dot{\vec{b}}\, dm\,, \qquad \vec{M}_C = \int\limits_{(V)} \vec{b} \times d\vec{F}\,, \tag{2.48}$$

where $\vec{b}$ is the position vector of the mass element dm with respect to the body-fixed coordinate system.

Principle of angular momentum:

The total time derivative of the angular momentum vector $\vec{D}_0$ equals the moment $\vec{M}_0$ of the resultant force $\vec{F}$, which is acting on the whole rigid body with respect to the origin of the inertial coordinate system 0.

$$\dot{\vec{D}}_0 = \vec{M}_0 . \tag{2.49}$$

Similarly, the total time derivative of the angular momentum vector $\vec{D}_C$ with respect to the center of mass of the rigid body C equals the moment $\vec{M}_C$ of the resultant force $\vec{F}$ on the entire rigid body relative to its center of mass.

$$\dot{\vec{D}}_C = \vec{M}_C . \tag{2.50}$$

The statement that the derivative of angular momentum equals the moment is valid for the origin of the inertial coordinate system and the center of mass of the rigid body and it is invalid for any other point on the rigid body. The principle of angular momentum for any other point other than the two aforementioned points, takes the form

$$\dot{\vec{D}}_A = \vec{M}_A + m\ddot{\vec{r}}_A \times \vec{a} , \tag{2.51}$$

where point A is an arbitrary point on the rigid body as shown in Figure 2.17 and $\vec{r}_A = \overrightarrow{OA}$ and $\vec{a} = \overrightarrow{AC}$.

The velocity vector of point P in the body-fixed coordinate system is $\dot{\vec{b}} = \vec{\omega} \times \vec{b}$. By applying this equation to the angular momentum vector with respect to the center of mass, equation (2.48) can be rewritten in the following form

$$\vec{D}_C = \int_{(V)} \vec{b} \times \dot{\vec{b}} \, dm = \int_{(V)} \vec{b} \times (\vec{\omega} \times \vec{b}) \, dm . \tag{2.52}$$

Carrying out the integration, the symmetrical inertia matrix $\boldsymbol{J}$ appears, consisting of

-    the mass moments of inertia

$$J_{xx} = \int_{(V)} (y^2 + z^2)\, dm\,,$$

$$J_{yy} = \int_{(V)} (x^2 + z^2)\, dm\,, \qquad (2.53)$$

$$J_{zz} = \int_{(V)} (x^2 + y^2)\, dm\,,$$

-    the products of mass moments of inertia

$$J_{xy} = J_{yx} = -\int_{(V)} xy\, dm\,,$$

$$J_{xz} = J_{zx} = -\int_{(V)} xz\, dm\,, \qquad (2.54)$$

$$J_{yz} = J_{zy} = -\int_{(V)} yz\, dm\,.$$

Using the acceptable description that $x =: 1,\ y =: 2,\ z =: 3,$ the inertia matrix becomes

$$\boldsymbol{J} = (J_{ik}) = \begin{pmatrix} J_{11} & J_{12} & J_{13} \\ J_{21} & J_{22} & J_{23} \\ J_{31} & J_{32} & J_{33} \end{pmatrix}, \qquad (2.55)$$

and angular momentum with respect to the center of mass of the rigid body takes the following compact form

$$\vec{D}_C = \sum_{i,k=1}^{3} J_{ik}\,\omega_i \vec{E}_k\ .$$

Thus, the angular momentum equation $\dot{\vec{D}}_C = \left(J_{ik}\omega_i\vec{E}_k\right)^{\cdot} = \vec{M}_C$ in component form in a principle axis system is

$$J_{11}\dot{\omega}_1 - J_{22}\omega_2\omega_3 + J_{33}\omega_3\omega_2 = M_{C1}\,,$$

$$J_{22}\dot{\omega}_2 - J_{11}\omega_1\omega_3 + J_{33}\omega_3\omega_1 = M_{C2}\,, \qquad\qquad (2.56)$$

$$J_{33}\dot{\omega}_3 - J_{11}\omega_1\omega_2 + J_{22}\omega_2\omega_1 = M_{C3}\,.$$

The following transformation equations of the inertia matrix describe the transition to a new coordinate system $\{C', \vec{E}_{i'}\}$, which can be obtained by parallel translational displacement (known as STEINER's theorem or the parallel axis theorem) or rotation of the original coordinate system $\{C, \vec{E}_i\}$.

- Applying the parallel translational displacement $\{C, \vec{E}_i\} \longrightarrow \{C', \vec{E}_i\}$ with linear displacement vector $\vec{a} = a_i\vec{E}_i$, it follows that

$$J_{i'k'} = J_{ik} + m\left(a_j a_j \delta_{ik} - a_i a_k\right). \qquad\qquad (2.57)$$

- Rotation of $\{C, \vec{E}_i\} \longrightarrow \{C', \vec{E}_{i'}\}$ with rotation matrix $\mathbb{E} = \left(E_{i'j}\right)$ yields

$$J_{i'k'} = E_{i'i}\, E_{k'k}\, J_{ik}\,. \qquad\qquad (2.58)$$

2.4.2   Analytical methods

2.4.2.1   D'ALEMBERT's principle

Explaining the principles of analytical mechanics the term "virtual displacement" plays an important role. For a point P on the moving rigid body with the position vector $\overrightarrow{OP} = \vec{r} = \vec{r}(x_i, q^1, q^2, ..., q^m, t)$, its <u>actual</u> displacement can be expressed as follows

$$d\vec{r} = \frac{\partial \vec{r}}{\partial q^a} dq^a + \frac{\partial \vec{r}}{\partial t} dt \, . \tag{2.59}$$

The <u>virtual</u> displacement $\delta \vec{r}$ is the set of differential changes of the position vector $\vec{r}$ with respect to a variation δq^a in a fixed time t as expressed in the following equation

$$\delta \vec{r} = \frac{\partial \vec{r}}{\partial q^a} \delta q^a \, . \tag{2.60}$$

In contrast to the actual displacement $d\vec{r}$, the virtual displacement $\delta \vec{r}$ is the possible displacement in the given time t with respect to the kinematic constraints of the described rigid body.

D'ALEMBERT's principle for the rigid bodies is

$$\int\limits_{(V)} \left(d\vec{F} - \ddot{\vec{r}} \, dm \right) \delta \vec{r} = 0 \, , \qquad \forall \, \delta \vec{r}, \tag{2.61}$$

where $d\vec{F}$ is an applied force on the mass element dm of the rigid body. D'ALEMBERT's principle is valid for rigid multibody systems with holonomic or nonholonomic constraints, when written in the form of a scalar product. It is certainly independent of the coordinate system.

2.4.2.2   LAGRANGE's equation of the second kind

Considering an MBS with holonomic kinematic constraints, it can be described by n independent generalized coordinates $q^a (a = 1, 2, ..., n)$ (n=degree of freedom). Using D'ALEMBERT's principle, it is possible to derive LAGRANGE's equation of the second kind. By applying

HELMHOLTZ identifiers, $\frac{\partial \dot{\vec{r}}}{\partial \dot{q}^a} = \frac{\partial \vec{r}}{\partial q^a}$ and $\frac{d}{dt}\left(\frac{\partial \vec{r}}{\partial q^a}\right) = \frac{\partial \dot{\vec{r}}}{\partial q^a}$ to the term $\ddot{\vec{r}}\frac{\partial \vec{r}}{\partial q^a}$ from equation (2.61), then it follows that

$$\ddot{\vec{r}}\frac{\partial \vec{r}}{\partial q^a} = \frac{1}{2}\frac{d}{dt}\left(\frac{\partial \dot{\vec{r}}^2}{\partial \dot{q}^a}\right) - \frac{1}{2}\left(\frac{\partial \dot{\vec{r}}^2}{\partial q^a}\right) \tag{2.62}$$

and with the generalized force Q_a

$$Q_a = \int\limits_{(V)} d\vec{F}\frac{\partial \vec{r}}{\partial q^a} \tag{2.63}$$

and kinetic energy T of the rigid MBS

$$T = \frac{1}{2}\int\limits_{(V)} \dot{\vec{r}}^2 \, dm \tag{2.64}$$

LAGRANGE's equation of the second kind then holds that

$$\frac{d}{dt}\left(\frac{\partial T}{\partial \dot{q}^a}\right) - \left(\frac{\partial T}{\partial q^a}\right) = Q_a, \qquad (a = 1,2,\dots,n). \tag{2.65}$$

The kinetic energy of a rigid MBS can be estimated using the following form

$$T = T_{Trans} + T_{Rot} = \frac{1}{2}m\dot{\vec{r}}_C^2 + \frac{1}{2}J_{ik}\omega_i\omega_k\,. \tag{2.66}$$

2.4.2.3   LAGRANGE's equation with multipliers

The derivation of LAGRANGE's equation of the second kind for a holonomic mechanical system was based on the linear independence of the virtual displacements δq^a. In the following calculations, it is assumed that there are r additional nonholonomic constraints

$$f_a^b(q^1, q^2, \dots, q^n)\,\dot{q}^a = 0\,,$$
$$(a = 1,2,\dots,n; b = 1,2,\dots,r < n)\,, \qquad \text{rank}(f_a^b) = r\,. \tag{2.67}$$

Sum (2.67) can be divided into two parts

$$f_{a_1}^b \, \dot{q}^{a_1} + f_{a_2}^b \, \dot{q}^{a_2} = 0 \, , (a_1 = 1,2, \dots, n-r; a_2 = n-r+1, \dots, n) \quad (2.68)$$

and therefore for the virtual displacements δq^a, it holds that

$$f_{a_1}^b \, \delta q^{a_1} + f_{a_2}^b \, \delta q^2 = 0 \, , \qquad\qquad (2.69)$$
$$(a_1 = 1,2, \dots, n-r; \ a_2 = n-r+1, \dots, n) \, .$$

Here virtual displacements δq^{a_1} are independent. Multiplying the equations with λ_b and considering the linear independence of δq^{a_1}, the LAGRANGE equations with multipliers follows in the from

$$\frac{d}{dt}\left(\frac{\partial T}{\partial \dot{q}^a}\right) - \left(\frac{\partial T}{\partial q^a}\right) = Q_a + \lambda_b \, f_a^b \, , \qquad (a = 1,2, \dots, n) \, . \qquad (2.70)$$

Here, $R_a = \lambda_b \, f_a^b$ represents the reaction forces on the MBS due to r additional constraints. The n generalized coordinates q^a and the r unknown multipliers λ_b can be determined by equations (2.67) and (2.70).

2.4.2.4   APPELL's equation

APPELL's equations are another useful kind of equation describing the dynamic behavior of a nonholonomic system. Again based on D'ALEMBERT's principle (2.61) and equations (2.68) with a regular matrix $f_{a_2}^b$ by introducing the acceleration energy

$$S = \frac{1}{2} \int\limits_{(V)} \ddot{\vec{r}}^2 \, dm \, , \qquad S = S(q^1, \dots, q^n, \dot{q}^1, \dots, \dot{q}^{n-r}, \ddot{q}^1, \dots, \ddot{q}^{n-r}) \, , \qquad (2.71)$$

and the generalized forces

$$\Pi_{a_1} = \int\limits_{(V)} d\vec{F} \, \vec{g}_{a_1} \, , \qquad\qquad (2.72)$$

a series of transformations leads to APPELL's equations

$$\frac{\partial S}{\partial \ddot{q}^{a_1}} = \Pi_{a_1}, \qquad (a_1 = 1, 2, \ldots, n - r).$$ (2.73)

where $\ddot{q}^{a_1}$ are $n - r$ generalized accelerations.

In the following chapter some of the equations, shortly described above will be used for the analysis of the dynamic behavior of several wheeled locomotion systems, applicable for disabled persons.

Everything should be
made as simple as
possible, but not simpler.
(A. Einstein)

3 Kinematic and dynamic analysis for different vehicle types with different types of wheels

3.1 The kinematics of different types of wheels

Here, different types of wheels will be presented and their kinematic constraints will be discussed briefly. The wheels used in industrial and laboratory fields can be classified into two main groups: the first is the classical wheel used in passenger and commercial vehicles. The second type is the omnidirectional wheel, which has additional motion capabilities. The omnidirectional wheel has a special mechanical design in which a set of free-rotating rollers is distributed along its circumference. These rollers rotate about their own rotational axis, which can be inclined with respect to the main rotating axis of the wheel by different angles, which is denoted here by δ. Omnidirectional wheels can also be classified into two subgroups: omnidirectional wheels with an inclination angle of the rotation axis of the rollers at 90°, which are referred to here as "classical omnidirectional wheels" and commonly found in robotics and the learning topics. The second type of omnidirectional wheel is known as the "Mecanum wheel", referring to the company which first developed the type. The Mecanum wheel design is unique and differs from the design of the first type of omnidirectional wheel because the inclination angle of the rotation axis of the rollers is 45° relative to the main rotation axis of the wheel as a whole, see Figure 3.2. The Mecanum wheel is widely used in industrial areas and the medical field, especially if there is a need to overcome the limitation in the area of the motion. Transport systems using Mecanum wheels offer a high degree of flexibility during motion.

3.1.1   Classical wheel

In this section, the classical wheel will be modeled as a thin disk with radius R rotating without slippage in the x-y-plane and with the wheel's plane perpendicular to the contact surface as shown in Figure 3.1. From the kinematic side, rotation without slippage means that the instantaneous velocity of the contact point between the wheel and the motion surface is zero. This condition is known as the kinematic constraint of the thin disk and can be further used to understand the behavior of the thin disk during motion on the surface.
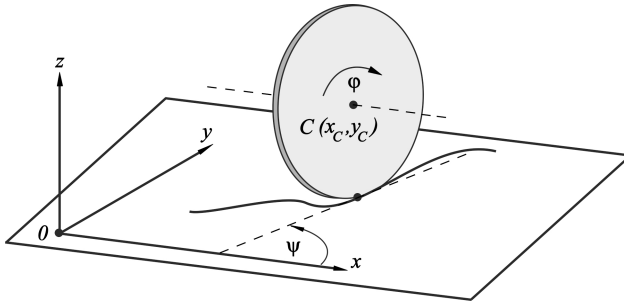
Figure 3.1 A classical wheel configuration during motion

The position of the wheel can now be defined using the coordinates (x_C, y_C, z_C) of the position of the wheel's center of mass C. Angle φ defines the rotation angle about a center line (i.e. a body-fixed axis) perpendicular to the wheel's plane and ψ is the angle between the wheel's plane and x-axis. The constraints are projected into the inertial coordinate frame $\{O, x, y, z\}$, in this particular case as follows

$$\dot{x}_C - R\dot{\varphi}\cos\psi = 0 , \;\; \dot{y}_C - R\dot{\varphi}\sin\psi = 0 .$$

Without taking into consideration the differential equations of motion, these constraints are not integrable as mentioned before in section 2.3.2. The kinematic constraints of these nonholonomic systems has already been discussed briefly.

3.1.2   Omnidirectional wheel

In general the omnidirectional wheel is a wheel with a set of additional freely rotating rollers distributed along the external circumference of the

wheel. The inclination of the rotation axes of these external rollers differs among designs. One very common design of omnidirectional wheel is commonly known as the Mecanum wheel, in which the rotation axes of the external rollers are inclined by an angle of 45°. Another definition for the inclination angle of the rollers, which is used when performing kinematic and dynamic analysis in most reviewed references, is the angle between the velocity vector of the contact point between the external roller and the motion plane and the velocity vector of the center of mass of the entire wheel. The inclination angle can be defined in different ways according to the objective of the study. The second type of omnidirectional wheel has already been mentioned in this thesis as the classical omnidirectional wheel, in which the inclination angle of the rotation axes of the external rollers are 90°. See Figure 3.2 for a visual overview of the classifications of omnidirectional wheels. In the following kinematic analysis, the inclination angle is denoted by δ to represent the general case of the omnidirectional wheel.
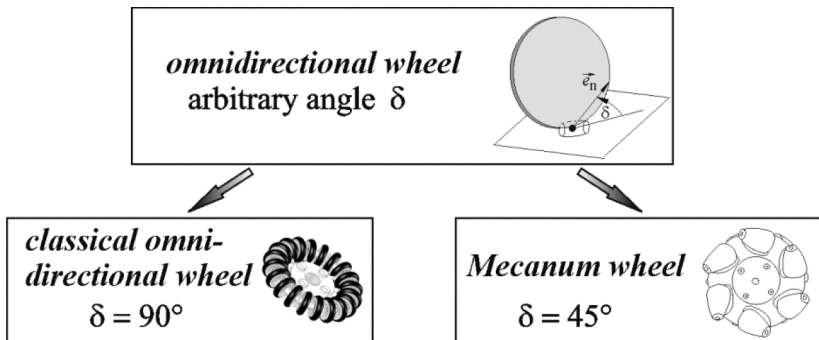
Figure 3.2 Classification of omnidirectional wheels

For a conventional wheel, contact between the wheel and the supporting plane is characterized by the condition that the wheel is rolling without slip. This means that the velocity of the point by which the wheel contacts the plane at each current instant is equal to zero. Then the projections of the velocity of the contact point onto the direction lying in the wheel plane as well as onto the direction perpendicular to this plane are equal to zero. For an omnidirectional wheel, there is only one direction in which the projection of the velocity of the wheel's point of contact with the supporting plane vanishes. This direction can be arbitrary but it is fixed relative to the wheel.

To avoid misunderstanding the term "omnidirectional wheel" as used in this thesis, this author has used it for an arbitrary angle δ (see Figure 3.3). In practice and in many publications the following special cases for δ are considered:

- The term "<u>classical</u> omnidirectional wheel" is used for the case in which $\delta = 90°$.
- The term "Mecanum wheel" is used for the case in which $\delta = 45°$.
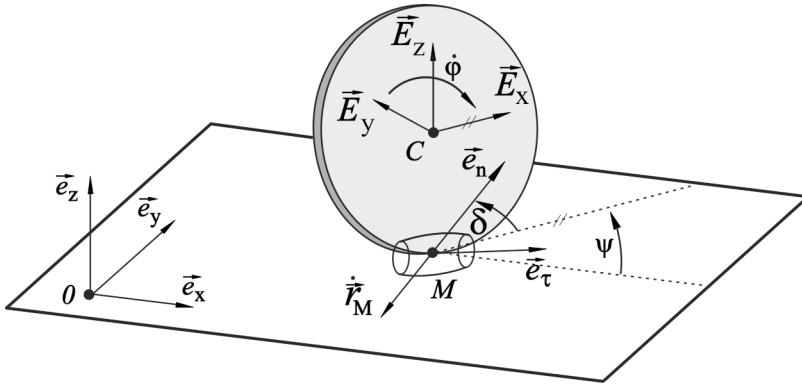
Figure 3.3 Mechanical model of an omnidirectional wheel with vectors and parameters describing the kinematics

As a model of an omnidirectional wheel, we will consider a rolling disk of radius R centered at point C on a horizontal plane. The plane of the disk is always vertical. Let $\vec{e}_\tau$ denote the unit vector along the axes of the rollers and δ **the angle between the plane of the wheel and the vector perpendicular to the roller axis (between vectors $\vec{e}_n$ and $\vec{E}_x$)**. Angle δ is constant. The kinematic constraint relationship for a Mecanum wheel implies that the projection of velocity vector $\dot{\vec{r}}_M$ of the point of contact M of the wheel with the plane onto the axis $\vec{e}_\tau$ is equal to zero as shown in Figure 3.3.

The kinematic constraint relation has the form

$$\dot{\vec{r}}_M \cdot \vec{e}_\tau = 0 \, , \tag{3.1}$$

where velocity $\dot{\vec{r}}_M$ is defined by the equation

$$\dot{\vec{r}}_M = \dot{\vec{r}}_C + \vec{\omega} \times \overrightarrow{CM} , \tag{3.2}$$

and $\dot{\vec{r}}_C$ is the velocity of the center of gravity C and $\vec{\omega}$ is the angular velocity of the disk.

Let $\{O, \vec{e}_x, \vec{e}_y, \vec{e}_z\}$ be a fixed reference frame (inertial system) and let C be the origin of a movable reference frame (body-fixed frame) $\{C, \vec{E}_x, \vec{E}_y, \vec{E}_z\}$. Unit vectors $\vec{E}_x$ and $\vec{E}_y$ are parallel to the horizontal plane, vector $\vec{E}_z$ lies in the disk plane and vector $\vec{E}_y$ is perpendicular to this plane. Let φ be the angle of rotation of the disk about the axis passing through point C perpendicular to the plane of the disk and ψ the angle formed by the disk plane with a line parallel to vector $\vec{E}_x$ (the angle between vector $\vec{E}_x$ and vector $\vec{e}_x$) as shown in Figure 3.3. Vectors $\vec{\omega}$ and $\overrightarrow{CM}$ are defined as

$$\vec{\omega} = \dot{\varphi}\vec{E}_y + \dot{\psi}\vec{E}_z , \qquad \overrightarrow{CM} = -R\vec{E}_z . \tag{3.3}$$

Let x_C, y_C and R be the coordinates of point C in the reference frame, then

$$\dot{\vec{r}}_C = (\dot{x}_C \cos\psi + \dot{y}_C \sin\psi)\vec{E}_x + (-\dot{x}_C \sin\psi + \dot{y}_C \cos\psi)\vec{E}_y , \\ \vec{\omega} \times \overrightarrow{CM} = -R\dot{\varphi}\vec{E}_x . \tag{3.4}$$

Substituting equation (3.4) into equation (3.2) yields

$$\dot{\vec{r}}_M = (\dot{x}_C \cos\psi + \dot{y}_C \sin\psi - R\dot{\varphi})\vec{E}_x + (-\dot{x}_C \sin\psi + \dot{y}_C \cos\psi)\vec{E}_y . \tag{3.5}$$

For the mechanical configuration in Figure 3.3, vector $\vec{e}_\tau$ is expressed as

$$\vec{e}_\tau = \sin\delta\, \vec{E}_x - \cos\delta\, \vec{E}_y . \tag{3.6}$$

Then, substituting equations (3.5) and (3.6) into kinematic constraint equation (3.1) yields the following relation

$$\begin{aligned} \dot{\vec{r}}_M \cdot \vec{e}_\tau &= \dot{x}_C \cos\psi \sin\delta + \dot{y}_C \sin\psi \sin\delta - R\dot{\varphi} \sin\delta \\ &\quad + \dot{x}_C \sin\psi \cos\delta - \dot{y}_C \cos\psi \cos\delta \\ &= \dot{x}_C \sin(\psi + \delta) - \dot{y}_C \cos(\psi + \delta) - R\dot{\varphi} \sin\delta = 0 . \end{aligned} \tag{3.7}$$

Finally, kinematic equation (3.1) becomes:

$$\dot{x}_C \sin(\psi + \delta) - \dot{y}_C \cos(\psi + \delta) = R\dot{\varphi} \sin \delta \,. \tag{3.8}$$

On the basis of the analysis of the kinematic constraints in equation (3.8), [14] shows that if a mechanical system is equipped with n Mecanum wheels in such a way that:

(a) $n \geq 3$
(b) Not all vectors $\vec{e}_{\tau_i}$ are parallel to each other
(c) The points of contact of the wheels with the plane do not lie on one line

then it is always possible to find control functions $\dot{\varphi}_i$ $(i = 1, \dots, n)$ that implement any prescribed motion of the system center of mass.

3.1.3   "Classical" omnidirectional wheel

Figure 3.4 shows the practical realization of an omnidirectional wheel with 20 external rollers, which are distributed along the circumference of the wheel.

Figure 3.4 Technical realization of a "classical" omnidirectional wheel

The kinematic constraint for this type of wheel is

$$\dot{x}_C \cos \psi + \dot{y}_C \sin \psi = R\dot{\varphi} \,. \tag{3.9}$$

3.1.4   Mecanum wheel

In Figure 3.5, the Mecanum wheel is presented from NEXUS ROBOT Inc. (Ref.: www.nexusrobot.com).

Figure 3.5 Mechanical design of a real Mecanum wheel

As mentioned before, this type of wheel is a special case of omnidirectional wheel, in which the inclination angle of the roller rotation axes is $45°$ $\left(\delta = \frac{\pi}{4}\right)$. Therefore, the kinematic constraint in (3.8) becomes

$$\dot{x}_C \sin\left(\psi + \frac{\pi}{4}\right) - \dot{y}_C \cos\left(\psi + \frac{\pi}{4}\right) = R\dot{\varphi} \sin\left(\frac{\pi}{4}\right) \tag{3.10}$$

and finally the kinematic constraint on the Mecanum wheel is expressed as

$$\dot{x}_C (\cos\psi + \sin\psi) + \dot{y}_C (\sin\psi - \cos\psi) = R\dot{\varphi}\,. \tag{3.11}$$

3.2   <u>Two-wheeled vehicle – basic model</u>

In this section, the kinematics and dynamics of a two-wheeled vehicle will be discussed with respect to a classic-wheel design. It is sometimes better to understand the behavior of these systems under different working conditions, mostly depending on the intended use and the working environment. A commonly used configuration for two-wheeled vehicles is one with classical wheels for moving on the street and other surfaces. The wheelchair is considered a direct application for two-wheeled vehicles because only two wheels are actually driving wheels, with the other wheels on the platform being used for support or steering purposes.

In general, the wheels can either be of the classical or omnidirectional type. The kinematic model of these wheels begins by finding the location of the vehicle center and the position of the center of mass for each wheel relative to global coordinates and as a function of the position of the vehicle's center of mass. The secondary wheels are used for supporting, balancing and steering the vehicle during motion. So far, those secondary wheels are not used in vehicle propulsion. Therefore, they are taken into account when analyzing the kinematics and dynamics of the vehicle as a whole. The secondary wheels are usually of the caster-wheel type because they offer a high degree of stability and maneuverability in all directions of travel.

Figure 3.6 shows a schematic drawing of a wheelchair with two classical wheels in the motion plane. The mechanical configuration presented consists of two wheels fixed on one axis, with the driving moments applied directly to the wheels.
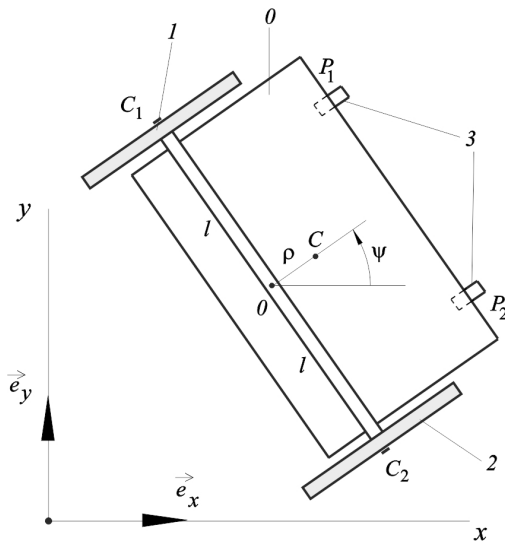
Figure 3.6 Model and geometric parameters of a wheelchair with classical wheels

The mass of each wheel 1,2 is denoted by m_1, the wheel radius is R, the distance between the centers of the wheels is $2l$ and the mass of the wheel's chassis 3 itself is designated m_0. The center of mass of the whole

system is located on a straight line perpendicular to the wheel axis. The distance between the center of whole system C and the center of the carrying axis of the wheel O is labeled ρ. J_C is the mass moment of the inertia for whole system with respect to the center of rotation of the vehicle. The following kinematic and dynamic analyses are valid for the mechanical system presented without taking into account slip between the wheels and the motion plane. Two caster wheels 4 are used here for supporting the frame during motion and for more maneuverability. Driving moments $\vec{M}_1$ and $\vec{M}_2$ and all other forces acting on the system are mentioned and drawn in Figure 3.7.
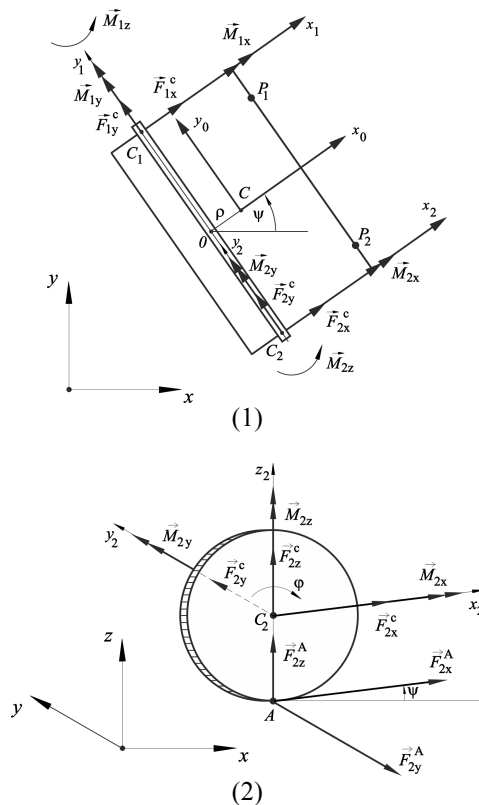
Figure 3.7 (1) The complete system with the applied driving moments and forces, (2) the right wheel with applied forces, moments and the reaction forces

3.2.1   Kinematic analysis

The position of the centers of mass for the left and right wheels, designated C_1 and C_2, can be derived as follows

$$
\begin{aligned}
x_1 &= x_0 - l \sin \psi \, , \\
y_1 &= y_0 + l \cos \psi \, , \\
x_2 &= x_0 + l \sin \psi \, , \\
y_2 &= y_0 - l \cos \psi \, , \\
x_C &= x_0 + \rho \cos \psi \, , \\
y_C &= y_0 + \rho \sin \psi \, .
\end{aligned}
\tag{3.12}
$$

The velocity of the previous centers of mass can be calculated as the first derivation with respect to the time as follows

$$
\begin{aligned}
\dot{x}_1 &= \dot{x}_0 - l \dot{\psi} \cos \psi \, , \\
\dot{y}_1 &= \dot{y}_0 - l \dot{\psi} \sin \psi \, , \\
\dot{x}_2 &= \dot{x}_0 + l \dot{\psi} \cos \psi \, , \\
\dot{y}_2 &= \dot{y}_0 + l \dot{\psi} \sin \psi \, , \\
\dot{x}_C &= \dot{x}_0 - \rho \dot{\psi} \sin \psi \, , \\
\dot{y}_C &= \dot{y}_0 + \rho \dot{\psi} \cos \psi \, .
\end{aligned}
\tag{3.13}
$$

Similarly, the acceleration is the second derivative of equation (3.12) with respect to time

$$
\begin{aligned}
\ddot{x}_1 &= \ddot{x}_0 - l \ddot{\psi} \cos \psi + l \dot{\psi}^2 \sin \psi \, , \\
\ddot{y}_1 &= \ddot{y}_0 - l \ddot{\psi} \sin \psi - l \dot{\psi}^2 \cos \psi \, , \\
\ddot{x}_2 &= \ddot{x}_0 + l \ddot{\psi} \cos \psi - l \dot{\psi}^2 \sin \psi \, , \\
\ddot{y}_2 &= \ddot{y}_0 + l \ddot{\psi} \sin \psi + l \dot{\psi}^2 \cos \psi \, , \\
\ddot{x}_C &= \ddot{x}_0 - \rho \ddot{\psi} \sin \psi - \rho \dot{\psi}^2 \cos \psi \, , \\
\ddot{y}_C &= \ddot{y}_0 + \rho \ddot{\psi} \cos \psi - \rho \dot{\psi}^2 \sin \psi \, .
\end{aligned}
\tag{3.14}
$$

The following kinematic constraints are valid for this mechanical system

$$
\begin{aligned}
\dot{x}_0 \cos \psi + \dot{y}_0 \sin \psi - l \dot{\psi} &= R \dot{\varphi}_1 \, , \\
\dot{x}_0 \cos \psi + \dot{y}_0 \sin \psi + l \dot{\psi} &= R \dot{\varphi}_2 \, , \\
-\dot{x}_0 \sin \psi + \dot{y}_0 \cos \psi &= 0 \, .
\end{aligned}
\tag{3.15}
$$

The kinematic constraint in equation (3.15) can be reformed as follows

$$\dot{x}_0 = l\dot{\psi}\cos\psi + R\dot{\varphi}_1\cos\psi\ ,$$
$$\dot{y}_0 = l\dot{\psi}\sin\psi + R\dot{\varphi}_1\sin\psi\ ,$$
$$\dot{\varphi}_2 = \dot{\varphi}_1 + \frac{2l}{R}\dot{\psi}\ , \tag{3.16}$$

and the time derivative of the last equation is

$$\ddot{x}_0 = l\ddot{\psi}\cos\psi - l\dot{\psi}^2\sin\psi + R\ddot{\varphi}_1\cos\psi - R\dot{\varphi}_1\dot{\psi}\sin\psi\ ,$$
$$\ddot{y}_0 = l\ddot{\psi}\sin\psi + l\dot{\psi}^2\cos\psi + R\ddot{\varphi}_1\sin\psi + R\dot{\varphi}_1\dot{\psi}\cos\psi\ ,$$
$$\ddot{\varphi}_2 = \ddot{\varphi}_1 + \frac{2l}{R}\ddot{\psi}\ . \tag{3.17}$$

3.2.2 Dynamic analysis

As presented in Figure 3.7, the driving moment components of $\vec{M}_{1y}$ and $\vec{M}_{2y}$ (the resultant internal moments between the mass of the chassis and the connected wheels) are assumed to be time-dependent functions, where $M_{1y} = M_1(t)$ and $M_{2y} = M_2(t)$. The whole vehicle as presented is divided into three separated bodies: the vehicle body (0), the left wheel (1) and the right wheel (2). The linear and angular momentum principles (see section 2.4.1) are used here to find the differential equations of motion to describe the dynamic behavior of the system. The body-fixed reference coordinates are used for each body, for example the reference coordinates $\left\{C, \vec{E}_{0\,1}, \vec{E}_{0\,2}, \vec{E}_{0\,3}\right\}$ for the chassis body of the two-wheeled wheelchair. C is the origin center of mass for the chassis body. By applying the same concept to the other two bodies, their reference body-fixed coordinates become $\left\{C_1, \vec{E}_{1\,1}, \vec{E}_{1\,2}, \vec{E}_{1\,3}\right\}$ for the first wheel and $\left\{C_2, \vec{E}_{2\,1}, \vec{E}_{2\,2}, \vec{E}_{2\,3}\right\}$ for the second wheel. The applied moments at the center of mass of each body are assumed to be $\vec{M}^C$, with corresponding components $\vec{M}_{1x}^C, \vec{M}_{1y}^C, \vec{M}_{1z}^C$ in the three body coordinates for first wheel. The same can be done for the reaction forces $\vec{F}^C$ on the center of mass of the body and its corresponding components $\vec{F}_{1x}^C, \vec{F}_{1y}^C, \vec{F}_{1z}^C$ and similarly for the other parts. The contact point between the wheel and the motion surface is denoted point A. $\vec{F}_{1x}^A, \vec{F}_{1y}^A, \vec{F}_{1z}^A$ are the three main components of reaction force $\vec{F}^A$. The mass moment of inertia relative to a certain axis and with the index of the body number is written J_{xx_1}, which denotes the mass moment of inertia for the first body relative to the x-axis

and J_{yy_1}, J_{zz_1} relative to the y- and z-axes. The mass moments of inertia for the other bodies follow the same rule. Generally, the mass moments of inertia for the first and second wheels are $J_{xx_1} = J_{xx_2} = J_{zz_1} = J_{zz_2} = J_{xx} = J_{zz} = \frac{m_1 R^2}{4}$ but $J_{yy_1} = J_{yy_2} = J_{yy} = \frac{m_1 R^2}{2}$. The mass moment of inertia of the vehicle chassis can be calculated as $J_{zz_0} = \frac{m_0}{12}(L^2 + 4l^2)$, where L is the chassis length and $2l$ is the width. m_1 is the wheel's mass, m_0 is the mass of wheelchair's base and R is the wheel radius.

Application of the linear momentum and angular momentum theorems (2.46) and (2.50) to the three parts of the analyzed wheelchair design yields the following equations

For body (0)

$$m_0 \ddot{\vec{r}}_C = -F_{1x}^C \vec{E}_{0}{}_1 - F_{1y}^C \vec{E}_{0}{}_2 - F_{2x}^C \vec{E}_{0}{}_1 - F_{2y}^C \vec{E}_{0}{}_2 . \qquad (3.18)$$

Substituting the acceleration vector $\ddot{\vec{r}}_C$ into the previous equation with its equivalent components in the x- and y-directions in the global reference frame $\{0, \vec{e}_x, \vec{e}_y, \vec{e}_z\}$ gives

$$\ddot{\vec{r}}_C = \ddot{x}_C \vec{e}_x + \ddot{y}_C \vec{e}_y .$$

Also since

$$\vec{e}_x = \cos \psi \, \vec{E}_{0}{}_1 - \sin \psi \, \vec{E}_{0}{}_2 ,$$
$$\vec{e}_y = \cos \psi \, \vec{E}_{0}{}_2 + \sin \psi \, \vec{E}_{0}{}_1 ,$$

then equation (3.18) can be rewritten in the following form

$$m_0 \left[\ddot{x}_C \left(\cos \psi \, \vec{E}_{0}{}_1 - \sin \psi \, \vec{E}_{0}{}_2 \right) + \ddot{y}_C \left(\cos \psi \, \vec{E}_{0}{}_2 + \sin \psi \, \vec{E}_{0}{}_1 \right) \right]$$
$$= -F_{1x}^C \vec{E}_{0}{}_1 - F_{1y}^C \vec{E}_{0}{}_2 - F_{2x}^C \vec{E}_{0}{}_1 - F_{2y}^C \vec{E}_{0}{}_2 .$$

Separating the coefficients of the unit vectors $\vec{E}_{0}{}_1$ and $\vec{E}_{0}{}_2$ from both sides of the last equation gives

$$m_0(\ddot{x}_C \cos\psi + \ddot{y}_C \sin\psi) = -F_{1x}^C - F_{2x}^C,$$
$$m_0(-\ddot{x}_C \sin\psi + \ddot{y}_C \cos\psi) = -F_{1y}^C - F_{2y}^C.$$

Substituting the corresponding values of $\ddot{x}_C$ and $\ddot{y}_C$ according to equation (3.14) into the last equations yields

$$m_0(\ddot{x}_0 \cos\psi + \ddot{y}_0 \sin\psi - \rho\dot{\psi}^2) = -F_{1x}^C - F_{2x}^C \tag{3.19}$$

and

$$m_0(-\ddot{x}_0 \sin\psi + \ddot{y}_0 \cos\psi + \rho\ddot{\psi}) = -F_{1y}^C - F_{2y}^C. \tag{3.20}$$

Using the angular momentum law yields

$$
\begin{aligned}
\dot{\vec{D}}_C &= -\vec{M}_1^C - \vec{M}_2^C + \left(l\underset{0}{\vec{E}}_2\right) \times \left(-F_{1x}^C \underset{0}{\vec{E}}_1\right) + \left(-\rho\underset{0}{\vec{E}}_1\right) \times \left(-F_{1y}^C \underset{0}{\vec{E}}_2\right) \\
&\quad + \left(-l\underset{0}{\vec{E}}_2\right) \times \left(-F_{2x}^C \underset{0}{\vec{E}}_1\right) + \left(-\rho\underset{0}{\vec{E}}_1\right) \times \left(-F_{2y}^C \underset{0}{\vec{E}}_2\right) \\
&= -M_{1x}^C \underset{0}{\vec{E}}_1 - M_{1y}^C \underset{0}{\vec{E}}_2 - M_{1z}^C \underset{0}{\vec{E}}_3 - M_{2x}^C \underset{0}{\vec{E}}_1 - M_{2y}^C \underset{0}{\vec{E}}_2 - M_{2z}^C \underset{0}{\vec{E}}_3 \\
&\quad + lF_{1x}^C \underset{0}{\vec{E}}_3 + \rho F_{1y}^C \underset{0}{\vec{E}}_3 - lF_{2x}^C \underset{0}{\vec{E}}_3 + \rho F_{2y}^C \underset{0}{\vec{E}}_3 \\
&= -M_{1x}^C \underset{0}{\vec{E}}_1 - M_{1y}^C \underset{0}{\vec{E}}_2 - M_{1z}^C \underset{0}{\vec{E}}_3 - M_{2x}^C \underset{0}{\vec{E}}_1 - M_{2y}^C \underset{0}{\vec{E}}_2 - M_{2z}^C \underset{0}{\vec{E}}_3 \\
&\quad + l(F_{1x}^C - F_{2x}^C)\underset{0}{\vec{E}}_3 + \rho(F_{1y}^C + F_{2y}^C)\underset{0}{\vec{E}}_3.
\end{aligned}
\tag{3.21}
$$

On the other hand,

$$\vec{D}_C = \underset{0}{J}_{xx}\underset{0}{\omega}_x \underset{0}{\vec{E}}_1 + \underset{0}{J}_{yy}\underset{0}{\omega}_y \underset{0}{\vec{E}}_2 + \underset{0}{J}_{zz}\underset{0}{\omega}_z \underset{0}{\vec{E}}_3$$

and since the chassis body of the wheelchair only rotates about the vertical axis $\underset{0}{E}_3$ by angle ψ and does not rotate about the other axes, then $\underset{0}{\omega}_x = \underset{0}{\omega}_y = 0$ and therefore

$$\vec{D}_C = \underset{0}{J}_{zz}\underset{0}{\omega}_z \underset{0}{\vec{E}}_3 = \underset{0}{J}_{zz}\dot{\psi}\underset{0}{\vec{E}}_3.$$

The first time derivative of the last equation leads to

$$\dot{\vec{D}}_C = \underset{0}{J}_{zz}\ddot{\psi}\underset{0}{\vec{E}}_3 + \underset{0}{J}_{zz}\dot{\psi}\underset{0}{\dot{\vec{E}}}_3.$$

Since from the beginning of the analysis there is consideration motion in a plane $\dot{\vec{E}}_3 = \vec{\omega} \times \vec{E}_3 = \left(\dot{\psi}\vec{E}_3\right) \times \vec{E}_3 = \vec{0}$ and the last equation will be

$$\dot{\vec{D}}_C = \underset{0}{J_{zz}}\ddot{\psi}\vec{E}_3 \,. \tag{3.22}$$

A comparison of the coefficients of the unity vectors in equations (3.21) and (3.22) delivers the following equation

$$\underset{0}{J_{zz}}\ddot{\psi} = l(F_{1x}^C - F_{2x}^C) + \rho(F_{1y}^C + F_{2y}^C) - M_{1z}^C - M_{2z}^C \,. \tag{3.23}$$

For the right wheel (2)

$$m_1\ddot{\vec{r}}_{C_2} = F_{2x}^C\vec{E}_1 + F_{2y}^C\vec{E}_2 + F_{2x}^A\vec{E}_1 + F_{2y}^A\vec{E}_2 \,,$$

Since

$$\ddot{\vec{r}}_{C_2} = \ddot{x}_2\vec{e}_x + \ddot{y}_2\vec{e}_y \,,$$

then

$$
\begin{aligned}
&m_1\left(\ddot{x}_2\vec{e}_x + \ddot{y}_2\vec{e}_y\right)\\
&= m_1\left[\ddot{x}_2\left(\cos\psi\,\vec{E}_1 - \sin\psi\,\vec{E}_2\right) + \ddot{y}_2\left(\cos\psi\,\vec{E}_2 + \sin\psi\,\vec{E}_1\right)\right]\\
&= m_1(\ddot{x}_2\cos\psi + \ddot{y}_2\sin\psi)\vec{E}_1 + m_1(-\ddot{x}_2\sin\psi + \ddot{y}_2\cos\psi)\vec{E}_2\\
&= F_{2x}^C\vec{E}_1 + F_{2y}^C\vec{E}_2 + F_{2x}^A\vec{E}_1 + F_{2y}^A\vec{E}_2 \,.
\end{aligned}
$$

Comparing the coefficients of the unit vectors in the last equation, follows

$$
\begin{aligned}
m_1(\ddot{x}_2\cos\psi + \ddot{y}_2\sin\psi) &= F_{2x}^C + F_{2x}^A \,,\\
m_1(-\ddot{x}_2\sin\psi + \ddot{y}_2\cos\psi) &= F_{2y}^C + F_{2y}^A \,.
\end{aligned}
$$

Substituting the corresponding value of $\ddot{x}_2$ and $\ddot{y}_2$ from equation (3.14) into the last two equations results in

$$m_1\left(\ddot{x}_0\cos\psi + \ddot{y}_0\sin\psi + l\ddot{\psi}\right) = F_{2x}^C + F_{2x}^A \,, \tag{3.24}$$

$$m_1\left(-\ddot{x}_0\sin\psi + \ddot{y}_0\cos\psi + l\dot{\psi}^2\right) = F_{2y}^C + F_{2y}^A \,. \tag{3.25}$$

An application of the angular momentum law yields

$$
\begin{aligned}
\dot{\vec{D}}_{C_2} &= \vec{M}_2^C + \left(-R\vec{\underset{2}{E}}_3\right) \times \left(F_{2x}^A\vec{\underset{2}{E}}_1 + F_{2y}^A\vec{\underset{2}{E}}_2\right) \\
&= M_{2x}^C\vec{\underset{2}{E}}_1 + M_{2y}^C\vec{\underset{2}{E}}_2 + M_{2z}^C\vec{\underset{2}{E}}_3 - RF_{2x}^A\vec{\underset{2}{E}}_2 + RF_{2y}^A\vec{\underset{2}{E}}_1 \; .
\end{aligned}
\tag{3.26}
$$

On the other hand,

$$
\vec{D}_{C_2} = \underset{2}{J}_{xx}\underset{2}{\omega}_x\vec{\underset{2}{E}}_1 + \underset{2}{J}_{yy}\underset{2}{\omega}_y\vec{\underset{2}{E}}_2 + \underset{2}{J}_{zz}\underset{2}{\omega}_z\vec{\underset{2}{E}}_3 \; .
$$

Since the second wheel rotates about the vertical axis $\underset{2}{E}_3$ by angle ψ and around $\underset{2}{E}_2$ by angle φ_2, it follows that $\underset{2}{\omega}_y = \dot{\varphi}_2$, $\underset{2}{\omega}_z = \dot{\psi}$ and $\underset{2}{\omega}_x = 0$ in the previous equation, allowing it to be rewritten as follows

$$
\vec{D}_{C_2} = \underset{2}{J}_{yy}\dot{\varphi}_2\vec{\underset{2}{E}}_2 + \underset{2}{J}_{zz}\dot{\psi}\vec{\underset{2}{E}}_3 \; .
$$

The first time derivative of the last relationship is:

$$
\begin{aligned}
\dot{\vec{D}}_{C_2} &= \underset{2}{J}_{yy}\ddot{\varphi}_2\vec{\underset{2}{E}}_2 + \underset{2}{J}_{yy}\dot{\varphi}_2\dot{\vec{\underset{2}{E}}}_2 + \underset{2}{J}_{zz}\ddot{\psi}\vec{\underset{2}{E}}_3 + \underset{2}{J}_{zz}\dot{\psi}\dot{\vec{\underset{2}{E}}}_3 \; , \\
&= \underset{2}{J}_{yy}\ddot{\varphi}_2\vec{\underset{2}{E}}_2 + \underset{2}{J}_{yy}\dot{\varphi}_2\left(\vec{\underset{2}{\omega}} \times \vec{\underset{2}{E}}_2\right) + \underset{2}{J}_{zz}\ddot{\psi}\vec{\underset{2}{E}}_3 + \underset{2}{J}_{zz}\dot{\psi}\left(\vec{\underset{2}{\omega}} \times \vec{\underset{2}{E}}_3\right) \; , \\
&= \underset{2}{J}_{yy}\ddot{\varphi}_2\vec{\underset{2}{E}}_2 + \underset{2}{J}_{yy}\dot{\varphi}_2\left[\left(\dot{\varphi}_2\vec{\underset{2}{E}}_2 + \dot{\psi}\vec{\underset{2}{E}}_3\right) \times \vec{\underset{2}{E}}_2\right] + \underset{2}{J}_{zz}\ddot{\psi}\vec{\underset{2}{E}}_3 \\
&\qquad + \underset{2}{J}_{zz}\dot{\psi}\left[\left(\dot{\varphi}_2\vec{\underset{2}{E}}_2 + \dot{\psi}\vec{\underset{2}{E}}_3\right) \times \vec{\underset{2}{E}}_3\right] \; , \\
&= \underset{2}{J}_{yy}\ddot{\varphi}_2\vec{\underset{2}{E}}_2 + \underset{2}{J}_{zz}\ddot{\psi}\vec{\underset{2}{E}}_3 - \underset{2}{J}_{yy}\dot{\varphi}_2\dot{\psi}\vec{\underset{2}{E}}_1 + \underset{2}{J}_{zz}\dot{\psi}\dot{\varphi}_2\vec{\underset{2}{E}}_1 \; .
\end{aligned}
\tag{3.27}
$$

A comparison of the unit vector coefficients in equations (3.26) and (3.27) yields the following differential equations of motion

$$
\left(\underset{2}{J}_{zz} - \underset{2}{J}_{yy}\right)\dot{\psi}\dot{\varphi}_2 = M_{2x}^C + RF_{2y}^A \; ,
\tag{3.28}
$$

$$
\underset{2}{J}_{yy}\ddot{\varphi}_2 = M_{2y}^C - RF_{2x}^A \; ,
\tag{3.29}
$$

$$
\underset{2}{J}_{zz}\ddot{\psi} = M_{2Z}^C \; .
\tag{3.30}
$$

The reaction force component F_{2y}^A at point A can be found from equation (3.28) as follows

$$F_{2y}^A = \frac{1}{R}\left[\left(J_{zz} - J_{yy}\right)\dot\psi\dot\varphi_2 - M_{2x}^C\right] \tag{3.31}$$

and the reaction force component F_{2x}^A from equation (3.29) becomes

$$F_{2x}^A = \frac{1}{R}\left(M_{2y}^C - J_{yy}\ddot\varphi_2\right). \tag{3.32}$$

By substituting equations (3.31) and (3.32) into equations (3.24)and (3.25) yields the following relationships

$$Rm_1\left(\ddot x_0 \cos\psi + \ddot y_0 \sin\psi + l\ddot\psi\right) = RF_{2x}^C + M_{2y}^C - J_{yy}\ddot\varphi_2 \,, \tag{3.33}$$

$$Rm_1\left(-\ddot x_0 \sin\psi + \ddot y_0 \cos\psi + l\dot\psi^2\right)$$
$$= RF_{2y}^C + \left(J_{zz} - J_{yy}\right)\dot\psi\dot\varphi_2 - M_{2x}^C \tag{3.34}$$

and

$$J_{zz}\ddot\psi = M_{2Z}^C \,. \tag{3.35}$$

The last three equations (3.33), (3.34) and (3.35) represent the dynamic model and describe the dynamic behavior of the right wheel (2) of the wheelchair with a two-wheeled steerable moving unit. The geometry of the wheelchair under investigation as well as the kinematic behavior derived from its movement shows that the difference between the right and left wheels is the location of the wheel relative to the center of the vehicle, i.e. center of mass C. Therefore, the dynamic model of the first wheel can be obtained by replacing the dimension $-l$ in place of l in the last three equations as follows

For the left wheel (1)

$$Rm_1\left(\ddot x_0 \cos\psi + \ddot y_0 \sin\psi - l\ddot\psi\right) = RF_{1x}^C + M_{1y}^C - J_{yy}\ddot\varphi_1 \,, \tag{3.36}$$

$$Rm_1\left(-\ddot{x}_0 \sin\psi + \ddot{y}_0 \cos\psi - l\dot{\psi}^2\right)$$
$$= RF_{1y}^C + \left(\underset{1}{J_{zz}} - \underset{1}{J_{yy}}\right)\dot{\psi}\dot{\varphi}_1 - M_{1x}^C\,, \tag{3.37}$$

and

$$\underset{1}{J_{zz}}\ddot{\psi} = M_{1Z}^C\,. \tag{3.38}$$

From the beginning of the dynamic analysis in this section, it has been assumed that the driving moments are known. The value of the moment is the driving torque of the electric motor or the effort expended by the user's hand in the case of manually driven wheelchairs, since $M_{1y} = M_1(t)$ and $M_{2y} = M_2(t)$. The driving situation and the resulting force, which determine the direction of the motion, will be not discussed here.

The problem in applying the synthetic method to finding a dynamic model of the mechanical system is simply the need to find the equivalents and corresponding values of the internal reaction force components between the connected mechanical parts, such as the two wheels and the wheelchair's chassis in the modeled system. Therefore, the corresponding values of the internal reaction forces and moments are F_{1x}^C, F_{1y}^C, F_{2x}^C, F_{2y}^C, M_{1x}^C, M_{2x}^C, M_{1Z}^C and M_{2Z}^C. It is important to mention here that this method for analyzing the dynamic behavior of the mechanical systems is needed to determine the internal forces and moments for design requirements. By applying both kinds of LAGRANGE equations or the APPELL equation, there is no longer a need to find the corresponding values of the internal forces and moments. In addition to the previously mentioned undetermined eight internal forces and moments, there are also undetermined motion coordinates x_0, y_0, ψ, φ_1 and φ_2. This means that there are thirteen unknowns that must be determined or replaced by their corresponding values in order to easily and concisely define the dynamic model of the two-wheeled wheelchair.

The undefined internal reaction moments components M_{1x}^C and M_{2x}^C can be determined by evaluating the rest of the unknown parameters in the dynamic model. That will help to reduce the number of unknowns to eleven; in other words, elimination of the undefined parameters in the dynamic model will reduce the required total number of equations needing to be solved in order to evaluate the dynamics of the system. Both the first and the second wheels are identical in their mechanical parameters and their

dimensions, which means that $\underset{1}{J_{zz}} = \underset{2}{J_{zz}} = J_{zz} = \frac{m_1 R^2}{4}$ for equations (3.35) and (3.38). Both equations will be equal and therefore $M_{1Z}^C = M_{2Z}^C = M_Z^C$. The internal reaction force components F_{1y}^C and F_{2y}^C are on the same working line, meaning it is not possible to determine their corresponding values separately but they can be determined as a summation, where $F_y^C = F_{1y}^C + F_{2y}^C$. It follows then for the latter assumptions that the number of unknowns can be further reduced to nine undetermined parameters, which can be estimated using equations (3.19), (3.20), (3.23), (3.33), (3.35)≡(3.38), (3.36) in addition to the three kinematic constraints in equation (3.16). Using the last assumptions regarding the internal reaction forces and moments, the model's differential equations (3.19), (3.20), (3.23), (3.33), (3.35)≡(3.38), (3.36) can be rewritten in the following forms

$$m_0\left(\ddot{x}_0 \cos\psi + \ddot{y}_0 \sin\psi - \rho\dot{\psi}^2\right) = -F_{1x}^C - F_{2x}^C , \tag{3.39}$$

$$m_0\left(-\ddot{x}_0 \sin\psi + \ddot{y}_0 \cos\psi + \rho\ddot{\psi}\right) = -F_y^C , \tag{3.40}$$

$$\underset{0}{J_{zz}}\ddot{\psi} = l(F_{1x}^C - F_{2x}^C) + \rho F_y^C - 2M_z^C , \tag{3.41}$$

$$Rm_1\left(\ddot{x}_0 \cos\psi + \ddot{y}_0 \sin\psi + l\ddot{\psi}\right) = RF_{2x}^C + M_2^C - J_{yy}\ddot{\varphi}_2 , \tag{3.42}$$

$$Rm_1\left(\ddot{x}_0 \cos\psi + \ddot{y}_0 \sin\psi - l\ddot{\psi}\right) = RF_{1x}^C + M_1^C - J_{yy}\ddot{\varphi}_1 , \tag{3.43}$$

$$J_{zz}\ddot{\psi} = M_Z^C . \tag{3.44}$$

The components of the internal reaction forces F_{1x}^C and F_{2x}^C can be estimated from equations (3.43) and (3.42), respectively, as follows

$$F_{1x}^C = m_1\left(\ddot{x}_0 \cos\psi + \ddot{y}_0 \sin\psi - l\ddot{\psi}\right) - \frac{M_1^C}{R} + \frac{J_{yy}}{R}\ddot{\varphi}_1 , \tag{3.45}$$

$$F_{2x}^C = m_1\left(\ddot{x}_0 \cos\psi + \ddot{y}_0 \sin\psi + l\ddot{\psi}\right) - \frac{M_2^C}{R} + \frac{J_{yy}}{R}\ddot{\varphi}_2 . \tag{3.46}$$

Substituting the corresponding values of the internal reaction forces F_{1x}^C and F_{2x}^C from equations (3.45) and (3.46) into equation (3.39) yields the following relationship

$$m_0\left(\ddot{x}_0 \cos\psi + \ddot{y}_0 \sin\psi - \rho\dot{\psi}^2\right)$$

$$= -m_1\left(\ddot{x}_0 \cos\psi + \ddot{y}_0 \sin\psi - l\ddot{\psi}\right) + \frac{M_1^C}{R} - \frac{J_{yy}}{R}\ddot{\varphi}_1$$

$$- m_1\left(\ddot{x}_0 \cos\psi + \ddot{y}_0 \sin\psi + l\ddot{\psi}\right) + \frac{M_2^C}{R} - \frac{J_{yy}}{R}\ddot{\varphi}_2 , \qquad (3.47)$$

$$(m_0 + 2m_1)\ddot{x}_0 \cos\psi + (m_0 + 2m_1)\ddot{y}_0 \sin\psi - m_0\rho\dot{\psi}^2$$

$$+ \frac{J_{yy}}{R}(\ddot{\varphi}_1 + \ddot{\varphi}_2) = \frac{1}{R}(M_1^C + M_2^C) .$$

Since $\underset{1}{J_{yy}} = \underset{2}{J_{yy}} = J_{yy} = \frac{m_1 R^2}{2}$ and the total mass of the wheelchair parts $m_t = m_0 + 2m_1$, then

$$Rm_t(\ddot{x}_0 \cos\psi + \ddot{y}_0 \sin\psi) - m_0\rho R\dot{\psi}^2 + J_{yy}(\ddot{\varphi}_1 + \ddot{\varphi}_2)$$

$$= M_1^C + M_2^C . \qquad (3.48)$$

In order to eliminate the internal reaction force components F_{1x}^C , F_{2x}^C , F_y^C and moment component M_z^C from the derived dynamic model, the equations (3.40), (3.44), (3.45) and (3.46) are substituted in equation (3.41), yielding

$$\underset{0}{J_{zz}}\ddot{\psi} = l\left(-2m_1 l\ddot{\psi} + \frac{1}{R}(M_2^C - M_1^C) + \frac{J_{yy}}{R}(\ddot{\varphi}_1 - \ddot{\varphi}_2)\right)$$

$$+ m_0\rho(\ddot{x}_0 \sin\psi - \ddot{y}_0 \cos\psi) - m_0\rho^2\ddot{\psi} - 2J_{zz}\ddot{\psi} ,$$

$$\left(\underset{0}{J_{zz}} + 2J_{zz} + m_0\rho^2 + 2m_1 l^2\right)\ddot{\psi} - m_0\rho(\ddot{x}_0 \sin\psi - \ddot{y}_0 \cos\psi)$$

$$+ \frac{l}{R}J_{yy}(\ddot{\varphi}_2 - \ddot{\varphi}_1) = \frac{l}{R}(M_2^C - M_1^C) .$$

From the assumption that $\bar{J}_{zz} = \underset{0}{J_{zz}} + 2J_{zz} + m_0\rho^2 + 2m_1 l^2$, then the last equation can be written in the following form

$$\bar{J}_{zz}\ddot{\psi} - m_0\rho(\ddot{x}_0 \sin\psi - \ddot{y}_0 \cos\psi) + \frac{l}{R}J_{yy}(\ddot{\varphi}_2 - \ddot{\varphi}_1)$$

$$= \frac{l}{R}(M_2^C - M_1^C) . \qquad (3.49)$$

In the next few steps, derivation of the equations is used to eliminate the parameters $\ddot{x}_0$ and $\ddot{y}_0$ from the dynamic system model. Therefore, the differential equations of the dynamic model will only be functions of φ_1,

φ_2, ψ and the corresponding time derivatives in addition to the known driving torques M_1^C and M_2^C. Based on the kinematic and geometrical constraints of the system in equation (3.17) and after substituting the corresponding values of $\ddot{x}_0$ and $\ddot{y}_0$ into equations (3.48) and (3.49), it appears that the differential equations of the dynamic model will be

$$m_t R\left(l\ddot{\psi} + R\ddot{\varphi}_1\right) - m_0 \rho R\dot{\psi}^2 + J_{yy}(\ddot{\varphi}_1 + \ddot{\varphi}_2) = M_1^C + M_2^C, \qquad (3.50)$$

$$\bar{J}_{zz}\ddot{\psi} + m_0\rho\left(l\dot{\psi}^2 + R\dot{\psi}\dot{\varphi}_1\right) + \frac{l}{R}J_{yy}(\ddot{\varphi}_2 - \ddot{\varphi}_1) = \frac{l}{R}(M_2^C - M_1^C), \qquad (3.51)$$

since

$$\ddot{x}_0 \cos\psi + \ddot{y}_0 \sin\psi$$
$$= l\ddot{\psi}\cos^2\psi - l\dot{\psi}^2\cos\psi\sin\psi + R\ddot{\varphi}_1\cos^2\psi - R\dot{\varphi}_1\dot{\psi}\cos\psi\sin\psi$$
$$+ l\ddot{\psi}\sin^2\psi + l\dot{\psi}^2\cos\psi\sin\psi + R\ddot{\varphi}_1\sin^2\psi + R\dot{\varphi}_1\dot{\psi}\cos\psi\sin\psi$$
$$= l\ddot{\psi} + R\ddot{\varphi}_1.$$

and

$$\ddot{x}_0 \sin\psi - \ddot{y}_0 \cos\psi$$
$$= l\ddot{\psi}\cos\psi\sin\psi - l\dot{\psi}^2\sin^2\psi + R\ddot{\varphi}_1\cos\psi\sin\psi - R\dot{\varphi}_1\dot{\psi}\sin^2\psi$$
$$- l\ddot{\psi}\cos\psi\sin\psi - l\dot{\psi}^2\cos^2\psi - R\ddot{\varphi}_1\cos\psi\sin\psi - R\dot{\varphi}_1\dot{\psi}\cos^2\psi$$
$$= -l\dot{\psi}^2 - R\dot{\varphi}_1\dot{\psi}.$$

Now, in order to reduce the dynamic model to eliminate parameter $\ddot{\varphi}_2$ from the last two differential equations, the corresponding value of $\ddot{\varphi}_2$ from equation (3.17) can be substituted into equations (3.50) and (3.51), respectively, which yields the following compact forms of the dynamic model for a two-wheeled wheelchair

$$m_t R\left(l\ddot{\psi} + R\ddot{\varphi}_1\right) - m_0 \rho R\dot{\psi}^2 + 2J_{yy}\left(\ddot{\varphi}_1 + \frac{l}{R}\ddot{\psi}\right) = M_1^C + M_2^C,$$

$$\left(2J_{yy} + m_t R^2\right)\ddot{\varphi}_1 + \left(2J_{yy}\frac{l}{R} + m_t Rl\right)\ddot{\psi} - m_0 \rho R\dot{\psi}^2 = M_1^C + M_2^C.$$

Also, by assuming that $\bar{J}_{yy} = 2J_{yy} + m_t R^2$ in the last equation, it follows that:

$$\bar{J}_{yy}\ddot{\varphi}_1 + \bar{J}_{yy}\frac{l}{R}\ddot{\psi} - m_0\rho R\dot{\psi}^2 = M_1^C + M_2^C. \qquad (3.52)$$

Using the second differential equation of the dynamic model

$$\bar{J}_{zz}\ddot{\psi} + m_0\rho\left(l\dot{\psi}^2 + R\dot{\psi}\dot{\varphi}_1\right) + 2J_{yy}\frac{l^2}{R^2}\ddot{\psi} = \frac{l}{R}(M_2^C - M_1^C),$$

$$\left(\bar{J}_{zz} + 2J_{yy}\frac{l^2}{R^2}\right)\ddot{\psi} + m_0\rho\dot{\psi}\left(l\dot{\psi} + R\dot{\varphi}_1\right) = \frac{l}{R}(M_2^C - M_1^C),$$

and assuming that $\bar{J} = \bar{J}_{zz} + 2J_{yy}\frac{l^2}{R^2}$ in the last equation results in

$$\bar{J}\ddot{\psi} + m_0\rho\dot{\psi}\left(l\dot{\psi} + R\dot{\varphi}_1\right) = \frac{l}{R}(M_2^C - M_1^C). \qquad (3.53)$$

Finally, this means that

$$\ddot{\varphi}_2 = \ddot{\varphi}_1 + \frac{2l}{R}\ddot{\psi}. \qquad (3.54)$$

From the last three differential equations (3.52), (3.53) and (3.54) of the dynamic model of a two-wheeled wheelchair, it is possible to estimate the motion of the vehicle in a defined period of time by using available numerical integration software. It is obvious that parameters φ_1, ψ, M_1^C and M_2^C are the basic parameters for this calculation and they are essential to compute the remainder of the system parameters for the dynamic model. Understanding the kinematic and dynamic behavior and also finding the internal reaction forces between the different mechanical sub-assemblies of the wheelchair can be determined directly through the previous derivation for the dynamic model, either by direct implementation or after integrating over the required operation time.

3.3 The suggested method for modeling the four-wheel Mecanum vehicle

This section discusses the four-wheel Mecanum vehicle concept from different points of view. Many scientific studies and sources have been published regarding the analysis of the four-wheel Mecanum vehicle, covering both kinematics and dynamics. The behavior of the four-wheel

Mecanum vehicle has been presented in many different works referenced here [18, 27, 90, 95, 129, 137, 154 and 157] beside WADA [140-153].

The kinematic and dynamic models of the four-wheel vehicle will be briefly discussed here, see Figure 3.8. This type of vehicle consists of two axles, each carrying two Mecanum wheels and driven using separate electric motors. The front axle is offset from the center of the vehicle C by distance ρ_1 and the rear axle is located behind the center point C by distance ρ_2. The width of the vehicle in most of cases studied is the same for the left and right sides, so it will be denoted here as $2l$. To simplify the study, the center of the vehicle is theoretically located equidistant from the left and right sides of the vehicle. The principle of operation of Mecanum vehicles mainly depends on the configuration of the wheel. The Mecanum vehicle as a locomotion system requires four Mecanum wheels, which can be classified into two categories:

1. Mecanum wheel with an inclination angle of 45° (referred to here as type A).
2. Mecanum wheel with an inclination angle of -45° (referred to here as type B).

Here, the inclination angle is the angle between the velocity vector of the roller and the relative velocity vector of the wheel. The inclination angles of the circumference rollers are denoted by angles (δ_1, δ_2, δ_3, δ_4) as shown in Figure 3.8 and carried through to the rest of the figures in this section.

It is important to remember that commonly used Mecanum wheels have standard inclination angles of either 45° or -45°. Mecanum vehicles typically employed in standard industrial applications use four wheels, namely two wheels of each type and one wheel of each type is typically located on each axis. Thus, the same wheel type is fixed on diagonal wheel positions in order to provide the required movement effect, referred to as the Mecanum effect. By applying the rotation moments on the four wheels, the traction force between the rollers in contact with the surface is split into two components. One component pushes the vehicle to move in the required direction and the second component provides opposing force components onto the vehicle chassis. Changing the installation position or installing the same wheel type on the same axle will cause significant irregularities during motion. Put simply, the vehicle will not be able to move along acceptable tracks and will not exhibit the expected maneuverability.
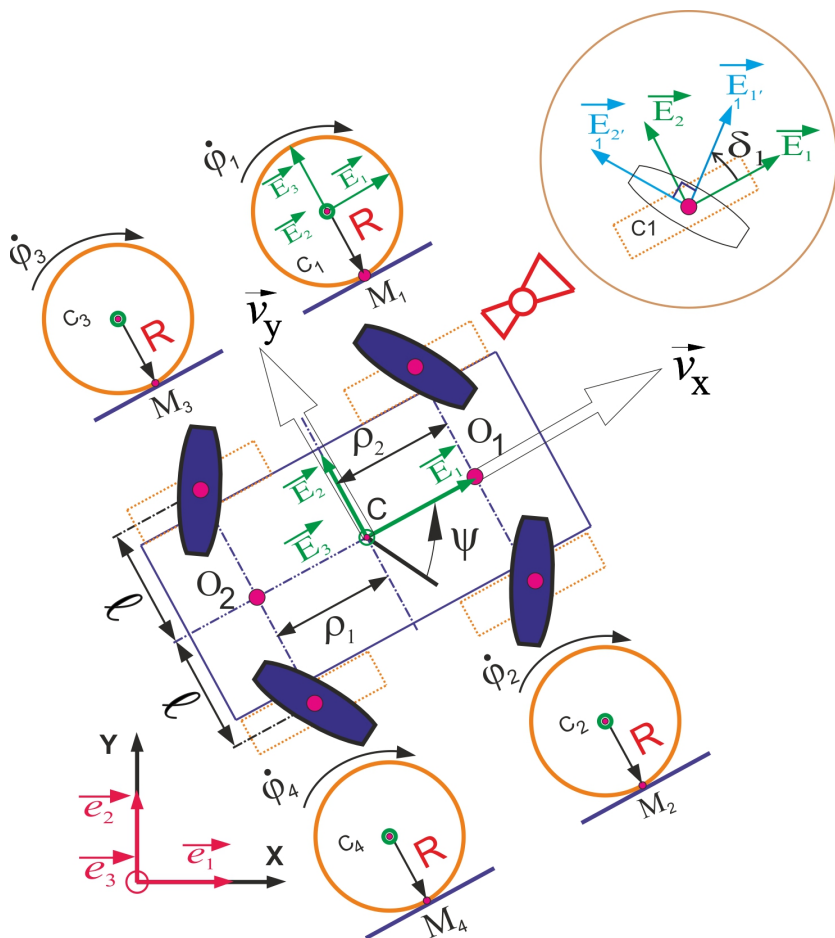
Figure 3.8 A sketch drawing of a four-wheel Mecanum vehicle – kinematic analysis

This study does not take into account any slip between the rollers of the Mecanum wheels and the surface during motion. This means that all applied moments from the electric motors will be converted into traction force between the wheels and the surface. There is also no need to assume an efficiency factor for the transmission of force between the rollers and the surface. Additionally, the motion is assumed to be on a flat surface without

any kind of obstacles, as there would be a loss of traction force while having to overcome those obstacles. Consideration of inclination angles different than 45° or -45° would lead to unexpected behavior during motion, especially if the cross-axle wheels were to have different inclination angles. Because the study here is a theoretical study, the common disadvantages of the Mecanum-wheel vehicle will not be taken into account when generating the kinematic or dynamic models. It is commonly known that the Mecanum-wheel vehicle suffers from a loss of kinetic energy during motion because of the slip that occurs between the plane surface and the rollers of the wheel. Any correction for this effect would be mathematically insufficient, which means the solution must come by a change in mechanical design.

Definition of the diagram symbols and orientation vectors

The diagram in Figure 3.8 gives an overhead view of the four-wheel Mecanum vehicle with additional side views of each of the Mecanum wheels located next to the corresponding wheel in the top view.

$\vec{e}_1, \vec{e}_2, \vec{e}_3$ are the unit vectors of the inertial coordinate system in the direction of the main x-, y- and z-axes in the motion diagram.

$\vec{E}_1, \vec{E}_2, \vec{E}_3$ are the unit vectors of the body-fixed coordinates in the directions of the main x-, y- and z-axes but relative to the moving body. These unity vectors are used to describe the movement of the vehicle center and the rotation centers of the wheels in their respective side views.

$\vec{E}_{1_i}, \vec{E}_{2_i}$ and $\vec{E}_{3_i}$ are unit vectors, located in the center of the rollers, where i represents the wheel number from 1 to 4. The unit vectors in this case are inclined by an angle of 45° or -45° corresponding to the type of wheel. The unit vectors point in the direction of the main x-, y-and z-axes.

O_1, O_2 are the middle points of the front and rear axles of the vehicle, respectively. C is the center of mass of the vehicle. C_i is the center of mass of the Mecanum wheel as well as its center of rotation. The variable n can assume a value in the range 1…4 corresponding to the wheel number. During motion, the Mecanum wheel rotates by angular velocity $\dot{\varphi}_i$. The wheel radius R is constant for all four wheels.

M_i is the contact point between the external surface of the wheel rollers and the motion surface located directly beneath the wheel center C_i. The suffix i corresponds to wheel number (1…4).

For the four-wheel Mecanum vehicle, it is assumed that the vehicle rotate about its center of mass C by angle ψ. The width of the vehicle is $2l$ and the distance between the vehicle center of mass C to the center of mass of the front axle O_1 is the distance ρ_1 and the distance between C and the center of mass of the rear axle O_2 is ρ_2.

The kinematic constraints and the dynamic model of the four-wheel Mecanum vehicle are determined using two different methods. The first method is the suggested procedure for modeling the kinematics and the dynamics of the four-wheel Mecanum vehicle using the principles of nonholonomic mechanics. A second method has been used in different references for a while. It is simple and suitable for control applications but it exhibits limited accuracy in describing the motion of the vehicle. The rest of this section briefly discusses the suggested method, first with respect to kinematics and then to dynamics.

3.3.1 The kinematic constraints

The general Mecanum vehicle has three degrees of freedom: translation in the x-y-plane and rotation about the z-axis. Movement of the center of the vehicle is denoted using displacements x_C, y_C and rotation is described using angular displacement ψ. These three parameters must be calculated in order to define the exact position of the vehicle center. The geometric constraints of the four-wheel Mecanum vehicle can be described using equations (3.55)…(3.62)

$$x_{C_1} = x_C + \rho_2 \cos \psi - l \sin \psi \tag{3.55}$$

$$y_{C_1} = y_C + \rho_2 \sin \psi + l \cos \psi \tag{3.56}$$

$$x_{C_2} = x_C + \rho_2 \cos \psi + l \sin \psi \tag{3.57}$$

$$y_{C_2} = y_C + \rho_2 \sin \psi - l \cos \psi \tag{3.58}$$

$$x_{C_3} = x_C - \rho_1 \cos \psi - l \sin \psi \tag{3.59}$$

$$y_{C_3} = y_C - \rho_1 \sin \psi + l \cos \psi \tag{3.60}$$

$$x_{C_4} = x_C - \rho_1 \cos \psi + l \sin \psi \tag{3.61}$$

$$y_{C_4} = y_C - \rho_1 \sin \psi - l \cos \psi \,. \tag{3.62}$$

The Mecanum vehicle under investigation has four wheels, the motion of which is determined by x_{C_i}, y_{C_i}, ψ and φ_{C_i}, where i is the wheel number. In total, the four-wheel Mecanum vehicle has 15 different parameters to describe its motion on the plane.

The kinematic constraints for the four Mecanum wheels are

$$\dot{\vec{r}}_{M_1} \cdot \vec{E}_{\underset{1}{2}} = 0 \tag{3.63}$$

$$\dot{\vec{r}}_{M_2} \cdot \vec{E}_{\underset{2}{2}} = 0 \tag{3.64}$$

$$\dot{\vec{r}}_{M_3} \cdot \vec{E}_{\underset{3}{2}} = 0 \tag{3.65}$$

$$\dot{\vec{r}}_{M_4} \cdot \vec{E}_{\underset{4}{2}} = 0 \,. \tag{3.66}$$

Based on EULER's equation (2.13), it follows that

$$\dot{\vec{r}}_{M_1} = \vec{v}_{M_1} = \dot{\vec{r}}_{C_1} + \vec{\omega}_1 \times \overrightarrow{C_1 M_1} \,. \tag{3.67}$$

Since

$$\begin{aligned}
\dot{\vec{r}}_{C_1} &= \dot{x}_{C_1} \vec{e}_1 + \dot{y}_{C_1} \vec{e}_2 \\
&= (\dot{x}_C - \rho_2 \dot{\psi} \sin \psi - l \dot{\psi} \cos \psi) \vec{e}_1 \\
&+ (\dot{y}_C + \rho_2 \dot{\psi} \cos \psi - l \dot{\psi} \sin \psi) \vec{e}_2
\end{aligned} \tag{3.68}$$

and

$$\vec{\omega}_1 = \dot{\psi} \vec{E}_3 + \dot{\varphi}_1 \vec{E}_2 \;; \overrightarrow{C_1 M_1} = -R \vec{E}_3 \,, \tag{3.69}$$

substituting equations (3.68) and (3.69) into equation (3.67) yields

$$\dot{\vec{r}}_{M_1} = \left(\dot{x}_C - \rho_2\dot{\psi}\sin\psi - l\dot{\psi}\cos\psi\right)\vec{e}_1$$
$$+ \left(\dot{y}_C + \rho_2\dot{\psi}\cos\psi - l\dot{\psi}\sin\psi\right)\vec{e}_2$$
$$+ \left(\dot{\varphi}_1\vec{E}_2 + \dot{\psi}\vec{E}_3\right)\times\left(-R\vec{E}_3\right) \tag{3.70}$$
$$= \left(\dot{x}_C - \rho_2\dot{\psi}\sin\psi - l\dot{\psi}\cos\psi\right)\vec{e}_1$$
$$+ \left(\dot{y}_C + \rho_2\dot{\psi}\cos\psi - l\dot{\psi}\sin\psi\right)\vec{e}_2 - R\dot{\varphi}_1\,\vec{E}_1\,.$$

By applying the cross-product rules to this case, then the local roller fixed coordinates $(\vec{E}_{1'},\vec{E}_{2'},\vec{E}_{3'})$ for the first Mecanum wheel in Figure 3.8, which is in direct contact with the motion surface, can be represented as a function of coordinates $(\vec{E}_1,\vec{E}_2,\vec{E}_3)$ with respect to the wheel center of mass as shown in Figure 3.9 as follows
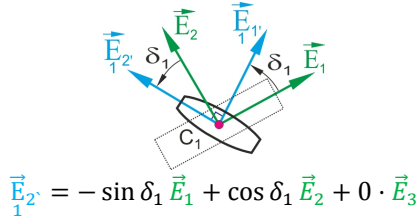
$$\vec{E}_{2'} = -\sin\delta_1\,\vec{E}_1 + \cos\delta_1\,\vec{E}_2 + 0\cdot\vec{E}_3$$

Figure 3.9 Analysis of local unit vector $\vec{E}_{2'}$ in the roller relative to the coordinates $(\vec{E}_1,\vec{E}_2,\vec{E}_3)$ with respect to the center of mass

$$\vec{E}_{1'} = \cos\delta_1\,\vec{E}_1 + \sin\delta_1\,\vec{E}_2 + 0\cdot\vec{E}_3\,,$$
$$\vec{E}_{2'} = -\sin\delta_1\,\vec{E}_1 + \cos\delta_1\,\vec{E}_2 + 0\cdot\vec{E}_3\,, \tag{3.71}$$
$$\vec{E}_{3'} = 0\cdot\vec{E}_1 + 0\cdot\vec{E}_2 + 1\cdot\vec{E}_3\,.$$

Converting center-of-mass-fixed coordinates $(\vec{E}_1,\vec{E}_2,\vec{E}_3)$ into global coordinates $(\vec{e}_1,\vec{e}_2,\vec{e}_3)$ results in

$$\vec{E}_1 = \cos\psi\,\vec{e}_1 + \sin\psi\,\vec{e}_2 + 0\cdot\vec{e}_3\,,$$
$$\vec{E}_2 = -\sin\psi\,\vec{e}_1 + \cos\psi\,\vec{e}_2 + 0\cdot\vec{e}_3\,, \tag{3.72}$$
$$\vec{E}_3 = 0\cdot\vec{e}_1 + 0\cdot\vec{e}_2 + 1\cdot\vec{e}_3\,,$$

therefore,

$$\begin{pmatrix} \vec{E}_1 \\ \vec{E}_2 \\ \vec{E}_3 \end{pmatrix} = \begin{pmatrix} \cos\psi & \sin\psi & 0 \\ -\sin\psi & \cos\psi & 0 \\ 0 & 0 & 1 \end{pmatrix} \begin{pmatrix} \vec{e}_1 \\ \vec{e}_2 \\ \vec{e}_3 \end{pmatrix}. \tag{3.73}$$

This means matrix $(\vec{e}_1, \vec{e}_2, \vec{e}_3)$ can be determined from the inverse of equation (3.73) as follows

$$\begin{pmatrix} \vec{e}_1 \\ \vec{e}_2 \\ \vec{e}_3 \end{pmatrix} = \begin{pmatrix} \cos\psi & -\sin\psi & 0 \\ \sin\psi & \cos\psi & 0 \\ 0 & 0 & 1 \end{pmatrix} \begin{pmatrix} \vec{E}_1 \\ \vec{E}_2 \\ \vec{E}_3 \end{pmatrix}. \tag{3.74}$$

Writing the matrix in equation form

$$\begin{aligned} \vec{e}_1 &= \cos\psi\, \vec{E}_1 - \sin\psi\, \vec{E}_2 + 0 \cdot \vec{E}_3\,, \\ \vec{e}_2 &= \sin\psi\, \vec{E}_1 + \cos\psi\, \vec{E}_2 + 0 \cdot \vec{E}_3\,, \\ \vec{e}_3 &= 0 \cdot \vec{E}_1 + 0 \cdot \vec{E}_2 + 1 \cdot \vec{E}_3\,, \end{aligned} \tag{3.75}$$

and analyzing unit vectors $\vec{e}_1$ and $\vec{e}_2$ in equation (3.70) using equation (3.75), it follows that

$$\begin{aligned} \dot{\vec{r}}_{M_1} &= (\dot{x}_C - \rho_2\dot{\psi}\sin\psi - l\dot{\psi}\cos\psi) \cdot (\cos\psi\, \vec{E}_1 - \sin\psi\, \vec{E}_2 + 0 \cdot \vec{E}_3) \\ &+ (\dot{y}_C + \rho_2\dot{\psi}\cos\psi - l\dot{\psi}\sin\psi) \cdot (\sin\psi\, \vec{E}_1 + \cos\psi\, \vec{E}_2 + 0 \cdot \vec{E}_3) \\ &\quad - R\dot{\varphi}_1\, \vec{E}_1\,. \end{aligned} \tag{3.76}$$

Applying the scalar product rules and substituting equations (3.76) and (3.71) into the kinematic constraint equation (3.63) results in

$$
\begin{aligned}
\dot{\vec{r}}_{M_1} \cdot \vec{E}_{2^{^{`}}_1} &= \{ (\dot{x}_C - \rho_2 \dot{\psi} \sin\psi - l\dot{\psi} \cos\psi) \\
&\quad \cdot (\cos\psi\, \vec{E}_1 - \sin\psi\, \vec{E}_2 + 0 \cdot \vec{E}_3) \\
&\quad + (\dot{y}_C + \rho_2 \dot{\psi} \cos\psi - l\dot{\psi} \sin\psi) \\
&\quad \cdot (\sin\psi\, \vec{E}_1 + \cos\psi\, \vec{E}_2 + 0 \cdot \vec{E}_3) - R\dot{\varphi}_1\, \vec{E}_1 \} \\
&\quad \cdot \{ -\sin\delta_1\, \vec{E}_1 + \cos\delta_1\, \vec{E}_2 + 0 \cdot \vec{E}_3 \} \\
&= \{ [(\dot{x}_C - \rho_2 \dot{\psi} \sin\psi - l\dot{\psi} \cos\psi) \cos\psi \\
&\quad + (\dot{y}_C + \rho_2 \dot{\psi} \cos\psi - l\dot{\psi} \sin\psi) \sin\psi - R\dot{\varphi}_1] \vec{E}_1 \\
&\quad + [-(\dot{x}_C - \rho_2 \dot{\psi} \sin\psi - l\dot{\psi} \cos\psi) \sin\psi \\
&\quad + (\dot{y}_C + \rho_2 \dot{\psi} \cos\psi - l\dot{\psi} \sin\psi) \cos\psi] \vec{E}_2 \} \\
&\quad \cdot \{ -\sin\delta_1\, \vec{E}_1 + \cos\delta_1\, \vec{E}_2 + 0 \cdot \vec{E}_3 \} \\
&= \{ [\dot{x}_C \cos\psi - l\dot{\psi} + \dot{y}_C \sin\psi - R\dot{\varphi}_1] \vec{E}_1 \\
&\quad + [-\dot{x}_C \sin\psi + \rho_2 \dot{\psi} + \dot{y}_C \cos\psi] \vec{E}_2 \} \\
&\quad \cdot \{ -\sin\delta_1\, \vec{E}_1 + \cos\delta_1\, \vec{E}_2 + 0 \cdot \vec{E}_3 \} \\
&= -(\dot{x}_C \cos\psi - l\dot{\psi} + \dot{y}_C \sin\psi - R\dot{\varphi}_1) \sin\delta_1 \\
&\quad + (-\dot{x}_C \sin\psi + \rho_2 \dot{\psi} + \dot{y}_C \cos\psi) \cos\delta_1 = 0
\end{aligned}
$$

The analysis of the velocity vectors of the vehicle can be seen in Figure 3.10
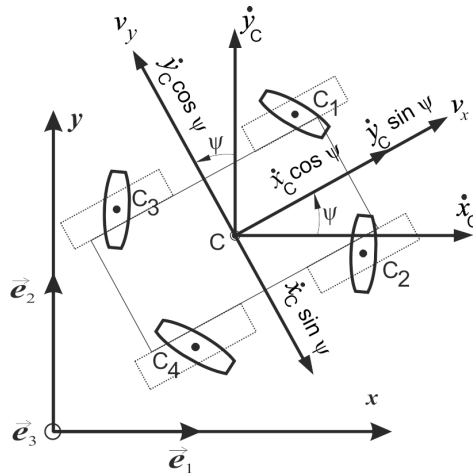
Figure 3.10 Analysis of the velocity vectors of the vehicle center of mass split into components relative to the global coordinate system

Therefore, the velocity vector can be written as follows

$$\dot{\vec{r}}_C = v_x \vec{E}_1 + v_y \vec{E}_2 = \dot{x}_C \vec{e}_1 + \dot{y}_C \vec{e}_2 \, .$$

Splitting the velocity vectors of the center of mass into components with respect to global coordinates leads to a kinematic model only containing functions of $\dot{x}_C$, $\dot{y}_C$ and $\dot{\psi}$. Analysis of the velocity vectors, as shown in Figure 3.10, yields

$$v_x = \dot{x}_C \cos\psi + \dot{y}_C \sin\psi \, , \qquad v_y = -\dot{x}_C \sin\psi + \dot{y}_C \cos\psi \, . \qquad (3.77)$$

First wheel:

The kinematic constraint for the first wheel can be written in the following form

$$\begin{aligned} -\left(\dot{x}_C \cos\psi + \dot{y}_C \sin\psi - l\dot{\psi} - R\dot{\varphi}_1 \right) \sin\delta_1 \\ + \left(-\dot{x}_C \sin\psi + \dot{y}_C \cos\psi + \rho_2 \dot{\psi} \right) \cos\delta_1 = 0 \end{aligned} \qquad (3.78)$$

➤ Assuming the special case of $\boldsymbol{\delta_1 = 45°}$ and cancelling out $\sin\delta_1$ and $\cos\delta_1$ from both sides results in

$$\begin{aligned} -(\dot{x}_C \cos\psi + \dot{y}_C \sin\psi) + (-\dot{x}_C \sin\psi + \dot{y}_C \cos\psi) \\ + l\dot{\psi} + \rho_2 \dot{\psi} + R\dot{\varphi}_1 = 0 \, . \end{aligned} \qquad (3.79)$$

Since

$$v_x = \dot{x}_C \cos\psi + \dot{y}_C \sin\psi \, , \qquad v_y = -\dot{x}_C \sin\psi + \dot{y}_C \cos\psi \, ,$$

then, equation (3.79) can be written in the form

$$-v_x + v_y + l\dot{\psi} + \rho_2 \dot{\psi} + R\dot{\varphi}_1 = 0 \, . \qquad (3.80)$$

Multiplying equation (3.80) by (-1) leads to

$$v_x - v_y - (l + \rho_2)\, \dot{\psi} = R\dot{\varphi}_1 \, . \qquad (3.81)$$

In order to find the kinematic constraints of the other wheels in the system, the last steps from equations (3.67) to (3.81) are repeated for each wheel in analogous way as following

<u>Second wheel:</u>

The kinematic constraint of the second wheel is

$$
\begin{aligned}
&\left(\dot{x}_C \cos\psi + \dot{y}_C \sin\psi + l\dot{\psi} - R\dot{\varphi}_2\right) \sin\delta_2 \\
&+ \left(-\dot{x}_C \sin\psi + \dot{y}_C \cos\psi + \rho_2\dot{\psi}\right) \cos\delta_2 = 0
\end{aligned}
\tag{3.82}
$$

➤   Assuming the special case of $\boldsymbol{\delta_2 = 45°}$, it follows that

$$
\begin{aligned}
&\left(\dot{x}_C \cos\psi + \dot{y}_C \sin\psi\right) + \left(-\dot{x}_C \sin\psi + \dot{y}_C \cos\psi\right) \\
&\qquad + \dot{\psi}(l + \rho_2) - R\dot{\varphi}_2 = 0\,,
\end{aligned}
\tag{3.83}
$$

therefore, according to equation (3.77), then equation (3.83) can be written in the following compact form of the kinematic constraint

$$
v_x + v_y + \dot{\psi}(l + \rho_2) = R\dot{\varphi}_2\,.
\tag{3.84}
$$

<u>Third Wheel:</u>

The kinematic constraint of the third wheel is

$$
\begin{aligned}
&\left(\dot{x}_C \cos\psi + \dot{y}_C \sin\psi - l\dot{\psi} - R\dot{\varphi}_3\right) \sin\delta_3 \\
&+ \left(-\dot{x}_C \sin\psi + \dot{y}_C \cos\psi - \rho_1\dot{\psi}\right) \cos\delta_3 = 0\,.
\end{aligned}
\tag{3.85}
$$

➤   Assuming the special case of $\boldsymbol{\delta_3 = 45°}$, then

$$
\begin{aligned}
&\left(\dot{x}_C \cos\psi + \dot{y}_C \sin\psi\right) + \left(-\dot{x}_C \sin\psi + \dot{y}_C \cos\psi\right) \\
&\qquad - \dot{\psi}(l + \rho_1) - R\dot{\varphi}_3 = 0\,.
\end{aligned}
\tag{3.86}
$$

Applying equation (3.77) yields that equation (3.86) can be written in the following compact form of the kinematic constraint

$$
v_x + v_y - \dot{\psi}(l + \rho_1) = R\dot{\varphi}_3\,.
\tag{3.87}
$$

Fourth wheel:

The kinematic constraint of the fourth wheel is

$$-\left(\dot{x}_C \cos\psi + \dot{y}_C \sin\psi + l\dot{\psi} - R\dot{\varphi}_4\right) \sin\delta_4$$
$$+ \left(-\dot{x}_C \sin\psi + \dot{y}_C \cos\psi - \rho_1\dot{\psi}\right) \cos\delta_4 = 0 \,. \tag{3.88}$$

➤   Assuming the special case of $\delta_4 = 45°$, it folllows that

$$-(\dot{x}_C \cos\psi + \dot{y}_C \sin\psi) + (-\dot{x}_C \sin\psi + \dot{y}_C \cos\psi)$$
$$- (l + \rho_1)\dot{\psi} + R\dot{\varphi}_4 = 0 \tag{3.89}$$

According to equation (3.77), then equation (3.89) can be written in the following compact form of the kinematic constraint

$$-v_x + v_y - (l + \rho_1)\dot{\psi} + R\dot{\varphi}_4 = 0 \,. \tag{3.90}$$

Multiplying equation (3.90) by (-1) yields

$$v_x - v_y + (l + \rho_1)\,\dot{\psi} = R\dot{\varphi}_4 \,. \tag{3.91}$$

3.3.2   The dynamic model

Because the four-wheel Mecanum vehicle is a nonholonomic system, it cannot be modeled dynamically using the second-order LAGRANGE equation. Therefore, the LAGRANGE equation with multipliers is used here for dynamic modeling.

The LAGRANGE equation with multipliers states that

$$\frac{d}{dt}\left(\frac{\partial T}{\partial \dot{q}^a}\right) - \frac{\partial T}{\partial q^a} = Q_a + \lambda_b f_a^b \; (a = 1,2,\dots,n; b = 1,2,\dots,r) \tag{3.92}$$

where
T is the general kinetic energy of the system and $T = T_{vehicle} + T_{wheels}$
q^a is the independent generalized coordinate
$\dot{q}^a$ is the first time derivative of the independent generalized coordinates (velocity)

n is the number of generalized coordinates, in this case $n = 7$ since
$\underbrace{q^1 = x_C,\ q^2 = y_C,\ q^3 = \psi}_{vehicle}$ and $\underbrace{q^4 = \varphi_1,\ q^5 = \varphi_2,\ q^6 = \varphi_3,\ q^7 = \varphi_4}_{wheels}$

r is the number of nonholonomic kinematic constraints of the system, here
$r = 4$

Q_a are the generalized forces (in this case driving moments)

λ_b are the multipliers in the LAGRANGE equation

f_a^b represents the coefficients of the independent coordinates for the motion constraints, in this case $a = 1, \dots, 7$ and $b = 1, \dots, 4$

The general form of kinetic energy in the LAGRANGE equation is

$$T = \frac{1}{2}m\dot{\vec{r}}_s^2 + \frac{1}{2}J_{ik}\omega_i\omega_k \ . \tag{3.93}$$

Assuming the special case for rotation in the plane, equation (3.93) can be rewritten in the form

$$T = \frac{1}{2}m\dot{\vec{r}}_s^2 + \frac{1}{2}J\omega^2. \tag{3.94}$$

Since $T = T_{vehicle} + T_{wheels}$, then

$$T_{vehicle} = \frac{1}{2}m_0(\dot{x}_C^2 + \dot{y}_C^2) + \frac{1}{2}J_0\dot{\psi}^2 \tag{3.95}$$

and

$$\begin{aligned}
T_{wheels} &= \frac{1}{2}m_1\left(\dot{x}_{C_1}^2 + \dot{y}_{C_1}^2\right) + \frac{1}{2}m_1\left(\dot{x}_{C_2}^2 + \dot{y}_{C_2}^2\right) + \frac{1}{2}m_1\left(\dot{x}_{C_3}^2 + \dot{y}_{C_3}^2\right) \\
&+ \frac{1}{2}m_1\left(\dot{x}_{C_4}^2 + \dot{y}_{C_4}^2\right) + \frac{1}{2}J_1\dot{\varphi}_1^2 + \frac{1}{2}J_1\dot{\varphi}_2^2 + \frac{1}{2}J_1\dot{\varphi}_3^2 \\
&+ \frac{1}{2}J_1\dot{\varphi}_4^2 + 4\cdot\frac{1}{2}J_2\dot{\psi}^2,
\end{aligned} \tag{3.96}$$

where m_0 is the mass of the vehicle's chassis without the wheels, m_1 is the mass of a Mecanum wheel, J_0 is the mass moment of inertia of the vehicle relative to body-fixed axis $\vec{E}_3$, J_1 is the mass moment of inertia of a wheel relative to the wheel's local rotating axis $\vec{E}_2^i$ and J_2 is the mass moment of inertia relative to the wheel's local axis $\vec{E}_3^i$. The parameters of the system are shown in Figure 3.11.
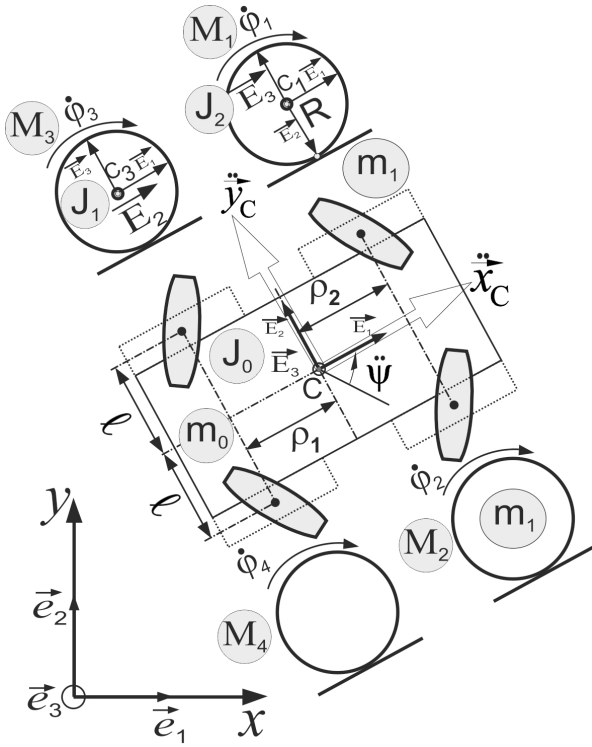
Figure 3.11 Diagram for the four-wheel Mecanum vehicle – dynamic analysis

   Using the wheel's coordinates as a function of the coordinates for the vehicles center of mass, for the first wheel it follows that

$$\dot{x}_{C_1} = \dot{x}_C - \rho_2 \dot{\psi} \sin\psi - l\dot{\psi} \cos\psi \ ,$$
$$\dot{y}_{C_1} = \dot{y}_C + \rho_2 \dot{\psi} \cos\psi - l\dot{\psi} \sin\psi \ , \tag{3.97}$$

for the second wheel

$$\dot{x}_{C_2} = \dot{x}_C - \rho_2 \dot{\psi} \sin\psi + l\dot{\psi} \cos\psi \ ,$$
$$\dot{y}_{C_2} = \dot{y}_C + \rho_2 \dot{\psi} \cos\psi + l\dot{\psi} \sin\psi \ , \tag{3.98}$$

for the third wheel

$$
\begin{aligned}
\dot{x}_{C_3} &= \dot{x}_C + \rho_1 \dot{\psi} \sin\psi - l\dot{\psi}\cos\psi \ , \\
\dot{y}_{C_3} &= \dot{y}_C - \rho_1 \dot{\psi} \cos\psi - l\dot{\psi}\sin\psi \ ,
\end{aligned}
\tag{3.99}
$$

and for the fourth wheel

$$
\begin{aligned}
\dot{x}_{C_4} &= \dot{x}_C + \rho_1 \dot{\psi} \sin\psi + l\dot{\psi}\cos\psi \ , \\
\dot{y}_{C_4} &= \dot{y}_C - \rho_1 \dot{\psi} \cos\psi + l\dot{\psi}\sin\psi \ .
\end{aligned}
\tag{3.100}
$$

From equation (3.96), the term $\left(\dot{x}_{C_i}^2 + \dot{y}_{C_i}^2\right)$ is repeated for each of the four wheels and the summation of this term can be found for all four Mecanum wheels as follows

$$
\begin{aligned}
\sum_{i=1}^{4}\left(\dot{x}_{C_i}^2 + \dot{y}_{C_i}^2\right) =\ & 4(\dot{x}_C^2 + \dot{y}_C^2) + 2\rho_2^2\dot{\psi}^2 + 4l^2\dot{\psi}^2 - 4\dot{x}_C\rho_2\dot{\psi}\sin\psi \\
& + 4\dot{x}_C\rho_1\dot{\psi}\sin\psi + 2\rho_1^2\dot{\psi}^2 + 4\dot{y}_C\rho_2\dot{\psi}\cos\psi \\
& - 4\dot{y}_C\rho_1\dot{\psi}\cos\psi \ .
\end{aligned}
\tag{3.101}
$$

Then, the total kinetic energy for whole system is shown to be

$$
\begin{aligned}
T =\ & \frac{1}{2}m_0(\dot{x}_C^2 + \dot{y}_C^2) + \frac{1}{2}J_0\dot{\psi}^2 \\
& + \frac{1}{2}m_1\big[4(\dot{x}_C^2 + \dot{y}_C^2) + (2\rho_1^2 + 2\rho_2^2 + 4l^2)\dot{\psi}^2 \\
& + 4\dot{x}_C\dot{\psi}\sin\psi\,(\rho_1 - \rho_2) + 4\dot{y}_C\dot{\psi}\cos\psi\,(\rho_2 - \rho_1)\big] \\
& + \frac{1}{2}J_1\dot{\phi}_1^2 + \frac{1}{2}J_1\dot{\phi}_2^2 + \frac{1}{2}J_1\dot{\phi}_3^2 + \frac{1}{2}J_1\dot{\phi}_4^2 + 2J_2\dot{\psi}^2 \ .
\end{aligned}
\tag{3.102}
$$

Performing some tedious but necessary calculation work yields the dynamic equations. Differentiation of the kinetic energy equation (3.102) can be calculated relative to the seven generalized coordinates of the system and for each case, the result is differentiated with respect to time.

For $a = 1$, then $q^1 = x_C$ and $\dot{q}^1 = \dot{x}_C$ and

$$
\frac{\partial T}{\partial \dot{q}^1} = \frac{\partial T}{\partial \dot{x}_C} = m_0\dot{x}_C + 4m_1\dot{x}_C + 2m_1\dot{\psi}(\rho_1 - \rho_2)\sin\psi
\tag{3.103}
$$

$$\frac{d}{dt}\left(\frac{\partial T}{\partial \dot{q}^1}\right) = \frac{d}{dt}\left(\frac{\partial T}{\partial \dot{x}_C}\right)$$
$$= (m_0 + 4m_1)\ddot{x}_C + 2m_1\ddot{\psi}(\rho_1 - \rho_2)\sin\psi$$
$$+ 2m_1\dot{\psi}^2(\rho_1 - \rho_2)\cos\psi \qquad (3.104)$$

$$\frac{\partial T}{\partial q^1} = \frac{\partial T}{\partial x_C} = 0 \,. \qquad (3.105)$$

For $a = 2$, then $q^2 = y_C$ and $\dot{q}^2 = \dot{y}_C$ and

$$\frac{\partial T}{\partial \dot{q}^2} = \frac{\partial T}{\partial \dot{y}_C} = m_0\dot{y}_C + 4m_1\dot{y}_C + 2m_1\dot{\psi}(\rho_2 - \rho_1)\cos\psi \qquad (3.106)$$

$$\frac{d}{dt}\left(\frac{\partial T}{\partial \dot{q}^2}\right) = \frac{d}{dt}\left(\frac{\partial T}{\partial \dot{y}_C}\right)$$
$$= (m_0 + 4m_1)\ddot{y}_C + 2m_1\ddot{\psi}(\rho_2 - \rho_1)\cos\psi$$
$$- 2m_1\dot{\psi}^2(\rho_2 - \rho_1)\sin\psi \qquad (3.107)$$

$$\frac{\partial T}{\partial q^2} = \frac{\partial T}{\partial y_C} = 0 \,. \qquad (3.108)$$

For $a = 3$, then $q^3 = \psi$ and $\dot{q}^3 = \dot{\psi}$ and

$$\frac{\partial T}{\partial \dot{q}^3} = \frac{\partial T}{\partial \dot{\psi}} = J_0\dot{\psi} + 2m_1(\rho_1^2 + \rho_2^2 + 2l^2)\dot{\psi}$$
$$+ 2m_1\dot{x}_C(\rho_1 - \rho_2)\sin\psi$$
$$+ 2m_1\dot{y}_C(\rho_2 - \rho_1)\cos\psi + 4J_2\dot{\psi} \qquad (3.109)$$

$$\frac{d}{dt}\left(\frac{\partial T}{\partial \dot{q}^3}\right) = \frac{d}{dt}\left(\frac{\partial T}{\partial \dot{\psi}}\right)$$
$$= \left(J_0 + 4J_2 + 2m_1(\rho_1^2 + \rho_2^2 + 2l^2)\right)\ddot{\psi}$$
$$+ 2m_1\ddot{x}_C(\rho_1 - \rho_2)\sin\psi + 2m_1\dot{x}_C\dot{\psi}(\rho_1 - \rho_2)\cos\psi$$
$$+ 2m_1\ddot{y}_C(\rho_2 - \rho_1)\cos\psi - 2m_1\dot{y}_C\dot{\psi}(\rho_2 - \rho_1)\sin\psi \qquad (3.110)$$

$$\frac{\partial T}{\partial q^3} = \frac{\partial T}{\partial \psi} = 2m_1\dot{x}_C\dot{\psi}(\rho_1 - \rho_2)\cos\psi$$
$$- 2m_1\dot{y}_C\dot{\psi}(\rho_2 - \rho_1)\sin\psi \,. \qquad (3.111)$$

For $a = 4$, then $q^4 = \varphi_1$ and $\dot{q}^4 = \dot{\varphi}_1$ and

$$\frac{\partial T}{\partial \dot{q}^4} = \frac{\partial T}{\partial \dot{\varphi}_1} = J_1 \dot{\varphi}_1 \tag{3.112}$$

$$\frac{d}{dt}\left(\frac{\partial T}{\partial \dot{q}^4}\right) = \frac{d}{dt}\left(\frac{\partial T}{\partial \dot{\varphi}_1}\right) = J_1 \ddot{\varphi}_1 \tag{3.113}$$

$$\frac{\partial T}{\partial q^4} = \frac{\partial T}{\partial \varphi_1} = 0 \; . \tag{3.114}$$

For $a = 5$, then $q^5 = \varphi_2$ and $\dot{q}^5 = \dot{\varphi}_2$ and

$$\frac{\partial T}{\partial \dot{q}^5} = \frac{\partial T}{\partial \dot{\varphi}_2} = J_1 \dot{\varphi}_2 \tag{3.115}$$

$$\frac{d}{dt}\left(\frac{\partial T}{\partial \dot{q}^5}\right) = \frac{d}{dt}\left(\frac{\partial T}{\partial \dot{\varphi}_2}\right) = J_1 \ddot{\varphi}_2 \tag{3.116}$$

$$\frac{\partial T}{\partial q^5} = \frac{\partial T}{\partial \varphi_2} = 0 \; . \tag{3.117}$$

For $a = 6$, then $q^6 = \varphi_3$ and $\dot{q}^6 = \dot{\varphi}_3$ and

$$\frac{\partial T}{\partial \dot{q}^6} = \frac{\partial T}{\partial \dot{\varphi}_3} = J_1 \dot{\varphi}_3 \tag{3.118}$$

$$\frac{d}{dt}\left(\frac{\partial T}{\partial \dot{q}^6}\right) = \frac{d}{dt}\left(\frac{\partial T}{\partial \dot{\varphi}_3}\right) = J_1 \ddot{\varphi}_3 \tag{3.119}$$

$$\frac{\partial T}{\partial q^6} = \frac{\partial T}{\partial \varphi_3} = 0 \; . \tag{3.120}$$

For $a = 7$, then $q^7 = \varphi_4$ and $\dot{q}^7 = \dot{\varphi}_4$ and

$$\frac{\partial T}{\partial \dot{q}^7} = \frac{\partial T}{\partial \dot{\varphi}_4} = J_1 \dot{\varphi}_4 \tag{3.121}$$

$$\frac{d}{dt}\left(\frac{\partial T}{\partial \dot{q}^7}\right) = \frac{d}{dt}\left(\frac{\partial T}{\partial \dot{\varphi}_4}\right) = J_1 \ddot{\varphi}_4 \tag{3.122}$$

$$\frac{\partial T}{\partial q^7} = \frac{\partial T}{\partial \varphi_4} = 0 \,. \tag{3.123}$$

In order to define the term for the driving moments in the LAGRANGE equation with multipliers, the virtual work δA can be written as follows for the system being described, which has four electric motors for driving, one motor for each wheel

$$\begin{aligned}
\delta A = Q_a \cdot \delta q^a &= Q_1 \cdot \delta q^1 + Q_2 \cdot \delta q^2 + Q_3 \cdot \delta q^3 + Q_4 \cdot \delta q^4 \\
&+ Q_5 \cdot \delta q^5 + Q_6 \cdot \delta q^6 + Q_7 \cdot \delta q^7 \\
&= M_1 \cdot \delta\varphi_1 + M_2 \cdot \delta\varphi_2 + M_3 \cdot \delta\varphi_3 + M_4 \cdot \delta\varphi_4 \,.
\end{aligned} \tag{3.124}$$

Thus, the generalized forces are $Q_4 = M_1$, $Q_5 = M_2$, $Q_6 = M_3$ and $Q_7 = M_4$.

In order to define the coefficients f_a^b, the kinematic constraints have to be rewritten. The first kinematic constraint has the following form

$$\begin{aligned}
-\dot{x}_C(\cos\psi + \sin\psi) + \dot{y}_C(\cos\psi - \sin\psi) \\
+ \dot{\psi}(l + \rho_2) + R\dot{\varphi}_1 = 0 \,,
\end{aligned} \tag{3.125}$$

the second

$$\dot{x}_C(\cos\psi - \sin\psi) + \dot{y}_C(\cos\psi + \sin\psi) + \dot{\psi}(l + \rho_2) - R\dot{\varphi}_2 = 0 \tag{3.126}$$

the third

$$\dot{x}_C(\cos\psi - \sin\psi) + \dot{y}_C(\cos\psi + \sin\psi) - \dot{\psi}(l + \rho_1) - R\dot{\varphi}_3 = 0 \tag{3.127}$$

and the fourth

$$\begin{aligned}
-\dot{x}_C(\cos\psi + \sin\psi) + \dot{y}_C(\cos\psi - \sin\psi) \\
- \dot{\psi}(l + \rho_1) + R\dot{\varphi}_4 = 0 \,.
\end{aligned} \tag{3.128}$$

The coefficients f_a^b can be estimated from the kinematic constraints of equations (3.125)…(3.128). The kinematic constraints are written in the following form

$$f_a^b(q^a) \cdot \dot{q}^a = 0 \,; \quad b = 1,2,3,4 \,. \tag{3.129}$$

If $b = 1$, the first kinematic constraint takes the following form

$$
\begin{aligned}
& f_1^1 \cdot \dot{q}^1 + f_2^1 \cdot \dot{q}^2 + f_3^1 \cdot \dot{q}^3 + f_4^1 \cdot \dot{q}^4 \\
& + f_5^1 \cdot \dot{q}^5 + f_6^1 \cdot \dot{q}^6 + f_7^1 \cdot \dot{q}^7 = 0 \,.
\end{aligned}
\tag{3.130}
$$

Comparing the coefficients for equations (3.125) and (3.130) shows that

$$
\begin{aligned}
& f_1^1 = -(\cos \psi + \sin \psi) \,; \; f_2^1 = (\cos \psi - \sin \psi) \,; \\
& f_3^1 = (l + \rho_2) \,; \; f_4^1 = R \,; f_5^1 = 0 \,; f_6^1 = 0 \,; f_7^1 = 0 \,;
\end{aligned}
\tag{3.131}
$$

If $b = 2$, the second kinematic constraint takes the following form

$$
\begin{aligned}
& f_1^2 \cdot \dot{q}^1 + f_2^2 \cdot \dot{q}^2 + f_3^2 \cdot \dot{q}^3 + f_4^2 \cdot \dot{q}^4 \\
& + f_5^2 \cdot \dot{q}^5 + f_6^2 \cdot \dot{q}^6 + f_7^2 \cdot \dot{q}^7 = 0 \,.
\end{aligned}
\tag{3.132}
$$

Comparing the coefficients for equations (3.126) and (3.132) shows that

$$
\begin{aligned}
& f_1^2 = (\cos \psi - \sin \psi) \,; \; f_2^2 = (\cos \psi + \sin \psi) \,; \; f_3^2 = (l + \rho_2) \,; \\
& f_4^2 = 0 \,; f_5^2 = -R \,; f_6^2 = 0 \,; f_7^2 = 0 \,;
\end{aligned}
\tag{3.133}
$$

If $b = 3$, the third kinematic constraint takes the following form

$$
\begin{aligned}
& f_1^3 \cdot \dot{q}^1 + f_2^3 \cdot \dot{q}^2 + f_3^3 \cdot \dot{q}^3 + f_4^3 \cdot \dot{q}^4 \\
& + f_5^3 \cdot \dot{q}^5 + f_6^3 \cdot \dot{q}^6 + f_7^3 \cdot \dot{q}^7 = 0 \,.
\end{aligned}
\tag{3.134}
$$

Comparing the coefficients for equations (3.127) and (3.134) shows that

$$
\begin{aligned}
& f_1^3 = (\cos \psi - \sin \psi) \,; \; f_2^3 = (\cos \psi + \sin \psi) \,; \; f_3^3 = -(l + \rho_1) \,; \\
& f_4^3 = 0 \,; f_5^3 = 0 \,; f_6^3 = -R \,; f_7^3 = 0 \,;
\end{aligned}
\tag{3.135}
$$

If $b = 4$, the fourth kinematic constraint takes the following form

$$
\begin{aligned}
& f_1^4 \cdot \dot{q}^1 + f_2^4 \cdot \dot{q}^2 + f_3^4 \cdot \dot{q}^3 + f_4^4 \cdot \dot{q}^4 + f_5^4 \cdot \dot{q}^5 \\
& + f_6^4 \cdot \dot{q}^6 + f_7^4 \cdot \dot{q}^7 = 0 \,.
\end{aligned}
\tag{3.136}
$$

Comparing the coefficients for equations (3.128) and (3.136) shows that

$$
\begin{aligned}
& f_1^4 = (\cos \psi + \sin \psi) \,; \; f_2^4 = (\sin \psi - \cos \psi) \,; \; f_3^4 = (l + \rho_1) \,; \\
& f_4^4 = 0 \,; f_5^4 = 0 \,; f_6^4 = 0 \,; f_7^4 = -R \,.
\end{aligned}
\tag{3.137}
$$

The LAGRANGE equation with multipliers can be written for each generalized coordinate q^a, where $a = 1, 2, 3, 4, 5, 6$ and 7.

If $a = 1$, then

$$
\frac{d}{dt}\left(\frac{\partial T}{\partial \dot{q}^1}\right) - \frac{\partial T}{\partial q^1} = Q_1 + \lambda_b f_1^b
$$
$$
= Q_1 + \lambda_1 f_1^1 + \lambda_2 f_1^2 + \lambda_3 f_1^3 + \lambda_4 f_1^4 \,. \tag{3.138}
$$

Substituting the terms of equation (3.138) with the corresponding calculated terms, equation (3.138) can be formed as follows

$$
(m_0 + 4m_1)\ddot{x}_C + 2m_1\ddot{\psi}(\rho_1 - \rho_2)\sin\psi
$$
$$
+ 2m_1\dot{\psi}^2(\rho_1 - \rho_2)\cos\psi
$$
$$
= -\lambda_1(\cos\psi + \sin\psi) + \lambda_2(\cos\psi - \sin\psi)
$$
$$
+ \lambda_3(\cos\psi - \sin\psi) + \lambda_4(\cos\psi + \sin\psi) \,. \tag{3.139}
$$

If $a = 2$, then

$$
\frac{d}{dt}\left(\frac{\partial T}{\partial \dot{q}^2}\right) - \frac{\partial T}{\partial q^2} = Q_2 + \lambda_b f_2^b
$$
$$
= Q_2 + \lambda_1 f_2^1 + \lambda_2 f_2^2 + \lambda_3 f_2^3 + \lambda_4 f_2^4 \,. \tag{3.140}
$$

Substituting the terms of equation (3.140) with the corresponding calculated terms, equation (3.140) can be formed as follows

$$
(m_0 + 4m_1)\ddot{y}_C + 2m_1\ddot{\psi}(\rho_2 - \rho_1)\cos\psi
$$
$$
- 2m_1\dot{\psi}^2(\rho_2 - \rho_1)\sin\psi
$$
$$
= \lambda_1(\cos\psi - \sin\psi) + \lambda_2(\cos\psi + \sin\psi)
$$
$$
+ \lambda_3(\cos\psi + \sin\psi) + \lambda_4(\sin\psi - \cos\psi) \,. \tag{3.141}
$$

If $a = 3$, then

$$
\frac{d}{dt}\left(\frac{\partial T}{\partial \dot{q}^3}\right) - \frac{\partial T}{\partial q^3} = Q_3 + \lambda_b f_3^b
$$
$$
= Q_3 + \lambda_1 f_3^1 + \lambda_2 f_3^2 + \lambda_3 f_3^3 + \lambda_4 f_3^4 \,. \tag{3.142}
$$

Substituting the terms of equation (3.142) with the corresponding calculated terms, equation (3.142) can be formed as follows

$$\left(J_0 + 4J_2 + 2m_1(\rho_1^2 + \rho_2^2 + 2l^2)\right)\ddot{\psi} + 2m_1\ddot{x}_C(\rho_1 - \rho_2)\sin\psi$$
$$+ 2m_1\dot{x}_C\dot{\psi}(\rho_1 - \rho_2)\cos\psi + 2m_1\ddot{y}_C(\rho_2 - \rho_1)\cos\psi$$
$$- 2m_1\dot{y}_C\dot{\psi}(\rho_2 - \rho_1)\sin\psi - 2m_1\dot{x}_C\dot{\psi}(\rho_1 - \rho_2)\cos\psi$$
$$+ 2m_1\dot{y}_C\dot{\psi}(\rho_2 - \rho_1)\sin\psi$$
$$= \lambda_1(l + \rho_2) + \lambda_2(l + \rho_2) - \lambda_3(l + \rho_1) + \lambda_4(l + \rho_1) .$$

$$\left(J_0 + 4J_2 + 2m_1(\rho_1^2 + \rho_2^2 + 2l^2)\right)\ddot{\psi} + 2m_1\ddot{x}_C(\rho_1 - \rho_2)\sin\psi$$
$$+ 2m_1\ddot{y}_C(\rho_2 - \rho_1)\cos\psi$$
$$= \lambda_1(l + \rho_2) + \lambda_2(l + \rho_2) - \lambda_3(l + \rho_1)$$
$$+ \lambda_4(l + \rho_1) . \tag{3.143}$$

If $a = 4$, then

$$\frac{d}{dt}\left(\frac{\partial T}{\partial \dot{q}^4}\right) - \frac{\partial T}{\partial q^4} = Q_4 + \lambda_b f_4^b$$
$$= Q_4 + \lambda_1 f_4^1 + \lambda_2 f_4^2 + \lambda_3 f_4^3 + \lambda_4 f_4^4 . \tag{3.144}$$

Substituting the terms of equation (3.144) with the corresponding calculated terms, equation (3.144) can be formed as follows

$$J_1\ddot{\varphi}_1 = M_1 + \lambda_1 R . \tag{3.145}$$

If $a = 5$, then

$$\frac{d}{dt}\left(\frac{\partial T}{\partial \dot{q}^5}\right) - \frac{\partial T}{\partial q^5} = Q_5 + \lambda_b f_5^b$$
$$= Q_5 + \lambda_1 f_5^1 + \lambda_2 f_5^2 + \lambda_3 f_5^3 + \lambda_4 f_5^4 . \tag{3.146}$$

Substituting the terms of equation (3.146) with the corresponding calculated terms, equation (3.146) can be formed as follows

$$J_1\ddot{\varphi}_2 = M_2 - \lambda_2 R . \tag{3.147}$$

If $a = 6$, then

$$\frac{d}{dt}\left(\frac{\partial T}{\partial \dot{q}^6}\right) - \frac{\partial T}{\partial q^6} = Q_6 + \lambda_b f_6^b$$
$$= Q_6 + \lambda_1 f_6^1 + \lambda_2 f_6^2 + \lambda_3 f_6^3 + \lambda_4 f_6^4 . \tag{3.148}$$

Substituting the terms of equation (3.148) with the corresponding calculated terms, equation (3.148) can be formed as follows

$$J_1 \ddot{\varphi}_3 = M_3 - \lambda_3 R \,. \tag{3.149}$$

If $a = 7$, then

$$\frac{d}{dt} \left(\frac{\partial T}{\partial \dot{q}^7} \right) - \frac{\partial T}{\partial q^7} = Q_7 + \lambda_b f_7^b$$
$$= Q_7 + \lambda_1 f_7^1 + \lambda_2 f_7^2 + \lambda_3 f_7^3 + \lambda_4 f_7^4 \,. \tag{3.150}$$

Substituting the terms of equation (3.150) with the corresponding calculated terms, equation (3.150) can be formed as follows

$$J_1 \ddot{\varphi}_4 = M_4 - \lambda_4 R \,. \tag{3.151}$$

Until now, the equations have contained 11 unknowns: x_C, y_C, ψ, φ_1, φ_2, φ_3, φ_4, λ_1, λ_2, λ_3 and λ_4. The unknowns can be estimated from the four kinematic constraint equations (3.125)…(3.128) and the seven LAGRANGE equations (3.139), (3.141), (3.143), (3.145), (3.147), (3.149) and (3.151).

From equation (3.145)

$$\lambda_1 = \frac{1}{R} (J_1 \ddot{\varphi}_1 - M_1) \,, \tag{3.152}$$

in which there are still two unknowns λ_1 and $\ddot{\varphi}_1$. Therefore, unknown $\ddot{\varphi}_1$ will be replaced by its corresponding value, which can be found by differentiating the kinematic constraint equation (3.125) with respect to time

$$\dot{\varphi}_1 = \frac{1}{R} \left[\dot{x}_C (\cos\psi + \sin\psi) - \dot{y}_C (\cos\psi - \sin\psi) - \dot{\psi}(l + \rho_2) \right] \tag{3.153}$$

$$\ddot{\varphi}_1 = \frac{1}{R} \left[\ddot{x}_C (\cos\psi + \sin\psi) + \dot{x}_C (-\dot{\psi}\sin\psi + \dot{\psi}\cos\psi) \right.$$
$$- \ddot{y}_C (\cos\psi - \sin\psi) - \dot{y}_C (-\dot{\psi}\cos\psi - \dot{\psi}\sin\psi)$$
$$\left. - \ddot{\psi}(l + \rho_2) \right]. \tag{3.154}$$

Then, substituting equation (3.154) into equation (3.152) gives

$$\lambda_1 = \frac{1}{R}\left\{\frac{J_1}{R}\left[\ddot{x}_C(\cos\psi + \sin\psi) + \dot{x}_C\dot{\psi}(\cos\psi - \sin\psi)\right.\right.$$
$$\left. + \ddot{y}_C(\sin\psi - \cos\psi) + \dot{y}_C\dot{\psi}(\cos\psi + \sin\psi)\right. \tag{3.155}$$
$$\left.\left. - \ddot{\psi}(l + \rho_2)\right] - M_1\right\}.$$

From equation (3.147)

$$\lambda_2 = \frac{1}{R}(M_2 - J_1\ddot{\varphi}_2), \tag{3.156}$$

in which there are still two unknowns λ_2 and $\ddot{\varphi}_2$. Therefore, unknown $\ddot{\varphi}_2$ will be replaced by its corresponding value, which can be found by differentiating the kinematic constraint equation (3.126) with respect to time

$$\dot{\varphi}_2 = \frac{1}{R}\left[\dot{x}_C(\cos\psi - \sin\psi) + \dot{y}_C(\cos\psi + \sin\psi) + \dot{\psi}(l + \rho_2)\right] \tag{3.157}$$

$$\ddot{\varphi}_2 = \frac{1}{R}\left[\ddot{x}_C(\cos\psi - \sin\psi) + \dot{x}_C(-\dot{\psi}\sin\psi - \dot{\psi}\cos\psi)\right.$$
$$\left. + \ddot{y}_C(\cos\psi + \sin\psi) + \dot{y}_C(\dot{\psi}\cos\psi - \dot{\psi}\sin\psi)\right. \tag{3.158}$$
$$\left. + \ddot{\psi}(l + \rho_2)\right].$$

Then, substituting equation (3.158) into equation (3.156) yields

$$\lambda_2 = \frac{1}{R}\left\{M_2 - \frac{J_1}{R}\left[\ddot{x}_C(\cos\psi - \sin\psi) - \dot{x}_C\dot{\psi}(\cos\psi + \sin\psi)\right.\right.$$
$$\left. + \ddot{y}_C(\cos\psi + \sin\psi) + \dot{y}_C\dot{\psi}(\cos\psi - \sin\psi)\right. \tag{3.159}$$
$$\left.\left. + \ddot{\psi}(l + \rho_2)\right]\right\}.$$

From equation (3.149)

$$\lambda_3 = \frac{1}{R}(M_3 - J_1\ddot{\varphi}_3), \tag{3.160}$$

in which there are still two unknowns λ_3 and $\ddot{\varphi}_3$. Therefore, unknown $\ddot{\varphi}_3$ will be replaced by its corresponding value, which can be found by differentiating the kinematic constraint equation (3.127) with respect to time

$$\dot{\varphi}_3 = \frac{1}{R}\left[\dot{x}_C(\cos\psi - \sin\psi) + \dot{y}_C(\cos\psi + \sin\psi) - \dot{\psi}(l + \rho_1)\right] \tag{3.161}$$

$$\ddot{\varphi}_3 = \frac{1}{R}\big[\ddot{x}_C(\cos\psi - \sin\psi) + \dot{x}_C\big(-\dot{\psi}\sin\psi - \dot{\psi}\cos\psi\big)$$
$$+ \ddot{y}_C(\cos\psi + \sin\psi) + \dot{y}_C\big(\dot{\psi}\cos\psi - \dot{\psi}\sin\psi\big)$$
$$- \ddot{\psi}(l + \rho_1)\big].$$

$$(3.162)$$

Then, substituting equation (3.162) into equation (3.160) yields

$$\lambda_3 = \frac{1}{R}\Big\{M_3 - \frac{J_1}{R}\big[\ddot{x}_C(\cos\psi - \sin\psi) - \dot{x}_C\dot{\psi}(\cos\psi + \sin\psi)$$
$$+ \ddot{y}_C(\cos\psi + \sin\psi) + \dot{y}_C\dot{\psi}(\cos\psi - \sin\psi)$$
$$- \ddot{\psi}(l + \rho_1)\big]\Big\}.$$

$$(3.163)$$

From equation (3.151)

$$\lambda_4 = \frac{1}{R}(M_4 - J_1\ddot{\varphi}_4),$$

$$(3.164)$$

in which there are still two unknowns λ_4 and $\ddot{\varphi}_4$. Therefore, unknown $\ddot{\varphi}_4$ will be replaced by its corresponding value, which can be found by differentiating the kinematic constraint equation (3.128) with respect to time

$$\dot{\varphi}_4 = \frac{1}{R}\big[\dot{x}_C(\cos\psi + \sin\psi) + \dot{y}_C(\sin\psi - \cos\psi) + \dot{\psi}(l + \rho_1)\big] \quad (3.165)$$

$$\ddot{\varphi}_4 = \frac{1}{R}\big[\ddot{x}_C(\cos\psi + \sin\psi) + \dot{x}_C\big(-\dot{\psi}\sin\psi + \dot{\psi}\cos\psi\big)$$
$$+ \ddot{y}_C(\sin\psi - \cos\psi) + \dot{y}_C\big(\dot{\psi}\cos\psi + \dot{\psi}\sin\psi\big)$$
$$+ \ddot{\psi}(l + \rho_1)\big],$$

$$(3.166)$$

Then, substituting equation (3.166) into equation (3.164) yields

$$\lambda_4 = \frac{1}{R}\Big\{M_4 - \frac{J_1}{R}\big[\ddot{x}_C(\cos\psi + \sin\psi) + \dot{x}_C\dot{\psi}(\cos\psi - \sin\psi)$$
$$+ \ddot{y}_C(\sin\psi - \cos\psi) + \dot{y}_C\dot{\psi}(\cos\psi + \sin\psi)$$
$$+ \ddot{\psi}(l + \rho_1)\big]\Big\}.$$

$$(3.167)$$

The next step is to substitute the corresponding values of $\lambda_1, \lambda_2, \lambda_3$ and λ_4 from equations (3.155), (3.159), (3.163) and (3.167) into equation (3.139) as shown in the following equation

$$(m_0 + 4m_1)\ddot{x}_C + 2m_1\ddot{\psi}(\rho_1 - \rho_2)\sin\psi + 2m_1\dot{\psi}^2(\rho_1 - \rho_2)\cos\psi =$$
$$-\frac{(\cos\psi + \sin\psi)}{R}\left\{\frac{J_1}{R}\left[\ddot{x}_C(\cos\psi + \sin\psi) + \dot{x}_C\dot{\psi}(\cos\psi - \sin\psi) + \right.\right.$$
$$\left.\ddot{y}_C(\sin\psi - \cos\psi) + \dot{y}_C\dot{\psi}(\cos\psi + \sin\psi) - \ddot{\psi}(l + \rho_2)\right] - M_1\Big\} +$$
$$\frac{(\cos\psi - \sin\psi)}{R}\left\{M_2 - \frac{J_1}{R}\left[\ddot{x}_C(\cos\psi - \sin\psi) - \dot{x}_C\dot{\psi}(\cos\psi + \sin\psi) + \right.\right.$$
$$\left.\ddot{y}_C(\cos\psi + \sin\psi) + \dot{y}_C\dot{\psi}(\cos\psi - \sin\psi) + \ddot{\psi}(l + \rho_2)\right]\Big\} +$$
$$\frac{(\cos\psi - \sin\psi)}{R}\left\{M_3 - \frac{J_1}{R}\left[\ddot{x}_C(\cos\psi - \sin\psi) - \dot{x}_C\dot{\psi}(\cos\psi + \sin\psi) + \right.\right.$$
$$\left.\ddot{y}_C(\cos\psi + \sin\psi) + \dot{y}_C\dot{\psi}(\cos\psi - \sin\psi) - \ddot{\psi}(l + \rho_1)\right]\Big\} +$$
$$\frac{(\cos\psi + \sin\psi)}{R}\left\{M_4 - \frac{J_1}{R}\left[\ddot{x}_C(\cos\psi + \sin\psi) + \dot{x}_C\dot{\psi}(\cos\psi - \sin\psi) + \right.\right.$$
$$\left.\ddot{y}_C(\sin\psi - \cos\psi) + \dot{y}_C\dot{\psi}(\cos\psi + \sin\psi) + \ddot{\psi}(l + \rho_1)\right]\Big\}.$$

Therefore, the final form of the dynamic second-order differential equation is as follows

$$
\boxed{
\begin{aligned}
&\ddot{x}_C\left[(m_0 + 4m_1) + \frac{4J_1}{R^2}\right] \\
&+ \ddot{\psi}\left[2m_1\sin\psi\,(\rho_1 - \rho_2) + \frac{2J_1}{R^2}\sin\psi\,(\rho_1 - \rho_2)\right] \\
&= -\frac{4J_1}{R^2}\dot{y}_C\dot{\psi} - 2m_1\dot{\psi}^2\cos\psi\,(\rho_1 - \rho_2) \\
&+ \frac{(\cos\psi + \sin\psi)}{R}\cdot(M_1 + M_4) + \frac{(\cos\psi - \sin\psi)}{R}\cdot(M_2 + M_3).
\end{aligned}
}
\tag{3.168}
$$

Repeating the last step of substituting the corresponding values of $\lambda_1, \lambda_2, \lambda_3$ and λ_4 from equations (3.155), (3.159), (3.163) and (3.167) into equation (3.141) gives the following equation

$$(m_0 + 4m_1)\ddot{y}_C + 2m_1\ddot{\psi}(\rho_2 - \rho_1)\cos\psi - 2m_1\dot{\psi}^2(\rho_2 - \rho_1)\sin\psi$$

$$= \frac{(\cos\psi - \sin\psi)}{R}\left\{\frac{J_1}{R}[\ddot{x}_C(\cos\psi + \sin\psi) + \dot{x}_C\dot{\psi}(\cos\psi - \sin\psi)\right.$$

$$+ \ddot{y}_C(\sin\psi - \cos\psi) + \dot{y}_C\dot{\psi}(\cos\psi + \sin\psi) - \ddot{\psi}(l + \rho_2)] - M_1\Big\}$$

$$+ \frac{(\cos\psi + \sin\psi)}{R}\left\{M_2 - \frac{J_1}{R}[\ddot{x}_C(\cos\psi - \sin\psi)\right.$$

$$- \dot{x}_C\dot{\psi}(\cos\psi + \sin\psi) + \ddot{y}_C(\cos\psi + \sin\psi) + \dot{y}_C\dot{\psi}(\cos\psi - \sin\psi)$$

$$+ \ddot{\psi}(l + \rho_2)]\Big\} + \frac{(\cos\psi + \sin\psi)}{R}\left\{M_3 - \frac{J_1}{R}[\ddot{x}_C(\cos\psi - \sin\psi)\right.$$

$$- \dot{x}_C\dot{\psi}(\cos\psi + \sin\psi) + \ddot{y}_C(\cos\psi + \sin\psi)$$

$$+ \dot{y}_C\dot{\psi}(\cos\psi - \sin\psi) - \ddot{\psi}(l + \rho_1)]\Big\}$$

$$+ \frac{(\cos\psi - \sin\psi)}{R}\left\{M_4 - \frac{J_1}{R}[\ddot{x}_C(\cos\psi + \sin\psi)\right.$$

$$+ \dot{x}_C\dot{\psi}(\cos\psi - \sin\psi) + \ddot{y}_C(\sin\psi - \cos\psi) + \dot{y}_C\dot{\psi}(\cos\psi + \sin\psi)$$

$$+ \ddot{\psi}(l + \rho_1)]\Big\}.$$

Therefore,

$$\boxed{\begin{aligned}
&\ddot{y}_C\left[(m_0 + 4m_1) + \frac{4J_1}{R^2}\right] - \ddot{\psi}\left[2m_1\cos\psi\,(\rho_1 - \rho_2)\right. \\
&+ \frac{2J_1}{R^2}\cos\psi\,(\rho_1 - \rho_2)\bigg] = \frac{4J_1}{R^2}\dot{x}_C\dot{\psi} - 2m_1\dot{\psi}^2\sin\psi\,(\rho_1 - \rho_2) \\
&- \frac{(\cos\psi - \sin\psi)}{R}\cdot(M_1 + M_4) + \frac{(\cos\psi + \sin\psi)}{R}\cdot(M_2 + M_3)\,.
\end{aligned}} \qquad (3.169)$$

Repeating the last step of substituting the corresponding values of $\lambda_1, \lambda_2, \lambda_3$ and λ_4 from equations (3.155), (3.159), (3.163) and (3.167) into equation (3.143) gives the following equation

$$(J_0 + 4J_2 + 2m_1(\rho_1^2 + \rho_2^2 + 2l^2))\ddot{\psi}$$
$$+ 2m_1\ddot{x}_C(\rho_1 - \rho_2)\sin\psi + 2m_1\ddot{y}_C(\rho_2 - \rho_1)\cos\psi$$
$$= \frac{(l + \rho_2)}{R}\left\{\frac{J_1}{R}\left[\ddot{x}_C(\cos\psi + \sin\psi) + \dot{x}_C\dot{\psi}(\cos\psi - \sin\psi)\right.\right.$$
$$\left.+ \ddot{y}_C(\sin\psi - \cos\psi) + \dot{y}_C\dot{\psi}(\cos\psi + \sin\psi) - \ddot{\psi}(l + \rho_2)] - M_1\right\}$$
$$+ \frac{(l + \rho_2)}{R}\left\{M_2 - \frac{J_1}{R}\left[\ddot{x}_C(\cos\psi - \sin\psi) - \dot{x}_C\dot{\psi}(\cos\psi + \sin\psi)\right.\right.$$
$$\left.+ \ddot{y}_C(\cos\psi + \sin\psi) + \dot{y}_C\dot{\psi}(\cos\psi - \sin\psi) + \ddot{\psi}(l + \rho_2)]\right\}$$
$$- \frac{(l + \rho_1)}{R}\left\{M_3 - \frac{J_1}{R}\left[\ddot{x}_C(\cos\psi - \sin\psi) - \dot{x}_C\dot{\psi}(\cos\psi + \sin\psi)\right.\right.$$
$$\left.+ \ddot{y}_C(\cos\psi + \sin\psi) + \dot{y}_C\dot{\psi}(\cos\psi - \sin\psi) - \ddot{\psi}(l + \rho_1)]\right\}$$
$$+ \frac{(l + \rho_1)}{R}\left\{M_4 - \frac{J_1}{R}\left[\ddot{x}_C(\cos\psi + \sin\psi) + \dot{x}_C\dot{\psi}(\cos\psi - \sin\psi)\right.\right.$$
$$\left.+ \ddot{y}_C(\sin\psi - \cos\psi) + \dot{y}_C\dot{\psi}(\cos\psi + \sin\psi) + \ddot{\psi}(l + \rho_1)]\right\}.$$

Therefore,

$$
\begin{aligned}
&\ddot{x}_C\left[2m_1\sin\psi\,(\rho_1 - \rho_2) + \frac{2J_1}{R^2}\sin\psi\,(\rho_1 - \rho_2)\right] \\
&- \ddot{y}_C\left[2m_1\cos\psi\,(\rho_1 - \rho_2) + \frac{2J_1}{R^2}\cos\psi\,(\rho_1 - \rho_2)\right] \\
&+ \ddot{\psi}\left[J_C + \frac{2J_1}{R^2}\cdot[(l + \rho_2)^2 + (l + \rho_1)^2]\right] \\
&= -\frac{2J_1}{R^2}\dot{x}_C\dot{\psi}\cos\psi\,(\rho_1 - \rho_2) - \frac{2J_1}{R^2}\dot{y}_C\dot{\psi}\sin\psi\,(\rho_1 - \rho_2) \\
&+ \frac{(l + \rho_2)}{R}\cdot(M_2 - M_1) + \frac{(l + \rho_1)}{R}\cdot(M_4 - M_3)\,.
\end{aligned}
\tag{3.170}
$$

$$J_C = J_0 + 4J_2 + 2m_1(\rho_1^2 + \rho_2^2 + 2l^2) \tag{3.171}$$

Assuming $\rho_1 = \rho_2 = \rho$, the differential equation of motion for the four-wheel Mecanum vehicle can be reduced to the following form

$$
\begin{aligned}
\ddot{x}_C\left(m + \frac{4J_1}{R^2}\right) = &-\frac{4J_1}{R^2}\dot{y}_C\dot{\psi} + \frac{(\cos\psi + \sin\psi)}{R}\cdot(M_1 + M_4) \\
&+ \frac{(\cos\psi - \sin\psi)}{R}\cdot(M_2 + M_3)
\end{aligned}
\tag{3.172}
$$

$$\ddot{y}_C \left(m + \frac{4J_1}{R^2} \right) = \frac{4J_1}{R^2} \dot{x}_C \dot{\psi} - \frac{(\cos\psi - \sin\psi)}{R} \cdot (M_1 + M_4)$$
$$+ \frac{(\cos\psi + \sin\psi)}{R} \cdot (M_2 + M_3) \tag{3.173}$$

$$\ddot{\psi} \left[J_C + \frac{4J_1}{R^2} \cdot (l + \rho)^2 \right] = \frac{(l + \rho)}{R} \cdot (M_2 - M_1 + M_4 - M_3), \tag{3.174}$$

where $m = m_0 + 4m_1$ and $J_C = J_0 + 4[J_2 + m_1 \cdot (l^2 + \rho^2)]$.

It is possible to find the vehicle rotation angle ψ analytically by integrating equation (3.174) when all driving moments are known functions of time. The initial conditions $\psi(t = 0)$ and $\dot{\psi}(t = 0)$ must be defined.

Here, we consider a special condition for motion, in which translational motion $\dot{\psi} = 0$, which makes it possible to analytically determine the integral of equations (3.172) and (3.173). The differential equations of motion take the following form

$$\ddot{x}_C \left(m + \frac{4J_1}{R^2} \right)$$
$$= \frac{(\cos\psi + \sin\psi)}{R} \cdot (M_1 + M_4) + \frac{(\cos\psi - \sin\psi)}{R} \cdot (M_2 + M_3), \tag{3.175}$$

$$\ddot{y}_C \left(m + \frac{4J_1}{R^2} \right)$$
$$= \frac{(\cos\psi - \sin\psi)}{R} \cdot (M_1 + M_4) + \frac{(\cos\psi + \sin\psi)}{R} \cdot (M_2 + M_3). \tag{3.176}$$

If angle ψ is given and the driving torques satisfy equation (3.174), then the vehicle motion $x_C(t)$ and $y_C(t)$ can be found by integrating with respect to time t. Furthermore, a general case from the presented dynamic model can be found in [166, 167].

3.4   Commonly used approximation method for modeling the 4WMV

This section briefly presents an approximation method for modeling the four-wheel Mecanum vehicle. This method uses a different strategy for modeling the four-wheel Mecanum vehicle from the kinematic and dynamic points of view and can be found in various sources, such as [137, 129, 27] and has been referenced to it in [11, 14-20, 25-29, 37, 48, 53, 63-65, 68, 69, 93, 95, 104, 105, 109, 110, 112, 114, 115, 121, 122, 125, 126, 128-134 and 155].

3.4.1   Kinematics of the approximation model

The assumption applies that no slip occurs between the rollers and the contact surface, as this is the main condition to guarantee the validation of the following kinematic and dynamic model for the four-wheel Mecanum vehicle. The approximation method for modeling the kinematics of the vehicle also assumes the coordinate frame is fixed to the vehicle center of mass and moves with it. $\vec{v}_{C_i}$ is the relative velocity vector of the wheel center, where $i = 1,2,3,4$ is the wheel number in the described system and $v_{C_i} = R\dot{\varphi}_i$. The radius of the vehicle is denoted R and $\dot{\varphi}_i$ is the angular velocity of the wheel. As a simplification for the study, the radius of the wheel R is assumed to be equal to the distance between wheel center and the contact point between the roller and the surface. Previous studies have considered this point and it was found that there is small nonlinear effect in the wheel kinematics due to the difference [154]. On the other hand $\vec{v}_{r_i}$ is the velocity vector for the freely rotating roller in contact with the surface. Practical applications have demonstrated that during motion there are multiple rollers contacting the surface simultaneously, which is not taken into account because the contact area can be considered a point. $\vec{v}_{r_i}$ can be analyzed as two vectors in the x- and y-directions. Velocity vector $\vec{v}_{r_i}$ is perpendicular to the roller centerline. Vector $\vec{v}_{r_i}$ forms an angle δ_i with $\vec{v}_{C_i}$.
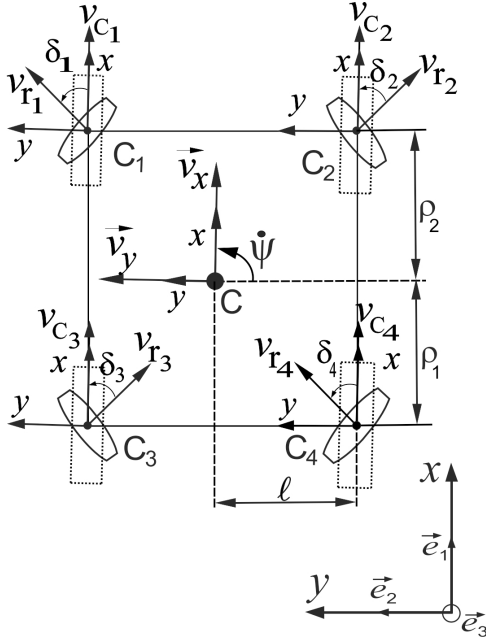
Figure 3.12 Diagram of the four-wheel Mecanum vehicle – kinematic analysis using the approximation method

The distance between the front wheel axis and the center of mass C of the locomotion system is ρ_2 and ρ_1 is the distance between the rear wheel axis and the center of mass. l is one-half the width of the transportation unit. The vehicle center of mass moves along velocity vectors $\vec{v}_x$ and $\vec{v}_y$. Weight transfer due to acceleration or braking has not been taking into account in this study in order to simplify the mathematical model. According to the method used here, the center of each wheel has two velocity coordinates v_{x_i} and v_{y_i}, which result from the analysis of the velocity vectors $\vec{v}_{C_i}$ and $\vec{v}_{r_i}$ in x- and y-body-fixed coordinates of the wheels as shown in Figure 3.12, resulting in the following derivation

$$v_{x_1} = v_{C_1} + v_{r_1} \cos \delta_1 , \quad v_{y_1} = v_{r_1} \sin \delta_1 , \tag{3.177}$$

$$v_{x_2} = v_{C_2} + v_{r_2} \cos \delta_2 , \quad v_{y_2} = -v_{r_2} \sin \delta_2 , \tag{3.178}$$

$$v_{x_3} = v_{C_3} + v_{r_3} \cos \delta_3 , \quad v_{y_3} = -v_{r_3} \sin \delta_3 , \tag{3.179}$$

$$v_{x_4} = v_{C_4} + v_{r_4} \cos \delta_4 \, , \quad v_{y_4} = v_{r_4} \sin \delta_4 \, . \tag{3.180}$$

Applying EULER's formula to find the velocity vectors $\vec{v}_x$ and $\vec{v}_y$ of the vehicle center of mass as functions of the wheel velocity coordinates v_{x_i} and v_{y_i} for the first wheel results

$$\begin{aligned} v_x &= v_{x_1} + l\dot{\psi} \, , \quad v_{x_1} = v_x - l\dot{\psi} \, , \\ v_y &= v_{y_1} - \rho_2 \dot{\psi} \, , \quad v_{y_1} = v_y + \rho_2 \dot{\psi} \, , \end{aligned} \tag{3.181}$$

for the second wheel

$$\begin{aligned} v_x &= v_{x_2} - l\dot{\psi} \, , \quad v_{x_2} = v_x + l\dot{\psi} \, , \\ v_y &= v_{y_2} - \rho_2 \dot{\psi} \, , \quad v_{y_2} = v_y + \rho_2 \dot{\psi} \, , \end{aligned} \tag{3.182}$$

for the third wheel

$$\begin{aligned} v_x &= v_{x_3} + l\dot{\psi} \, , \quad v_{x_3} = v_x - l\dot{\psi} \, , \\ v_y &= v_{y_3} + \rho_1 \dot{\psi} \, , \quad v_{y_3} = v_y + \rho_1 \dot{\psi} \end{aligned} \tag{3.183}$$

and for the fourth wheel

$$\begin{aligned} v_x &= v_{x_4} - l\dot{\psi} \, , \quad v_{x_4} = v_x + l\dot{\psi} \, , \\ v_y &= v_{y_4} + \rho_1 \dot{\psi} \, , \quad v_{y_4} = v_y - \rho_1 \dot{\psi} \, . \end{aligned} \tag{3.184}$$

Comparing equations (3.177)-(3.180) with equations (3.181)-(3.184) demonstrates that for the first wheel

$$v_{C_1} + v_{r_1} \cos \delta_1 = v_x - l\dot{\psi} \text{ and } v_y + \rho_2 \dot{\psi} = v_{r_1} \sin \delta_1 \tag{3.185}$$

and substituting the value of v_{r_1} in the previous equation gives

$$v_{C_1} = v_x - v_y \tan \delta_1 - \dot{\psi}(l + \rho_2 \tan \delta_1) \, . \tag{3.186}$$

For the second wheel

$$v_{C_2} + v_{r_2} \cos \delta_2 = v_x + l\dot{\psi} \text{ and } v_y + \rho_2 \dot{\psi} = -v_{r_2} \sin \delta_2 \tag{3.187}$$

and substituting the value of v_{r_2} in the previous equation gives

$$v_{C_2} = v_x + v_y \tan \delta_2 + \dot{\psi}(l + \rho_2 \tan \delta_2). \tag{3.188}$$

For the third wheel

$$v_{C_3} + v_{r_3} \cos \delta_3 = v_x - l\dot{\psi} \text{ and } v_y - \rho_1\dot{\psi} = -v_{r_3} \sin \delta_3 \tag{3.189}$$

and substituting the value of v_{r_3} in the previous equation gives

$$v_{C_3} = v_x + v_y \tan \delta_3 - \dot{\psi}(l + \rho_1 \tan \delta_3). \tag{3.190}$$

For the fourth wheel

$$v_{C_4} + v_{r_4} \cos \delta_4 = v_x + l\dot{\psi} \text{ and } v_y - \rho_1\dot{\psi} = v_{r_4} \sin \delta_4 \tag{3.191}$$

and substituting the value of v_{r_3} in the previous equation gives

$$v_{C_4} = v_x - v_y \tan \delta_4 + \dot{\psi}(l + \rho_1 \tan \delta_4). \tag{3.192}$$

Since $v_{C_i} = R\dot{\varphi}_i$, then the kinematic constraint of the 4WMV can be written as follows

$$\begin{aligned}
\dot{\varphi}_1 &= \frac{1}{R}\left[v_x - v_y \tan \delta_1 - \dot{\psi}(l + \rho_2 \tan \delta_1)\right], \\
\dot{\varphi}_2 &= \frac{1}{R}\left[v_x + v_y \tan \delta_2 + \dot{\psi}(l + \rho_2 \tan \delta_2)\right], \\
\dot{\varphi}_3 &= \frac{1}{R}\left[v_x + v_y \tan \delta_3 - \dot{\psi}(l + \rho_1 \tan \delta_3)\right], \\
\dot{\varphi}_4 &= \frac{1}{R}\left[v_x - v_y \tan \delta_4 + \dot{\psi}(l + \rho_1 \tan \delta_4)\right].
\end{aligned} \tag{3.193}$$

From the inverse kinematic equation, which states that

$$[\dot{\varphi}_i] = \frac{1}{R} \cdot \mathbb{J} \cdot [V_C], \tag{3.194}$$

where $[V_C] = (v_x, v_y, \dot{\psi})^T$ is the velocity vector of the center of mass relative to the body-fixed coordinates and $[V_C] \in \mathbb{R}^{3 \times 1}$ and $\mathbb{J}$ is a transformation matrix and $\mathbb{J} \in \mathbb{R}^{4 \times 3}$, the kinematic constraints can be represented as follows

$$
\begin{bmatrix} \dot\varphi_1 \\ \dot\varphi_2 \\ \dot\varphi_3 \\ \dot\varphi_4 \end{bmatrix} = \frac{1}{R} \cdot \begin{bmatrix} 1 & -\tan\delta_1 & -(l + \rho_2 \tan\delta_1) \\ 1 & \tan\delta_2 & (l + \rho_2 \tan\delta_2) \\ 1 & \tan\delta_3 & -(l + \rho_1 \tan\delta_3) \\ 1 & -\tan\delta_4 & (l + \rho_1 \tan\delta_4) \end{bmatrix} \cdot \begin{bmatrix} v_x \\ v_y \\ \dot\psi \end{bmatrix}.
\tag{3.195}
$$

The advantage of this approximation method is the ability to find an approximate value for the vehicle velocity vector $[V_C] = (v_x, v_y, \dot\psi)^T$ from the wheel angular velocities $(\dot\varphi_1, \dot\varphi_2, \dot\varphi_3, \dot\varphi_4)^T$ using the pseudo-inverse matrix method to solve the over-defined equations such as equation (3.195). The pseudo-inverse matrix for solving the over-defined equation set, which contains a number of equations more than the number of unknowns and in order to minimize the Euclidean norm $\|\mathbb{J} \cdot [V_C] - R \cdot [\dot\varphi_i]\|$, is formed as follows

$$
[V_C] = R \cdot \mathbb{J}^+ \cdot [\dot\varphi_i],
\tag{3.196}
$$

where $\mathbb{J}^+ = (\mathbb{J}^T \cdot \mathbb{J})^{-1} \cdot \mathbb{J}^T$, the diagonal matrix $\mathbb{I} = \mathbb{J}^+ \cdot \mathbb{J}$.

In this case, the following solution was found in [137, 129, 27]

$$
\begin{bmatrix} v_x \\ v_y \\ \dot\psi \end{bmatrix} = \frac{R}{4} \cdot \begin{bmatrix} 1 & 1 & 1 & 1 \\ -\tan\delta_1 & \tan\delta_2 & \tan\delta_3 & -\tan\delta_4 \\ -1 & 1 & -1 & 1 \\ \overline{l + \rho_2 \tan\delta_1} & \overline{l + \rho_2 \tan\delta_2} & \overline{l + \rho_1 \tan\delta_3} & \overline{l + \rho_1 \tan\delta_4} \end{bmatrix} \cdot \begin{bmatrix} \dot\varphi_1 \\ \dot\varphi_2 \\ \dot\varphi_3 \\ \dot\varphi_4 \end{bmatrix},
\tag{3.197}
$$

and the velocity vector elements $(v_x, v_y, \dot\psi)^T$ of the vehicle center of mass can be calculated directly from the following equations

$$
\begin{aligned}
v_x &= \frac{R}{4}(\dot\varphi_1 + \dot\varphi_2 + \dot\varphi_3 + \dot\varphi_4), \\
v_y &= \frac{R}{4}(-\dot\varphi_1 \tan\delta_1 + \dot\varphi_2 \tan\delta_2 + \dot\varphi_3 \tan\delta_3 - \dot\varphi_4 \tan\delta_4), \\
\dot\psi &= \frac{R}{4}\left(-\frac{\dot\varphi_1}{l + \rho_2 \tan\delta_1} + \frac{\dot\varphi_2}{l + \rho_2 \tan\delta_2} - \frac{\dot\varphi_3}{l + \rho_1 \tan\delta_3} \right. \\
&\quad \left. + \frac{\dot\varphi_4}{l + \rho_1 \tan\delta_4}\right).
\end{aligned}
\tag{3.198}
$$

In the Mecanum vehicle in the consideration, the rollers of the wheels are inclined by constant angle of 45°. Substituting the assumption of $\delta_1 = \delta_2 = \delta_3 = \delta_4 = \frac{\pi}{4}$ into equation (3.198) and assuming $\rho_1 = \rho_2 = \rho$ yields the following simplified forms for the velocity vector equation

$$v_x = \frac{R}{4}(\dot{\varphi}_1 + \dot{\varphi}_2 + \dot{\varphi}_3 + \dot{\varphi}_4),$$

$$v_y = \frac{R}{4}(-\dot{\varphi}_1 + \dot{\varphi}_2 + \dot{\varphi}_3 - \dot{\varphi}_4),$$

$$\dot{\psi} = \frac{R}{4\,(1+\rho)}(-\dot{\varphi}_1 + \dot{\varphi}_2 - \dot{\varphi}_3 + \dot{\varphi}_4).$$

(3.199)

Based on equation (3.199), it is possible to find the parameters of the velocity vector directly by substituting the rotation velocities of the wheels into the equation. Numerically integrating the substituted results produces the linear displacement of the vehicle center x_C, y_C and the angular displacement about the center ψ. Motion of the vehicle can be visualized using special programs such as the visual reality toolbox found in MATLAB/SIMULINK® from The Mathworks.

3.4.2   Dynamics of the approximation model

By applying the pseudo-inverse matrix to estimate the parameters of the vehicle velocity vector as a function in the wheel's rotation velocities, then it is now valid to use the LAGRANGE equation directly to estimate the differential equation of motion for the 4WMV, where the system is now considered holonomic. This section briefly presents the approximation procedure. Using the notations from the previous section, the generalized coordinates are $q^4 = \varphi_1, q^5 = \varphi_2,\ q^6 = \varphi_3$ and $q^7 = \varphi_4$, where $a = 4, \ldots, 7$ and the general form of the LAGRANGE equation of the second kind is

$$\frac{d}{dt}\left(\frac{\partial T}{\partial \dot{q}^a}\right) - \frac{\partial T}{\partial q^a} = Q_a - \left(\frac{\partial D}{\partial \dot{q}^a} + F_R(\dot{q}^a)\right), \qquad a = 4, \ldots, 7, \qquad (3.200)$$

where D represents losses due to viscous friction in the system and can be found from:

$$\frac{\partial D}{\partial \dot{q}^a} = \frac{1}{2}D_\varphi(\dot{\varphi}_1^2 + \dot{\varphi}_2^2 + \dot{\varphi}_3^2 + \dot{\varphi}_4^2), \qquad (3.201)$$

and D_φ is the coefficient of viscous friction in the wheel bearings. An additional resistance force due to dry friction in the bearings can take the form

$$F_R(\dot{q}^a) = \begin{bmatrix} fc_1 \cdot \text{sgn}(\dot{\varphi}_1) \\ fc_2 \cdot \text{sgn}(\dot{\varphi}_2) \\ fc_3 \cdot \text{sgn}(\dot{\varphi}_3) \\ fc_4 \cdot \text{sgn}(\dot{\varphi}_4) \end{bmatrix}. \tag{3.202}$$

Since the friction term can be neglected in the model, then $\left(\frac{\partial D}{\partial \dot{q}^a} + F_R(\dot{q}^a) \right) = 0$.

The generalized force Q_a in equation (3.200) is replaced by the driving moments of the four wheels, $(M_1, M_2, M_3, M_4)^T$. The kinetic energy can be written as follows

$$T = \frac{1}{2} m (v_x^2 + v_y^2) + \frac{1}{2} J_3 \dot{\psi}^2 + \frac{1}{2} J_1 (\dot{\varphi}_1^2 + \dot{\varphi}_2^2 + \dot{\varphi}_3^2 + \dot{\varphi}_4^2), \tag{3.203}$$

where $m = m_0 + 4m_1$, J_3 is the mass moment of inertia of the vehicle and all four wheels relative to the vehicle-fixed coordinate $\vec{E}_3$. This can be found from the relation $J_C = J_0 + 4(J_2 + m_1 \cdot (l^2 + \rho^2))$ according to the STEINER rule and $J_2 = \frac{1}{12} m_1 (b^2 + 3R^2)$, where b is the width of the Mecanum wheel, which is considered here to be zero. In order to simplify the analysis, the contact between the wheel and the surface is considered as a point. Therefore, the wheel width $b = 0$ and the mass moment of inertia $J_2 = \frac{1}{4} m_1 R^2$. $J_0 = \frac{m_0}{3} (l^2 + \rho^2)$ and $J_1 = \frac{1}{2} m_1 R^2$, yielding

$$J_C = m_1 R^2 + \left(\frac{m_0}{3} + 4m_1 \right) (l^2 + \rho^2). \tag{3.204}$$

Substituting equation (3.199) into equation (3.203) gives

$$T = \frac{mR^2}{32}(2\dot{\varphi}_1^2 + 2\dot{\varphi}_2^2 + 2\dot{\varphi}_3^2 + 2\dot{\varphi}_4^2 + 4\dot{\varphi}_1\dot{\varphi}_4 + 4\dot{\varphi}_2\dot{\varphi}_3)$$

$$+ \frac{J_C R^2}{32(l+\rho)^2}(\dot{\varphi}_1^2 + \dot{\varphi}_2^2 + \dot{\varphi}_3^2 + \dot{\varphi}_4^2 - 2\dot{\varphi}_1\dot{\varphi}_2 + 2\dot{\varphi}_1\dot{\varphi}_3$$

$$- 2\dot{\varphi}_1\dot{\varphi}_4 - 2\dot{\varphi}_2\dot{\varphi}_3 + 2\dot{\varphi}_2\dot{\varphi}_4 - 2\dot{\varphi}_3\dot{\varphi}_4)$$

$$+ \frac{1}{2}J_1(\dot{\varphi}_1^2 + \dot{\varphi}_2^2 + \dot{\varphi}_3^2 + \dot{\varphi}_4^2) \tag{3.205}$$

$$= \frac{1}{2}\left(\frac{mR^2}{8} + \frac{J_C R^2}{16(l+\rho)^2} + J_1\right)(\dot{\varphi}_1^2 + \dot{\varphi}_2^2 + \dot{\varphi}_3^2 + \dot{\varphi}_4^2)$$

$$+ \left(\frac{mR^2}{8} + \frac{J_C R^2}{16(l+\rho)^2}\right)(\dot{\varphi}_1\dot{\varphi}_4 + \dot{\varphi}_2\dot{\varphi}_3)$$

$$- \frac{J_C R^2}{16(l+\rho)^2}(\dot{\varphi}_1\dot{\varphi}_2 - \dot{\varphi}_1\dot{\varphi}_3 - \dot{\varphi}_2\dot{\varphi}_4 + \dot{\varphi}_3\dot{\varphi}_4).$$

Next, substituting equation (3.205) into equation (3.200) and calculating the derivatives of the kinetic energy according to LAGRANGE equation for the 4 different coordinates yields the following in the various cases

If $a = 4$, then $\dot{q}^a = \dot{q}^4 = \dot{\varphi}_1$, therefore

$$\frac{\partial T}{\partial \dot{q}^4} = \frac{\partial T}{\partial \dot{\varphi}_1} = \left(\frac{mR^2}{8} + \frac{J_C R^2}{16(l+\rho)^2} + J_1\right)\dot{\varphi}_1 - \left(\frac{J_C R^2}{16(l+\rho)^2}\right)\dot{\varphi}_2$$

$$+ \left(\frac{J_C R^2}{16(l+\rho)^2}\right)\dot{\varphi}_3 + \left(\frac{mR^2}{8} - \frac{J_C R^2}{16(l+\rho)^2}\right)\dot{\varphi}_4, \tag{3.206}$$

and

$$\frac{d}{dt}\left(\frac{\partial T}{\partial \dot{q}^4}\right) = \frac{d}{dt}\left(\frac{\partial T}{\partial \dot{\varphi}_1}\right)$$

$$= \left(\frac{mR^2}{8} + \frac{J_C R^2}{16(l+\rho)^2} + J_1\right)\ddot{\varphi}_1 - \left(\frac{J_C R^2}{16(l+\rho)^2}\right)\ddot{\varphi}_2 \tag{3.207}$$

$$+ \left(\frac{J_C R^2}{16(l+\rho)^2}\right)\ddot{\varphi}_3 + \left(\frac{mR^2}{8} - \frac{J_C R^2}{16(l+\rho)^2}\right)\ddot{\varphi}_4.$$

On the other hand, since $\frac{\partial T}{\partial q^4} = \frac{\partial T}{\partial \varphi_1} = 0$, $Q_4 = M_1$. Therefore, substituting that into the LAGRANGE equation yields the second-order differential equation

$$
\left(\frac{mR^2}{8} + \frac{J_C R^2}{16(l+\rho)^2} + J_1 \right) \ddot{\varphi}_1 - \left(\frac{J_C R^2}{16(l+\rho)^2} \right) \ddot{\varphi}_2
$$
$$
+ \left(\frac{J_C R^2}{16(l+\rho)^2} \right) \ddot{\varphi}_3 + \left(\frac{mR^2}{8} - \frac{J_C R^2}{16(l+\rho)^2} \right) \ddot{\varphi}_4 \qquad (3.208)
$$
$$
= M_1 .
$$

Assuming $H_1 = \frac{mR^2}{8}$ and $H_2 = \frac{J_C R^2}{16(l+\rho)^2}$ and substituting the assumed values for H_1 and H_2 into equation (3.208) yields

$$
(H_1 + H_2 + J_1)\ddot{\varphi}_1 - H_2\ddot{\varphi}_2 + H_2\ddot{\varphi}_3 + (H_1 - H_2)\ddot{\varphi}_4 = M_1 . \qquad (3.209)
$$

If $a = 5$, then $\dot{q}^a = \dot{q}^5 = \dot{\varphi}_2$, therefore

$$
\frac{\partial T}{\partial \dot{q}^5} = \frac{\partial T}{\partial \dot{\varphi}_2}
$$
$$
= -\left(\frac{J_C R^2}{16(l+\rho)^2} \right)\dot{\varphi}_1 + \left(\frac{mR^2}{8} + \frac{J_C R^2}{16(l+\rho)^2} + J_1 \right)\dot{\varphi}_2 \qquad (3.210)
$$
$$
+ \left(\frac{mR^2}{8} - \frac{J_C R^2}{16(l+\rho)^2} \right)\dot{\varphi}_3 + \left(\frac{J_C R^2}{16(l+\rho)^2} \right)\dot{\varphi}_4 ,
$$

and

$$
\frac{d}{dt}\left(\frac{\partial T}{\partial \dot{q}^5} \right) = \frac{d}{dt}\left(\frac{\partial T}{\partial \dot{\varphi}_2} \right)
$$
$$
= -\left(\frac{J_C R^2}{16(l+\rho)^2} \right)\ddot{\varphi}_1 + \left(\frac{mR^2}{8} + \frac{J_C R^2}{16(l+\rho)^2} + J_1 \right)\ddot{\varphi}_2 \qquad (3.211)
$$
$$
+ \left(\frac{mR^2}{8} - \frac{J_C R^2}{16(l+\rho)^2} \right)\ddot{\varphi}_3 + \left(\frac{J_C R^2}{16(l+\rho)^2} \right)\ddot{\varphi}_4 .
$$

On the other hand, since $\frac{\partial T}{\partial q^5} = \frac{\partial T}{\partial \varphi_2} = 0$, $Q_5 = M_2$. Therefore, substituting that into the LAGRANGE equation yields the second-order differential equation

$$-\left(\frac{J_C R^2}{16(l+\rho)^2}\right)\ddot{\varphi}_1 + \left(\frac{mR^2}{8} + \frac{J_C R^2}{16(l+\rho)^2} + J_1\right)\ddot{\varphi}_2$$

$$+\left(\frac{mR^2}{8} - \frac{J_C R^2}{16(l+\rho)^2}\right)\ddot{\varphi}_3 + \left(\frac{J_C R^2}{16(l+\rho)^2}\right)\ddot{\varphi}_4 = M_2 \,. \qquad (3.212)$$

Then, substituting the assumed values for H_1 and H_2 into equation (3.212) yields

$$-H_2\ddot{\varphi}_1 + (H_1 + H_2 + J_1)\ddot{\varphi}_2 + (H_1 - H_2)\ddot{\varphi}_3 + H_2\ddot{\varphi}_4 = M_2 \,. \qquad (3.213)$$

If $a = 6$, then $\dot{q}^a = \dot{q}^6 = \dot{\varphi}_3$, therefore

$$\frac{\partial T}{\partial \dot{q}^6} = \frac{\partial T}{\partial \dot{\varphi}_3}$$

$$= \left(\frac{J_C R^2}{16(l+\rho)^2}\right)\dot{\varphi}_1 + \left(\frac{mR^2}{8} - \frac{J_C R^2}{16(l+\rho)^2}\right)\dot{\varphi}_2 \qquad (3.214)$$

$$+\left(\frac{mR^2}{8} + \frac{J_C R^2}{16(l+\rho)^2} + J_1\right)\dot{\varphi}_3 - \left(\frac{J_C R^2}{16(l+\rho)^2}\right)\dot{\varphi}_4 \,,$$

and

$$\frac{d}{dt}\left(\frac{\partial T}{\partial \dot{q}^6}\right) = \frac{d}{dt}\left(\frac{\partial T}{\partial \dot{\varphi}_3}\right)$$

$$= \left(\frac{J_C R^2}{16(l+\rho)^2}\right)\ddot{\varphi}_1 + \left(\frac{mR^2}{8} - \frac{J_C R^2}{16(l+\rho)^2}\right)\ddot{\varphi}_2 \qquad (3.215)$$

$$+\left(\frac{mR^2}{8} + \frac{J_C R^2}{16(l+\rho)^2} + J_1\right)\ddot{\varphi}_3 - \left(\frac{J_C R^2}{16(l+\rho)^2}\right)\ddot{\varphi}_4 \,.$$

On the other hand, since $\frac{\partial T}{\partial q^6} = \frac{\partial T}{\partial \varphi_3} = 0$, $Q_6 = M_3$. Therefore, substituting that into the LAGRANGE equation yields the second-order differential equation

$$\left(\frac{J_C R^2}{16(l+\rho)^2}\right)\ddot{\varphi}_1 + \left(\frac{mR^2}{8} - \frac{J_C R^2}{16(l+\rho)^2}\right)\ddot{\varphi}_2$$

$$+\left(\frac{mR^2}{8} + \frac{J_C R^2}{16(l+\rho)^2} + J_1\right)\ddot{\varphi}_3 - \left(\frac{J_C R^2}{16(l+\rho)^2}\right)\ddot{\varphi}_4 = M_3 \,. \qquad (3.216)$$

Then, substituting the assumed values for H_1 and H_2 into equation (3.216) yields

$$H_2 \ddot{\varphi}_1 + (H_1 - H_2) \ddot{\varphi}_2 + (H_1 + H_2 + J_1) \ddot{\varphi}_3 - H_2 \ddot{\varphi}_4 = M_3 \,. \qquad (3.217)$$

If $a = 7$, then $\dot{q}^a = \dot{q}^7 = \dot{\varphi}_4$, therefore

$$
\begin{aligned}
\frac{\partial T}{\partial \dot{q}^7} = \frac{\partial T}{\partial \dot{\varphi}_4} &= \left(\frac{mR^2}{8} - \frac{J_c R^2}{16(l + \rho)^2} \right) \dot{\varphi}_1 + \left(\frac{J_c R^2}{16(l + \rho)^2} \right) \dot{\varphi}_2 \\
&\quad - \left(\frac{J_c R^2}{16(l + \rho)^2} \right) \dot{\varphi}_3 + \left(\frac{mR^2}{8} + \frac{J_c R^2}{16(l + \rho)^2} + J_1 \right) \dot{\varphi}_4 \,,
\end{aligned}
\qquad (3.218)
$$

and

$$
\begin{aligned}
\frac{d}{dt} \left(\frac{\partial T}{\partial \dot{q}^7} \right) &= \frac{d}{dt} \left(\frac{\partial T}{\partial \dot{\varphi}_4} \right) \\
&= \left(\frac{mR^2}{8} - \frac{J_c R^2}{16(l + \rho)^2} \right) \ddot{\varphi}_1 + \left(\frac{J_c R^2}{16(l + \rho)^2} \right) \ddot{\varphi}_2 \\
&\quad - \left(\frac{J_c R^2}{16(l + \rho)^2} \right) \ddot{\varphi}_3 + \left(\frac{mR^2}{8} + \frac{J_c R^2}{16(l + \rho)^2} + J_1 \right) \ddot{\varphi}_4 \,.
\end{aligned}
\qquad (3.219)
$$

On the other hand, since $\dfrac{\partial T}{\partial q^7} = \dfrac{\partial T}{\partial \varphi_4} = 0$, $Q_7 = M_4$. Therefore, substituting that into the LAGRANGE equation yields the second-order differential equation

$$
\begin{aligned}
&\left(\frac{mR^2}{8} - \frac{J_c R^2}{16(l + \rho)^2} \right) \ddot{\varphi}_1 + \left(\frac{J_c R^2}{16(l + \rho)^2} \right) \ddot{\varphi}_2 \\
&- \left(\frac{J_c R^2}{16(l + \rho)^2} \right) \ddot{\varphi}_3 + \left(\frac{mR^2}{8} + \frac{J_c R^2}{16(l + \rho)^2} + J_1 \right) \ddot{\varphi}_4 = M_4 \,.
\end{aligned}
\qquad (3.220)
$$

Then, substituting the assumed values for H_1 and H_2 into equation (3.220) yields

$$(H_1 - H_2) \ddot{\varphi}_1 + H_2 \ddot{\varphi}_2 - H_2 \ddot{\varphi}_3 + (H_1 + H_2 + J_1) \ddot{\varphi}_4 = M_4 \,. \qquad (3.221)$$

The general form of the approximated dynamic model is

$$[N] \cdot [\ddot{\varphi}] = [M] \,, \qquad (3.222)$$

where

$$[N] = \begin{bmatrix} H_1 + H_2 + J_1 & -H_2 & H_2 & H_1 - H_2 \\ -H_2 & H_1 + H_2 + J_1 & H_1 - H_2 & H_2 \\ H_2 & H_1 - H_2 & H_1 + H_2 + J_1 & -H_2 \\ H_1 - H_2 & H_2 & -H_2 & H_1 + H_2 + J_1 \end{bmatrix}$$

and $[\ddot{\varphi}] = (\ddot{\varphi}_1, \ddot{\varphi}_2, \ddot{\varphi}_3, \ddot{\varphi}_4)^T$; $[M] = (M_1, M_2, M_3, M_4)^T$ is the driving moment vector and $[M] \in \mathbb{R}^{4 \times 1}$.

3.5   <u>Comparison of the dynamic models</u>

The dynamic model from the second method discussed is a function of $\ddot{\varphi}_1, \ddot{\varphi}_2, \ddot{\varphi}_3$ and $\ddot{\varphi}_4$. Therefore, it is not possible to compare it directly with the dynamic model from the first method, which is function of $\ddot{x}_C$, $\ddot{y}_C$ and $\ddot{\psi}$. However, it is possible to convert the dynamic model analytically to be a function of the parameters in $\ddot{x}_C$, $\ddot{y}_C$ and $\ddot{\psi}$ in order to facilitate the comparison. The first step in the conversion process is to find the time derivative of equation (3.199) as follows

$$\dot{v}_x = \frac{R}{4}(\ddot{\varphi}_1 + \ddot{\varphi}_2 + \ddot{\varphi}_3 + \ddot{\varphi}_4),$$
$$\dot{v}_y = \frac{R}{4}(-\ddot{\varphi}_1 + \ddot{\varphi}_2 + \ddot{\varphi}_3 - \ddot{\varphi}_4), \qquad (3.223)$$
$$\ddot{\psi} = \frac{R}{4(l+\rho)}(-\ddot{\varphi}_1 + \ddot{\varphi}_2 - \ddot{\varphi}_3 + \ddot{\varphi}_4),$$

The time derivative of equation (3.77) is

$$\dot{v}_x = \ddot{x}_C \cos\psi - \dot{x}_C \dot{\psi} \sin\psi + \ddot{y}_C \sin\psi + \dot{y}_C \dot{\psi} \cos\psi, \qquad (3.224)$$

and also

$$\dot{v}_y = -\ddot{x}_C \sin\psi - \dot{x}_C \dot{\psi} \cos\psi + \ddot{y}_C \cos\psi - \dot{y}_C \dot{\psi} \sin\psi. \qquad (3.225)$$

Then, multiplying $\dot{v}_x$ in equation (3.224) by $\cos\psi$ results in

$$\dot{v}_x \cos\psi = \ddot{x}_C \cos^2\psi - \dot{x}_C \dot{\psi} \cos\psi \sin\psi + \ddot{y}_C \cos\psi \sin\psi \\ + \dot{y}_C \dot{\psi} \cos^2\psi. \qquad (3.226)$$

Similarly, multiplying $\dot{v}_x$ in equation (3.224) by $\sin\psi$ results in

$$\dot{v}_x \sin \psi = \ddot{x}_C \cos \psi \sin \psi - \dot{x}_C \dot{\psi} \sin^2 \psi + \ddot{y}_C \sin^2 \psi \\ + \dot{y}_C \dot{\psi} \cos \psi \sin \psi \,. \tag{3.227}$$

The same steps are then repeated for equation (3.225). Multiplying $\dot{v}_y$ in equation (3.225) by $\cos \psi$ results in

$$\dot{v}_y \cos \psi = -\ddot{x}_C \cos \psi \sin \psi - \dot{x}_C \dot{\psi} \cos^2 \psi + \ddot{y}_C \cos^2 \psi \\ - \dot{y}_C \dot{\psi} \cos \psi \sin \psi \,, \tag{3.228}$$

Then, multiplying $\dot{v}_y$ in equation (3.225) by $-\sin \psi$ results in

$$-\dot{v}_y \sin \psi = \ddot{x}_C \sin^2 \psi + \dot{x}_C \dot{\psi} \cos \psi \sin \psi - \ddot{y}_C \cos \psi \sin \psi \\ + \dot{y}_C \dot{\psi} \sin^2 \psi \,. \tag{3.229}$$

Summing equations (3.226) and (3.229) gives

$$\dot{v}_x \cos \psi - \dot{v}_y \sin \psi = \ddot{x}_C + \dot{y}_C \dot{\psi} \tag{3.230}$$

and summing equations (3.227) and (3.228) gives

$$\dot{v}_x \sin \psi + \dot{v}_y \cos \psi = \ddot{y}_C - \dot{x}_C \dot{\psi} \,. \tag{3.231}$$

Substituting equation (3.223) into equation (3.230) yields

$$\ddot{x}_C + \dot{y}_C \dot{\psi} = \frac{R}{4} (\ddot{\varphi}_1 + \ddot{\varphi}_2 + \ddot{\varphi}_3 + \ddot{\varphi}_4) \cos \psi \\ + \frac{R}{4} (\ddot{\varphi}_1 - \ddot{\varphi}_2 - \ddot{\varphi}_3 + \ddot{\varphi}_4) \sin \psi \tag{3.232}$$

and substituting equation (3.223) into equation (3.231) yields

$$\ddot{y}_C - \dot{x}_C \dot{\psi} = \frac{R}{4} (\ddot{\varphi}_1 + \ddot{\varphi}_2 + \ddot{\varphi}_3 + \ddot{\varphi}_4) \sin \psi \\ + \frac{R}{4} (-\ddot{\varphi}_1 + \ddot{\varphi}_2 + \ddot{\varphi}_3 - \ddot{\varphi}_4) \cos \psi \,. \tag{3.233}$$

From the previous derivation, it is known that

$$\ddot{\psi} = \frac{R}{4 (l + \rho)} (-\ddot{\varphi}_1 + \ddot{\varphi}_2 - \ddot{\varphi}_3 + \ddot{\varphi}_4) \,.$$

According to equations (3.209), (3.213), (3.217) and (3.221), the differential equations of the dynamic model for the four-wheel Mecanum vehicle are

$$(H_1 + H_2 + J_1)\ddot{\varphi}_1 - H_2\ddot{\varphi}_2 + H_2\ddot{\varphi}_3 + (H_1 - H_2)\ddot{\varphi}_4 = M_1 \,,$$

$$-H_2\ddot{\varphi}_1 + (H_1 + H_2 + J_1)\ddot{\varphi}_2 + (H_1 - H_2)\ddot{\varphi}_3 + H_2\ddot{\varphi}_4 = M_2 \,,$$

$$H_2\ddot{\varphi}_1 + (H_1 - H_2)\ddot{\varphi}_2 + (H_1 + H_2 + J_1)\ddot{\varphi}_3 - H_2\ddot{\varphi}_4 = M_3 \,,$$

$$(H_1 - H_2)\ddot{\varphi}_1 + H_2\ddot{\varphi}_2 - H_2\ddot{\varphi}_3 + (H_1 + H_2 + J_1)\ddot{\varphi}_4 = M_4 \,.$$

Summing equations (3.209), (3.213), (3.217) and (3.221), i.e. the last four differential equations, results in

$$(2H_1 + J_1)\ddot{\varphi}_1 + (2H_1 + J_1)\ddot{\varphi}_2 + (2H_1 + J_1)\ddot{\varphi}_3 + (2H_1 + J_1)\ddot{\varphi}_4$$
$$= M_1 + M_2 + M_3 + M_4 \,,$$
$$\ddot{\varphi}_1 + \ddot{\varphi}_2 + \ddot{\varphi}_3 + \ddot{\varphi}_4 = \frac{1}{(2H_1 + J_1)}(M_1 + M_2 + M_3 + M_4) \tag{3.234}$$

and summing equations (3.209) and (3.221) and subtracting both (3.213) and (3.217) yields

$$(2H_1 + J_1)\ddot{\varphi}_1 - (2H_1 + J_1)\ddot{\varphi}_2 - (2H_1 + J_1)\ddot{\varphi}_3 + (2H_1 + J_1)\ddot{\varphi}_4$$
$$= M_1 - M_2 - M_3 + M_4 \,,$$
$$\ddot{\varphi}_1 - \ddot{\varphi}_2 - \ddot{\varphi}_3 + \ddot{\varphi}_4 = \frac{1}{(2H_1 + J_1)}(M_1 - M_2 - M_3 + M_4) \,. \tag{3.235}$$

Similarly, summing equations (3.209) and (3.217) and subtracting equations (3.213) and (3.221) yields

$$(4H_2 + J_1)\ddot{\varphi}_1 - (4H_2 + J_1)\ddot{\varphi}_2 + (4H_2 + J_1)\ddot{\varphi}_3 - (4H_2 + J_1)\ddot{\varphi}_4$$
$$= M_1 - M_2 + M_3 - M_4 \,,$$
$$\ddot{\varphi}_1 - \ddot{\varphi}_2 + \ddot{\varphi}_3 - \ddot{\varphi}_4 = \frac{1}{(4H_2 + J_1)}(M_1 - M_2 + M_3 - M_4) \,. \tag{3.236}$$

It then follows from substituting equations (3.234) and (3.235) into equation (3.232) that

$$\ddot{x}_C + \dot{y}_C\dot{\psi} = \frac{R}{4(2H_1 + J_1)}(M_1 + M_2 + M_3 + M_4)\cos\psi$$
$$+ \frac{R}{4(2H_1 + J_1)}(M_1 - M_2 - M_3 + M_4)\sin\psi\,,$$
$$\ddot{x}_C + \dot{y}_C\dot{\psi} = \frac{R}{4(2H_1 + J_1)}[M_1(\cos\psi + \sin\psi)$$
$$+ M_2(\cos\psi - \sin\psi) + M_3(\cos\psi - \sin\psi)$$
$$+ M_4(\cos\psi + \sin\psi)]$$

(3.237)

and it follows from substituting equations (3.234) and (3.235) into equation (3.233) that

$$\ddot{y}_C - \dot{x}_C\dot{\psi} = \frac{R}{4(2H_1 + J_1)}(M_1 + M_2 + M_3 + M_4)\sin\psi$$
$$- \frac{R}{4(2H_1 + J_1)}(M_1 - M_2 - M_3 + M_4)\cos\psi\,,$$
$$\ddot{y}_C - \dot{x}_C\dot{\psi} = \frac{R}{4(2H_1 + J_1)}[M_1(\sin\psi - \cos\psi)$$
$$+ M_2(\sin\psi + \cos\psi) + M_3(\sin\psi + \cos\psi)$$
$$+ M_4(\sin\psi - \cos\psi)]\,.$$

(3.238)

Substituting equation (3.236) into the differential equation of $\ddot{\psi}$ as in (3.223) results in

$$\ddot{\psi} = \frac{R}{4\,(l + \rho)(4H_2 + J_1)}(-M_1 + M_2 - M_3 + M_4)\,.$$

(3.239)

Then, substituting coefficients H_1 and H_2 by their corresponding values $H_1 = \frac{mR^2}{8}$ and $H_2 = \frac{J_C R^2}{16(l+\rho)^2}$ results in the following comparable form of the differential equations of the approximation model

$$\ddot{x}_C + \dot{y}_C\dot{\psi} = \frac{R}{(mR^2 + 4J_1)}[M_1(\cos\psi + \sin\psi)$$
$$+ M_2(\cos\psi - \sin\psi) + M_3(\cos\psi - \sin\psi)$$
$$+ M_4(\cos\psi + \sin\psi)]\,,$$

(3.240)

$$\ddot{y}_C - \dot{x}_C\dot{\psi} = \frac{R}{(mR^2 + 4J_1)}[M_1(\sin\psi - \cos\psi)$$
$$+ M_2(\sin\psi + \cos\psi) + M_3(\sin\psi + \cos\psi)$$
$$+ M_4(\sin\psi - \cos\psi)]\,,$$

(3.241)

$$\ddot{\psi} = \frac{R}{\left(\frac{J_C R^2}{(l+\rho)} + 4J_1(l+\rho)\right)}(-M_1 + M_2 - M_3 + M_4).$$

(3.242)

Now, the last three differential equations of motion can be reformed to obtain a mathematical form that can be compared with the differential equations of motion of the suggested modeling method, which is based on the LAGRANGE equation with multipliers, as follows

$$\boxed{\begin{aligned} &(\ddot{x}_C + \dot{y}_C\dot{\psi})\left(m + \frac{4J_1}{R^2}\right) \\ &= \frac{1}{R}[(\cos\psi + \sin\psi)(M_1 + M_4) + (\cos\psi - \sin\psi)(M_2 + M_3)], \end{aligned}}$$

(3.243)

$$\boxed{\begin{aligned} (\ddot{y}_C - \dot{x}_C\dot{\psi})\left(m + \frac{4J_1}{R^2}\right) \\ = \frac{1}{R}[-(\cos\psi - \sin\psi)(M_1 + M_4) \\ + (\cos\psi + \sin\psi)(M_2 + M_3)], \end{aligned}}$$

(3.244)

$$\boxed{\ddot{\psi}\left(J_C + \frac{4J_1(l+\rho)^2}{R^2}\right) = \frac{(l+\rho)}{R}(-M_1 + M_2 - M_3 + M_4).}$$

(3.245)

Equations (3.172)-(3.174), which were estimated from nonholonomic mechanics principles, and equations (3.243)-(3.245), which are based on holonomic mechanics, deliver identical results in the case of $\dot{x}_C\dot{\psi} = 0$ and $\dot{y}_C\dot{\psi} = 0$. An equivalent case can also be achieved where $\dot{\psi} = 0$, i.e. $\psi = const$, or $\dot{x}_C = \dot{y}_C = 0$, i.e. $x_C = const$ and $y_C = const$.

In other words, the result of the comparison between the two different methods is that both methods lead to the same result in the particular case in which the vehicle exhibits only translational motion or only rotates about its center of mass. In both of these cases, the constraints become holonomic. The next chapter discusses a case study based on the 4WMV from the company Nexusrobot® using simulation and presented as an application for both the suggested and the approximation dynamic models. The simulation results can help in determining which methodology is more suitable for achieving accurate kinematic and dynamic modeling for all possible motion trajectories.

4   Simulation results and experiments

This chapter aims to realize the mathematical equations into simulations and experiments and presents several trajectories of motion for the 4WMV. The simulation covers the translational and rotational motion of the vehicle. A virtual reality environment will be introduced to visualize the motion of the system and converts the data into real motion, which combines the translation and rotation in one object. Finally, the designed platforms and their motion characteristics will be discussed.

4.1   Numerical integration methods

The numerical integration methods, which have been used in this thesis can be categorized in two classes, the first integration method is for the fully implicit differential equations system and the second category is for the explicit differential equations. The estimated differential equations of the dynamic model, which are presented in Chapter 3- Section 3.3.2; equations (3.168), (3.169) and (3.170) are implicit differential equations of second order. They are coupled in the term with highest derivative order, i.e. $\ddot{x}_C$, $\ddot{y}_C$ and $\ddot{\psi}$. Therefore a special routine for the numerical integration in MATLAB® has been used to integrate the set of equations numerically. It is called ODE15i and the required parameters have been passed to enhance the accuracy of the integration.

The numerical integration routines can handle only the differential equations of first order; therefore the order of the differential equations will be reduced from the second to the first order by assuming that

$$y_1 = x_C , \qquad y_2 = y_C , \qquad y_3 = \psi ,$$

and

$$y_4 = \dot{x}_C, \qquad y_5 = \dot{y}_C, \qquad y_6 = \dot{\psi}.$$

Therefore, the first time derivative for the last expressions will be

$$\dot{y}_1 = y_4 = \dot{x}_C, \qquad \dot{y}_2 = y_5 = \dot{y}_C, \qquad \dot{y}_3 = y_6 = \dot{\psi},$$

and

$$\dot{y}_4 = \ddot{x}_C, \qquad \dot{y}_5 = \ddot{y}_C, \qquad \dot{y}_6 = \ddot{\psi}.$$

The previous procedure is used to transform three differential equations of second order into six equations of first order, which can be integrated numerically using any numerical integration software, but in this thesis, MATLAB® and SIMULINK® have been used to handle this task. The transformation procedure has been done for both the implicit and explicit form of the differential equations.

In case of the approximation method, the system of differential equations consists of four equations of second order. These equations will be transformed again into 8 differential equations of second order as following

$$y_1 = \varphi_1, \qquad y_2 = \varphi_2, \qquad y_3 = \varphi_3, \qquad y_4 = \varphi_4,$$

and

$$y_5 = \dot{\varphi}_1, \qquad y_6 = \dot{\varphi}_2, \qquad y_7 = \dot{\varphi}_3, \qquad y_8 = \dot{\varphi}_4.$$

The time derivative for the last assumptions will be

$$\dot{y}_1 = y_5 = \dot{\varphi}_1, \qquad \dot{y}_2 = y_6 = \dot{\varphi}_2,$$
$$\dot{y}_3 = y_7 = \dot{\varphi}_3, \qquad \dot{y}_4 = y_8 = \dot{\varphi}_4,$$

and

$$\dot{y}_5 = \ddot{\varphi}_1, \qquad \dot{y}_6 = \ddot{\varphi}_2, \qquad \dot{y}_7 = \ddot{\varphi}_3, \qquad \dot{y}_8 = \ddot{\varphi}_4.$$

This set consists of eight differential equations of first order and they are not coupled. They will be passed to an integration routine in MATLAB® called ODE45. The initial conditions and the integration period beside the

accuracy will be passed to the routine ODE45 to get the similar accuracy as mentioned before in the case of the suggested model.

Another solution has been used to integrate the equations of the dynamic model numerically by changing the equations of (3.168), (3.169) and (3.170) into an explicit form as following

$$
\begin{aligned}
\ddot{x}_C = & -\frac{2m_1 R^2}{A}(\rho_1 - \rho_2)\cos\psi\,\dot{\psi}^2 \\
& +\frac{2J_1 m_0 \alpha}{J \cdot A}(\rho_1 - \rho_2)^2 \sin 2\psi\,\dot{x}_C \dot{\psi} \\
& +\frac{4J_1}{A}\left[\frac{m_0 \alpha}{J}(\rho_1 - \rho_2)^2 \sin^2 \psi - 1\right]\dot{y}_C \dot{\psi} \\
& -\frac{2\alpha}{J \cdot R}(\rho_1 - \rho_2)[l(M_2 - M_1 + M_4 - M_3) + \rho_2(M_2 - M_1) \\
& + \rho_1(M_4 - M_3) - 2\alpha(\rho_1 - \rho_2)(M_1 - M_2 - M_3 + M_4)]\sin\psi \\
& +\frac{R}{A}[(M_1 + M_2 + M_3 + M_4)\cos\psi \\
& + (M_1 - M_2 - M_3 + M_4)\sin\psi]\,,
\end{aligned}
\tag{4.1}
$$

$$
\begin{aligned}
\ddot{y}_C = & \frac{-2m_1 R^2}{A}(\rho_1 - \rho_2)\sin\psi\,\dot{\psi}^2 \\
& -\frac{4J_1}{A}\left[\frac{m_0 \alpha}{J}(\rho_1 - \rho_2)^2 \cos^2 \psi - 1\right]\dot{x}_C \dot{\psi} \\
& -\frac{2J_1 m_0 \alpha}{J \cdot A}(\rho_1 - \rho_2)^2 \sin 2\psi\,\dot{y}_C \dot{\psi} \\
& +\frac{2\alpha}{J \cdot R}(\rho_1 - \rho_2)[l(M_2 - M_1 + M_4 - M_3) + \rho_2(M_2 - M_1) \\
& + \rho_1(M_4 - M_3) - 2\alpha(\rho_1 - \rho_2)(M_1 - M_2 - M_3 + M_4)]\cos\psi \\
& +\frac{R}{A}[(M_1 + M_2 + M_3 + M_4)\sin\psi \\
& - (M_1 - M_2 - M_3 + M_4)\cos\psi]\,,
\end{aligned}
\tag{4.2}
$$

$$
\begin{aligned}
\ddot{\psi} = & -\frac{2J_1 m_0}{J \cdot A}(\rho_1 - \rho_2)(\dot{x}_C \cos\psi + \dot{y}_C \sin\psi)\dot{\psi} \\
& +\frac{1}{J \cdot R}[l(M_2 - M_1 + M_4 - M_3) + \rho_2(M_2 - M_1) \\
& + \rho_1(M_4 - M_3) - 2\alpha(\rho_1 - \rho_2)(M_1 - M_2 - M_3 + M_4)]\,.
\end{aligned}
\tag{4.3}
$$

$A = mR^2 + 4J_1$, $B = m_1R^2 + J_1$ and $\alpha = \frac{B}{A}$. Also, the mass moments of inertia can be defined as following, where $J = J_0 + 4J_2 + 2m_1(\rho_1^2 + \rho_2^2 + 2l^2) + \frac{4J_1}{R^2}((l + \rho_1)^2 + (l + \rho_2)^2) - \frac{4B}{R^2}\alpha(\rho_1 - \rho_2)^2,$ $J_0 = \frac{m_0}{12}(4l^2 + (\rho_1 + \rho_2)^2)$, $J_1 = \frac{m_1R^2}{2}$ and $J_2 = \frac{m_1R^2}{4}$.

The virtual reality model uses the RUNGE-KUTTA algorithm for the numerical integration and forwards the results of the integration to the virtual Environment, which simulates the motion. A 4WMV has been built and a trajectory for the motion of the mass center will be plotted during the simulation. The structure of the SIMULINK® model for the virtual reality environment has been used to realize the motion of the vehicle.
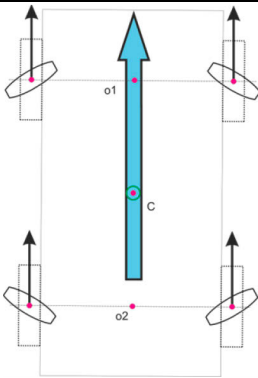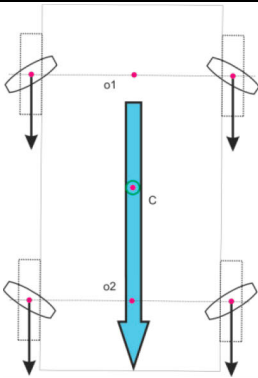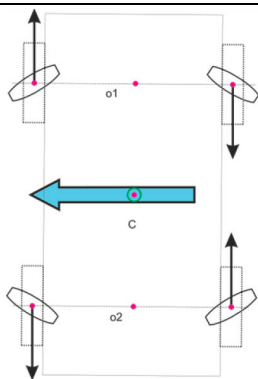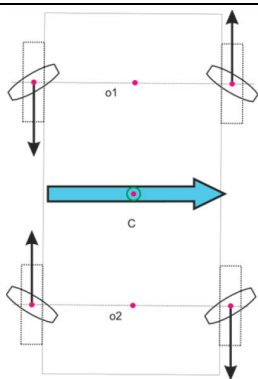
4.2   <u>Motion trajectories and the simulated mathematical models</u>
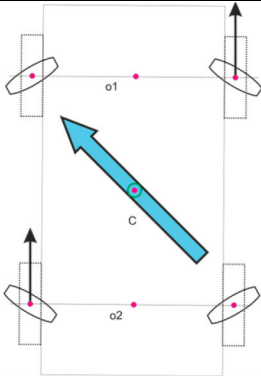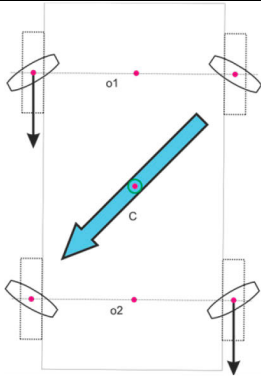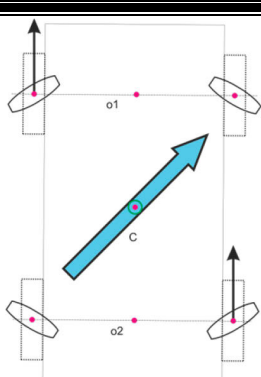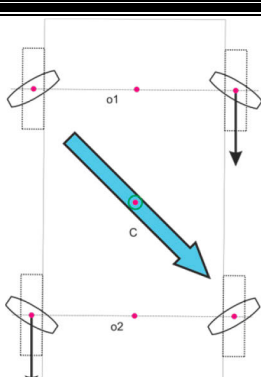
The 4WMV can move along different motion trajectories. They are classified into simple trajectories and combined trajectories. The simple trajectories are called also the main directions of motion (for example the motion to forward, backward, left and right). The combined trajectories consist of a set of simple motion trajectories which lead to a motion along a complex trajectory in the plane. In this study, the simple trajectories will be considered as shown in the following subsections.
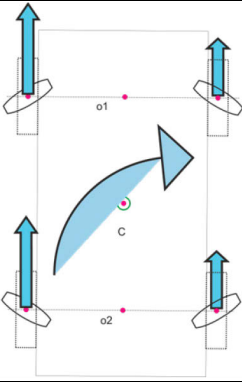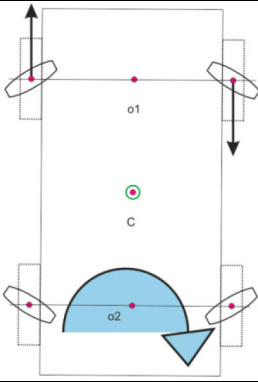
4.2.1   The main directions of motion

The 4WMV can move to any point on the plane using certain directions of motion. The main directions can be simulated by applying driving moments on each wheel. For each motion trajectory, the driving moments are constant within the simulation timeframe. The direction of the arrow on each wheel shows the direction of rotation, which is also fixed within the simulation. In the case of motion along a curve, the length of the arrow indicates the magnitude of the driving moment for each wheel. The blue arrow shows the resultant direction of motion for whole vehicle. Both the suggested dynamic model and the approximated dynamic model will be examined to simulate the following motion trajectories and the capability of modeling the trajectory will be indicated directly under each trajectory as follows:
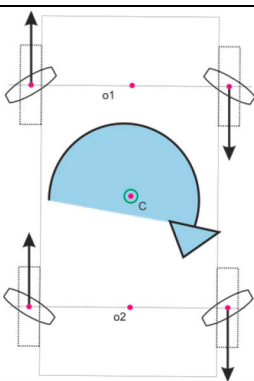
Table 4.1 Main motion trajectories

Forward	Backward
Both models can simulate forward motion	Both models can simulate backward motion
Left	Right
Both models can simulate motion to the left	Both models can simulate motion to the right

Forward – Left (diagonal motion)	Backward – Left (diagonal motion)
Both models can simulate diagonal motion forward and left	Both models can simulate diagonal motion backward and left
Forward – Right (diagonal motion)	Backward – Right (diagonal motion)
Both models can simulate diagonal motion forward and right	Both models can simulate diagonal motion backward and right

Curve	Lateral arc
The suggested model can simulate motion along a curve but the approximated model cannot	The suggested model can simulate motion along a lateral arc but the approximated model cannot

Rotation about the center of mass

Both models can simulate rotational motion about the center of mass

It was found in numerical simulations of the presented suggested model, that the center of mass must be in the middle of the vehicle. That means ρ_1 and ρ_2 in Figure 3.8 or in Figure 3.11 must be equal.

4.2.2   The resulted variables from the simulation

First, the following 4WMV parameters will be given to the MATLAB code to be numerically integrated and delivers the simulated parameters of the vehicle. The transitional period has not been taken in consideration, because it is assumed that the maximum driving moment will reach the maximum limit after 2 sec from the beginning to the end of the simulation time as shown in Figure 4.1. The used vehicle is a 4WD 100mm Mecanum Wheel robot kit 10011 - Nexus Robot.

Table 4.2 Vehicle parameters of the 4WMV

m_0 (kg)	20
m_1 (kg)	0.3
$\rho_1 + \rho_2$ (m)	0.4
l (m)	0.18
R (m)	0.05
M_i (Nm) where $i = 1, 2, 3, 4$	0-0.9- variable within the simulation time
Electrical Motor Specifications	
Max. Power (W)	17
Max. Rotation Speed (RPM)	120
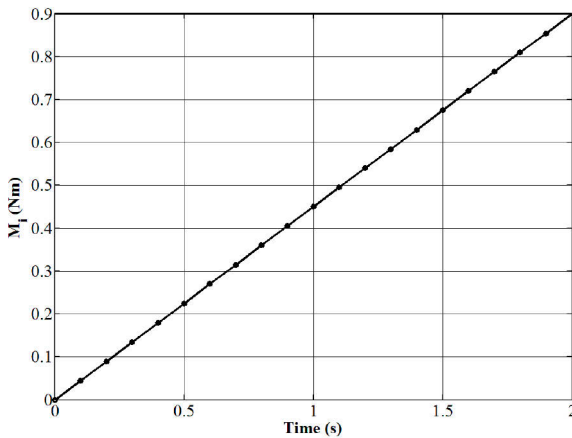
Figure 4.1 The driving moment

   In the simulation, the numerical integration of the suggested model will be denoted by "Sugg." and it will be the result of the numerical integration for the equations (3.168), (3.169) and (3.170) to estimate the parameters x_C , y_C and ψ. By simulating the approximation method in equation (3.222) results the parameters $\dot\varphi_1$, $\dot\varphi_2$, $\dot\varphi_3$ and $\dot\varphi_4$, then they will be substituted in equation (3.199) to find the parameters $\dot x_C$, $\dot y_C$ and $\dot\psi$ and after integrating them numerically along the simulation time, the integration results will be denoted by "Aprox." and plotted in comparison to the first method as shown in Figure 4.2.
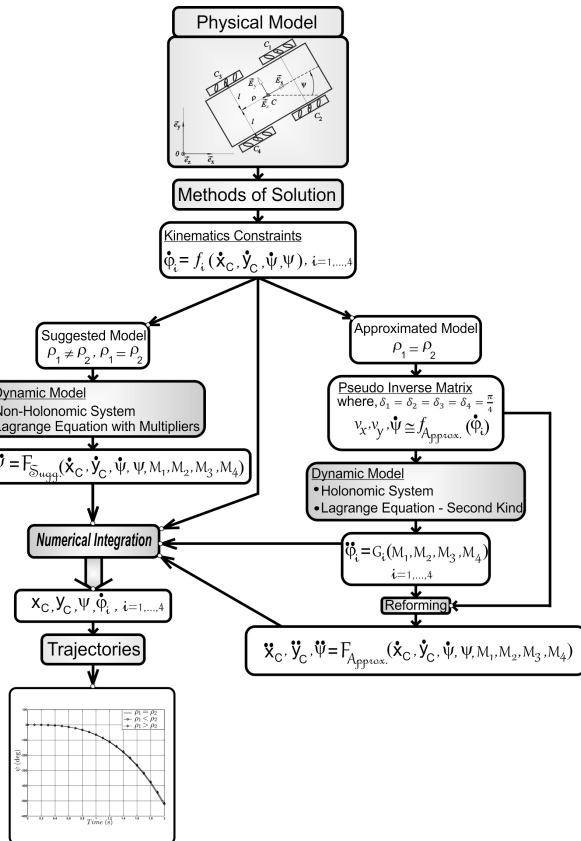
Figure 4.2 Flow chart for the mathematical derivations and programming sequence

Regarding to the angular speeds of the Mecanum wheels, the numerical integration of the equations (3.168), (3.169) and (3.170) of the suggested model give the parameters $\dot{x}_C$, $\dot{y}_C$ and $\dot{\psi}$, which will be substituted in the equations of the kinematic constraints (3.79), (3.83), (3.86) and (3.89) to find the rotation speeds $\dot{\varphi}_1$, $\dot{\varphi}_2$, $\dot{\varphi}_3$ and $\dot{\varphi}_4$, respectively. In the following parts, the rotation speeds of the wheel will be used in the virtual reality simulation of the real motion of the 4WMV, where the angular displacement of each wheel is required. Therefore, the numerical integration will applied to integrate the rotation speeds numerically within the simulation in the SIMULINK® model.

In all simulated motion trajectories, a variable driving moment will be given as input to the system, which is changing from 0 to 0.9 Nm in 2 seconds. For each motion trajectory, a separate simulation will be carried out to find its corresponding motion parameters. They will be plotted and compared with the used mathematical models. The driving moments can have different absolute values or different rotation direction for each wheel, all that depend on the motion trajectory which is simulated. The driving moments must be proportional to the rotation speeds of each wheel during the simulation. They will be denoted by $\vec{M}_1$, $\vec{M}_2$, $\vec{M}_3$ and $\vec{M}_4$ with respect to its corresponding wheel.

4.3   Simulation results

Now, after analyzing the system from the kinematics and dynamics point of views and having differential equations from the second order which are representing the behavior of the 4WMV, it is possible to integrate these equations numerically and find out the characteristics of the motion of the 4WMV. The studied trajectories, in the motion plane, are classified into simple and complex trajectories as has been discussed in the following parts.

4.3.1   Simple trajectories

The simple trajectories are all the trajectories which can be realized by applying direct variable or constant moments on the wheels of the 4WMV separately. The simple trajectories are the base of all the complex forms or motion trajectories, in the case of using the approximated method. In this part, a comparison between the suggested and the approximated models was held, to find the advantages and disadvantages of each method. The effect of shifting the center of mass will be studied. In addition, the virtual reality

environment has been used to show the behavior of the system under different operation conditions.

Forward Motion	
Sugg. and Aprox. @ $\rho_1 = \rho_2$	Sugg. @ $\rho_1 = \rho_2$, $\rho_1 < \rho_2$, $\rho_1 > \rho_2$
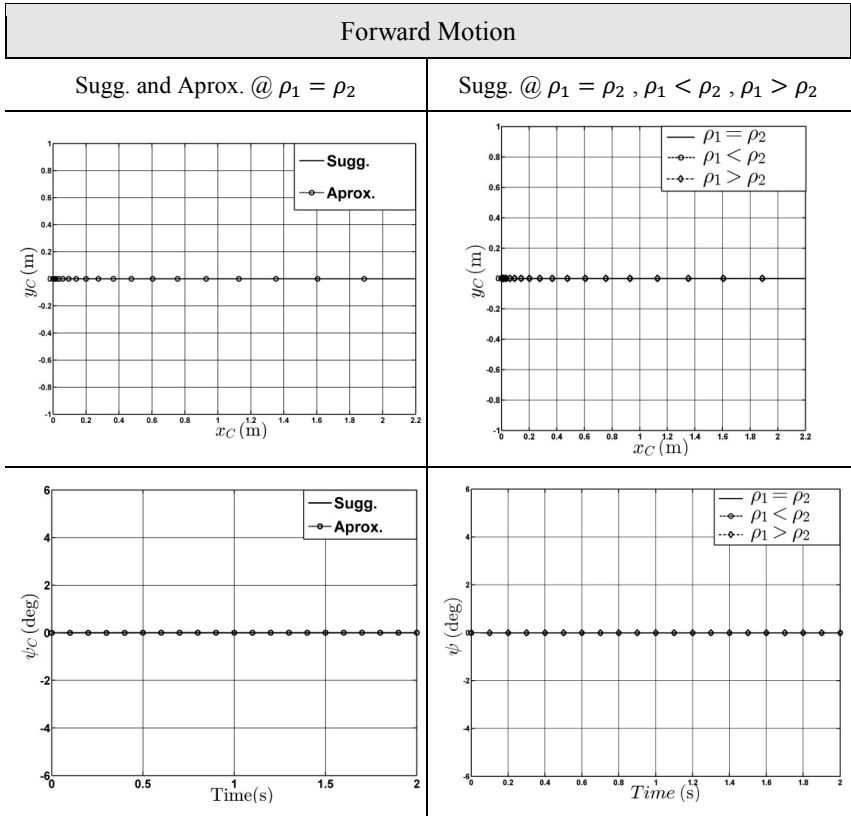
Figure 4.3 Forward motion simulation using the suggested and the approximated methods at different cases of shifting the vehicle mass center
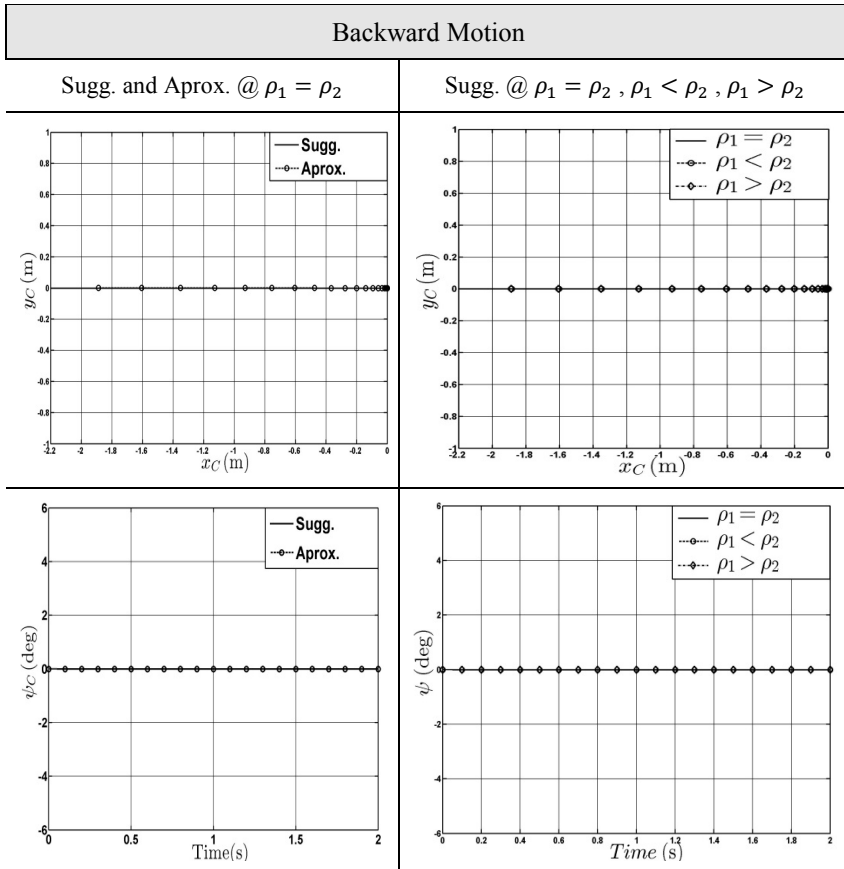
Figure 4.4 Backward motion simulation using the suggested and the approximated methods at different cases of shifting the vehicle mass center

Left Motion	
Sugg. and Aprox. @ $\rho_1 = \rho_2$	Sugg. @ $\rho_1 = \rho_2$, $\rho_1 < \rho_2$, $\rho_1 > \rho_2$
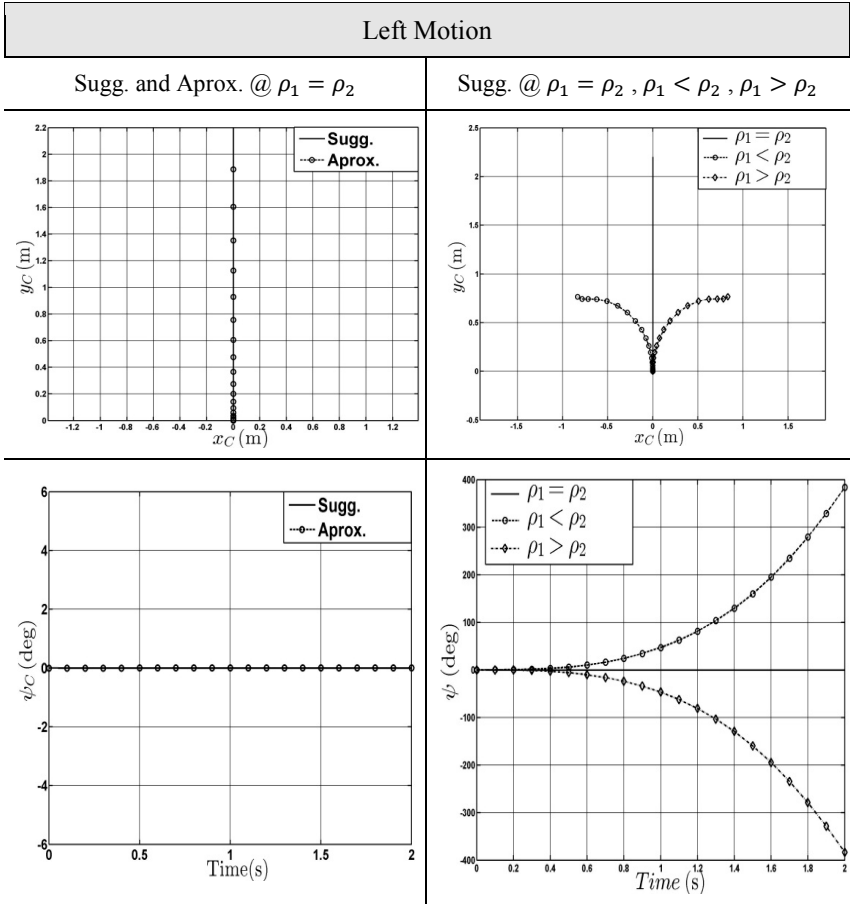
Figure 4.5 Left motion simulation using the suggested and the approximated methods at different cases of shifting the vehicle mass center

The effect of shifting the center of mass of the vehicle appears on the resulted motion trajectory, the whole vehicle rotation angle ψ and the displacements x_C and y_C as shown in Figure 4.5. The accuracy of the resulted parameters from the numerical integration can be differ from the exact behavior of the real system due to the slip of wheels, which leads to losses kinetic energy, which has not been taken in consideration in the mathematical equations. It is expected that the shifting of center of mass for the real 4WMV will not change the motion parameters dramatically as

appeared in the simulation results. The previous declaration for the simulation results is valid for all next results. In case $\rho_1 < \rho_2$, it was noticed that the whole vehicle moves along a curve to the left backward direction. But in case of $\rho_1 > \rho_2$, the vehicle moves to the left forward direction along a curve. In both previous cases, the 4WMV rotates by angle ψ around the center of mass. Therefore, it can be said that the vehicle moves in the same direction to the load concentration of the vehicle mass. If the mass concentrated on the frontal axle, then the 4WMV moves forward left and by changing the mass concentration to be on the rear axle, then the 4WMV moves in the backward left direction.
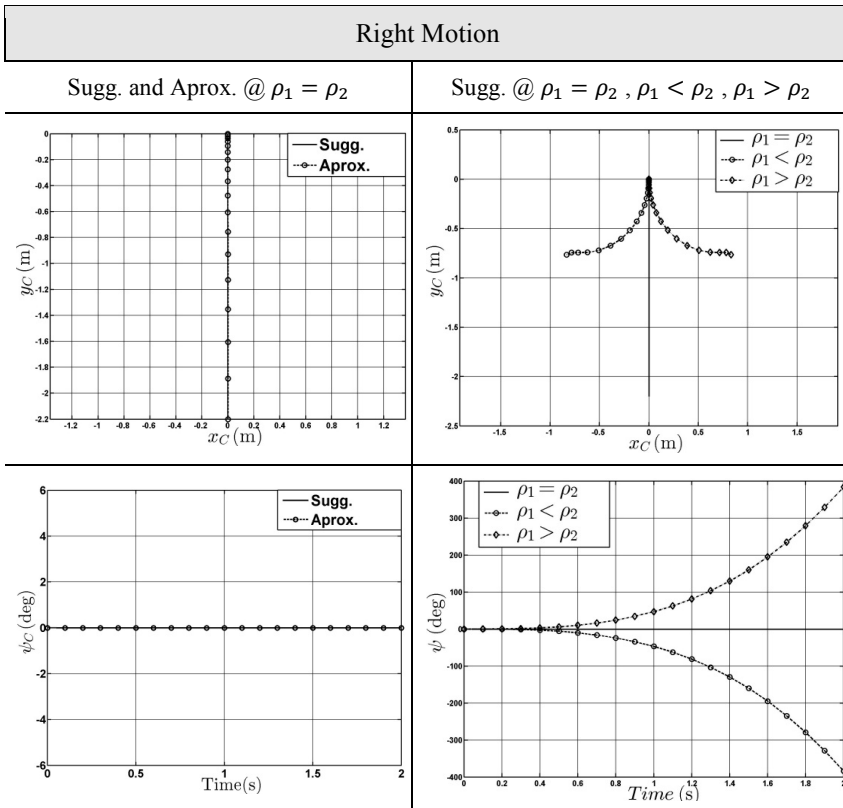
Figure 4.6 Right motion simulation using the suggested and the approximated methods at different cases of shifting the vehicle mass center

Forward-Left Motion	
Sugg. and Aprox. @ $\rho_1 = \rho_2$	Sugg. @ $\rho_1 = \rho_2$, $\rho_1 < \rho_2$, $\rho_1 > \rho_2$
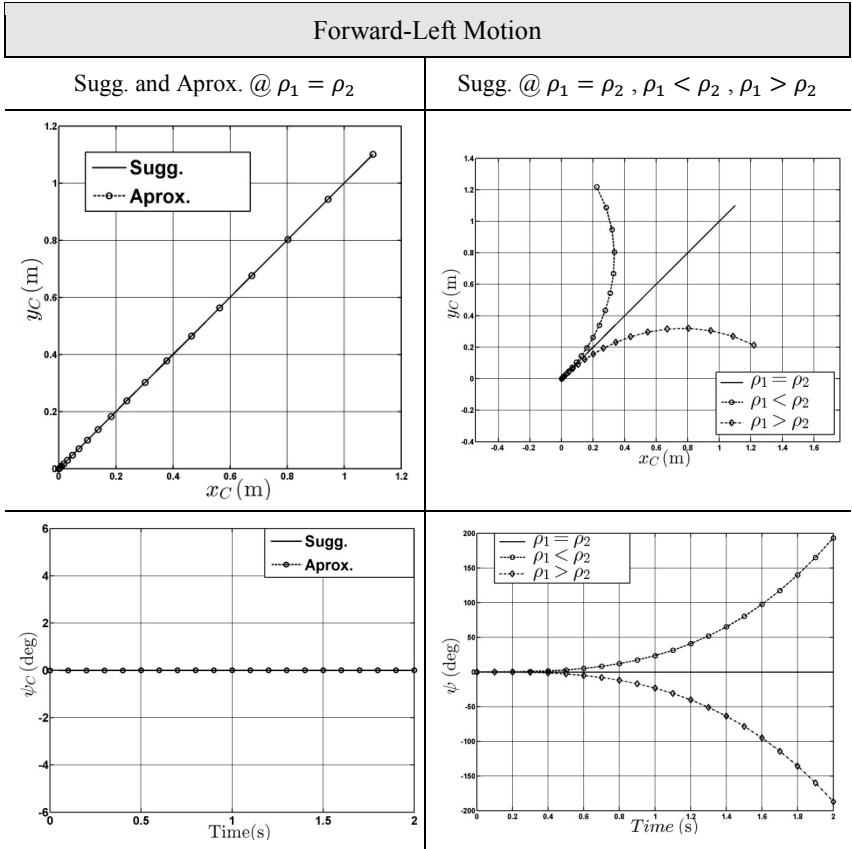
Figure 4.7 Forward-Left motion simulation using the suggested and the approximated methods at different cases of shifting the vehicle mass center

Backward-Left Motion	
Sugg. and Aprox. @ $\rho_1 = \rho_2$	Sugg. @ $\rho_1 = \rho_2$, $\rho_1 < \rho_2$, $\rho_1 > \rho_2$
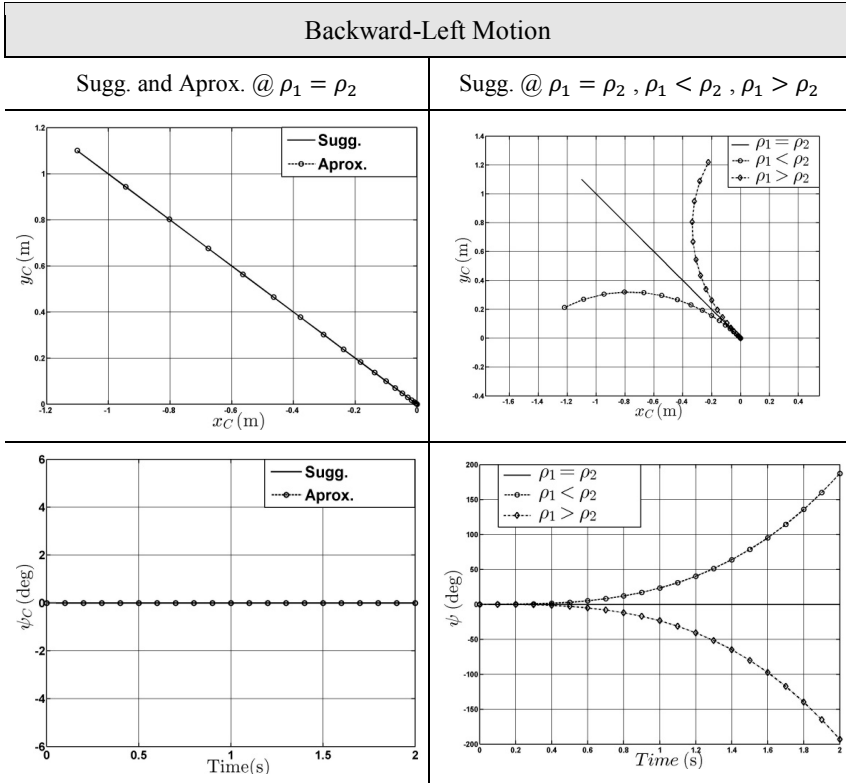
Figure 4.8 Backward-Left motion simulation using the suggested and the approximated methods at different cases of shifting the vehicle mass center

Forward-Right Motion	
Sugg. and Aprox. @ $\rho_1 = \rho_2$	Sugg. @ $\rho_1 = \rho_2$, $\rho_1 < \rho_2$, $\rho_1 > \rho_2$

Figure 4.9 Forward-Right motion simulation using the suggested and the approximated methods at different cases of shifting the vehicle mass center

Backward-Right Motion	
Sugg. and Aprox. @ $\rho_1 = \rho_2$	Sugg. @ $\rho_1 = \rho_2$, $\rho_1 < \rho_2$, $\rho_1 > \rho_2$
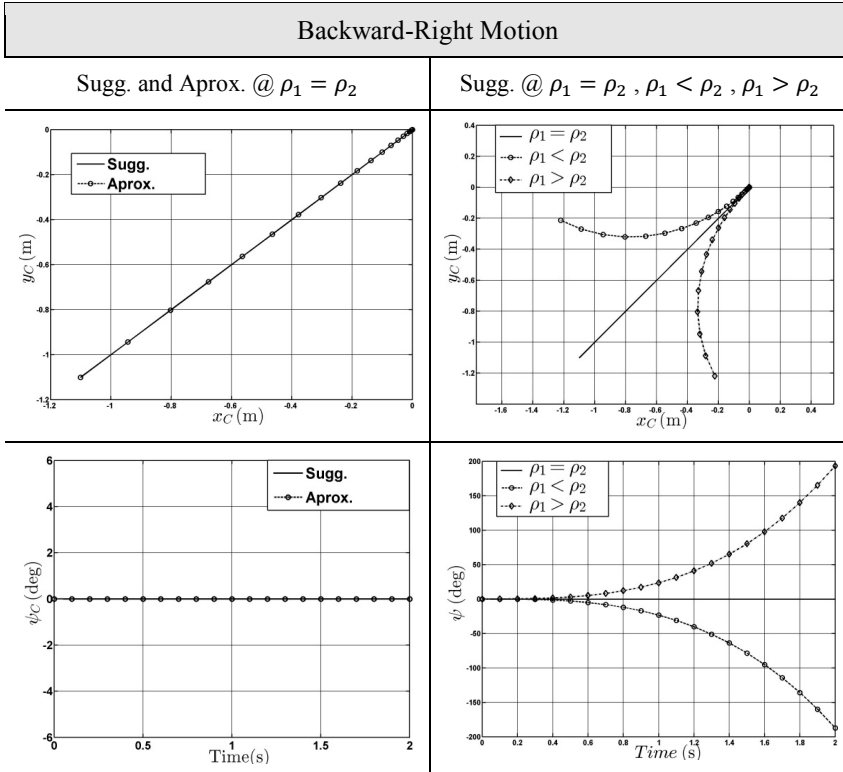
Figure 4.10 Backward-Right motion simulation using the suggested and the approximated methods at different cases of shifting the vehicle mass center

In Figure 4.7, Figure 4.8, Figure 4.9 and Figure 4.10, the 4WMV took the axle of weight concentration as a rotation center and began in rotating around it. Here, it is clear that the 4WMV showed translational and rotational behavior in respect to the weight concentration. If the mass is shifted near from the frontal axle, then the 4WMV moves forward and vice versa.

The suggested and approximated models show the same behavior during the motion in case the center of mass of the vehicle is in the middle of the 4WMV, i.e. $\rho_1 = \rho_2$. The centralization of the mass leads to uniform distribution of the traction forces which cause standardized translational and rotational motion as expected from the 4WMV.
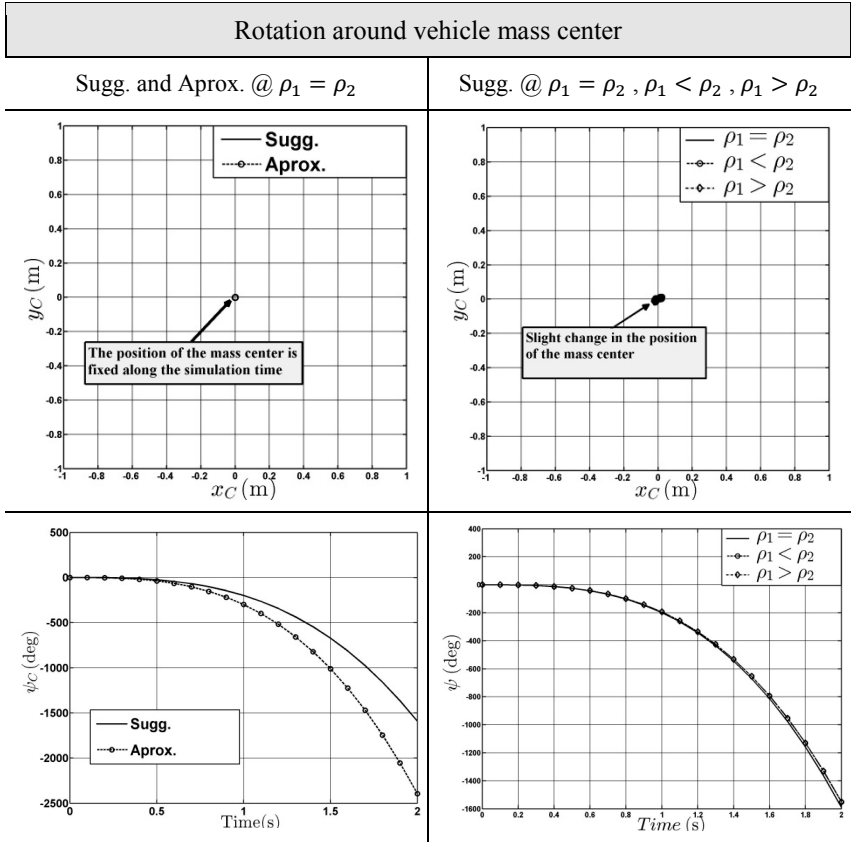
Figure 4.11 Simulation of the rotation around the vehicle mass center using the suggested and the approximated methods at different cases of shifting the vehicle mass center

During the rotation around the center of mass, the 4WMV shows the same behavior of both the suggested and the approximated models during the translational motion. However, the rotational motion is greater in case the approximated model in comparison to the suggested one. The approximated model results change rapidly by increasing the simulation time. On the other hand, the suggested model shows a slight shift in the position of the mass center in the cases of $\rho_1 < \rho_2$, $\rho_1 > \rho_2$, shifting the mass center produces residual forces, which are pushing the mass center to be translated locally as shown in Figure 4.11.

Curved Motion	
Sugg. and Aprox. @ $\rho_1 = \rho_2$	Sugg. @ $\rho_1 = \rho_2$, $\rho_1 < \rho_2$, $\rho_1 > \rho_2$
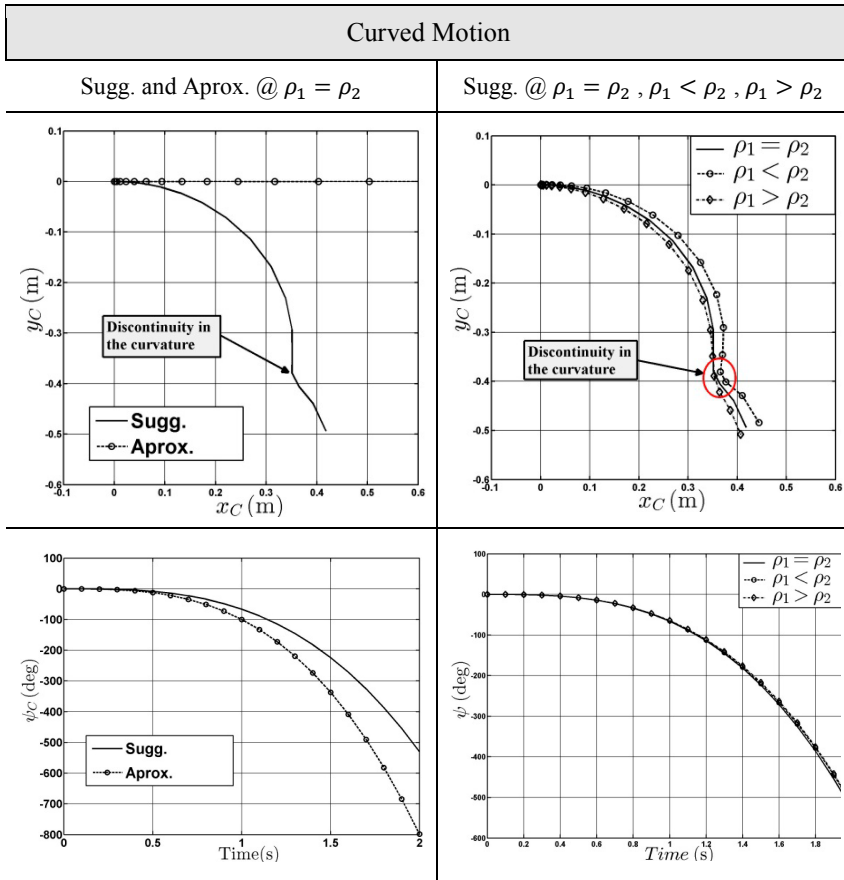
Figure 4.12 Curved motion simulation using the suggested and the approximated methods at different cases of shifting the vehicle mass center

It was noticed, that there is no fixed rotation center during the curved motion. The shifting of the center of mass produces shifting for the center of the rotation. There is a slight difference in the angular displacements due to shifting the mass center of the 4WMV. The approximated model cannot simulate the translational motion in this case and also produces rapidly increased angular displacements. The 4WMV rotates around a rotation center which is shifted in the direction of shifting the mass center. The components of the traction forces, on the contact point, produce shift not

only in the center of the curvature (rotation) but also in shifting the whole trajectory in the direction of shifting the mass center as shown in Figure 4.12.

In the case of the nonholonomic mechanics, the following assumptions are used:

1. The contact is realized just only in one point.
2. The rolling without slippage is considered.

These assumptions, in practice, are realized only approximately. Also, the suggested method did not consider the friction in the axes or the effect of the reduction mechanism. There is no slippage between the roller in contact with the motion surface and the motion plan. Therefore, the driving moment will be converted without losses into motion.
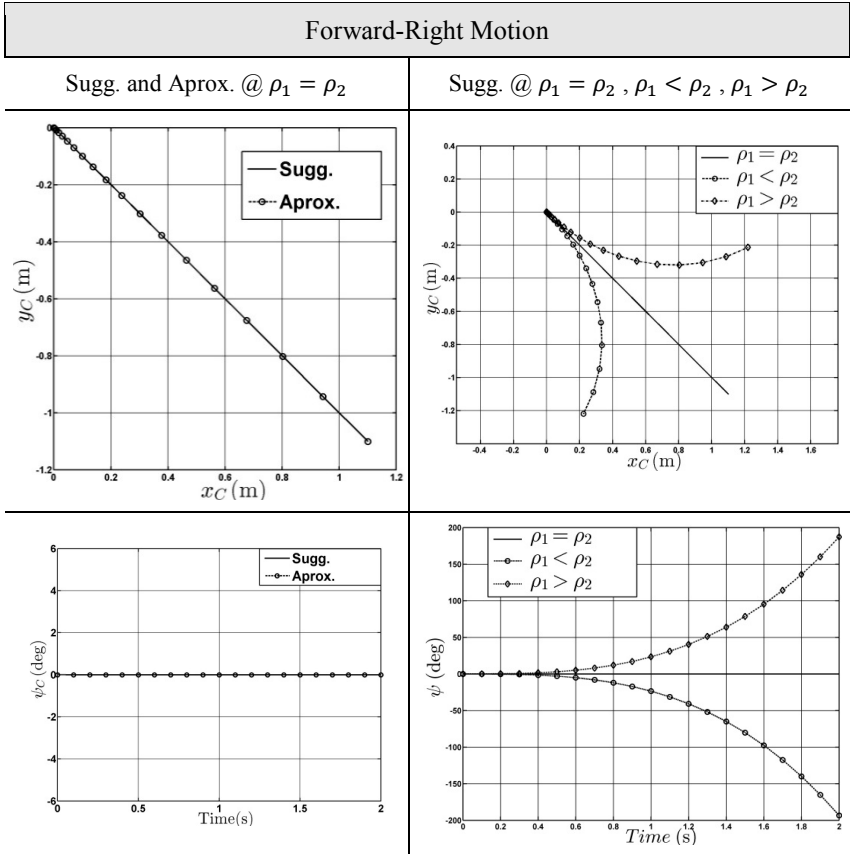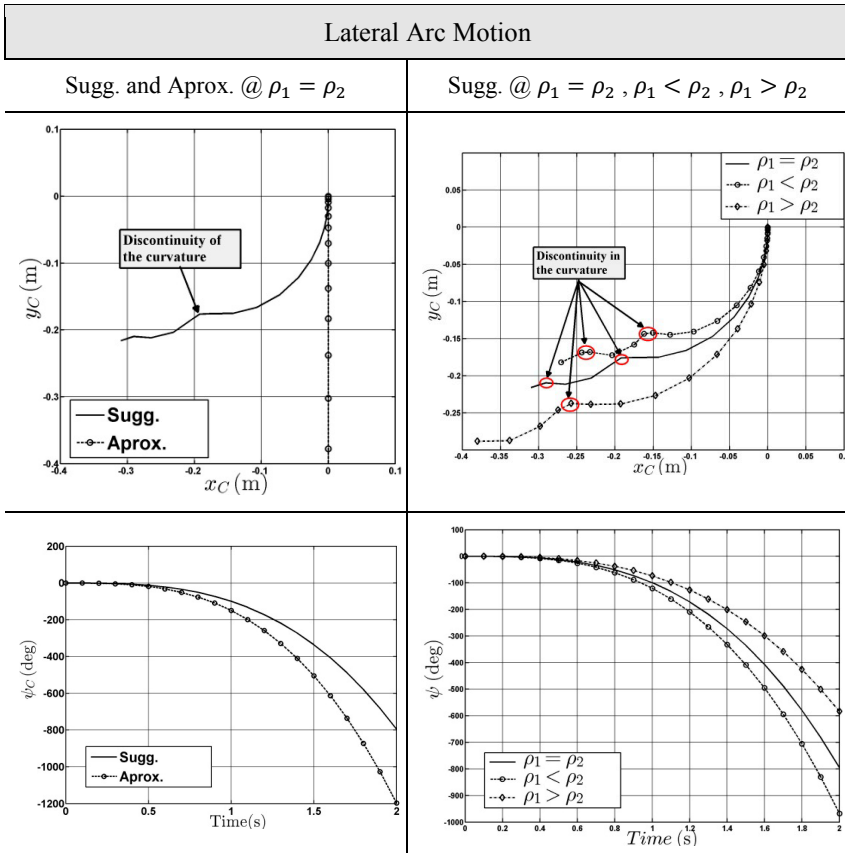
Figure 4.13 Lateral arc motion simulation using the suggested and the approximated methods at different cases of shifting the vehicle mass center

From Figure 4.13, the suggested model shows that the 4WMV rotates around unfixed rotation center, which will change periodically depending on the magnitude of the traction components and their direction along the simulation time. By shifting the center of mass, the translational trajectory will change and the rotation center will change, too. There is interaction between the location of the center of mass and the driving forces direction. This interaction will determine the direction of the translation and how fast the curvature center will be changed.

   As mentioned before, if there is no driving moment applied on the wheel, then the wheel itself will not rotate, but the roller, which is in contact with the surface, will slip.

   In the next part, a virtual simulation environment has been developed to simulate the 4WMV in the 3D environment using Simulink model and the Simulink 3D animation toolbox. The virtual 3D environment shows the 4WMV during the motion and combines all the motion parameters simultaneously. It shows not only the vehicle itself and the motion trajectory in the 3D but also the simulation parameters will be presented in text box nearby, see Figure 4.14.
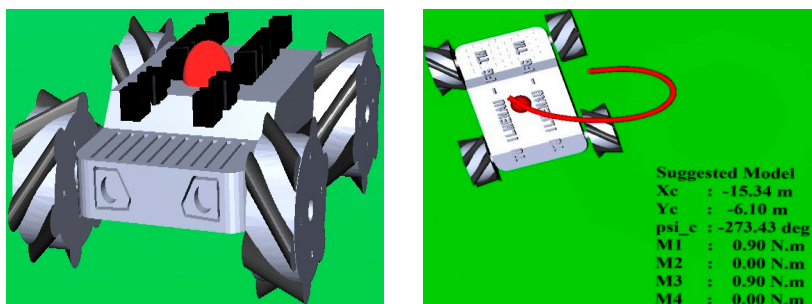
Figure 4.14 The 3D virtual simulation environment using Simulink® and Simulink® 3D animation toolbox

   The case of the motion in the forward – right direction has been selected to show the effect of shifting the center of mass on the trajectory animation of the 4WMV.

Approximated Model
Xc   :   17.61 m
Yc   : -17.61 m
psi_c :   0.00 deg
M1   :   0.90 N.m
M2   :   0.00 N.m
M3   :   0.00 N.m
M4   :   0.90 N.m

Suggested Model
Xc   :   -1.83 m
Yc   :   -3.06 m
psi_c : -3085.17 deg
M1   :   0.90 N.m
M2   :   0.00 N.m
M3   :   0.00 N.m
M4   :   0.90 N.m
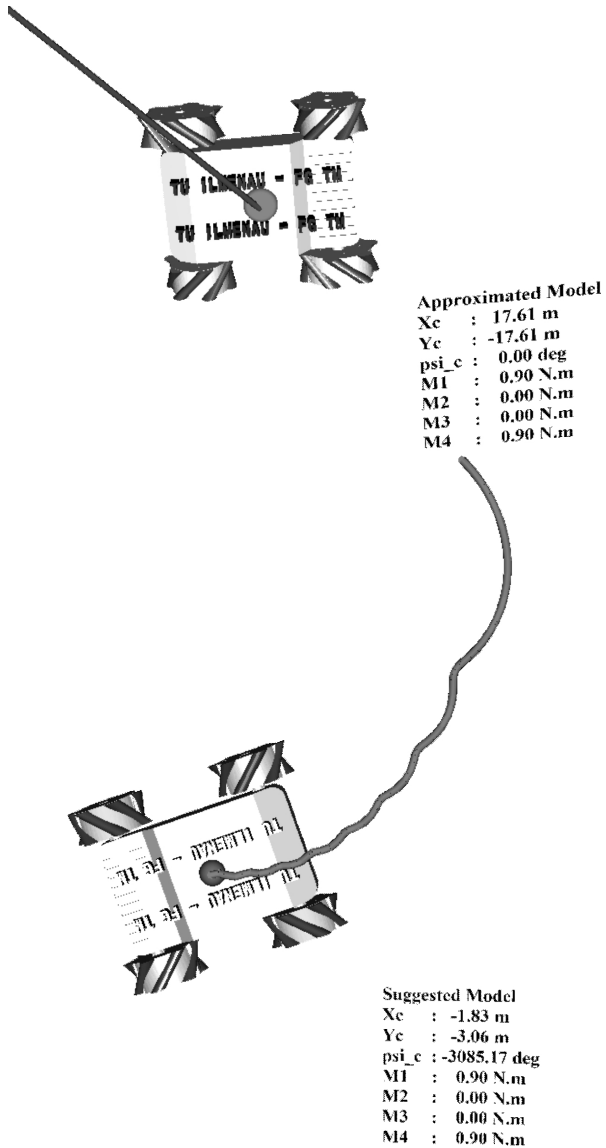
Figure 4.15 Forward right motion trajectory in case of mass center shifting for both the suggested and the approximated models

As shown in Figure 4.15– up, the center of mass shifting leads to combination of changes in the translational trajectory and additional rotation angle for the whole body relative to the center of mass reaches to 8.6 revolution after 8 sec form the beginning of the simulation but on the other side, the approximated model, where the mass center has been considered to be fixed, the vehicle will move diagonally without rotation around its center of mass. The discontinuity of the curvature is an indication of unfixed rotation center during the motion.

For the curved motion, without shifting the mass center, it is found that the motion trajectory of the suggested model is differing from the resulted trajectory of the approximated model due to the difference of the driving moments from a side to another. The differential equations of the approximated model cannot generate the expected trajectory along the simulation time. The suggested model has produced a spiral trajectory after 8 sec from the simulation as shown in Figure 4.16. It is expected for the long simulation period, the vehicle will rotate around its center of mass. The approximated model cannot handle the difference in the driving moments between the left and right sides of the vehicle, so that it produced a linear trajectory parallel to x axis with continuous rotation for the vehicle around its mass center reached to 37 revolutions at the end of the simulation time. Both of the models agree in the continuous rotation of the vehicle around its center of mass but finally they produced different trajectories. The spiral trajectory contains discontinuity in the curvature due to changing of the rotation center during the motion.

```
Approximated Model
Xc    :   22.91 m
Yc    :   -0.00 m
psi_c : -13400.76 deg
M1    :    0.90 N.m
M2    :    0.27 N.m
M3    :    0.90 N.m
M4    :    0.27 N.m
```

```
Suggested Model
Xc    :   -0.15 m
Yc    :   -0.83 m
psi_c : -8903.00 deg
M1    :    0.90 N.m
M2    :    0.27 N.m
M3    :    0.90 N.m
M4    :    0.27 N.m
```
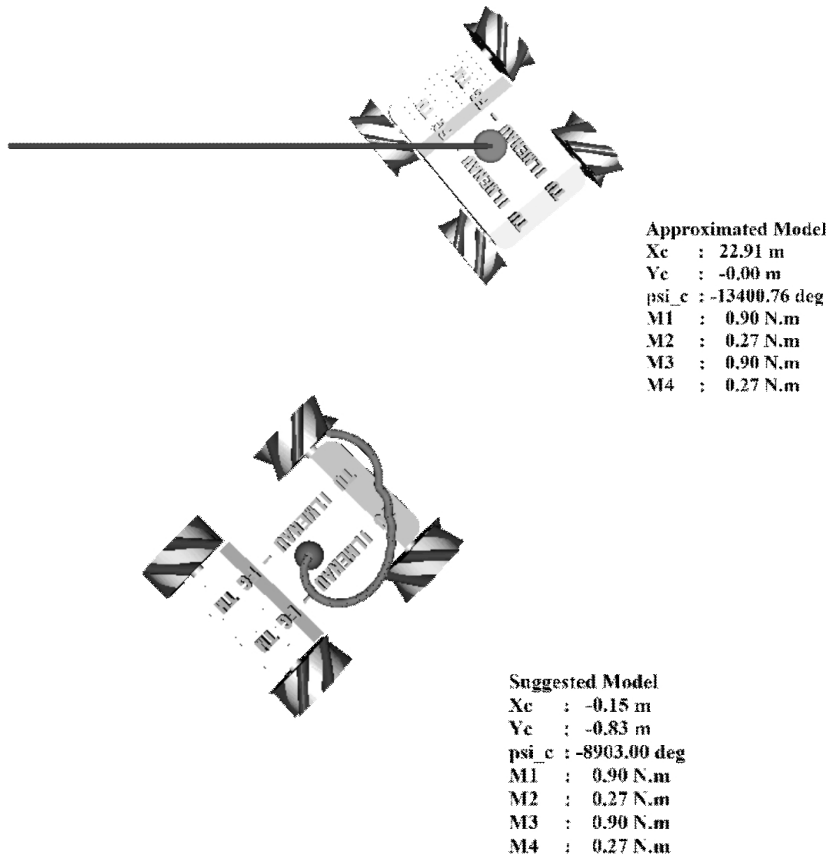
Figure 4.16 Curvature motion with centralized mass center

In case of shifting the center of mass and applying different driving moments on the both sides of the 4WMV, then the suggested model produced similar spiral trajectory like before as shown in Figure 4.17 .
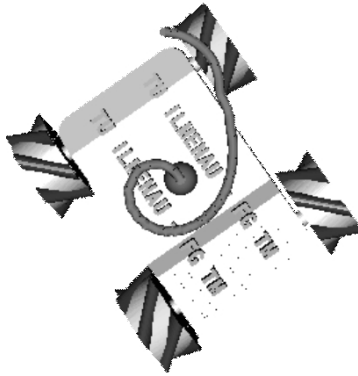
Suggested Model
Xc   :   0.09 m
Yc   : -0.87 m
psi_c : -13572.09 deg
M1   :   0.90 N.m
M2   :   0.27 N.m
M3   :   0.90 N.m
M4   :   0.27 N.m

Figure 4.17 Curvature motion with shifting in mass center

The lateral arc is a special case from the curved motion, it is produced from applying driving moments on just two wheels either the wheels of the frontal axle or the rear axle in different direction to force the whole vehicle to rotate around the middle center of the non-driving axle either frontal or rear it does not matter just to reach the determined point. Therefore, the previous declaration of the curved motion is valid also in case of the motion along a lateral arc. The discontinuity of the curvature can be seen from the presented trajectory in Figure 4.18. The residuals from the traction force components cause a continuous change in the center of the rotation for the whole vehicle. In this case, the loss of the kinetic energy is noticeable due to the free rotation of the rollers at the non-driven wheels. The accumulation of the residuals at end of each turn pushes the whole vehicle to change its center position, therefore the end point of the curvature will most of the time found at the end of the complete rotation.
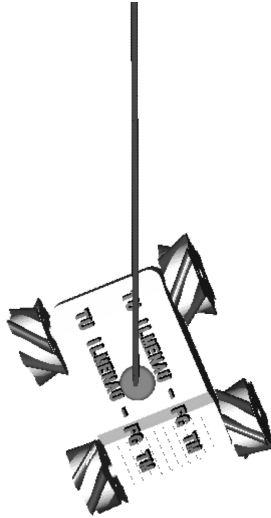
Approximated Model
Xc   :   0.00 m
Yc   : -27.52 m
psi_c : -29931.41 deg
M1   :   0.90 N.m
M2   : -0.90 N.m
M3   :   0.00 N.m
M4   :   0.00 N.m

Suggested Model
Xc   :   -0.51 m
Yc   :   0.05 m
psi_c : -19885.38 deg
M1   :   0.90 N.m
M2   : -0.90 N.m
M3   :   0.00 N.m
M4   :   0.00 N.m

Figure 4.18 Lateral arc motion with centralized mass center

The approximated model has produced a linear trajectory parallel to y axis combined with continuous rotation around the mass center of the vehicle, the reason behind that the differential equations of the approximated model can't deal with the driving moments on one axle either in case the applied moments were in same direction or in different directions. The differential equations can't recognize the different between the driving and the slippage of the wheel without effective driving moment. As it is mentioned before, as long as the model cannot distinguish between the rotation due to driving moment or the slippage of the contact roller, besides producing angular velocities for stationary wheels, i.e., no driving moment applied on it, then the results must be considered as not accurate results and don't meet the expected trajectory of motion. On the other hand, the suggested model can simulate and estimate the expected trajectory beside the continuous rotation around the vehicle center during the simulation.

4.3.2   Complex trajectories

The complex trajectories are constructed from sequential sets from the simple trajectories, which are governed by the applied driving moments and the driving duration. The variation of the given moments is proportional directly with time and limited by simulation time 2 sec. The complicated trajectories can be produced also by applying driving moments in different forms like sine wave, triangular wave or even connected parabolas. The input form of the driving moments can be the same of all wheels or variable for each wheel separately. An example for the complicated trajectories will be discussed here.

In this study, the driving moments have been given to the equations of the dynamic model of the 4WMV. These equations will be integrated numerically to find the motion of the 4WMV. In the case of the complex trajectories, a variable driving moments will be applied as following $M_1 = 1\,\text{Nm}$, $M_2 = -0.8\,\text{Nm}$, $M_3 = -0.5\,\text{Nm}$ and $M_4 = 1\,\text{Nm}$. The simulated trajectory will be as shown in Figure 4.19. The 4WMV shows a translational motion and continuous rotational motion around its center of mass. The vehicle has translated a long a semi curve or a set of connected curves. The discontinuity of the curvature is resulted from the change of the position of the vehicle center of mass during the motion, which is characterized by the combination between the translation and the continuous rotation. By the end of the simulation time, it was found that the total translational motion of the 4WMV is around 5 m to the right direction or in the negative direction of the x axis and around 3 m to backward or the

negative direction of the y axis. The total number of the revolutions of the 4WMV around its mass center was 6 complete revolutions.

Suggested Model
Xc   : -4.98 m
Yc   : -2.79 m
psi_c : -2121.11 deg
M1   :   0.90 N.m
M2   : -0.80 N.m
M3   : -0.50 N.m
M4   :   0.90 N.m
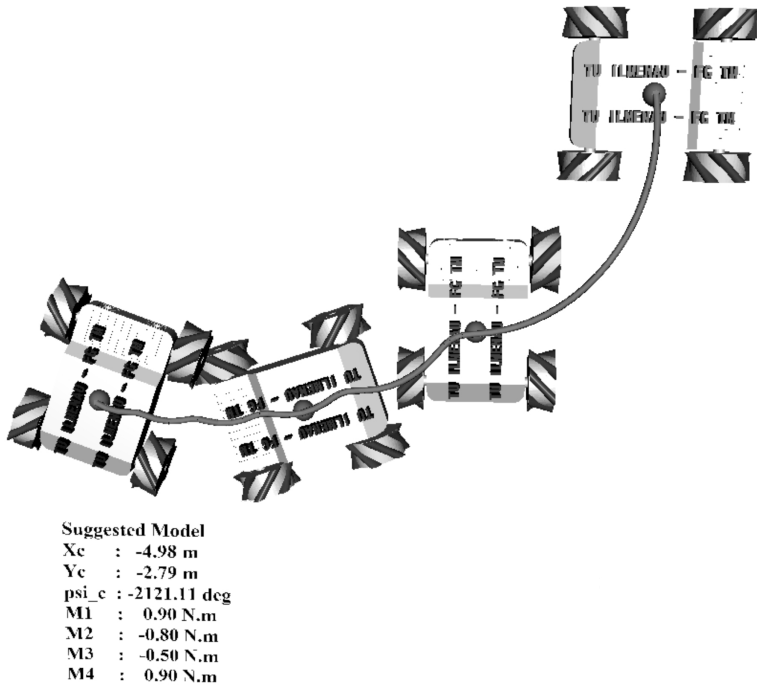
Figure 4.19 The simulation resulted trajectory according to MATLAB®

By comparing the real trajectory of Figure 4.20 with the simulation results, it was found that the real trajectory is free from the discontinuity and the vehicle will rotate continuously during the translation. The experiment on the real system shows, after 10 seconds from the beginning of the operation, a translation and rotation a long a curve as shown in Figure 4.20. The real system has moved just like the simulation results in the first segment from the curve.
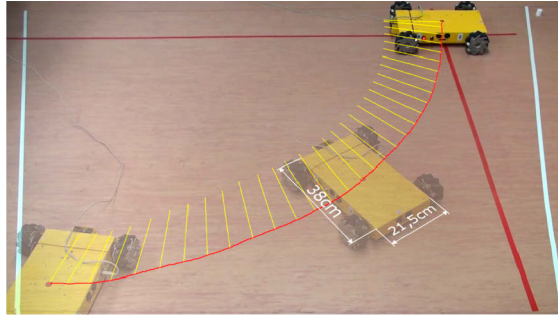
Figure 4.20 The real trajectory resulted from a motion sequence of a moving 4WMV

The deviation between the simulation results and the real trajectory can be reasoned by the friction forces and the wheel slip. The parameters of the simulation have not influenced by such friction or the slip. The question which still opened is how this deviation can be minimized or even eliminated. No doubt, the first idea appears on the mind is applying the control theories and specially the artificial intelligent one. The fuzzy logic can play an important role in this case.

4.4   Experimental setups

As practical application for the studied theories of the motion of the Mecanum wheels and the 4WMV, an experimental test unit has been prepared to examine the possible motion trajectories. In order to show the differences between the ordinary vehicle and the 4WMV during the translational and rotational motion, a simple ordinary experimental vehicle has been modified and used to be a platform for a handicapped seat. The designed seat is suitable for the standard dimensions of the handicapped people and can be fixed on the tested platforms.

The ordinary platform with steerable wheels is used widely in the field of the vehicle for the handicapped persons. In order to show the advantages and the high translational and rotational capabilities of the suggested special-purpose vehicle based on the Mecanum wheels, a comparison between the two types has been held. The both vehicles are equipped with portable seat with a model for a handicapped person and the selected speeds are moderate to avoid the over turning or unbalanced motion. The tested

vehicles are moving within a test area which is free from all types of the obstacles.

The real life time, especially for the handicapped persons, is full with the hard situations and motion obstacles. The simulation purposes obliged the need for design a special test track for testing the motion of the suggested vehicle. The track has to be constrained by certain dimensions and defined obstacles separated by determined distances. The steers are considered to be real obstacle in front of the handicapped and both the introduced platforms cannot deal with such obstacle. The motion of the introduced platforms has not been tested on the real roads or in the open surroundings.

Both of the mathematical models cannot distinguish between the rotation of the whole wheel and the slippage of the rollers. The kinematic constraints of the 4WMV produce corresponding rotation speeds as long as there are changes in the linear and angular displacements of the whole vehicle. It is recommended to study further the relation between the rotation speeds and the applied moments on the wheel. A mathematical model for the electric motor and the attached mechanical units is recommended, that to combine the effect of the electrical part from the system of the vehicle with the dynamical model. Also, the reduction mechanism has to be taken in account. As simplification for estimating the rotation speed of each wheel, the corresponding value can be found from the relation between the driving power, the mechanical efficiency and the corresponding driving moment. Experimentally, the driving power and the corresponding parameters like driving moment, rotation speed, mechanical efficiency and the applied current, have been measured and plotted as shown in Figure 4.21.

$$\dot{\varphi} = \frac{60}{2\pi} \cdot \frac{\eta \cdot P}{M} \, , \qquad \text{(rev/min)}$$

where, $\dot{\varphi}$ is the rotation speed for each wheel in rev/min, P is the driving electric power in watt, η is the mechanical efficiency and finally M is the driving moment, which has been assumed to be 0 - 0.9 Nm therefore, the expected maximum rotation speed according to the previous relationship and the measurement is around 90 rev/min. It is recommended to select the applied driving moments to be within the given range as shown in the Figure 4.21. The corresponding rotation speed is the actual rotation speed of each wheel under operation conditions free from friction or slippage. The driving moment is proportional directly with the driving current of the motor; therefore, the loading on the vehicle must not exceed a certain limit

to avoid reaching to the higher levels of the currents and failing the system. Based on the fact, that the introduced systems are small models and are operating in different areas rather than the real vehicles which can carry a real handicapped, and then it is expected to find deviation between the simulation results, the small models and the real vehicles.
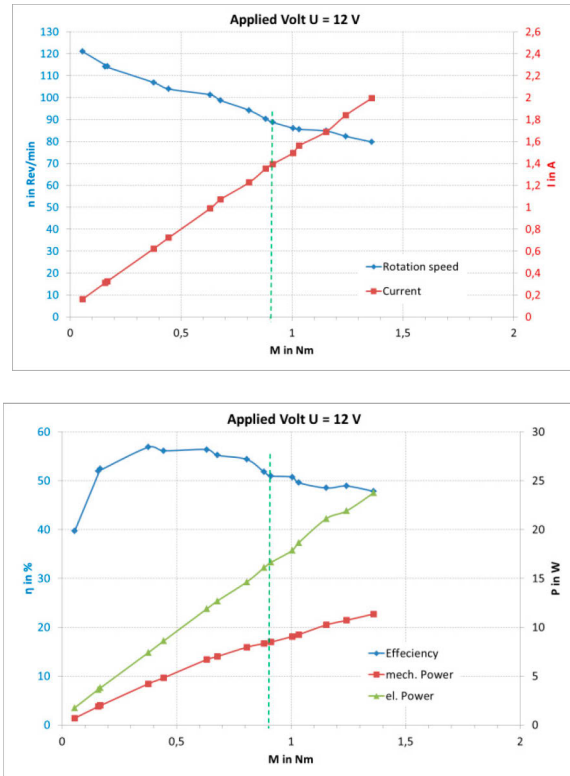
Figure 4.21 The driving power and the corresponding parameters at applied voltage 12 V. (small electrical devices group, TU Ilmenau)

Now, the introduced platforms can be classified according the motion trajectories point of view into

A platform for simple trajectories

The frontal steerable axle is the base for all the vehicles moving on the roads nowadays. The system is characterized by the simple design and the limited motion capability. In the market of the handicapped vehicles, this design is used commonly alone of coupled by steering by differentiating the rotation speeds of the driving motors. In our model, the steering will be executed by additional mechanical mechanism, which is driven by additional electric motor. The platform will be remotely controlled. The remote control can send separate commands for both the driving motors and the steering system. The commands of the speed are controlling the change in the travelling speed during the motion and the commands of the steering command the change in the steering angle. The sensitivity for the change and the response time are moderate.

The common characteristics between the introduced platform and the real system are the used tires and the used steering system but in different scale. The real system still has the advantage of the matching between the response time of steering the vehicle and the driving speeds but on the other hand the small electric motors, which are used in the introduced platform, are pushing the vehicle with higher rotation speeds and the steering system cannot show smooth steering angles.

Figure 4.22 The front axle steerable platform – suitable for simple motion trajectories

The modified remotely controlled vehicle is shown in Figure 4.22, the vehicle can introduce all the expected simple trajectories like the motion in forward, backward directions or even along a curve with constant rotation radius. The stability during the motion has not been tested, where the motion surface is extended soft without obstacles. The wheels of the platform are normal tires from rubber and have a limited carrying capacity. The handicapped seat is not fixed permanently to the platform, but the weight of the seat played a role in keeping the system balanced during the motion.

Mecanum wheels based platform for both simple and complex trajectories

This platform is based on the NEXUS® Mecanum robot vehicle. This platform, as shown in Figure 4.23 , can introduce all the simple and even the complicated trajectories just by applying the suitable driving moments or the platform wheels separately.

Figure 4.23 The 4WMV – suitable for simple and complicated motion trajectories

The platform can be controlled remotely for the standard trajectories as mentioned before, but for the complicated trajectories, it must be programmed using special software. Different motion trajectories have been executed to test the translational and rotational capabilities of the platform.

Also, the effect of shifting the mass center has been examined and the platform has shown results similar to the results of the simulation.

It is planned to design a set of complicated trajectories and compare the behavior of the systems during these trajectories with the resulted trajectories from the simulation, in order to define the strength and the weakness points in the suggested dynamic mathematical model. For more enhancement for both the real system and the mathematical model, it is recommended to measure the translational motion, rotational angle of the whole system and the rotation speeds of each wheel during the motion and if there is possibility to determine or to measure the driving moments too, that increases rapidly the accuracy of the comparison and leads for better results on the long term.

The Mecanum wheels based platform can move freely to any direction to reach any point on the motion surface but the exactness is limited. No control system is used to increase the accuracy of the motion or the exactness of the targeting. Only the used control in the introduced system, is a regulator to the rotation speeds of the wheels, to keep a small difference between the demanded speeds and the actual rotating speeds.

It is recommended also, to test the exactness of the motion from both the translational and rotational behaviors, in case that the driving moments have different time varying characteristics , for example varying as a time function looks like a sine wave, triangular wave or even a combined parabolas.

The greatest engineering challenges in manual wheelchair design are optimizing interaction between the user and the wheelchair, which requires knowledge of materials, biomechanics, ergonomics, anthropometrics, and human physiology, as well as motor learning to train the user in the skills necessary to achieve maximum mobility.

(R.A. Cooper)

5 <u>Biomechanical analysis of wheelchair user movement with mobility aids</u>

Biomechanical engineering plays an important role in athletic life and has been used widely in sports science by applying the experience and increasing knowledge of specialists in this field. Scientific research in the field of biomechanical engineering is a critical task and is facing a lot of obstacles according to MILLER/NELSON [84, 83]. The main objective of sports science, especially for professional athletes, is to achieve the highest possible performance and the best finishes during races. On the other hand, sports science can help to decrease and limit incorrect overloading on the athlete during training and competitions.

In order to understand and optimize motion flow in the fields of sport, rehabilitation and orthopedics, biomechanics can be applied to the training of professional athletes, SHAN [113]. In addition, new facilities have been created to perform more detail-oriented analyses, using modern technical measuring methods and special computer-aided evaluation.

This chapter investigates wheelchair motion, including strategies employed by wheelchair users when driving. With respect the sports world, motion of a disabled athlete as an experienced test volunteer will be analyzed and compared with the motion of an inexperienced test volunteer, who has no disability at all and is moving in a wheelchair for the first time.

Their respective performance under different driving conditions will be analyzed and compared.

The objective of such an analysis is to understand the differences between the test volunteers while using the wheelchair under different motion scenarios. Additionally, where possible, an additional objective of this study is to provide new suggestions and recommendations for training methods or novel enhancements for the configurations used and for manual wheelchair design. Therefore, the motion of the test volunteers were recorded optically and mapped to a digital anthropometric modified human model for evaluation purposes.

5.1   State of the art of motion capturing and digital evaluation

5.1.1   Methods of motion capturing

Since the 19th century, experimental methods have been developed to capture the motion of animals using optical methods according to MUYBRIDGE (1885) [92] and MAREY (1868) [75]. Initial trials for capturing motion involved a set of timed triggered cameras, creating an experimental "video" camera. A similar design used equally spaced rotational photographical plates equipped with additional pressure sensors. Nowadays, motion capturing systems use different physical properties to sense motion but in general all of these systems produce digitally measured information. Motion capturing methods can be categorized into mechanical, optical, magnetic, acoustical and inertia-based systems, depending on the technical system employed.

An example of a mechanical motion capturing system is a set of goniometers fixed to the body of the test volunteer to measure the change in body joints angles. This system distinguishes itself through high accuracy and robustness against motion disturbances, with the primary disadvantages being added difficulty for the test subject to perform motion due to the fixation of mechanical parts on the body.

Optical motion capturing systems are categorized into marker-based or marker-less systems. The markers are mechanical objects with either active self-lighting or passive light reflecting units. These markers can be detected within the test area by special cameras and software. The markers are fixed to the body of the test volunteers and their motions are captured using a set

of special cameras during the experiment. Then the motion of the markers can be analyzed and evaluated using special software according to the objective of the experiment and the test personnel. Two different methods can be used to determine the exact position coordinates of different body parts. They are:

1. Body contour monitoring.
2. Automatic body part monitoring.

Optical motion capturing systems exhibit high accuracy and have no effects on the health of test volunteer; the system is 100% safe and does not employ dangerous materials. The test subjects are not exposed to harmful waves or radiation in contrast to other techniques used. But, these systems are complex and expensive, both upfront and during operation, in addition to additional costs incurred to evaluate the experimental data. Another disadvantage of these systems is the need for continuous visual contact between the capturing system and the moving objects under test in order to ensure reasonable correctness of the captured motion. Also, some modifications of the optical characteristics of the surroundings may be required, such as:

1. Constant light source.
2. Contrast between the markers used and the background in test area.

Magnet-based motion capturing system produces, three linearly independent magnetic fields for the three world coordinates x, y and z for each measured point on the body. During motion, special sensors are fixed to the body of the test volunteer. These sensors measure the strength of the magnetic field, allowing the position of the moving part to be calculated. This technique does not require visual contact. Therefore, the technique used here is simpler and more flexible. Moreover, the operation and use of small sensors is relatively easy. The disadvantage of this technique is the possible disruption due to magnetic field in the surrounding area, such as ferromagnetic or metallic materials. The second disadvantage of magnetic-based systems is that the test volunteer is prevented from moving freely due to the cable connections with the extremities.

Acoustics-based motion capturing systems use ultrasound signals to determine the position of the moving object. They depend on fixing a set of special sensors to the test volunteer, after which ultrasound signals can be sent to the moving body to be received by the stationary sensors. The time

required for the signals to reach the sensors is determined and the location can be found based on that time. On the other hand, acoustics-based systems using acoustic wave reflection can determine the position of a moving object by evaluating the phase difference between the sent and received signals. This technique is robust and simple to use. Electromagnetic fields do not affect the measurements. The main disadvantages of these techniques for motion capture are the limited accuracy and the sensitivity toward the filling material.

Using micro-mechanical acceleration and velocity sensors, changes in the position of a moving body can be calculated over a certain time period based on numerical integration methods for the measured acceleration and velocity data from the test volunteer. This is the simple working principle of inertia-based motion capturing systems. By using batteries and transmission units to transmit the measured data to a computer, the test volunteer can freely move without any effects from the surroundings on the quality of the measured data. The sensors used must be fixed to the body of the test volunteer, which might cause annoyance. In order to determine the absolute position of the test volunteer, it is necessary to know the previous initial position before beginning a motion sequence using a secondary measurement system. If only the velocities and the relative change in the position of the moving body are available, then the measurements cannot be trusted at our current level of technology. The measured data from these systems can then be transferred to the computer and a digital biomechanical model created to visualize and evaluate the data using special software.

5.1.2   Biomechanical model of the human body

Principally, there are two human models that can be used to analyze human motion and to visualize the human body from a biomechanical point of view. They are:

1.   Deformable body model
2.   Rigid multibody model

The deformable model is suitable for measuring and evaluating the local deformation for different body parts. Using the finite element method, the deformation of body segments can be modeled numerically and analyzed. The deformable human model is not suitable for describing motion assistance systems such as wheelchairs because it is difficult to estimate the relative motion of the body segments connected together by

joints. On the other hand, the rigid multibody model consists of a set of rigid bodies connected together by joints, as illustrated in Figure 2.2 and Figure 2.3. There are several pieces of computer software that can create these models and simulate motion. The disadvantage of the rigid multibody model is the difficulty in implementing the elastic properties of the body segments. The solution is to combine both models, making use of their advantages but the number of required calculations and analysis processes can increase rapidly.

Analysis of human body motion in this section uses the rigid multibody model. According to the available references, it can be assumed that the effect of elastic deformation of the test volunteer body segments is negligible. Also, it can be assumed that the body biomechanical model being used consists of a number of non-deformable (rigid) segments connected together by joints and the body segments have constant density. Generally, it is well-known that by simplifying the human body model the number of model segments will decrease. From a practical point of view, the level of simplification for the human body model mostly depends on the research objectives, so that in most of the cases, the exact model of the fingers and toes can be neglected when studying motion of the human body in its environment.

The first human models were suggested by SIMONS/GARDNER [118] and KULWICKI. In both models, the extremities and the trunk of the body are represented as one single rigid segment. Therefore, such models cannot be used to model and analyze the movements and propulsion of the mechanical wheelchair because the relative motion of the arms to the body trunk is important. While considering US spaceships and initial trials for space exploration, WHITTSETT [158] and HANAVAN [41] suggested new human models, in which the extremities of those models, namely the arms and legs, consist of three segments connected together by spherical joints in order to facilitate the study of leg and arm motion. ZATSIORSKY's model [106] consists of 16 segments, where the extremities and the trunk each consist of three segments. Another important property for ZATSIORSKY's model is that the separation plane between the upper part of the thigh and the hip is set at an angle of 37° with respect to the perpendicular plane when the model is in a standing position.

WHITTSETT (1964)   ZATSIORSKY (1983)
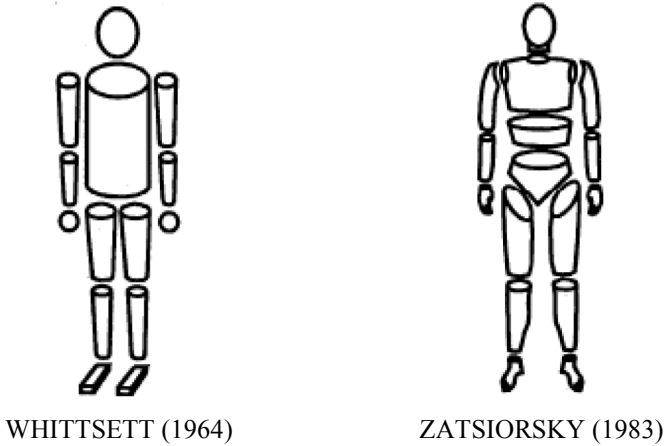
Figure 5.1 Representation of two example biomechanical models [158],[163] and [113]

WHITTSETT's (1964) [158] and ZATSIORSKY's (1983) [106] models (both shown in Figure 5.1) form the basis of current digital human models, which are used in different motion capturing software. The digital human body model known as JACK was developed between 1980 and 1990 at the University of Pennsylvania for studying human ergonomics in civil and military projects, before it was bought by Siemens AG, which markets the model under the name TECNOMATRIX JACK® [116]. The main application for this model is the study of ergonomics in a virtual digitalized environment. The RAMSIS® model design by Human Solutions GmbH (see MEULEN/SEIDL [82]) is based on the model suggested by ZATSIORSKY [106]. That human biomechanical model is used in a large amount of computer-aided research for human motion and is distinguished by the flexibility regarding the anthropometric data. The RAMSIS model is also used in the program package ALASKA/DYNAMICUS® according to the INSTITUT FÜR MECHATRONIK E.V. [101, 52], which is used in this study. Another modern biomechanical human model with similar functionality is implemented in the program environment AnyBody®, according to ANYBODY TECHNOLOGY A/S [8], which can simulate material changes, muscles reactions and mechanical forces and moments according to the given motion data of the body being tested. It has been mentioned in different references such as TECNOMATIX GMBH [124] and DASSAULT SYSTEMS [23]. Other program packages can also perform the same function and are mostly based on the RAMSIS® and

JACK® models. The entertainment industry usually only utilizes the human models for motion animating and for the graphical visualization of human bodies, RATNER [100]. From the mechanical point of view and not from the biomechanical point of view, there is no use for anthropometric information other than as just for presentation and visualization of for the data being analyzed.

In conclusion, it can be said that modern programs used to study the motion of humans can use very complex human models by applying modern computer techniques and their utilization can reach across domains. The models can be categorized into rigid vs. elastic or even into technical vs. biological. Interaction between the human body and the motion system can also be defined as a closed chain of rigid body in a multibody system (MBS) as previously shown in Figure 2.3.

5.1.3   Anthropometric information

Anthropometric information comprises the specific mass distribution within the human body as well as the dimensions of body segments. It includes parameters such as the geometrical dimensions of the whole body and the individual segments, the center of mass of the body and the different parts in addition to the masses and moments of inertia for the whole body and its segments. Anthropometric information can be considered "design" information of humans, making it important for simulating the dynamics of the human body. When studying the kinematics of human motion, it is enough to know the geometrical dimensions of the moving human body under study.

Investigation of anthropometric information has been carried out since 1860. According to [113] and [106], anthropometry has been performed on different test volunteers and documented in various published scientific references over the years. Anthropometric information can be taken from living or dead persons using different methods. Measuring exact anthropometric values for living persons is a complex and expensive procedure. Analysis of anthropometric statistics, which has been carried out over many years during continuous research in biomechanical engineering, can help to provide the exact anthropometric information required for any specific application. Using this collection of information, the geometrical dimensions and the weight of a test volunteer can be measured and all other typical parameters can then be estimated, including mass, moment of inertia and center of mass of body segments. According to [113], anthropometric

information has an accuracy of 10%, which is enough for dynamic analysis of the human body. Propulsion of wheelchairs and other topics regarding human body models are discussed in [136, 22, 117, 32, 67, 79, 135 and 138].

5.2   Experimental motion capture setup, test volunteers and test procedure

5.2.1   Technical description of the motion capture system

This section briefly describes the preparation process for capturing the motion of the test volunteers.

(a)   (b)
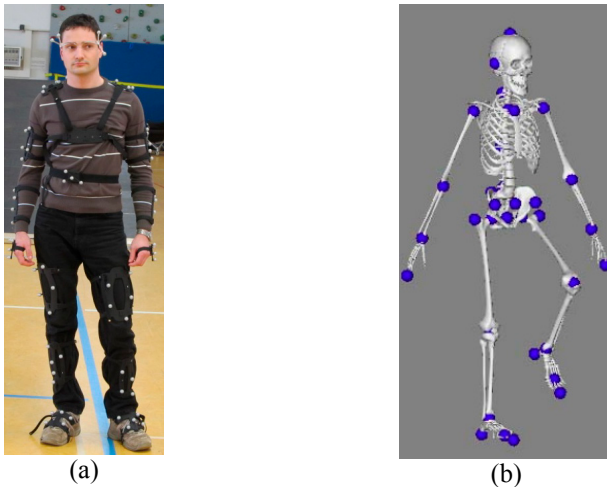
Figure 5.2 Body markers on the test volunteer (a) in comparison to the digitalized representation in ALASKA/DYNAMICUS® (b) INSTITUT FÜR MECHATRONIK E.V. [101,52]

After installing the motion capture equipment, it is connected to the computer used to record and analyze the motion data. The motion capture system consists of a set of high-resolution cameras for motion detection, which are located on each side of the motion track, see Figure 5.4. The test volunteers are outfitted with white markers, which have specialized reflection capabilities for infrared light. A calibration process is then carried out on the motion capture system. Recording the motion of a test volunteer

using a wheelchair is a complicated process. It not only requires preparation for the motion track under different conditions but also keeping the capturing cameras in the same orientation throughout the capturing process. Any change in the orientation or in the location of the recording cameras requires the team to recalibrate the system.

The motion capture procedure consisted of testing the capability of two different test volunteers during motion on a flat plane or on an inclined surface at different speeds. That required changing the location of the capturing cameras and recalibrating the system. The most important technical specifications of the capturing system are highlighted briefly below.

A set of special cameras is used for motion capture. There were 12 different cameras distributed around the area of motion: four Atrack3 cameras and eight Atrack2 cameras. The cameras have a reasonable operation frequency around 60 Hz, that means the system can produce 60 frames per second for all moved targets. Within capturing the motion of the test volunteers, they wear a special suite to capture their motion which consists of 17 body targets. Beside that additional moved targets have been fixed on the wheelchair chassis and its wheels, two motion targets for each. Special software called Dtrack2 has been used to calculate the 3D world coordinates based on the gathered 2D photo pixels coordinates of each used camera during the sensing and capturing the position of the moved targets. Then, the captured data are sent to a monitoring computer through UTP (universal transmission port) to be monitored using the software Dynamics recorder, which records the captured data and presents them simultaneously. Finally, the position and the orientation of the moved targets are modified and settled to its positions on the human body model, for the system details see Figure 5.4. The expert version of DYNAMICUS /ALSAKA® is used for combining the captured data of the targets with the opposite points on the body model.

1 Glasses target (AGT4)
2 Shoulder targets (UT)
1 Dorsal target (DT)
2 Upper arm targets (HBT)
2 Forearm targets (UBT)
2 Hand targets (HT)
1 Waist target (WT, one-piece)
1 Waist target (WT, multi-part),
2 Upper leg targets (FBT)
2 Lower leg targets (TBT)
2 Foot targets (FT)

Figure 5.3 Overview on the Motion capturing targets [5]

After wearing the measurement suite which is shown in Figure 5.3, the tests volunteer moves, using the wheelchair, within the motion area of the motion capturing system. The setup of the motion capturing system is presented in the following Figure 5.4.
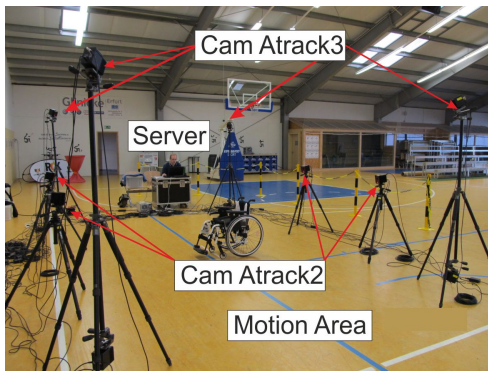
Figure 5.4 The setup of the motion capturing system

The captured motion was taken on two different motion surfaces, one of them the ground surface with inclination angle 0° and the second motion

surface was a ramp which is inclined on the ground by angle around 9°. The ramp is presented in Figure 5.5. The shown ramp has the following dimensions, length 10m; width 2m; end height 1.2m. The same set of cameras have been distributed around the ramp, to capture the motion during the climbing the ramp. All the test procedures have been carried out before capturing and during the capturing from calibrating the system till preparing the test volunteers for the test.
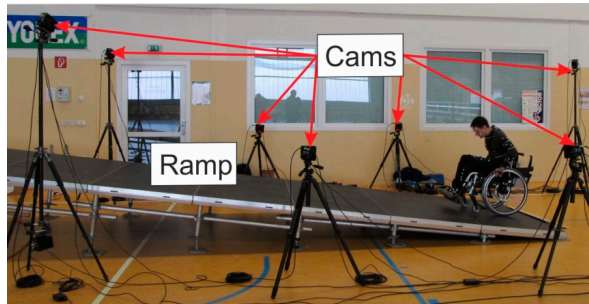
Figure 5.5 The setup of the motion capturing system on the ramp

The captured motion on both the ground and the ramp has been transmitted from the cameras to the main frame or the main server for fitting the captured data on the human body model and to produce the final human body motion simulation. The system may produce a slightly small percentage of error within the acceptable level.

The first step in preparing the capturing system for the measurement is inserting the anthropometric data of both test volunteers to estimate the length and the distance between the white markers, which indicates a certain segment on the human biomechanical model RAMSIS®.

5.2.2   Human model in the ALASKA/DYNAMICUS® simulation environment

The data collected from the motion capture system is loaded into a human model in the ALASKA/DYNAMICUS® program package to be analyzed and visualized using a subprogram called DYNAMICUS/MOTION ANALYSIS®. The methods of inverse kinematic and dynamic analysis can be employed on the captured motion with the human model.

The RAMSIS® human model is implemented in s/w ALASKA/DYNAMICUS®, which is abstracted from the ZATSIORSKY's multibody model [106] as shown in Figure 5.7. It consists of eight main parts: trunk, head and neck, left and right arms, left and right legs and feet. Each main part is devided into one or more subparts. The smallest subpart is called a segment. The fragmentation of the main part of the body into subparts or segments mostly depends on the motion capability of human skeleton. In particular, the spine and the thorax are very finely subdivided into small segements, with each segment considered as a rigid body with a body-fixed coordinate system used to find the orthopometric information.
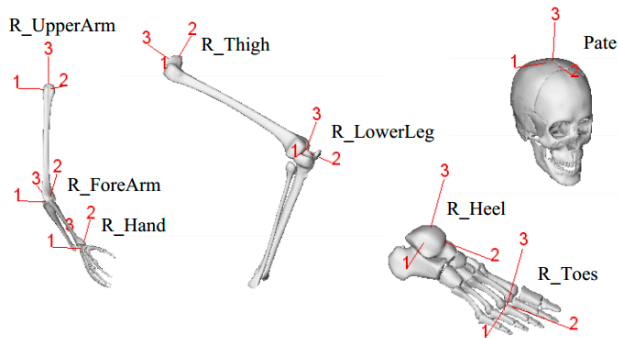
Figure 5.6 Body-fixed coordinate system for the segments of the human body model in ALASKA/DYNAMICUS® – INSTITUT FÜR MECHATRONIK E.V. [101,52]

The segments are connected together by ball joints with a guiding element and a following element. For any studied segment, the guiding body is near the body centerline. The orientation of a joint's coordinate system is parallel to the world coordinate system if the human body model is in relaxed standing position. The rotation of the jointed segments can be described by three different angles, but two of these angles remain constant when dealing with rotating joints. When motion is starting, all angles of the connecting joints are zero.
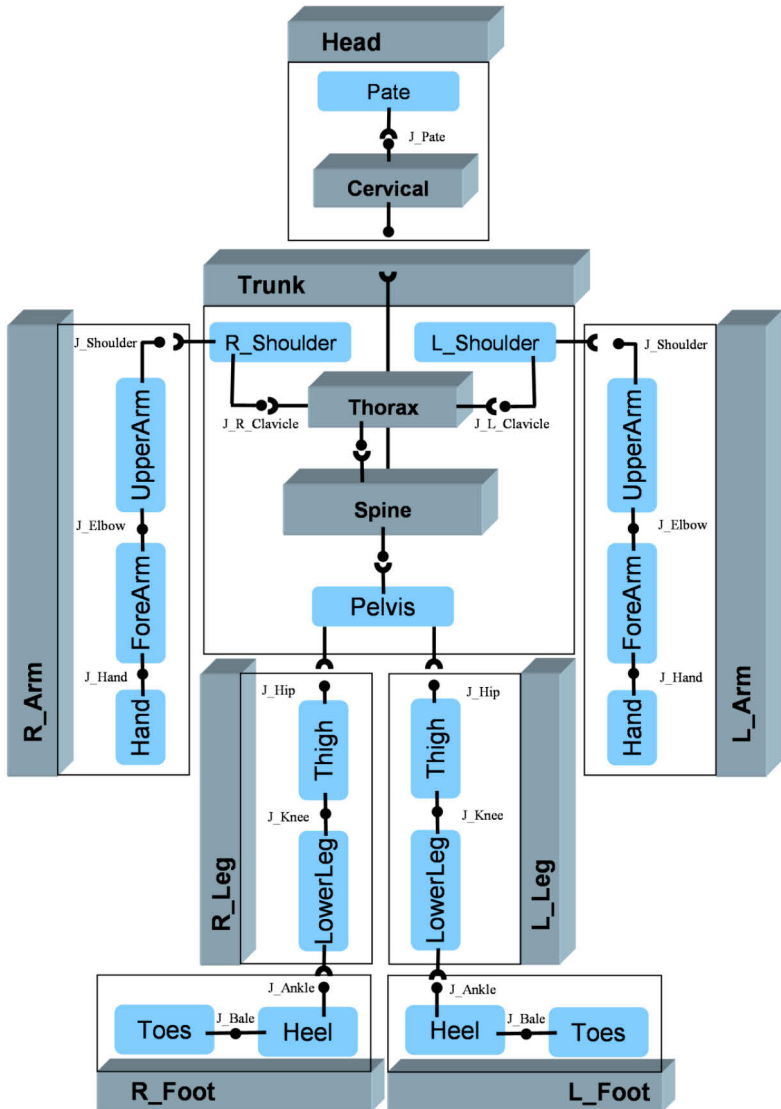
Figure 5.7 Schematic diagram of the human model in ALASKA/DYNAMICUS® – INSTITUT FÜR MECHATRONIK E.V. [101,52]

5.2.3   Test volunteers

The study being discussed here deals with the movement of wheelchair users using the example of two test volunteers. The first test volunteer is Mr. J, an experienced wheelchair user, who has used a wheelchair since early childhood, because he was born with a leg disability. Mr. J is a professional wheelchair basketball player, who has been practicing the game for a long time and has taken part in various championships. The second test volunteer, Mr. K, has no experience with wheelchair driving. Both test volunteers are young men both of age 20 with normal body builds. Neither of them has suffered any major health problems before the test.

The primary anthropometric parameters of each test subject were determined before any motion measurements. In this test, the dimensions of legs and feet were neglected because they do not have any effect on the captured motion of the wheelchair user. Using ALASKA/DYNAMICUS®, it was possible to estimate the complete anthropometric information of the test volunteers based on the measured dimensions in Table 5.1.

Table 5.1 Anthropometric information of the test volunteers

Test volunteer	Normal (Mr. K)	Disabled (Mr. J)
Gender	Male	Male
Mass (kg)	65	60
Height (m)	1.76	1.63
Upper arm length (m)	0.34	0.305
Lower arm length (m)	0.26	0.275
Hand length (m)	0.2	0.19
Shoulder width (m)	0.45	0.43

The wheelchairs used in the measurements can be classified into two different categories. The OTTOBOCK® wheelchair is a light-weight model of the starter M1 type. The second wheelchair was provided by the sports center in which the measurements took place, see Figure 5.19.

5.2.4   The evaluated parameters and measurement procedures

The motion of the segments, trunk and both left and right arms will be analyzed in the following measurement evaluations. Generally, the analysis deals with the angular motion of the connecting joints about the x-axis, between the shoulder and the upper arm (J_Shoulder) and the upper and lower arm (J_Elbow). The position of the hands and shoulders is considered

as a movement in a level parallel to the side of the wheelchair for each test subject. Diagrams of the required coordinate systems are shown in Figure 5.8.

Figure 5.8 Position of the coordinate systems for investigating the motion of the wheelchair compared to the position of the markers

The following situations were the subject of the motion capture investigation:

1. The motion trajectories of both test volunteers in slow motion.
2. The position of the body parts (i.e. the absolute or relative positions of the following parts: hand, arm, shoulder, trunk etc.) and a comparison of the motion trajectories for Mr. J during fast and slow motion sequences.
3. The body position and the motion trajectory of Mr. J when climbing a ramp, driving over a ramp with around a 9° inclination and comparing the motion on the ramp with the motion on the ground level.

The motion was recorded for the fixed white points on the measurement suit. The white points do not represent an exact point on the body part such as the center of mass and it can only be considered a reference point for tracking the motion of its corresponding body part. The body part's absolute position or relative position with respect to another part, such as the relation between the shoulder and the arm, was collected and modified by the software.

During the motion capture, the volunteers moved using the test wheelchair on different surface types and by different speeds along different tracks. The motion surfaces were either flat ground or an inclined ramp. The movement variables are summarized in Table 5.2. It is important to mention that the disabled athlete (Mr. J) used an additional seat pillow to make the seat more comfortable for him. The study of the relative motion of the body parts with respect to each other was one of the objectives in addition to understanding the relative angular motion between them as in the case of the shoulder and the upper arm or the elbow angle between the upper arm and the lower arm.

Table 5.2 Movement variables

Variable type	Description
Speed	Slow motion Fast motion
Wheelchair type	Ottobock-modified wheelchair Sport wheelchair
Surface inclination	Flat Inclined (ramp)
Track	One-way path → Round-trip path ⇄
Surface cover	Rough surface, covered with carpet Smooth surface

Important terminology

Figure 5.9 Important terminology for the analysis of motion capture

The analysis of the test subject behavior and driving strategies necessitated defining important parameters to be used to describe and understand the nature of the motion. The required terminology is outlined in Figure 5.9, such as θ_P as the propulsion angle or the effective pushing cycle, θ_R as the release angle, θ_C as the contact angle, RD as the direction of rotation for the entire wheel [22] and θ_S as the angle between the horizontal line and the start of propulsion.

Mr. K and Mr. J naturally exhibited different styles of driving the wheelchairs, mostly depending on the difference in their wheelchair experience levels. Generally, the motion capture process was not influenced by a specific standard or discipline; it mostly depends on the motivation and

demands of the researchers performing the experiments. The objective for the capture process here can be summarized in the following points:

- Comparison of the driving behavior of abled and disabled subjects
- Analysis of the personal characteristics of the disabled expert operator when driving the wheelchair under different operating conditions
- General evaluation of the driving strategies exhibited by the test volunteers
- Enhancement of wheelchair design based on the conclusions drawn from the measurements in accordance with users needs.

5.2.5   Comparison of the rotational and translational motion of body parts at different motion speeds

To begin the motion capture analysis, the captured data is first visualized for different body parts under the same experimental conditions, e.g. the Ottobock® wheelchair at slow-moderate speed on a flat surface. The figures in the next few sections show the motion data captured from each of the test subjects, the athlete Mr. J and the inexperienced user Mr. K, highlighting the difference between the motion characteristics of the right and left sides of each volunteer. Next, the motion space trajectories for the segments, for example a hand, are introduced to detect the effect of training and experience in determining a suitable and more effective driving style which is comfortable at the same time. It is important to mention that the motion data is analyzed but not modified. The test volunteers were presented with the same surrounding conditions, including temperature and humidity, and the test was carried out in the same place for both test volunteers.

Left	Right
Elbow rotational motion relative to the x-axis – slow motion	

| Shoulder rotational motion relative to the x-axis – slow motion | |
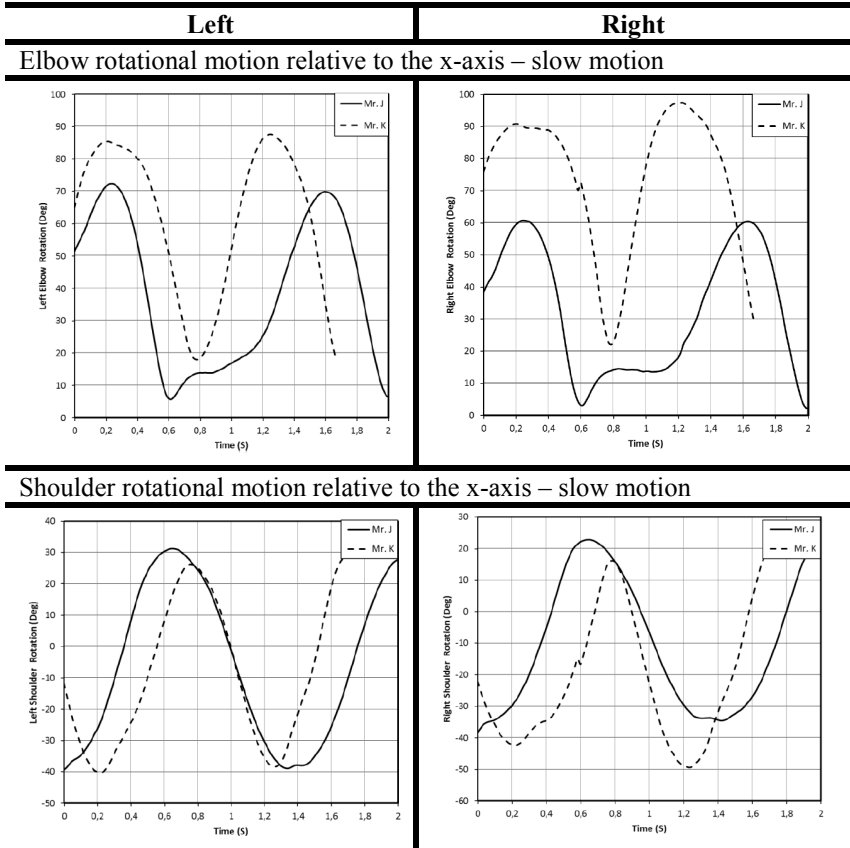
Figure 5.10 Comparison of angular motion of the shoulder and elbow for both Mr. J and Mr. K in the Ottobock® wheelchair during slow motion

The comparison in Figure 5.10 makes it clear that both elbows and shoulders are rotating periodically around their center of rotation, in this case the x-axis according to Figure 5.8. The periodic motion of the left and right shoulders and elbows are quite similar over the recorded time period. In the case of Mr. J's elbow motion, the curves exhibit discontinuity but little deviation from pure sinusoidal rotation, which is due to relaxing the arm or freezing the arm at a vertical position by rotating the wheels. Synchronization of the motion between the left and right parts is visible and the harmony in motion is achieved for both test persons, which shows that even without wheelchair driving experience, synchronization and harmony
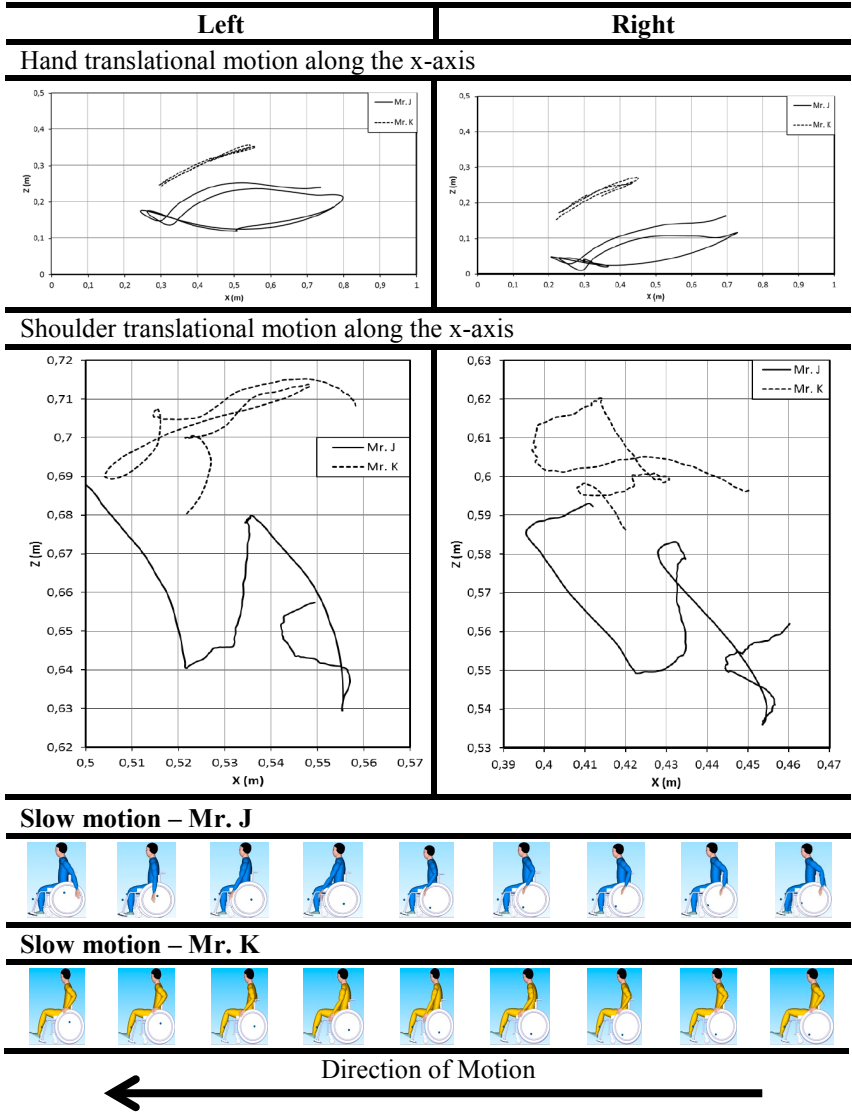
in the motion are easily realized, especially if there is no disability in the user's hand. For electric wheelchairs, whether fully or semi-electrically driven, harmony in the motion between right and left body parts is not required, allowing the user to compensate any discontinuities causing a lack of harmonious motion.

Due to Mr. J's experience in driving different types of wheelchairs, he demonstrated a clear capability of using the full range of hand motion compared to Mr. K as shown in Figure 5.11. Homogeneity in the motion of the Mr. J's right and left hands is clearly visible. A thorough analysis for Mr. J's hand motion showed that he kept his hand in contact with the rim of the wheel for a longer time than Mr. K, which simply means that Mr. J rarely moved his hand behind his body center line. Most of the time, Mr. J's arm was straightened and moved in systematic, relaxed way. Mr. J's hand introduced an elliptical trajectory for its translational motion on the x-z-plane. In contrast, Mr. K's hand trajectory was nearly linear, which indicates the intensive forward and backward motion of the Mr. K's upper body during motion capture.

Analysis of the captured motion for the left and right shoulders of the test persons found a clear difference in the motion working range. Mr. K moved his upper body faster and intensively at sharp angles. The resulting diagrams show a motion range for his shoulders with very limited motion space along the z-axis. Mr. K's shoulders did not travel up and down, which prevented him from introducing additional force to push the wheels. He overcame the smaller driving force by adding fast, intensive motion of his hand. The conclusion from this is that Mr. J used a markedly different strategy based on experience to push the wheels than did Mr. K. In Mr. J's case, motion of the shoulder is very important to introduce the required force for pushing the wheels with minimal effort and reduce stress on the arm muscles. On the other hand, Mr. K has weaker, less trained muscles but still had to apply the same pushing force to the wheels for forward locomotion. He compensated for the weakness of the muscles and the lack of driving experience by employing much faster motion of his hands mostly in straight line.

His shoulder muscles were not able to contribute much when applying the required pushing force because he mostly kept his shoulders in a position parallel to the seatback of the wheelchair. Unfortunately, this position added stresses to the muscles of Mr. K's upper body. An analysis of the shoulder trajectory of Mr. J during motion, also found that the synchronization between the right and left was not complete.

Left	Right

Hand translational motion along the x-axis

Shoulder translational motion along the x-axis

Slow motion – Mr. J

Slow motion – Mr. K

Direction of Motion

Figure 5.11 Comparison of translational motion of the hand and the shoulder for both Mr. J and Mr. K on the Ottobock® wheelchair during slow motion

The relative lack of synchronization between the left and right shoulders can be explained by:

1. Missing some captured data due to the intermediate accuracy of the motion capture system in use.
2. Slightly unsynchronized motion due to different relaxing time during the pushing cycle.

A careful study of the captured motion for the test persons at different traveling speeds found that the change in driving and pushing cycle style is sometimes completely different from the starting point to the motion trajectory within the x-z-plane or even the x-y-plane. It is worthwhile to analyze the motion for the same test person during fast and slow motion in order to recognize the change in driving strategies for the wheelchair in addition to the change in pushing cycle for the wheels and finally the motion trajectories for the operating space of the body part being analyzed.

By comparing the resultant animation from the captured motion of both test volunteers as shown in Figure 5.11, it becomes clear that Mr. J moved his hand behind the centerline of his body and extended his arm to reach the farthest point behind his body centerline that his arm would allow, which allowed him to pull the wheel through the first half of the propulsion stroke and push it to the farthest point his hand could reach in front of his body through the second half of the stroke.

Mr. J's hand made a half-circle during the wheel propulsion stroke, which begins from the farthest point behind Mr. J's back and pushed fully to the farthest point his hand could reach in front of his body. On the other hand, Mr. K did not extend his arm behind his body centerline. He caught the point on the wheel just beside his body and pushed it forward in fast, short continuous motion. The motion trajectory of Mr. K's hands made a semi-circle in the motion space. This difference in the starting point of the propulsion stroke for the wheel made a clear different in the moving force and the pushing moment achieved.

| Mr. J | Mr. K |
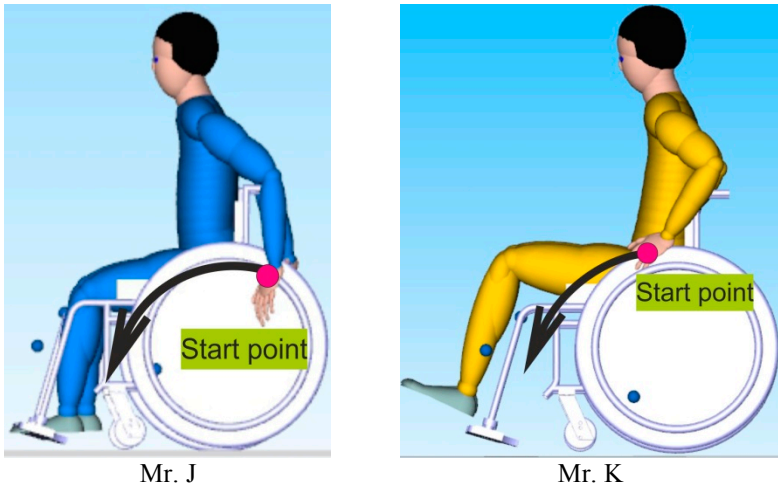
Figure 5.12 Mr. J vs. Mr. K during slow motion

From Figure 5.12, it is clear that the start point of the propulsion stroke is different. Mr. J's hand is behind his body centerline whereas Mr. K. only brings his hand to the centerline. The difference in the starting point of the propulsion leads to a change in the propulsion force and the amount of driving power induced. Using this simple technique, Mr. J produced more pushing force and moment during motion.

Left	**Right**

Elbow rotational motion relative to the x-axis – fast motion

Shoulder rotational motion relative to the x-axis – fast motion
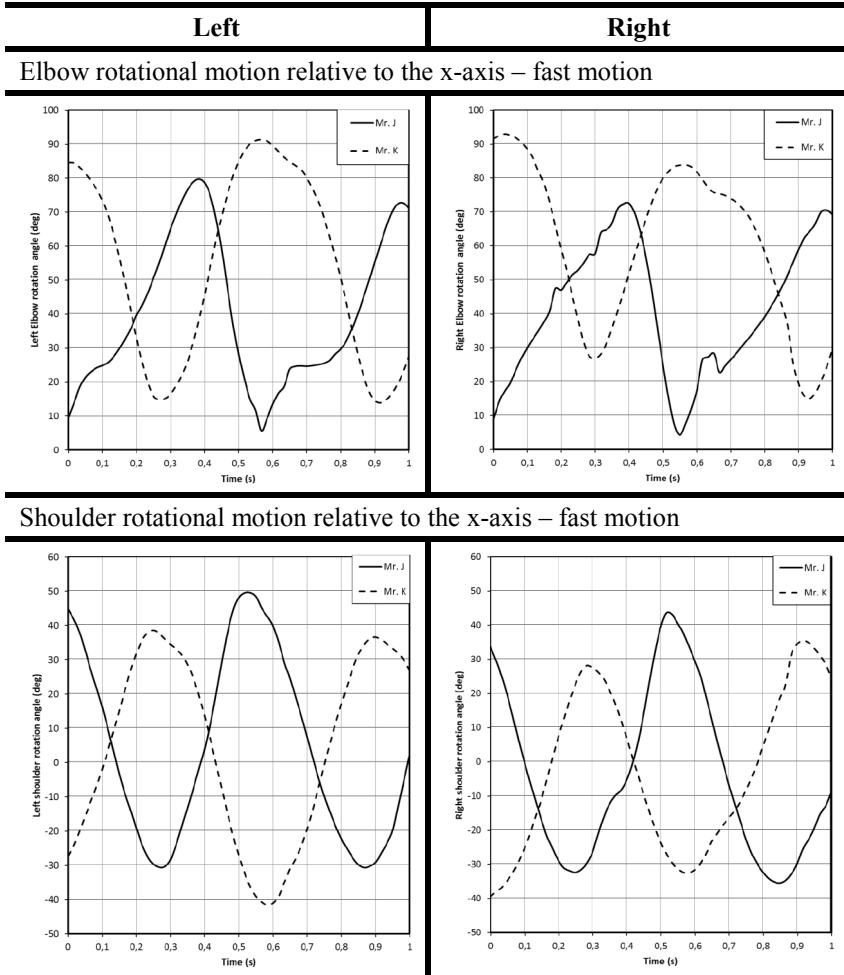
Figure 5.13 Comparison of the angular motion of the shoulder and elbow for both Mr. J and Mr. K on the Ottobock® wheelchair during fast motion

The harmonious periodical motion is evident for both Mr. J and Mr. K; also, due to the fast pushing cycle used by both test persons, the motion of their shoulders followed an identical clear periodical sinusoidal trajectory in the motion space. Synchronization between the right and left parts of the

body can be seen in the Figure 5.13. Nevertheless, because of the fast motion and, as a consequence, the resulting continuous pushing cycles for both right and left wheels, the shoulders do not experience a true relaxing cycle, only a short interruption of the otherwise continuous pushing in order to keep the induced force at the required level to attain the allowable maximum speed during the test. It is important to mention here that the test subjects were asked to follow a fast pushing cycle and give their maximum effort to reach their maximum traveling speed for the wheelchair. The elbows move along trajectories within the motion range which seem to be identical along the length of the test track. However, in a few trials, Mr. J's right elbow showed a discontinuity in the pushing cycle arising either to resynchronize the motion of the left and right sides of the body or to correct the path of his wheelchair, which allowed him to utilize the relaxation and stress of the muscles to develop the maximum possible pushing force especially during fast motion.

He avoided motion irregularity by holding his arms parallel to the wheels for a few seconds and then moving his arm in a motion that appeared almost random. But it is clear that it is a professional move to re-catch the rim of the wheel and push the wheels starting from a selected attack angle. This may be slightly different on the right side than the left side but the end effect of such move is to decrease the irregularity and correct the motion path. Mr. K, who was using a wheelchair for the first time in his life, would not have been expected to demonstrate such sensitivity or capability to understand it immediately. Any attempts by Mr. K to correct the motion path or even synchronize the pushing motion led to delays in the motion and stress in the arm muscles without real output of pushing force.

A comparison of the arm and shoulder trajectories will be discussed briefly below to understand the main motion characteristics and the critical driving mistakes made by the untrained test person. The trajectory positions are shown and analyzed, especially commenting on the differences and highlighting the essentials of the developed strategies for assuring effective pushing cycles θ_P, see Figure 5.9, when quickly driving the wheelchair.

Left	**Right**
Hand translational motion along the x-axis	
Shoulder translational motion along the x-axis	
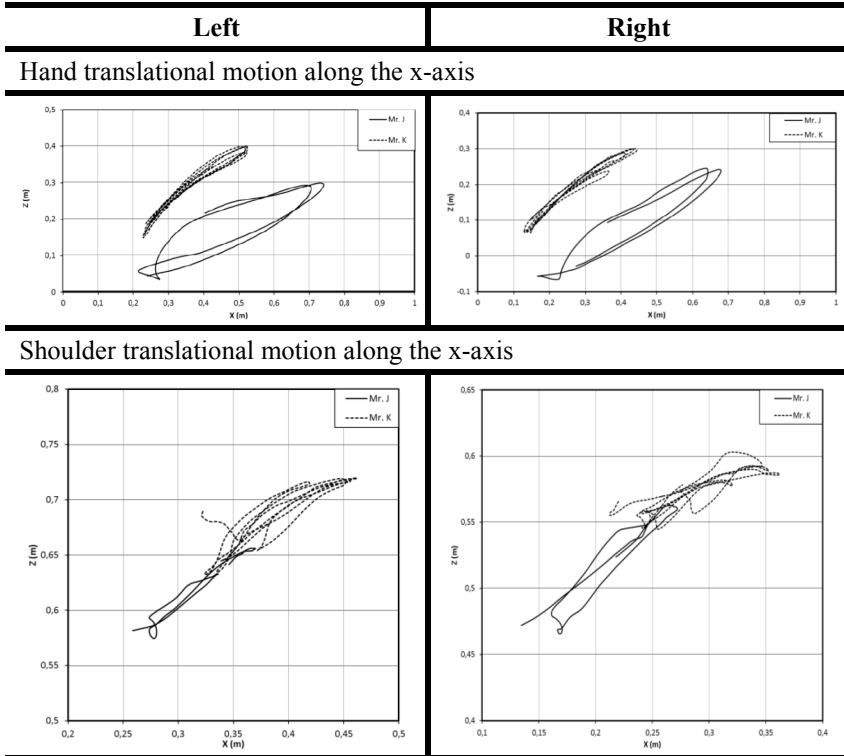
Figure 5.14 Comparison of the translational motion of the hand and the shoulder for both Mr. J and Mr. K in the Ottobock® wheelchair during fast motion

The motion trajectories of the right and left hand for each of the test volunteers have been identical so far. Each of them moved his left and right hands in a similar way to push the wheelchair wheels. Mr. J's hands followed more identical trajectories which were in an elliptical configuration. His hand trajectory was inclined at an angle of around 45° with respect to the vertical body centerline. This means that he pushed his upper body forward to produce more force during travel. Mr. K followed the same strategy by bending his upper body at a very sharp angle and moved his hand fast to push the wheels in short bursts to reach the maximum derived force and allowable speed. However, the trajectory of Mr. K's hand showed a linear configuration with multiple strikes on slightly different positions on the rim. The lack of experience on the part of Mr. K

was very evident in his driving strategy, which can be comfortable for him and effective for the amount of pushing force induced. The motion of the shoulders when traveling quickly was not promising, where a detailed analysis of the moving trajectories within their effective motion space showed inhomogeneities in the driving style for the same volunteer between his left and right hand. But the main conclusion indicates that both of the test volunteers inclined their back at a sharp angle to gain more force when pushing the wheel. The force gained mostly depends on not only the angle of the back but also the moving speed of the hand and the contact point on the rim relative to the hand position within the effective motion range. The shoulders trajectories shown in Figure 5.14 involve motion in the x-z-plane. It is not clear whether Mr. J achieved the optimal driving strategy during the captured test but his performance is definitely better than Mr. K in most of the cases.

5.2.6   Comparison between the fast and slow motion of Mr. J

To understand the main characteristics of the driving strategy during the different driving situations, it is important to compare the available motion speeds. Body orientation, back inclination angle, the instantaneous contact point between the volunteer's hand and the rim of the wheelchair play very important roles in enhancing and increasing the pushing force induced and the corresponding moments. Moreover, the driving strategy used may help to relax the muscles and provide the users with a more comfortable situation and at the same time allow them to push the wheelchair forward without excessive effort or additional stresses on hands or shoulders.

From Figure 5.15 it is noteworthy that during Mr. J's fast pushing cycle (who is the expert volunteer) he bent his back at an angle of around 45°, whereas his back remained parallel to the wheelchair seatback during slow motion. Mr. J used to extend his arm to its full length to reach the most far contact point of the wheel rim to pull it to the half way of the rotation track and then begin to push it away and he extended his arm to reach its full length during the pushing cycle. The pushing and pulling strokes have similar characteristics for both fast and slow motion. However, in the fast motion, the arm is not extended to its full length parallel to the wheelchair, which is a movement that helps to regulate the speed of the wheelchair during slow motion and achieve the desired synchronicity in the motion of both sides of the body. Mr. J's back angle, see Figure 5.16, J is not constant over the time period captured. The angle is mainly proportional to the pushing or pulling force desired, in other words proportional to the rotating

moment required to push the wheelchair in the direction of travel at the desired or allowable speed. The technique used by Mr. J to maximize his pushing and pulling forces can be summarized as follows:

1. Bending his back at an angle of about 45°.
2. Extending his arm to its full length to reach the fartherst point on the wheel rim during the pushing and pulling cycles while the wheel is rotating.

Left	Right

Hand translational motion along the x-axis

Shoulder translational motion along the x-xis

Slow motion

Fast motion

Direction of Motion
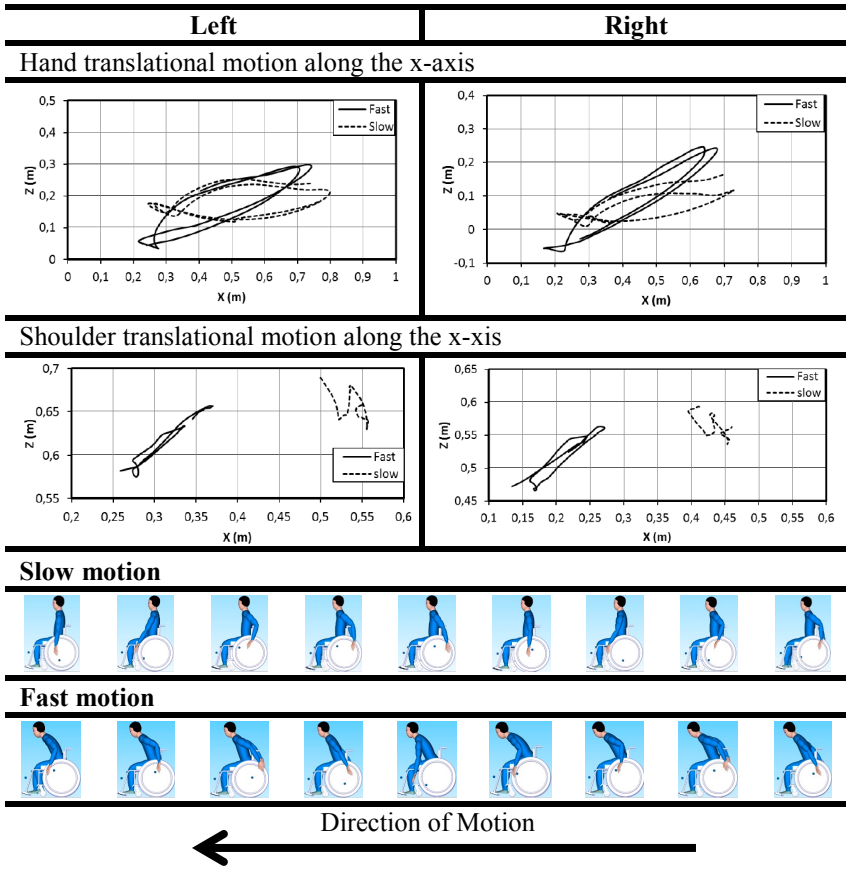
Figure 5.15 Comparison of the translational motion of the hand and the shoulder for Mr. J in the Ottobock® wheelchair during fast and slow motion

It can be concluded from the previous measurements that the acceleration techniques demonstrated by Mr. J developed after a large amount of training as a basketball player. The speed-up techniques do not only depend on the back angle or the point of grip on the wheel rim but also by attaining a high degree of synchronization between the right and left sides of the body, especially in hand motion. From the previous figure, it is evident that the motion trajectories of Mr. J's right and left hands are similar for both fast and slow speeds. In the slow motion case, the hand trajectory is parallel to the traveling track whereas the fast motion track is inclined at an angle of 45° with respect to the body centerline. The motion space of the shoulders seems to be comparable between the fast and slow speeds. The shoulder movement helps to increase the range of motion of the hand to reach the farthest point on the rim in addition to helping to induce the required rotation moment without stressing the muscles of the arm or using more effort than usually required.

Fast Motion   Slow Motion
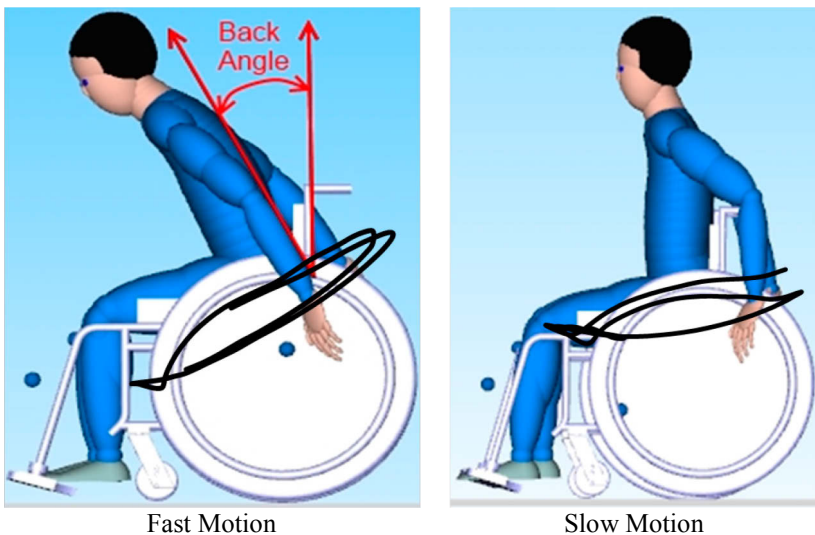
Figure 5.16 Fast and slow travelling of Mr. J in the Ottobock® wheelchair

The conclusions to be drawn from Figure 5.16 is that a new wheelchair users should be advised to pay attention to back position during travel and to train their hands to find a suitable contact point in order to achieve smooth motion. They should be made aware that fast movements of the hands are not enough to reach a desired speed but rather that the method of

hand movement and location on the rim are also very important. A suitable amount of training time is required to enhance the capability of users to drive and maneuver a wheelchair with reasonable quality. Even for advanced users, achieving synchronization between the hand and back movement is a difficult task. In order to reach full synchronization between the hand and other body parts, concentration and training are required in addition to sensitivity to surrounding conditions. To reduce the traveling speed of the wheelchair, it is recommended to follow Mr. J's strategy in this situation, which is to extend both arms parallel to the wheels and let the wheelchair brake itself using the weight of the user and in extreme cases using the hands on the external wheel rim. For users with a high degree of disability or those who want to keep traveling speeds low, it is recommended for them to keep their backs parallel to the back of the wheelchair seat and to push the wheels in regular cycles, in which the trajectory of their hands within the motion space should appear as a continuous ellipse.

Table 5.3 contains the maximum, minimum and average speed of the wheelchair for both test volunteers while motion was being captured at each speed of travel.

Table 5.3 Wheelchair speed during motion capture

| Traveling mode	Test volunteer	Max. speed (m/s)	Min. speed (m/s)	Average speed (m/s)
Slow motion	Mr. J	1.039	0.58	0.81
	Mr. K	0.85	0.43	0.64
Fast motion	Mr. J	2.97	2.1	2.54
	Mr. K	1.98	0.91	1.45

5.2.7   Motion on a ramp

Based on the experience acquired in the previous sections using motion analysis of traveling with an Ottobock wheelchair, the study of the motion captured from use of the sport wheelchair, including on the ramp obstacle, can be simplified by concentrating on just the hand motion and the angle of the user's back, see Figure 5.5. Traveling over the ramp represents a particular challenge, especially in overcoming the front part of the obstacle; reaching the specified end point requires a continuously increasing amount of effort.

Next, the analysis covers the motion captured from both Mr. J and Mr. K on a ramp with an inclination angle of about 9° and with a track length of about 10 m. The test volunteers were asked to start their motion from around one-half meter before the starting point of the ramp to gain additional pushing force in order to overcome the obstacle at the front of the ramp. Then, the volunteer was to travel on the ramp until reaching a specified end point. The distance travelled on the ramp is not more than 5 m but the real challenge is in expending the required effort to produce enough force to push the wheelchair and keep its speed of travel at the same level from beginning to end.

Due to the huge amount of effort required to climb the ramp, Mr. K was unable to maintain synchronization between the left and right rotation of his elbows during the pushing motion, as shown in Figure 5.17; on the other hand, Mr. K showed a real capability of handling the situation with synchronization between the rotation of his left and right elbows and shoulders. The harmony and full synchronization between the motion of Mr. K's left and right arms helped him to produce the required force to keep the climbing motion of the wheelchair regular and continuous without disturbance due to the lack of sufficient pushing force. Mr. K succeeded in keeping the rotation angle of his left and right arms within the same range, despite the huge effort required to push the wheelchair upward along the ramp. Due to a lack of the experience, Mr. K exhibited irregularity in his pushing cycles and therefore irregularity in the path traveled along the ramp.

Left	**Right**

Elbow rotational motion relative to the x-axis – on the ramp

Shoulder rotational motion relative to the x-axis – on the ramp
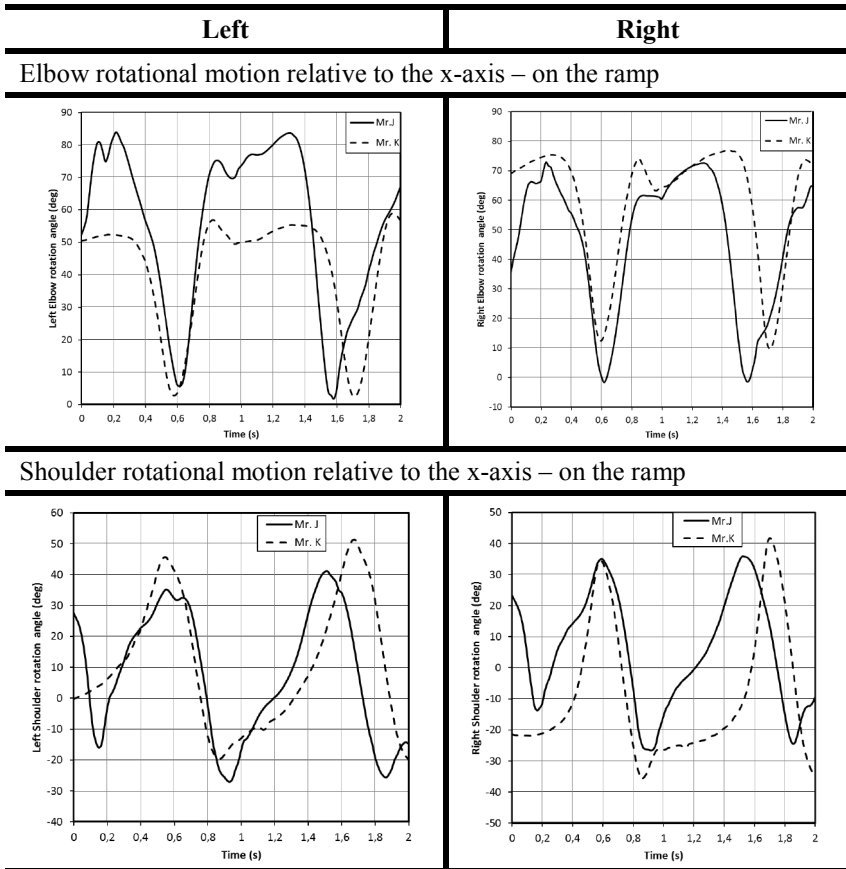
Figure 5.17 Comparison of the angular motion of the shoulder and the elbow for both Mr. J and Mr. K in the Ottobock® wheelchair during motion on the ramp

Left	Right

Hand translational motion along the x-axis
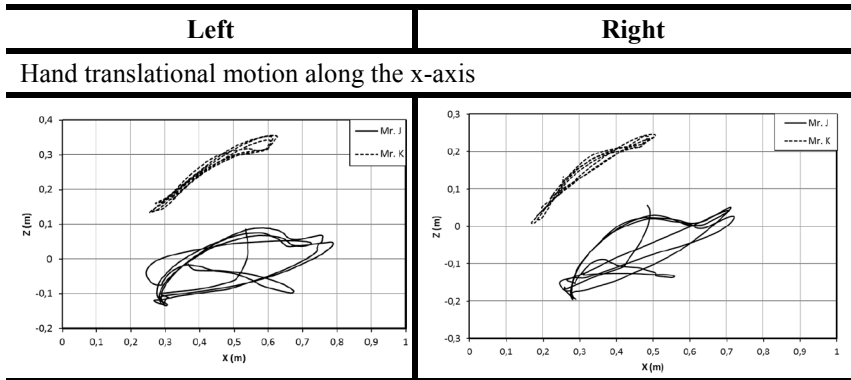
Figure 5.18 Comparison of the translational motion of the hand for both Mr. J and Mr. K in the Ottobock® wheelchair during motion on the ramp

As shown in Figure 5.18, the motion span of Mr. J's hand is larger than that of Mr. K, meaning Mr. J handled the situation and controlled his pushing cycles to produce the effort required to push the wheelchair along the ramp. Mr. J and Mr. K both kept their hands on the rim; therefore, the upper parts of the trajectories of the hand's translational motion look like semi-circles. Analysis of the return stroke of Mr. J's hand showed that he tried to grip the farthest contact point his hand could reach to pull the wheel. He continuously did his best to catch the farthest point and pull it. The return strokes of his left and right hands seemed to be synchronized and in harmony, which helped him to in avoid motion disruptions and decreased deviations from the traveling path.

5.2.8   Sport vs. OttoBock wheelchair

(a) Ottobock® wheelchair   (b) Sport wheelchair

Figure 5.19 The wheelchairs used in the motion capture measurements

The first type of wheelchair used in the study was from Ottobock®. The model is modified in design and weight to be more suitable for users with different levels of motion disability. The weight of the wheelchair used here was reduced to make it easy to push. It needs less driving moment than other similar wheelchairs from similar categories oriented toward the same users. In the category of manually driven wheelchairs, the weight and the design of the wheelchair are important parameters for specifying a suitable wheelchair for each disability case. Some companies, of which Ottobock® is one, have invested a reasonable amount of capital into adding more enhancements for their wheelchairs products in order to improve the motion and enhance the stability of the wheelchair under different driving and environmental circumstances.

The second type used is a special wheelchair designed for sports activities, especially for basketball players with disabilities. The wheelchair is equipped with a wide base to increase stability when pushing and maneuvering about the playing surface. The wheelchair has a simple design and construction but exhibits very stable capabilities during motion. The sport wheelchair, as in this case, gives the player additional advantages during play and improves on the shortcomings of other designs [136, 22, 79 and 135].

The question now is whether there is a difference in driving style or maneuvering characteristics of each of the wheelchairs used. And, if the answer is yes, then which can be classified as "easy to drive" and which "difficult to drive". The main characteristics of the wheelchairs, such as stability and maneuverability, will not discussed here because the focus is on the driving style of the test volunteers. The main objective here is to understand the main differences in the pushing cycles for both wheelchairs and the general configuration of the user in each case. Hand position during the motion will be used as a comparison parameter for different driving speeds.

Here, data are available for driving at high and low speeds in addition to motion on the ramp with moderate speed. Motion on the ramp, specifically, is a challenge even for experienced users because of the wheelchair weight and the need for an additional pushing force to overcome the inclination. The motion span will be presented on the illustrated motion trajectories of the user hand, which is a direct indicator for the difficulty level of wheelchair control. Increasing the motion span of the hand means the driver expends more effort during the pull and push strokes to move the wheelchair.

The analysis found next will concentrate on Mr. J's motion because of his high level of experience in wheelchair use due to his disability and because he has trained using the sports wheelchair for a number of years when practicing basketball. When driving the wheelchairs, Mr. J seemed quite capable of maneuvering the wheelchair, whereas Mr. K's lack of experience was evident in that his motion was strange and showed a loss of concentration in comparison with Mr. K. Therefore, the results of the analysis will be more accurate and more closely represent reality without the need to repeat motion sequences. The goal of the analysis is then to investigate the differences between the different chairs in different conditions.

Left	Right
Hand translational motion – slow motion	
Hand translational motion – fast motion	
Hand translational motion – motion on the ramp	
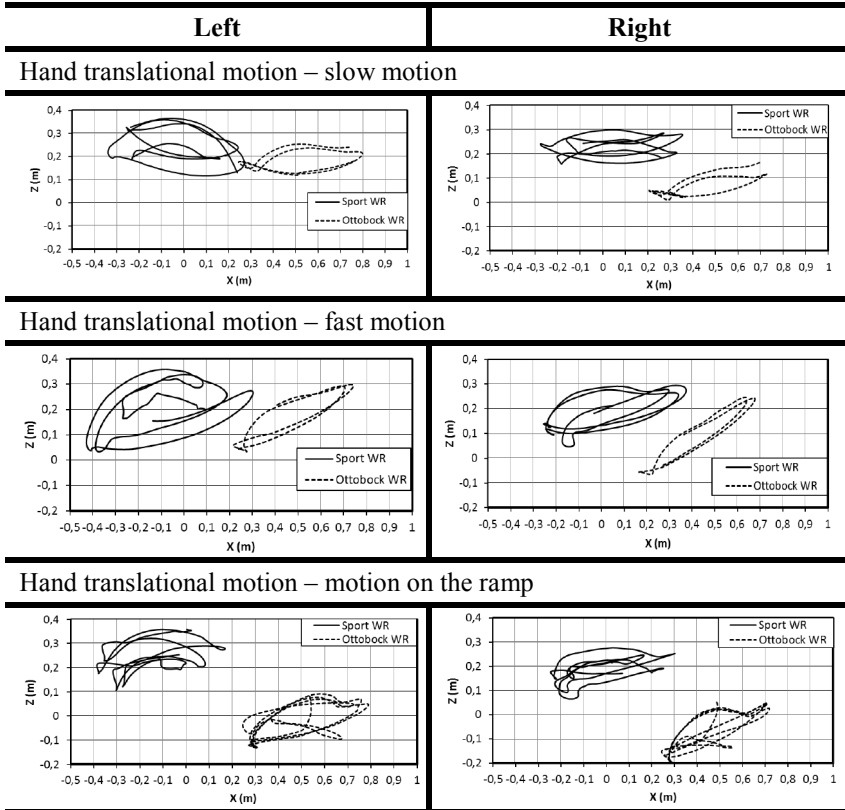
Figure 5.20 Sport vs. Ottobock ®wheelchair at different motion speeds and on the ramp

The motion span (MS) is defined as the span of the motion boundary of the hand, defined by the farthest points which the hand can reach by pulling and pushing the wheel. The motion boundary can be determined from two points on the motion path and used to characterize the motion and the boundary. The working boundary or motion space of the hand cannot be exactly determined; rather, it is just an experimental way to determine roughly how users move their hands during motion capture. The motion span is an indicator for the simplicity of control driving, where increasing the span shows that the user expended more effort to move the wheelchair. Under all driving conditions, it seemed that the sport wheelchair needed more driving force from the same user, which is reflected in the dimensions

of the motion span. The main reason behind the relatively large motion span in the case of the sport wheelchair and thus of the driving effort is simply the weight of the wheelchair.

5.2.9   Comparison of hand trajectory

The hand trajectory which arises during propulsion of the wheelchair has been previously discussed in various sources [79, 135]. It depends on the type of disability. These measurements confirmed that the hand trajectory captured complied with the commonly known trajectories as shown in Figure 5.21. Mr. J moved his hand along a uniform trajectory, which MASON called a single looping [79]. The trajectories exhibited by Mr. J and those shown in the literature are quite similar, with the primary difference being the starting angle θ_S, see Figure 5.9.

(a) Mr. J's hand trajectory   (b) Single looping from Mason [79]
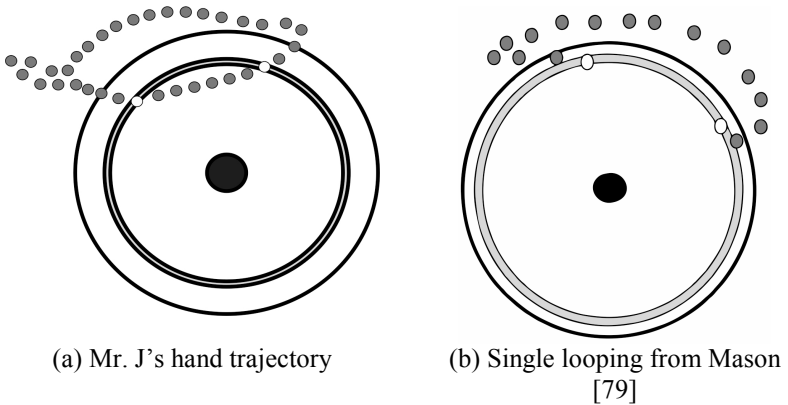
Figure 5.21 Single looping hand trajectory in Mr. J's case

In theory, there is no difference between theory and practice. But, in practice, there is.

(J. L. A. van de Snepscheut)

6   <u>Conclusion and further work</u>

This chapter presents the final results and a conclusion for each studied point in this thesis. The recommendations derived from this work are summarized and introduced here to cover the following points:

- Developing a new concept for wheel-based locomotion systems
- Analyzing human motion within the full locomotion system

The focus on developing a new concept for wheel-based locomotion systems demonstrated the importance of analyzing the performance of that locomotion system based on Mecanum wheels. Generally, studying the 4WMV covers many subjects. They can be categorized into three main groups:

- Design
- Mathematical modeling
- Control

6.1   <u>Design</u>

The mechanical design covers not only the suggested conceptual designs and modifications for new locomotion systems but also the analysis of the dynamical behavior and the analysis of mechanical stress and deformation in the suggested systems. New concepts will be introduced under:

New conceptual design for a wheel with varied rollers inclination angles

For more stability during the motion, it is recommended to use the wheels with continuous profile. Such wheels can be steered separately and they can achieve the same performance of the 4WMV by applying the suitable steering angle on each wheel. In case of the need to overcome the obstacles, it is still possible within the allowed rang for the classical wheels. The stairs climbing also can be achieved by using suitable motors. The chained wheeled vehicle can be an answer for all the previous situations. The chained wheeled vehicle is a vehicle equipped with four separate chained wheels or wheel combination. Each chain can be steered separately by its own mechanism. The Mecanum effect can be obtained by steering the chained units separately by the suitable steering angles and simultaneously they can overcome the high obstacles as an advantage for the chained locomotion systems.
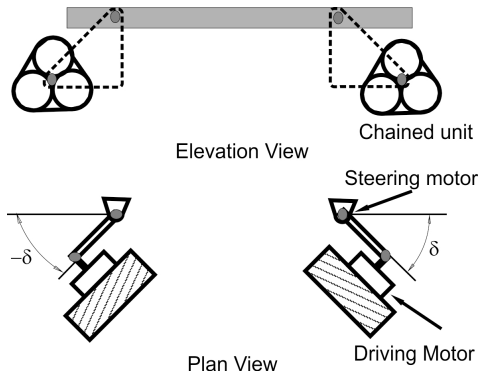
Figure 6.1 Chained –Mecanum wheeled vehicle

A conversion kit using Mecanum wheels

The conversion kit facilitates the conversion of an ordinary wheelchair into a 4WMV in a few simple steps. Removing the ordinary wheels and installing the conversion kit by pressing a fixing button. The electrical attachments such as the battery and the driving joystick can be supplied separately or added as part of installation of the conversion kit.

Section Plan
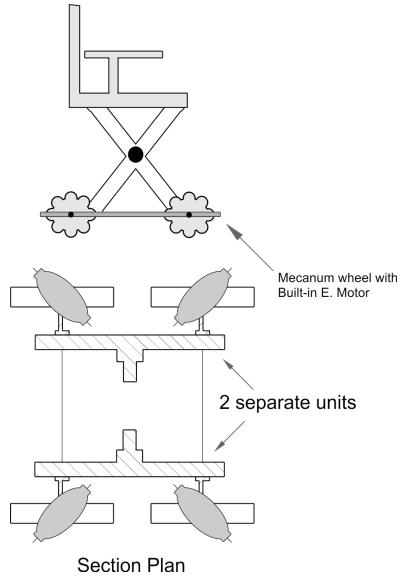
Figure 6.2 Conversion kit using Mecanum wheels for wheelchairs

Multi-angle Rollers for the Mecanum wheel

The inclination angle of the rollers of the Mecanum wheel can be changed from 0°-90°. There is a special mechanism to rotate the rollers simultaneously in the same direction by the same angle. This mechanism is driven by a central gear, which can be rotated by additional electric motor or manually. It is recommended to set the inclination angle before the motion to avoid the instability of the system during the motion. This design is facing a problem which is the continuous vibration due to the gap between the rollers, so that as a solution, it is suggested to increase the number of the rotating rollers. The rollers will be closer and the vibration will decrease. Such design has not been examined practically but has been discussed theoretically in different references.
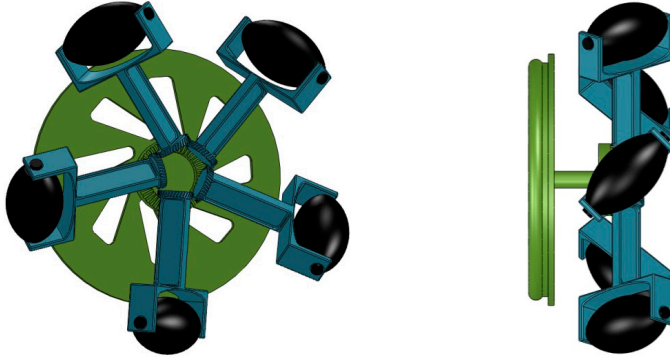
Figure 6.3 Mecanum wheel with rotating rollers

6.2   <u>Mathematical modeling</u>

Building kinematic and dynamic mathematical models for the nonholonomic 4WMV was achieved successfully in this study. The advantages of the dynamic model introduced, can be summarized in finding optimal motion trajectories, save the design costs and examine different operation conditions like shifting the mass center or fluctuation of the driving moments.

In the further studies for the 4WMV, it is recommended to build a complete Mecanum test vehicle, equipped with acceleration sensors to measure acceleration in the x- and y-directions and the angular acceleration relative to the z-axis. The measured parameters can be digitally integrated to calculate the displacements along the x- and y-axes in addition to the angular velocity and the angular displacement relative to the z-axis. The driving moments and the corresponding rotation speeds for each wheel must be measured or estimated mathematically to prove the correctness of the dynamic and kinematic models introduced in this thesis. The measured parameters from the test Mecanum vehicle can also be used to identify a model for the 4WMV. One goal is the correction of the deviation between the suggested model and the commonly used approximation model on the one hand and the suggested model and the practical measurements from a real system on the other hand. That can enhance the developed models and help to develop suitable control methodologies to decrease the amount of deviation.

The suggested model supports the determination of the dynamic behavior of Mecanum vehicles with different dimensions, especial when the center of gravity of the Mecanum vehicle is not located at its middle. Irrespective of whether the center of mass shifts forward or backward, the suggested model can handle it. On the other hand, the commonly used approximation model assumes that the vehicle center of gravity is located exactly in the middle, meaning the center of gravity is located at exactly half the distance between the front and the rear wheels, which is an ideal case not actually found in reality.

In case of the load transfer, it can be said that the vehicle moves in the same direction to the load concentration of the vehicle mass. If the mass concentrated on the frontal axle, then the 4WMV moves forward left and by changing the mass concentration to be on the rear axle, then the 4WMV moves in the backward left direction.

For the future scope, the study showed the need for estimation a mathematical dynamic model, which is a function of the various wheel inclination angles δ_1 , δ_2 , δ_3 and δ_4. This model can help in finding the required moments for each wheel in order for the 4WMV to follow a predefined trajectory. The model expands the coverage of dynamic investigations, not only for the 4WMV but also for the classic electrical vehicle with an independent steering system for each wheel, which is called wheel unit. The later model was introduced by CONTINENTAL® and SIEMENS VDO® at the end of the 20th century. Furthermore, governments of various developed countries are encouraging the electrical vehicle industry and introducing this type from the dynamic models to help in optimizing the required driving moments and achieve more complex maneuverability.

Certain constraints can help tighten the motion of the independent steering wheel vehicle, such as having the inclination angles of the front wheels be similar but in the opposite direction of the rear wheels:

$$\delta_1 = \delta_2, \qquad \delta_3 = \delta_4 \ ,$$

and at the same time:

$$\delta_1 = -\delta_3, \qquad \delta_2 = -\delta_4 \ ,$$

that will tighten the motion trajectory but is still the only valid way to reach a desired location with sufficient maneuvering, especially if classical wheels are being used, which have a complete continuous circumference.

It is important to study the change of the driving moments during the traveling due to the change in the motion direction or due to the brake or the acceleration. The effect of weight transfer during the motion must be further studied, that to compensate the driving moments to keep the stability of the vehicle. For the future work, it is recommended to study how to overcome the obstacles using the compensation of the driving moments, to overcome the obstacle and in the same time to keep the motion with steady speed. The effect of changing the direction of the motion and the required time for changing the state from direction to another and how to minimize these transient periods are also demands for the future research in this field. The sensors-actuators-setups have to be taken in consideration to measure the important parameters of the vehicle during the motion and to develop the suitable compensation algorithm.

Expanding the studied parameters of the dynamic model leads to the need for deploying different theories in estimating the model, therefore deploying MAGGI equation will help in avoiding the additional mathematical processes of eliminating the LAGRANGE multipliers from the equations as mentioned in [55].

Analyzing and studying further the effect of the electric motors and the electrical parts from the system on the overall behavior is recommended. It is suitable also, estimating a mathematical model for the combination of the electric effects and the mechanical parts of the electric motor as known widely under the title the DC motor physical and mathematical models. As mentioned before, it will be better to find the actual angular velocities of the wheels based on the electrical characteristics of the motor used in the mechanical setup. One from the feature of modeling electric motor is combining the effects of the mechanical and electrical parts of the system and increases the accuracy by determining exact motion characteristics.

6.3   <u>Developing a model based controller for the 4WMV</u>

For the future work, from the control scope, it has been found a real need to develop a model based controller for the 4WMV. It is recommended to examine the effect of the feedback controllers. Also, the effect of the intelligent controllers like the Fuzzy logic, Genetic search and optimization algorithms and the Neural Network must be examined to enhance the motion capabilities of the 4WMV. Many artificial intelligent algorithms are used nowadays, in many industrial applications, to supervise the system directly or supervise the other types of feedback or even the nonlinear controllers.
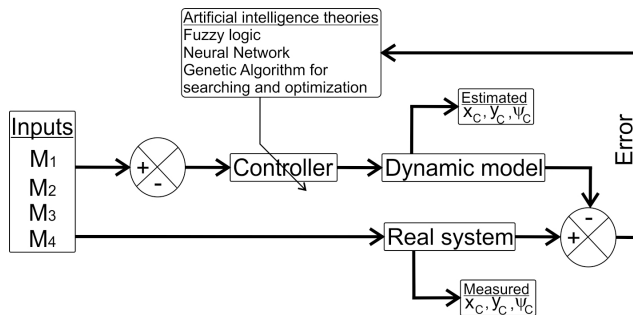
Figure 6.4 Design a supervised controller for the 4WMV

In Figure 6.4, the supervised controller is presented. The controller will decrease the difference between the measured and the estimated parameters to be minimum.

6.4   <u>Analysis of the human motion behavior while using a wheelchair</u>

In chapter 5, the motion of the wheelchair user has been captured using special cameras and has been analyzed to understand the differences between the healthy and handicapped persons during the propulsion of the wheelchair. Two different tracks have been prepared for the experiments. The first one was a flat track but the second was a ramp with inclination angle around 9°.

The slow and fast motions for two volunteers have been captured for the comparison purposes. This study has concentrated on the analysis of primary parts of the human body, where the motion of the arm, shoulders and body trunk. It has been found, according to many references, that the type of disability has a direct relationship with the propulsion method for the wheelchair. The important results have been summarized and plotted for the corresponding speed and for the corresponding movable part.

The analysis of the motion has been carried out using ALASKA® and ERGO TOOL®. The capturing cameras, which have been used in the experiments, are delivered from the research partners of the institute of Mechatronics Chemnitz. They provided the experiments by a digital human body model; the captured motion has been clipped to that model, that to visualize the captured data in 3D. The virtual model of the human body is used to present the detailed motion of each body part during the propulsion of the wheelchair.

The test volunteers have dressed a special suit, which consist of a set of white nodes, these nodes will be detected and their displacements and rotations will be captured during the motion. The motion of each body part has been captured and stored under the corresponding node. Each part can have both translational and rotational motion. The captured data is analyzed immediately and compared with the stored digital model of the human body.

A task for the future research is the integration of the motion capturing data into a complete virtual human model in ALASKA®.

References

1. Abdelrahman, M.; Zeidis, I.; Bondarev, O.; Adamov, B.; Becker, F.; Zimmermann, K.: A description of the dynamics of a four-wheel Mecanum mobile system as a basis for a platform concept for special purpose vehicles for disabled persons.submitted to 54th International Scientific Colloquium, September 8-12, 2014, Ilmenau, Germany.

2. Abdelrahman, M.; Zeidis, I.; Bondarev, O.; Adamov, B.; Zimmermann, K.: An approach to the kinematics and dynamics of a four-wheel Mecanum vehicles. submitted to Scientific Journal of IFToMM "Problems of Mechanics".

3. Abrahm, R., Marsden, J.E. (1978): Foundations of mechanics, Benjamin Currings, London.

4. Adascalitei, F.; Doroftei, I. (2011): Practical applications for mobile robots based on Mecanum wheels – a systematic survey. The Romanian review precision mechanics, Optics & Mechatronics, No. 40.

5. Advanced Realtime Tracking (ART) GmbH(2012): System user manaul of ARTtrack R , Trackpack & DTrack; Am Öferl 6, 82362 Weilheim, Germany.

6. Agulló, J.; Cardona, S.; Vivancos, J. (1987): Kinematics of vehicles with directional sliding wheels. Mechanism and Machine Theory, vol.22, no. 4, pp. 295-301.

7. Americans With Disabilities and Disability Resources (2010): online website under http://www.dol.gov /dol/topic/disability/ statistics.htm.

8. Anybody Technology A/S (2013): The AnyBody Managed Model Repository (ANMR). http://www.anybodytech.com /?id=20. Last visited: 08-08-2013.

9. Arczewski, K.; Pietrucha, J. (1993): Mathematical Modelling of Complex Mechanical Systems. vol.1, Discrete Models, Ellis Horwood, Chichester.

10. Arnold, V.I. (1988): Mathematische Methoden der klassischen Mechanik; VEB Deutscher Verlag der Wissenschaften, Berlin.

11. Barraquand, J.; Latombe, J.-C. (1989): On nonholonomic mobile robots and optimal maneuvering. In: Intelligent Control Proceedings., IEEE International Symposium, pp. 340–347.

12. Bates, L.; Sniatycki, J. (1993): Nonholonomic reduction, Reports on Mathematical Physics 32, 99–115.

13. Becker, F. et al (2013): Das rollende Bein – eine Kombination aus Rollen und Schreiten für die Nahfeldmöbilität. Konstruktion Zeitschrift für Produktentwick-lung und Ingenieur-Werkstoffe, Springer-VDI-Verl. vol. 653, no. 9, pp. 88-90, Düsseldorf.

14. Borisov A.V., Kilin A.A., Mamaev I.S. (2011): An omni-wheel vehicle on a plane and a sphere. Russian J. Nonlin. Dyn.,vol. 7, no. 4, pp.785–801.

15. Bullo, F.; Lewis, A.D (2004): Geometric Control of Mechanical Systems. Springer Sceince + Bussiness media, New York. ISBN:0387221956, 9780387221953.

16. Byun, K.; Song, J. (2003): CVT control of an omnidirectional mobile robot with steerable omnidirectional wheels for energy efficient drive. Proceedings of IEEE International Conference ICRA '03 on Robotics and Automation, vol. 1, pp. 503–508.

17. Chenier, F.; Bigras, P.; Aissaoui, R. (2011): A new dynamic model of the manual wheelchair for straight and curvilinear propulsion. In: Rehabilitation Robotics ICORR, IEEE International Conference, pp. 1–5.

18. Chenier, F.; Bigras, P.; Aissaoui, R. (2011): An Orientation Estimator for the Wheelchair's Caster Wheels. Control Systems Technology, IEEE Transactions. vol. 19, no. 6, pp. 1317–1326.

19. Colyer, R. E.; Economou, J. T. (1998): Comparison of steering geometries for multi-wheeled vehicles by modelling and simulation. In: Proceedings of the 37th IEEE Conference. Decision and Control, vol. 3, pp. 3131–3133.

20. Conceigao, O. S.; Moreira, A. P.; Costa, P. J. (2005): Architecture Control and Model Identification of a Omni-Directional Mobile Robot. Portuguese Conference on Artificial Intelligence epia, pp. 247–251.

21. Cooper, R. (2009): Wheeled mobility and manipulation technologies. The Bridge Washington National Academy of Engineering; vol. 39, no. 1, pp. 13–20, ISSN: 0737-6278.

22. Crespo-Ruiz, B.M. et al (2011): Relation Between Kinematic Analysis of Wheelchair Propulsion and Wheelchair Functional Basketball Classification. Adapt Phys Activ Q, vol. 28, no.2 , pp.157-172.

23. Dassault Systems (2013): DELMIA – Virtual Ergonomics Solution. http://www2.3ds.com/fileadmin/PRODUCTS/DELMIA/OFFE RS/Virtual-Ergonomics-Solutions/PDF/DELMIA-Virtual-Ergonomics-brochure.pdf. Last visited: 09-08-2013.

24. De Villiers, M.; G. Bright (2010): Development of a control model for a four wheel Mecanum vehicle; 25th international conference for CAD/CAM, Robotics and factories of the future conference, Pretoria, South Africa.

25. Dickerson, S. L.; Lapin, B. D. (1991): Control of an omni-directional robotic vehicle with Mecanum wheels. In: National Telesystems Conference Proceedings NTC '91, Vol.1, pp. 323–328.

26. Diegel, O.; Badve, A.; Bright, G.; Potgieter, J. and Tlale, S. (2002): Improved Mecanum wheel design for omni-directional robots. Australasian Conference on Robotics and Automation, Auckland.

27. Doroftei, I.; Grosu, V.; Spinu, V. (2008): Design and Control of an Omni-directional Mobile Robot. Novel Algorithms and Techniques In Telecommunications, Automation and Industrial Electronics: Springer Netherlands, pp. 105-110. Online verfügbar unter http://dx.doi.org/10.1007/978-1-4020-8737-0_19.Kolp.

28. Dresscher, D.; Brodskiy, Y.; Breedveld, P.; Broenink, J.; Stramigioli, S. (2010): Modeling of the youBot in a serial link structure using twists and wrenches in a bond graph. 2nd International Conference on Simulantion, Modeling, and Programming for Autonomous Robots, SIMPAR 2010 Workshops. Germany: SIMPAR, pp. 385–400.

29. Economou, J. T.; Colyer, R. E. (2000): Modelling of skid steering and fuzzy logic vehicle ground interaction. American Control Conference Proceedings, vol. 1, pp. 100–104.

30. Enos, M.J. (1993): Dynamics and Control of Mechanical Systems. American Mathematical Society, Providence.

31. Essen, H. (1994): Geometry of nonholonomic dynamics. Journal of Applied Mechanics 61,689–694.

32. Finley, MA. at el (2004): The biomechanics of wheelchair propulsion in individuals with and without upper-limb impairment. J Rehabil Res Dev., vol. 41, no. 3B, pp.385-395.

33. Gantmacher, F.R. (1960): The Theory of Matrices. Chelsea Publishing Company, N.Y., 462 p.

34. Guidelines on the provision of manual wheelchairs in less-resourced settings (2013): online website under http://www.who.int/disabilities/publications/ technology/wheel chairguidelines/en/.

35. Gutowski, R.; Radziszewski. B. (1971): The behavior of the solutions of equations of motion of the mechanical system with program constraints. Bull. Acad. Polon. Sci. Ser. Sci. Tech. vol. 17, no. 2, pp. 17–25.

36. Hamel, G. (1949): Theoretische Mechanik, Springer-Verlag, Berlin.

37. Han, F.; Yamada, T.; Watanabe, K.; Kiguchi, K.; Izumi, K. (2000): Construction of an Omnidirectional Mobile Robot Platform Based on Active Dual-Wheel Caster Mechanisms and Development of a Control Simulator. Journal of Intelligent and Robotic Systems, vol. 29, no. 3, pp. 257-275.

38. Han, K. et al (2008): Design and control of omni-directional mobile robot for Mobile Haptic Interface. International Conference on Control, Automation and Systems ICCAS, pp. 1290–1295.

39. Han, K. et al (2009): Design and control of mobile robot with Mecanum wheel. ICCAS-SICE, pp. 2932–2937.

40. Han, K.; Kim, H.; Lee, J. S. (2010): The sources of position errors of omni-directional mobile robot with Mecanum wheel.

IEEE International Conference on Systems Man and Cybernetics SMC, pp. 581–586.

41. Hanavan, E.P. (1964): A mathematical model of the human body. AMRL-TR, pp. 64-102, Wright Patterson Air Force Base, Ohio.

42. Haug, J. (1996): Zur Modellierung aktiv geregelter elastischer Mehrkörpersysteme, Fortschritt-Berichte, Reihe 11, Nr. 230, VDI-Verlag, Düsseldorf.

43. Hering, E.; Steinhart, H.; et al (2005): Taschenbuch der Mechatronik. Fachbuchverl. Leipzig im Carl-Hanser-Verlag. ISBN: 978-3-446-22881-8.

44. Hertz, H.R. (1899): Prinzipien der Mechanik in neuem Zusammenhange dargestellt. Barth-Verlag, Leipzig.

45. Hiller, M. (1983): Mechanische Systeme. Springer-Verlag, Berlin.

46. Hiller, M.; Kecskemethy , A. (1989): equations of motion of complex multibody systems using kinematical differentials. Transactions of the CSME, vol. 13, no. 4, pp. 113-121.

47. Hiller, M.; Kecskemethy, A. (1986): Eine vereinfachte Methode zur Aufstellung der Bewegungsgleichungen ebener Mechanismen. Zeitschrift für Angewandte Mathematik und Mechanik, vol. 66, no. 4, T42-T43.

48. Huang, H.; Tsai ,C. (2009): Simultaneous tracking and stabilization of an omnidirectional mobile robot in polar coordinates: a unified control approach. Robotica, 27, pp 447-458. doi:10.1017/S0263574708004852.

49. Ilon; Bengt Erland. November 13, 1972. Patent title: Wheels for a course stable selfpropelling vehicle movable in any desired direction on the ground or some other base, B60B 19/12 (20060101); B60b 019/00, REF/3876255, Sweden.

50. Indiveri, G. (2009): Swedish Wheeled Omnidirectional Mobile Robots: Kinematics Analysis and Control. On Robotics, IEEE Transactions, vol. 25, no.1, pp.164-171.

51. Inklusive Mobility. UK Government, Department for Transport (2005): online website under _ https://www.gov.uk/

government/uploads/system/uploads/attach   ment_data/   file/ 3695/inclusive-mobility.pdf.

52.   Institut Für Mechatronik E.V. (2012): Dynamicus 8 – Modellierung und Simulation von mehrkörperdynamischen Menschmodellen – Referenz- und Benutzerhandbuch; Institut für Mechatronik e.V.; Reichenhainer Str. 88, 09126 Chemnitz.

53.   Jamali, P.; Tabatabaei, S. M.; Sohrabi, O.; Seifipour, N. (2013): Software based modeling, simulation and fuzzy control of a Mecanum wheeled mobile robot. In: First RSI/ISM International Conference on Robotics and Mechatronics ICRoM, pp. 200–204.

54.   Jarzebowska, E. (2008): Advanced programmed motion tracking control of nonholonomic mechanical systems. On Robotics, IEEE Transactions, vol. 24, no. 6, pp. 1315–1328.

55.   Jarzebowska, E. (2012): Model-Based Tracking Control of Nonlinear Systems, CRC Press Taylor & Francis Group, Boca Raton.

56.   Jerrold E. M.; Jürgen, S. (1993): The reduced EULER-LAGRANGE equations. Fields Institute Comm 1, pp. 139–164.

57.   Jerrold, E. M.; Jürgen, S. (1993): Lagrangian reduction and the double spherical pendulum. ZAMP 44, pp. 17–43.

58.   Kalaba, R.E. and Udwadia, F.E. (1993): Equations of motion for nonholonomic, constrained dynamical systems via Gauss's principle. Journal of Applied Mechanics, vol. 60, pp. 662–668.

59.   Kamenetz, H. L. (1969): A Brief History of the Wheelchair. Journal of the History of Medicine and Allied Sciences, vol. XXIV, no. 2, pp. 205–210.

60.   Kane T.R. (1961): Dynamics of nonholonomic systems. ASME. J. Appl. Mech., vol.28, pp. 574-578, December. 1961.

61.   Kang, J. W.; Kim, B. S.; Chung, M. (2008): Development of Assistive Mobile Robots Helping the Disabled Work in a Factory Environment. IEEE/ASME International Conference on Mechtronic and Embedded Systems and Applications MESA, pp. 426–431.

62.   Kang, J. W.; Kim, B. S.; Chung, M. (2008): Development of omni-directional mobile robots with mecanum wheels assisting the disabled in a factory environment. International Conference on Control, Automation and Systems ICCAS, pp. 2070–2075.

63.   Kiddee, P.; Shimada, A. (2007): A controller design on person following omni-directional vehicle robots. SICE Annual Conference, pp. 1043–1047.

64.   Killpack, M.; Deyle, T.; Anderson, C.; Kemp, C. C. (2010): Visual odometry and control for an omnidirectional mobile robot with a downward-facing camera. In: Intelligent Robots and Systems (IROS), IEEE/RSJ International Conference, pp. 139–146.

65.   Kitagawa, H.; Miyoshi, T.; Terashima, K. (2009): Skill-assist control of omnidirectional wheelchair using human-friendly interface. Robotics and Biomimetics, IEEE International Conference ROBIO, pp. 1002–1007.

66.   Klingbeil, E. (1966): Tensorrechnung für Ingenieure, Bibliographisches Institut Mannheim.

67.   Kotajarvi, B. et al (2004): The effect of seat position on wheelchair propulsion biomechanics. J Rehabil Res Dev, vol. 41, no. 3B, pp. 403–414.

68.   Kumile, C. M.; Tlale, N. S. (2005): Intelligent distributed fuzzy logic control system (IDFLCS) of a mecanum wheeled autonomous guided vehicle. Mechatronics and Automation, IEEE International Conference, vol. 1, pp. 131–137.

69.   Li, X.; Zell, A. (2009): Motion Control of an Omnidirectional Mobile Robot. Joaquim Filipe, JuanAndrade Cetto and Jean-Louis Ferrier (Hg.); Informatics in Control, Automation and Robotics, Bd. 24; Springer Berlin Heidelberg (Lecture Notes in Electrical Engineering), pp. 181-193. Online available under http://dx.doi.org/ 10.1007/978-3-540-85640-5_14.

70.   Liang, L. (1993): Variational problem of general displacement in nonholonomic systems. Acta Mechanica Solida Sinica, vol.6, pp. 357–364.

71.   Liu, Y.; Wu, X.; Zhu, J. J.; Lew, J. (2003): Omni-directional mobile robot controller design by trajectory linearization.

American Control Conference Proceedings, vol. 4, pp. 3423-3428.

72.   Luo, S. (1991): Generalized Noether's theorem of nonholonomic nonpotential system in noninertial reference frames. Applied Mathematics and Mechanics, vol. 12, pp. 927–934.

73.   Luo, Y.; Zhao, Y. (1993): Routh's equations for general nonholonomic mechanical systems of variable mass. Applied Mathematics and Mechanics, vol. 14, pp. 285–298.

74.   Makatchev, M.; McPhee, J. J.; Tso, S. K.; Sherman Y. T. (2000): System Design, Modelling, and Control of a Four-Wheel-Steering Mobile Robot. Proc. of the 19th Chinese Control Conference, Hong Kong.

75.   Marey, E.-J. (1868): Du mouvement dans les fonctions de la vie. Lecons faites au; College de France, Bailliere, Paris.

76.   Martynenko, Yu. G. (2007): Motion Control of Mobile Wheeled Robots. Journal of Mathematical Sciences, Vol. 147, No. 2.

77.   Martynenko, Yu. G. (2010): Stability of steady motions of a mobile robot with roller-carrying wheels and a displaced centre of mass. Journal of Applied Mathematics and Mechanics, vol. 74, No. 4, pp. 436-442.

78.   Martynenko, Yu. G.; Formal'skii, A. M. (2007): On the motion of a mobile robot with roller-carrying wheels. Journal of Computer and Systems Sciences International, vol. 46, no. 6, pp 976-983.

79.   Mason, B. S. et al (2013): The ergonomics of wheelchair configuration for optimal performance in the wheelchair court sports. Sports Med, vol. 43, no. 1, pp. 23–38.

80.   Matthew, T. M. (2012): Mechanics of Manipulation -Lectures Notes.

81.   Mckee, C. (2010): A market-based approach to inclusive mobility, 12th International Conference on Mobility and Transport for Eldery and Disabled Persons (TRANSED 2010); Hong Kong.

82. Meulen, P., Seidl, A. (2007): Ramsis – The Leading CAD Tool for Ergonomic Analysis of Vehicles; First International Conference on Digital Human Modeling; Beijing, China, Lecture Notes in Computer Science, Springer; Berlin, Heidelberg.

83. Miller, D. I., Nelson, R. C. (1973): Biomechanics of Sport. Philadelphia, Lea & Febiger.

84. Miller, D.I. (1979): Modeling in Biomechanics; An Overview; Medicine and Science in Sports, vol. 11, no. 2, pp. 115-122.

85. Mladenova, C.D. (1994): Kinematics and dynamics of a rigid body in nonholonomic coordinates, Systems & Control Letters, vol. 22, pp. 257–265.

86. Modi,V.J.; Suleman, A.C. (1991): Approach to dynamics and control of orbiting flexible structures, International Journal for Numerical Methods in Engineering, vol. 32, pp. 1727–1748.

87. Morales, R.; Feliu, V.; Gonzalez, A.; Pintado, P. (2006): Coordinated motion of a new staircase climbing wheelchair with increased passenger comfort. Robotics and Automation ICRA, IEEE International Conference, pp. 3995–4001.

88. Morales, R.; Gonzalez, A.; Feliu, V. (2007): Mechanical and Kinematics Design Methodology of a New Wheelchair with Additional Capabilities, Bioinspiration and Robotics Walking and Climbing Robots, Maki K. Habib (Ed.), ISBN: 978-3-902613-15-8.

89. Moravec, H. P. (1983): The Stanford Cart and the CMU Rover. Proceedings of the IEEE , vol.71, no. 7, pp. 872-884.

90. Muir, P. F.; Neuman, C. P. (1987): Kinematic modeling for feedback control of an omnidirectional wheeled mobile robot. IEEE International Conference Proceedings on Robotics and Automation, vol. 4, pp. 1772–1778.

91. Murray, R.M; Li, Z.; Sastry, S.S (1994): A Mathematical Introduction to Robotic Manipulation, Taylor & Francis.

92. Muybridge, E. (1885): Animal Location – An Electrophotographic Investigation of Consecutive Phases of Animal Movement. Philadelphia.

93.   Nagatani, K.; Tachibana, S.; Sofue, M.; Tanaka, Y. (2000):
       Improvement of odometry for omnidirectional vehicle using
       optical flow information. Proceedings of the IEEE/RSJ
       international conference on intelligent robots and systems, vol.
       1, pp. 468-473.

94.   Neimark, J.I.; N.A. Fufaev (1972): Dynamics of
       Nonholonomic Systems; American Mathematical Society.

95.   Oetomo, D.; Li, Y. P.; Ang, V. M. H.; Lim, C. (2005):
       Omnidirectional mobile robots with powered caster wheels:
       design guidelines from kinematic isotropy analysis. Intelligent
       Robots and Systems. IEEE/RSJ International Conference on
       Intelligent Robots and Systems, IROS 2005, pp. 3034–3039.

96.   Pfeiffer, F.; Gebler, B. (1988): A multistage-approach to the
       dynamics and control of elastic robots, IEEE International
       Conference on Robotics and Automation, IEEE Comput. Soc.
       Press, Washington, vol. 1, pp. 2-8.

97.   Pichler, V. (1999): Modellbildung der Dynamik von
       Kraftfahrzeugen unter Anwendung objektorientierter
       Konzepte. (Dissertation), Fachgebiet Mechatronik ,
       Maschinenbau, Gerhard-Mercator-Universität – GH Duisburg,
       VDI Verlag, Düsseldorf.

98.   Popp, K. and Schiehlen, W. (1993): Fahrzeugdynamik,
       Teubner, Stuttgart.

99.   Ramirez-Serrano, A.; Kuzyk, R. (2010): Modified Mecanum
       wheels for traversing rough terrains, Sixth conference on
       autonomic and autonomous systems.

100.   Ratner, P. (2009): 3-D human modeling and animation.
       Hoboken; NJ, Willey.

101.   Reference and user handbook for DYNAMICUS 7.0 (2011):
       Institute of Mechatronics; Chemnitz.

102.   Rismantab-Sany, J.; Shabana, A.A. (1988): Impulsive motion
       of nonholonomic deformable multibody systems. Part I,
       Kinematic and dynamic equations, Journal of Sound and
       Vibration, vol. 127, pp. 193–204.

103.   Rismantab-Sany, J.; Shabana, A.A. (1989): Numerical solution
       of differential-algebraic equations of motion of deformable

mechanical systems with nonholonomic constraints ,
Computers & Structures, vol. 33, pp. 1017–1029.

104. Röhrig, C.; Hess, D.; Kirsch, C.; Künemund, F. (2010):
Localization of an omnidirectional transport robot using IEEE
802.15.4a ranging and laser range finder. Intelligent Robots
and Systems, IEEE/RSJ International Conference IROS, pp.
3798–3803.

105. Ru, D.; Tong, Z.; Li, Z.; Gang L. (2008): Design and
Realization of Omni-directional Mobile Robot Body Based on
Zigbee Technology. Embedded Computing, Fifth IEEE
International Symposium SEC '08, pp. 207–211.

106. Saziorski, W., Aruin, A., Selujanow, W. and Friedrich, G.
(1987): Biomechanik des menschlichen Bewegungsapparates.
Sportverlag, Berlin.

107. Schiehlen, W. (1994): Dynamics and control of nonholonomic
mobile robot systems , In: L. Sciavicco, C. Bonivento and F.
Nicolo (eds), Preprints of Symposium on Robot Control, vol. 1,
pp. 329-334, Napoli.

108. Schiehlen, W. (1997): Multibody System Dynamics: Roots and
Perspectives. Institute B of Mechanics, University of Stuttgart,
Germany. Multibody System Dynamics 1: pp. 149–188,
Kluwer Academic Publishers. Printed in the Netherlands.

109. Schramm, D.; Hiller, M.; Bardini, R. (2010): Modelbildung
und Simulation der Dynamik von Fahrzeugen; Springer-Verlag
Berlin, ISBN 978-3-540-89313-4.

110. Schuster, C. (1999): Strukturvariante Modelle zur Simulation
der Fahrdynamik bei niedrigen Geschwindigkeiten. Aachen:
Shaker, ISBN: 3-8265-4874-4.

111. Schweitzer, G.; Mansour, M. (1989): Dynamics of Controlled
Mechanical Systems, Springer-Verlag, Berlin.

112. Segel, L. (1996): The Dynamics of Vehicles on Roads and
Tracks, Swets& Zeitlinger, Lisse.

113. Shan, G. (1999): Ein biomechanisches Modell auf Basis von
individuellen anthropometrischen Daten für das
Bewegungslernen von Flugphasen bei sportlichen

Bewegungsabläufen. Univ. Diss., Münster. ISBN: 3-8258-4274-6.

114. Shimada, A.; Yajima, S.; Viboonchaicheep, P.; Samura, K. (2005): Mecanum-wheel vehicle systems based on position corrective control. Industrial Electronics Society, 31st Annual Conference of IEEE IECON, vol.23, pp. 2077-2082.

115. Sidibe, M. B.; Yulin, M. (2006): Wheels of wheeled mobile robots. Proceedings of the 5th WSEAS International Conference on Signal Processing, Robotics and Automation. World Scientific and Engineering Academy and Society (WSEAS), Madrid, Spain; pp. 119-124.

116. SIEMENS AG (2013): Jack and Process Simulate Human. http://www.plm. automation .siemens.com/en_us/products/ tecnomatix/assembly_planning/jack/index. shtml. Last visited: 08-08-2013.

117. Silber, G. (2013): Eine neue Methode in der präventiven Biomechanik. Orthopädie-Technik, vol. 64, no. 3, pp. 48.

118. Simons, J. C., Gardener, M. S. (1960): Self maneuvring for the orbital worker. WADD Technical Report, pp. 60-748; Wright Patterson Air Force Base, Ohio.

119. Simpson, R. C. (2005): Smart wheelchairs: A literature review. J Rehabil Res Dev,vol. 42, no. 4, pp. 423-436.

120. Simpson, R. C.; LoPresti, E. F.; Cooper, R. A. (2008): How many people would benefit from a smart wheelchair?; J Rehabil Res Dev., vol. 45, no. 1, pp. 53-71.

121. Song, J.; Byun, K. (2006): Design and Control of an Omnidirectional Mobile Robot with Steerable Omnidirectional Wheels, Mobile Robotics, Moving Intelligence, Jonas Buchli (Ed.), ISBN: 3-86611-284-X, InTech, DOI: 10.5772/4723. Available from: http://www.intechopen.com/books/mobile_ robotics_moving_intelligence/design_and_control_of_an_omni directional_mobile_robot_with_steerable_omnidirectional_whe els.

122. Spenko, M.; Yu, H.; Dubowsky, S. (2002): Analysis and design of an omnidirectional platform for operation on non-

ideal floors. Robotics and Automation. IEEE International Conference Proceedings, ICRA '02, vol. 1, no. 1, pp. 726-731.

123.   Stadler, W. (1995): Analytical Robotics and Mechatronics, McGraw-Hill, London.

124.   TECNOMATIX GMBH (2013): RAMSIS in eM-Human. http://www.human-solutions.com/download/pdf/eMPower_ Ramsis_de.pdf. Last visited: 09-08-2013.

125.   Terashima, K.; Miyoshi, T.; Urbano, J.; Kitagawa, H. (2004): Frequency shape control of omni-directional wheelchair to increase user's comfort. the Proceedings of IEEE International Conference on Robotics and Automation ICRA '04, vol. 3, pp. 3119–3124.

126.   Tlale, N. S. (2006): On distributed mechatronics controller for omni-directional autonomous guided vehicles. Industrial Robot: An International Journal, vol. 33, no. 4, pp.278-284.

127.   Tlale, N.; Villiers, M. (2008): Kinematics and Dynamics Modelling of a Mecanum Wheeled Mobile Platform. Mechatronics and Machine Vision in Practice, 15th International Conference M2VIP, pp. 657-662.

128.   Toth, F.; Krasnansky, P.; Gulan, M.; Rohal'-Ilkiv, B. (2013): Control systems in omni-directional robotic vehicle with mecanum wheels. International Conference, Process Control PC, pp. 516–521.

129.   Tsai, C. and Wu, H. (2010): Nonsingular terminal sliding control using fuzzy wavelet networks for Mecanum wheeled omni-directional vehicles. Fuzzy Systems (FUZZ), IEEE International Conference Fuzzy Systems, pp.1-6. doi:10.1109/FUZZY.2010.5584223.

130.   Tsai, C.; Tai F.; Lee Y. (2011): Motion controller design and embedded realization for Mecanum wheeled omnidirectional robots. 9th World Congress. Intelligent Control and Automation WCICA, pp. 546–551.

131.   Udengaard, M.; Iagnemma, K. (2007): Kinematic analysis and control of an omnidirectional mobile robot in rough terrain. IEEE/RSJ International Conference on Intelligent Robots and Systems IROS, pp. 795-800.

132. Ueno, Y.; Ohno, T.; Terashima, K.; Kitagawa, H. (2009): The development of driving system with Differential Drive Steering System for omni-directional mobile robot. International Conference on Mechatronics and Automation ICMA, pp. 1089-1094.

133. Urbano, J.; Terashima, K.; Kitagawa, H. (2006): Neuro-fuzzy control of a power assist Omni-directional Wheelchair to enhance maneuverability. In: Computer Aided Control System Design, IEEE International Conference on Control Applications, IEEE International Symposium on Intelligent Control, pp. 939–946.

134. Usher, K.; Dunbabin, M.; Ridley, P. (2004): Robust position estimation for a car-like vehicle. Robotics and Automation, IEEE International Conference Proceedings ICRA '04., vol. 5, pp. 5129-5134.

135. Van der Woude, L.; et al (2009): Evaluation of Manual Wheelchair Performance in Everyday Life. Topics in Spinal Cord Injury Rehabilitation, vol. 15, no. 2, pp. 1-15.

136. Vegter R.JK.; de Groot, S.; et al (2011): Design of a manually propelled wheelchair: optimizing a wheelchair user combination. International Encyclopedia of Rehabilitation. Center for International Rehabilitation Research Information and Exchange (CIRRIE).

137. Viboonchaicheep, P., Shimada, A. and Kosaka, Y. (2003): Position rectification control for Mecanum wheeled omni-directional vehicles; Industrial Electronics Society, IECON '03. The 29th Annual Conference of the IEEE , vol.1, pp.854,859, 2-6 Nov. doi:10.1109/IECON.2003.1280094.

138. Vladimir Medved (2000): Measurement of Human Locomotion.CRC Press. Print ISBN: 978-0-8493-7675-7; eBook ISBN: 978-1-4200-3698-5.

139. Vukobratovic, M.; Stokic, D. (1982): Control of Manipulation Robots, Springer-Verlag, Berlin.

140. Wada, M. (2005): An omnidirectional 4WD mobile platform for wheelchair applications. Advanced Intelligent

Mechatronics, IEEE/ASME International Conference Proceedings, pp. 576-581.

141. Wada, M. (2005): Omnidirectional control of a four-wheel drive mobile base for wheelchairs. Advanced Robotics and its Social Impacts, IEEE Workshop, pp. 196-201.

142. Wada, M. (2006): Omnidirectional Control of 4WD Robotic Base. International Joint Conference, SICE-ICASE, pp. 2064-2067.

143. Wada, M. (2006): Virtual link model for redundantly actuated holonomic omnidirectional mobile robots. Robotics and Automation, Proceedings IEEE International Conference on ICRA 2006, pp. 3201-3207.

144. Wada, M. (2007): Holonomic and omnidirectional wheelchairs with synchronized 4WD mechanism. Intelligent Robots and Systems, IEEE/RSJ International Conference IROS, pp. 1196-1202.

145. Wada, M. (2008): A 4WD omnidirectional wheelchair with a chair tilting mechanism for enhancing step climbing capability. Advanced Motion Control, 10th IEEE International Workshop AMC '08, pp. 474-479.

146. Wada, M. (2008): A 4WD omnidirectional wheelchair with a chair tilting system. Mechatronics and Automation, IEEE International Conference, pp. 21-26.

147. Wada, M. (2008): Development of a 4WD omnidirectional wheelchair. SICE Annual Conference, pp. 1767-1771.

148. Wada, M. (2008): Step climbing capability of a 4WD omnidirectional wheelchair. Intelligent Robots and Systems Conferance, IEEE/RSJ International Conference, IROS 2008, pp. 266-272.

149. Wada, M. (2009): Mechanism and control of a 4WD robotic platform for omnidirectional wheelchairs. IEEE/RSJ International Conference on Intelligent Robots and Systems, IROS 2009, pp. 4855-4862.

150. Wada, M.; Hirama, T.; Inoue, Y. (2013): Traction analysis for active-caster omnidirectional Robotic drive with a Ball Transmission (ACROBAT). IEEE/ASME International

Conference on Advanced Intelligent Mechatronics (AIM), pp. 274-279.

151.   Wada, M.; Inoue, Y.; Hirama, T. (2012): A new active-caster drive system with a dual-ball transmission for omnidirectional mobile robots. In: Intelligent Robots and Systems (IROS), IEEE/RSJ International Conference, pp. 2525-2532.

152.   Wada, M.; Mori, S. (1996): Holonomic and omnidirectional vehicle with conventional tires. Robotics and Automation, IEEE International Conference Proceedings, vol. 4, pp. 3671-3676.

153.   Wada, M.; Mori, S. (1996): Modeling and control of a new type of omnidirectional holonomic vehicle. 4th International Workshop Proceedings on Advanced Motion Control AMC '96-MIE, vol. 1, pp. 265-270.

154.   Wampfler, G.; Salecker, M.; Wittenburg, J. (1989): Kinematics, Dynamics, and Control of Omnidirectional Vehicles with Mecanum Wheels. Journal Mechanics of Structures and Machines, vol.17, no. 2, pp. 165-177.

155.   Wang, D.; Xu, G. (2003): Full-state tracking and internal dynamics of non holonomic wheeled mobile robots. Mechatronics, IEEE/ASME Transactions, vol. 8, no. 2, pp. 203–214.

156.   Wang, Y.; Linnett, J. A.; Roberts, J. W. (1996): A unified approach to inverse and direct kinematics for four kinds of wheeled mobile robots and its applications. Robotics and Automation, IEEE International Conference Proceedings, vol. 4, no. 4, pp. 3458-3465.

157.   Watanabe, K. (1998): Control of an omnidirectional mobile robot. Proceedings of Second International Conference on Knowledge-Based Intelligent Electronic Systems, pp. 51-60.

158.   Whitsett, C.E. (1964): A mathematical model to represent weightless man. Aerospace Med, vol. 35, pp. 11-16.

159.   Woernle, C. (1988): Ein systematisches Verfahren zur Aufstellung der geometrischen Schließbedingungen in kinematischen Schleifen mit Anwendung bei der

Rückwärtstransformation für Industrieroboter. Fortschritt - Berichte VDI Reihe 18 Nr. 59, VDI-Verlag, Düsseldorf.

160. Yu, H.; Zhang, J.; Xu, Y. (1993): Noether's theory for nonholonomic systems relative to non-inertial reference frame. Applied Mathematics and Mechanics, vol. 14, pp. 527-536.

161. Yunan ,Z. et al (2010): Research on motion Characteristic of omnidirectional robot based on Mecanum Wheel. International Conference on Digital Manufacturing and Automation ICDMA, vol. 2, pp. 237-241.

162. Yunan, Z.; Shuangshuang, W. et al (2011): Research on motion characteristic of omnidirectional device based on Mecanum wheel. Electric Information and Control Engineering, International ICEICE, pp. 6094-6097.

163. Zatsiorsky, V.; Selvyanov, V. (1983): The Mass and Inertia characteristics of the Main Segments of the Human body. Biomechanics VIII-B, Illinois.

164. Zhao, D.; Deng, X.; Yi, J. (2009): Motion and Internal Force Control for Omnidirectional Wheeled Mobile Robots. Mechatronics, IEEE/ASME Transactions, vol. 14, no. 3, pp. 382–387.

165. Zimmermann, K., Zeidis, I.; Behn, C. (2009): Mechanics of Terrestrial Locomtion with a Focus on Non-pedal Motion Systems. Springer, Dordrecht, ISBN 978-3-540-88840-6.

166. Zimmermann, K.; Zeidis, I.; Abdelrahman, M. (2013): Dynamics of mechanical systems with mecanum wheels. 12th Conference on Dynamical Systems – Theory and Applications. Lodz, Poland, Book of Abstracts, pp. 190.

167. Zimmermann, K.; Zeidis, I.; Abdelrahman, M.(2014): Dynamics of mechanical systems with mecanum wheels. submitted to International Journal of Dynamics and Control, Springer publishing.

168. Zobova, A.A; Tatarinov, Ya.V (2009): Dynamics of an omni-mobile vehicle. Prikl. Mat. Mekh, vol. 73, no. 1, pp. 13-22.